Abstract

Barker, Jason Alan. Investigations of Liposome/Water Partitioning Using Electrokinetic Chromatography. (Under the direction of Morteza G. Khaledi)

The main goal of this research progress was to investigate different aspects of liposome/water partitioning using liposome electrokinetic chromatography (LEKC) with various lipid bilayer membrane pseudostationary phases and a wide variety of different test solutes.

The predictive and descriptive abilities of Linear Solvation Energy Relationships (LSER) models were used extensively over the course of this research project. The predictive ability of the LSER model was first tested by comparing experimental retention factors with retention factors predicted using LSER models determined using a set of simple test molecules for a set of neutral drugs. Later in the study, a similar approach was used to predict retention factors for aliphatic compounds that cannot be detected using UV absorbance. The descriptive ability was used to study the interactions that control liposome/water partitioning and to compare the selectivity of lipid phases of varied compositions. LSER models describing liposome/water partitioning behavior were also compared to those describing different biological processes such as intestinal and skin permeability.

The use of pseudostationary phases comprised of spontaneous unilamellar vesicles formed by the mixing of short-chain and long-chain lipids was also investigated. The sizes of these vesicles was characterized using dynamic light scattering and

retention properties were characterized using a set of 50 test solutes. The temperature dependence and thermodynamic parameters of vesicle/water partitioning for these lipid phases were studied by fitting partition coefficients determined over a range of temperatures to nonlinear van't Hoff plots.

Finally, a quantative structure activity relationship (QSAR) was developed to predict skin permeability coefficients using LEKC retention factors, molecular weight, and a descriptor of hydrogen bonding determined using the solute structure. This model was favorably compared with other models used for the prediction of skin permeability coefficients using similar descriptors.

Investigations of Liposome/Water Partitioning Using Electrokinetic Chromatography

by

Jason Alan Barker

A dissertation submitted to the Graduate Faculty of
North Carolina State University
in partial fulfillment of the
requirements for the Degree of
Doctor of Philosophy

Department of Chemistry

Raleigh, NC

December 17, 2004

APPROVED BY:

Charles B. Boss	**Edmond F. Bowden**
Daniel L. Feldheim	**Morteza G. Khaledi** (Chair of Advisory Committee)

This dissertation is dedicated to my friends and family.
I could not have gotten here without you.

Well, I probably could have, but I sure am glad you guys were around to keep things interesting.

Biography

Jason Alan Barker was born on April 24, 1975 to Terry and Kaye Barker in Wilmington, NC. After stays in Wilmington; Tampa, Florida; Myrtle Beach, South Carolina; and Atlanta, Georgia; the Barker family settled in Chapel Hill, North Carolina in January of 1987. In 1993, Jason graduated from Chapel Hill High School and began his undergraduate course work in chemistry major at North Carolina State University. In 1997, he completed his Bachelor of Science degree in chemistry. After working in industry for two years, Jason's interest in chromatography and other modes of analytical separations drove him to begin his graduate work at North Carolina State University under the direction of Dr. Morteza G. Khaledi in August of 1999.

Acknowledgments

Bear with me, folks, I've got a lot of people that I want to thank. I am certain that I will forget at least a couple of people that have made a positive contribution to this document.

First of all, I absolutely have to thank Dr. William Switzer and Dr. William Tucker for taking the time to talk to me way back in 1992 when I first visited the NCSU Department of Chemistry. Without their encouragement, I might have gone to Carolina.

I'd like to thank Dr. Charles Boss, whose Instrumental Analysis class got me interested in analytical chemistry as a senior in college. I'd also like to thank Dr. Anton Schreiner for his insistences that I one day pursue graduate school in chemistry.

I was lucky enough to start graduate school with an incredibly supportive class in 1999. In particular, I need to acknowledge Dr. Ryan Fuierer for his dedication to rock and roll and obscene finger gestures, Joe Ryan for his patience in all of those organic and inorganic study sessions, and all of the guys that were lucky enough to play Saturday morning basketball in my company. I consider myself very lucky to have spent some time in graduate school with Miles Andersen. I doubt that there is anyone who ever met Miles that will ever forget him. I know that I will not.

Next, I have to thank Dr. Morteza G. Khaledi for his support and mentorship during my graduate school career. Dr. Khaledi did an excellent job of walking the fine line between teaching me and allowing me to learn on my own. Additionally, I have learned volumes (and it mostly was not even chemistry) from my fellow Khaledi group members: Dr. Scott Burns, Dr. Hai Bui, Juan Pablo Mack, Dr. Jennifer Carrozino, Emnet Yitbarek, Neha Frantz, Chairman Yang Shen, Ceixiong Fu, Suzy Yeh, and Sam Jenkins.

I am extremely fortunate to have very good friends who were able to distract me from my work; sometimes even at the appropriate times when I needed a distraction. I'd like to thank Amanda Wagner, Vincent Turner, and Rebecca Semcer for their uncanny ability to share various apartments with me while I was in graduate school. I need to specifically thank Vincent for all of the weight room trips, games of Madden, episodes of the Sopranos, and late night swims that we had in Sumter Square. I'd also like to thank Steven Green and Catherine Pozarycki for their friendship, support, and also for letting me live in their house for those six months in 2000. Andrew and Vanessa Neal, my great friends in Chapel Hill, have offered me support, encouragement, and Pepper's Pizza whenever I needed it. Without your friendships, the last five and a half years would have been a lot less fun.

I'm never exactly sure how to answer people when they ask me how I got into chemistry. I have always known that I was going to be a scientist, and more specifically a chemist. I strongly suspect that the driving force behind that desire was the first chemist I ever met, my grandfather, James Barker. Although I never learned much chemistry from him, and although I never got to spend as much time with him as I would have liked, the memories that I have of my grandfather will influence me and guide me for the rest of my life.

Having my brother, Clay, at the same school with me has been very special. Without the football games, basketball games, and trips to the gym that we have had, I would have lost my sanity somewhere along the way. Not to mention all of the free statistics consultations that he has given me. Finally, and certainly most of all, I need to thank my parents. They raised me to be the person I am today and have supported me through everything I have ever done. To paraphrase Jim Valvano, they have given me the greatest gift that anyone can give; they have believed in me.

Thanks, everybody.

Table of Contents

List of Tables

List of Figures

Chapter 1

Introduction

Nearly countless techniques exist that use widely varied molecular properties to separate the individual components of mixtures; solvent extraction, thin-layer chromatography, gas chromatography, liquid chromatography, size-exclusion chromatography, ion exchange chromatography and electrophoretic methods separate compounds using properties such as hydrophobicity, molecular size, electrostatic interactions and electrophoretic mobility. Each technique has its own specific strengths and weaknesses.

Capillary Electrophoresis

In general, electrophoretic techniques are used to separate compounds by differential mobilities under the influence of an electric field. Capillary electrophoresis is used to separate ions in a fused silica capillary. Two distinct phenomena contribute to separations by capillary electrophoresis: electrophoresis and electroosmosis.

Electrophoresis refers to the movement of an ion under the influence of an electric field. In the presence of a constant electric field, an ion in solution moves at a constant velocity (u_{ep} **,** in m/s) that is dependant upon the magnitude of the electric field (E , in V/m), the charge of the ion (q , in coulombs), and the friction coefficient of the ion in the specific solution (f). Electrophoretic mobility refers to the proportionality constant between the velocity of the ion and the electric field. These quantities are related by:

$$u_{ep} = \frac{q}{f} E = \mu_{ep} E \qquad \textbf{Equation 1-1}$$

Assuming the ion is spherical in shape, the friction coefficient of the ion is related to its radius (***r***) and the viscosity of the solution (η) by:

$$f = 6\pi\eta r \qquad \textbf{Equation 1-2}$$

Combining **Equations 1-1** and 1-**2**:

$$u_{ep} = \frac{q}{6\pi\eta r} E \qquad \textbf{Equation 1-3}$$

From **Equation 1-3**, given constant solution viscosity and electric field, the velocity of an ion under the influence of an electric field depends upon the ratio of the charge to the radius of the ion.

Therefore, an electrophoretic separation of two distinct ions depends upon differential charge-to-size ratios of the two ions.

Electroosmosis refers to the net flow of a buffer solution in a fused silica capillary under an electric field from the anode to the cathode. The interior walls of a fused silica capillary are covered by silanol (SiOH) groups. When the pH of the buffer solution in the capillary is above pH = 2, the silanol groups are deprotonated to SiO^-, imparting a net negative charge to the interior walls of the capillary. Interactions between the negatively charged groups on the capillary walls and the buffer cations form an electrical double layer at the surface of the walls. Two populations of buffer cations are attracted to the deprotonated silanol groups. One layer of immobile cations is tightly bound to the deprotonated silanol groups by electrostatic interactions. Another layer of mobile cations are loosely attracted to the surface of the capillary walls. These mobile cations constitute the diffuse part of the electrical double layer. When the electric field is applied, the mobile buffer cations are attracted to the anodic end of the capillary; because excess cations are localized in the diffuse part of the double layer, the momentum of the cations are able to create a net flow of buffer from the cathodic end of the capillary to the anodic end of the capillary. This flow is often referred to as the electroosmotic flow (EOF). The electroosmotic mobility (μ_{eo}) is defined as the proportionality constant between the velocity of the electroosmotic flow (u_{eo}) and the magnetic field as described below:

$$u_{eo} = \mu_{eo} E \qquad \textbf{Equation 1-4}$$

In any given electrophoretic separation, the electroosmotic mobility is constant for all ions involved.

The presence of the electroosmotic flow in electrophoretic and electrokinetic separations offers improved resolution relative to liquid chromatographic methods. Electroosmotic flow is characterized by a uniform flow profile, i.e. the velocity of the electroosmotic flow center of the capillary is equal to the velocity of the electroosmotic flow at the surface of the capillary wall. In contrast, liquid chromatography systems are characterized by a laminar or parabolic velocity profile, i.e. the velocity of the flow is greater in the middle of the cross-section than at the walls of the column. Systems that display a uniform flow profile always exhibit less band broadening than systems that display a hydrodynamic flow profile.

The observed or apparent mobility (μ_{app}) of an ion in an electrophoretic separation is the proportionality constant between the net velocity of the ion (u_{net}) and the electric field. Apparent mobility depends on both the electrophoretic mobility and the electroosmotic mobility:

$$\mu_{app} = \mu_{ep} + \mu_{eo} = \frac{u_{net}}{E} \qquad \textbf{Equation 1-5}$$

Analyte cations have electrophoretic mobility towards the cathode. Therefore, electrophoretic mobility and electroosmotic mobility always have the same sign and apparent mobility is therefore greater in

magnitude than electroosmotic mobility. Conversely, analyte anions have electrophoretic mobility towards the anode. At neutral or basic pH, the electroosmotic mobility will be opposite in sign and larger in magnitude than analyte anions. Therefore, at neutral or basic pH, analyte anions will have an apparent mobility towards the cathode and smaller in magnitude than electroosmotic mobility. At acidic pH, electroosmotic mobility may be smaller than the electrophoretic mobility of analyte anions. Under these conditions, analyte anions may have an apparent mobility towards the anode.

Up to this point, this discussion of electrophoretic separations has neglected non-ionic species. By definition, the charge on a neutral species is zero. Therefore, by **Equation 1-1** the electrophoretic mobility of a neutral species will be zero and by **Equation 1-5** the apparent mobility of a neutral species will be equal to the electroosmotic mobility. Separation of a mixture of species by capillary electrophoresis is dependant upon differential apparent mobilities and therefore differential electrophoretic mobilities; because neutral species do not have differential electrophoretic mobilities, they cannot be separated by conventional capillary electrophoresis methods.

Capillary electrophoresis separations offer several theoretical advantages over liquid chromatography methods. As mentioned above, the uniform flow profile that is characteristic of electroosmotically-driven separations offers decreased band broadening relative to the hydrodynamic flow profile characteristic of pressure-driven liquid chromatography methodologies. Band broadening (quantified by *H*, theoretical plate height) in liquid chromatography is often described using the van Deemter equation:

$$H = A + \frac{B}{u_x} + Cu_x \qquad \textbf{Equation 1-6}$$

Where A represents the multiple paths term, $\frac{B}{u_x}$ represents the longitudinal diffusion term and Cu_x represents the mass transfer term. Capillary electrophoresis minimizes band broadening by eliminating the multiple paths term because of the open tubular capillary and the mass transfer term because there is no stationary phase. For these reasons, capillary electrophoresis methods often exhibit an order of magnitude more theoretical plates than analogous liquid chromatography methods.[1]

Electrokinetic Chromatography

Electrokinetic chromatography methods combine the high resolution of capillary electrophoresis with the ability to separate neutral compounds. In 1984, Terabe, et al. introduced micellar electrokinetic chromatography (MEKC).[2,3] Traditional MEKC uses anionic or cationic surfactant micelles as a

separation medium for neutral compounds. This separation medium is often referred to as the pseudostationary phase; it is similar in function to the stationary phase in other forms of chromatography, yet it is not stationary due to its electrophoretic and electroosmotic mobilities. The most common pseudostationary phase for MEKC separations is a buffered aqueous solution of micelles made from a simple anionic surfactant such as sodium dodecylsulfate (SDS). Assuming that the buffer solution is at neutral pH or higher, the mobility of the electroosmotic flow will be from the anode/injection end of the capillary, towards the cathode/detector end of the capillary. The electrophoretic mobility of the anionic micelles will oppose the electroosmotic flow; the negatively charged micelles will be attracted to the anode/injection end of the capillary. If the mobility of the electroosmotic flow is greater than the electrophoretic mobility of the micelles, the micelles will therefore have an apparent mobility towards the cathode/detector end of the capillary that is smaller in magnitude than the electroosmotic flow.

Separation of neutral solutes by MEKC depends on differential partitioning of the solutes between the micelle phase and the aqueous phase. When a neutral solute molecule is distributed to the aqueous phase, its apparent mobility is equal to the electroosmotic mobility. Conversely, when the same neutral solute molecule is distributed to the micelle phase, its apparent mobility is identical to the apparent mobility of the micelle. Therefore, the elution time of a given solute in an MEKC separation is influenced by the electroosmotic mobility, the electrophoretic mobility of the micelle phase, and the micelle/water partition coefficient (K_{mw}) of the given solute.

The electroosmotic mobility and the electrophoretic mobility of the micelle phase impose a fundamental limitation upon MEKC separations. A neutral compound that has little or no interaction with the micellar phase (i.e., an unretained solute with a small K_{mw}) will travel from the anode/injection end to the cathode/detector end of the capillary at a velocity determined by the electroosmotic mobility. This solute will be eluted first in a given MEKC separation. A neutral compound that has little or no interaction with the aqueous phase (ie. a solute with a very large K_{mw}) will travel across the capillary with a velocity determined by the apparent mobility of the micellar phase. This solute will be eluted last in an MEKC separation. All other neutral solutes must elute between the elution times defined by these two limits in the order of their respective micelle/water partition coefficients. This phenomenon is referred to as the elution window of MEKC.

MEKC and other electrokinetic chromatography separations represent a “best of both worlds” situation relative to capillary electrophoresis and liquid chromatography. MEKC retains an efficiency advantage over liquid chromatography because the open tubular capillary and the uniform flow profile are maintained. The addition of the micellar pseudostationary phase reintroduces the mass transfer

term (Cu_x) to the van Deemter equation describing band broadening in a given MEKC separation. The Cu_x term is much smaller for most MEKC separations relative to liquid chromatography.

Investigating Partitioning Behavior Using Electrokinetic Chromatography

Electrokinetic chromatography methods, including MEKC, offer alternative high-resolution methods for separating a diverse population of charged or uncharged analytes. An excellent review of different MEKC methods is included in *High Performance Capillary Electrophoresis: Theory, Techniques, and Applications*.[4]

It is important to note that electrokinetic chromatography also offers a tool for studying different partitioning phenomena. As stated above, the elution time of a given solute in an MEKC separation is influenced by the electroosmotic mobility, the electrophoretic mobility of the micelle phase, and the micelle/water partition coefficient (K_{mw}) of the given solute. The same statement holds true if the micellar phase is replaced with a different separation medium such as vesicles or liposomes.

As in all partition chromatography, the retention factor (k) in MEKC is defined as the ratio of moles of a given solute in the micellar phase (n_{mc}) to the number of moles of the same solute in the aqueous phase (n_{aq}). From this definition, it is possible to algebraically relate the retention factor to the solute's micelle/water partition coefficient and the volume phase ratio (Φ) for the MEKC system:

$$k = \frac{n_{mc}}{n_{aq}} = \frac{[solute]_{mc}}{[solute]_{aq}} * \frac{V_{mc}}{V_{aq}} = K_{mw}\Phi \quad \textbf{Equation 1-7}$$

For many chromatography systems, the volume phase ratio cannot be experimentally determined. For most electrokinetic chromatography systems, the volume phase ratio can be directly determined using the physical properties of the pseudostationary phase:

$$\Phi = \frac{\nu(C_{sf} - CMC)}{1 - \nu(C_{sf} - CMC)} \quad \textbf{Equation 1-8}$$

ν is the molar volume of the surfactant, C_{sf} is the concentration of the surfactant, and CMC is the critical micelle concentration of the surfactant. All of the quantities can be directly determined experimentally.

The apparent mobility of any solute in any EKC experiment is directly dependant on the amount of solute distributed to the pseudostationary phase and the aqueous phase at any given time and the respective apparent mobilities of the pseudostationary phase and the aqueous phase. Therefore, for these LEKC experiments, it is possible to describe the apparent mobility of any solute, μ, as a

weighted sum of the apparent mobility of the solute in the liposome phase (μ_{lip}) and the apparent mobility of the solute in the aqueous phase (μ_0):

$$\mu = \left(\frac{n_{lip}}{n_{lip} + n_{aq}} \right) \mu_{lip} + \left(\frac{n_{aq}}{n_{lip} + n_{aq}} \right) \mu_0 \quad \textbf{Equation 1-9}$$

The retention factor is defined as the ratio of the number of moles of solute distributed to the liposome phase (n_{lip}) and the number of moles of solute distributed to the aqueous phase (n_{aq}). Therefore, it is possible to algebraically rearrange **Equation 1-9** to:

$$\mu = \left(\frac{k}{k+1} \right) \mu_{lip} + \left(\frac{1}{k+1} \right) \mu_0 \quad \textbf{Equation 1-10}$$

For any solute, μ_{lip} is equivalent to the mobility of the lipid phase. μ_{lip} is easily determined by adding a hydrophobic marker (octanophenone) to the sample solution to mark the migration of the liposome phase through the detection window. For neutral solutes, the mobility of the solute in the aqueous phase will be equivalent to the electroosmotic mobility. Therefore, the apparent mobility of a neutral solute in the aqueous phase, μ_0, will be zero and **Equation 1-10** may be simplified to:

$$\mu = \left(\frac{k}{k+1} \right) \mu_{lip} \quad \textbf{Equation 1-11}$$

By rearrangement,

$$k = \frac{\mu}{\mu_{lip} - \mu} \quad \textbf{Equation 1-12}$$

In any EKC experiment, the apparent mobility of any solute or marker may be determined from the migration time using:

$$\mu = \left(\frac{1}{t_r} - \frac{1}{t_{eo}} \right) \left(\frac{L_t L_d}{V} \right) \quad \textbf{Equation 1-13}$$

Where t_r represents the migration time of the solute or marker (minutes), t_{eo} represents the migration time of the unretained EOF marker (minutes), L_t represents the total length of the capillary (cm), L_d represents the length of the capillary to the detection window, and V represents the applied voltage.

Therefore the apparent mobility of a neutral solute may be expressed using **Equation 1-13**, and μ_{lip} may be expressed using:

$$\mu_{lip} = \left(\frac{1}{t_{lip}} - \frac{1}{t_{eo}} \right) \left(\frac{L_t L_d}{V} \right) \quad \textbf{Equation 1-14}$$

where t_{lip} is the migration time of the hydrophobic marker.

By inserting **Equation 1-13** and **Equation 1-14** into **Equation 1-12** above and subsequent rearrangement,

$$k = \frac{t_r - t_{eo}}{t_{eo}\left[1 - \frac{t_r}{t_{lip}}\right]} \qquad \textbf{Equation 1-15}$$

Calculation of retention factors for ionized solutes require consideration of the electrophoretic mobility of the solute, μ_0. From **Equation 1-10** above, the apparent mobility of any solute in an LEKC experiment may be expressed as a weighted sum of the μ_{lip} and μ_0 using the retention factor (k) as a measure of the amount of solute distributed to each phase respectively:

$$\mu = \left(\frac{k}{k+1}\right)\mu_{lip} + \left(\frac{1}{k+1}\right)\mu_0 \quad \textbf{Equation 1-10}$$

For partially ionized solutes, each solute has a distinct electrophoretic mobility related to the fraction of the solute that is ionized and the size of the solute. Therefore, μ_0 is not equal to zero for partially ionized solutes.

By rearrangement of **Equation 1-10**, the retention factor of a partially ionized solute may be expressed using:

$$k = \frac{\mu - \mu_0}{\mu_{lip} - \mu} \quad \textbf{Equation 1-16}$$

For each partially ionized solute, μ and μ_{lip} may be calculated from LEKC data using **Equation 1-13** and **Equation 1-4**, respectively. μ_0 may be calculated from CZE data using:

$$\mu_0 = \left(\frac{1}{t_r} - \frac{1}{t_{eo}}\right)\left(\frac{L_t L_d}{V}\right) \qquad \textbf{Equation 1-17}$$

Finally, retention factors for ionizable solutes were calculated from μ, μ_{lip}, and μ_0 using **Equation 1-16**.

Many studies in the Khaledi research group have focused on the use of electrokinetic chromatography to study partitioning behavior for many different systems including micelle/water[5-10], vesicle/water[11-13], and liposome/water[14,15].

Linear Solvation Energy Relationship (LSER) Models

Linear solvation energy relationships were first used by Kamlet and Taft to model various solvation systems.[16-19] This model was then revised by Abraham et al. to better describe selectivity chromatographic systems.[20] The LSER model has been extensively used by Khaledi et al. to characterize selectivity of micellar,[5-9,21-23] vesicular,[11-13] and lipid-based pseudostationary phases in electrokinetic chromatography systems.[14,15] Other groups have used the LSER model to characterize

various micellar pseudostationary phases,[24] the effect of organic modifiers in MEKC,[25,26] and polymeric micellar pseudostationary phases.[27-31]

The LSER model used to describe selectivity in this study is:

$$\log k = vV + bB + aA + sS + eE + C \quad \textbf{Equation 1-18}$$

where lower case coefficients describe pseudostationary phase properties and upper case descriptors describe solute properties. These system coefficients and solute descriptors are described in **Appendix A-3**. The solute descriptor V is the solute's McGowan's volume, B is the solute's hydrogen bond acceptor ability/basicity, A is the solute's hydrogen bond donor ability/acidity, S is the solute's dipolarity/polarizability, and E is the solute's excess molar refraction. The coefficient v is a measure of the system's cohesiveness. The coefficient b is a measure of the system's hydrogen bond donor ability/acidity coefficient; the coefficient a is a measure of the system's hydrogen bond acceptor ability/basicity. The coefficient s is a measure of the system's dipolarity/polarizability. The system coefficient e is the measure of the system's dependence on interactions with the solute's *n*- or *π*- electrons. It is important to note that all of the system coefficients are determined relative to the aqueous phase, ie, the v coefficient refers to the cohesiveness of the system relative to the aqueous phase. C is a regression constant and includes information about the chromatographic phase ratio and thus varies with pseudostationary phase composition.

Like any model, the LSER model can serve a dual purpose. First of all, when log k values are experimentally determined for a set of solutes with known descriptor values, system coefficients can be determined and used to characterize the selectivity of the given system. Also, known solute descriptors and system coefficients can be used to predict log k values for solutes without running additional experiments.

Significance of Liposome/Water Partitioning

Since Meyer and Overton noticed a strong correlation between the olive oil/water partitioning behavior and the narcotic activity of simple organic compounds in the late nineteenth century[32], partitioning behavior has been investigated as a predictor of bioavailability/permeability. Often, the partition coefficient, K, of a molecule between a hydrophobic phase such as a long-chain alcohol or hydrocarbon is used as a measure of the molecule's affinity for a lipid phase or "lipophilicity." Using the octanol/water system as an example, K_{ow} may be calculated using:

$$K_{ow} = \frac{[solute]_{oct}}{[solute]_{aqueous}} \quad \textbf{Equation 1-10}$$

$[solute]_{oct}$ is the concentration of the solute in the octanol phase and $[solute]_{aqueous}$ is the concentration of the solute in the aqueous phase.

Many compounds are transported in the body by passive transport across a barrier membrane composed mainly of lipids and cholesterol. In the case of octanol/water partitioning, the octanol is used to model the lipid environment of the cell membrane and the water is used to model the aqueous environment that surrounds the cell membrane. It is reasonable to theorize that a lipophilic molecule, that is, a molecule with a relatively high octanol/water partition coefficient, would be distributed mainly to the lipid phase and would therefore be more bioavailable than a less lipophilic molecule.

Lipophilicity estimation using partitioning between a hydrophobic solvent and aqueous solvent has limitations. The simplest limitation is that determination of partition coefficients for a system like octanol/water requires direct determination of the concentration of a solute in the separated aqueous and hydrophobic phases. This experiment is generally performed by a shake flask method to allow equilibrium distribution of the solute between the two solvent phases and then spectrophotometric determination of the concentration of the solute in each phase. This method is obviously very time-consuming, labor-intensive, and difficult to automate. A second and more abstract limitation of lipophilicity estimation based on octanol/water partitioning is the inherent assumption that distribution of a solute between two bulk solvent phases accurately models distribution of a solute in an interfacial system like a biological membrane.

To this point, the terms *vesicles* and *liposomes* have been used but not yet defined. Vesicles and liposomes are very similar to the more familiar micelles; all three are aggregates formed by the dispersion of amphiphilic molecules in an aqueous solvent. The aggregation of amphiphilic molecules occurs to segregate the hydrophobic regions of the molecule from the aqueous solvent. Amphiphiles with small hydrophobic regions relative to their hydrophilic regions form micelles. Amphiphiles with larger hydrophobic regions relative to their hydrophilic regions form vesicles. Vesicles are spherical aggregates of amphiphiles arranged in bilayers surrounding an aqueous core.[32] Liposomes are simply vesicles formed specifically by phospholipids. The simplest phosphodiglyceride, phosphatidic acid (PA), is synthesized by adding two fatty acids to L-glycerol phosphate by esterification. The resultant molecule has a phosphate head group and glycerol backbone attached to two long acyl chains. A variety of different neutral, anionic, cationic or zwitterionic phosphodiglycerides are made by linking the acidic phosphate head group of PA to bases such as choline, ethanolamine, inositol or serine. The most common phosphodiglyceride, phosphatidylcholine (PC), results from the linkage of a basic choline molecule to a PA molecule to form a zwitterionic lipid. Due to their spherical shape and lipid composition, liposomes are often used to model biological cell membranes.

The liposome/water system offers a unique opportunity to study partitioning of a molecule to a hydrophobic phase composed of lipids and cholesterol similar to the composition of a biological membrane. Studies of liposome/water partitioning can be performed using equilibrium dialysis[33], calorimetry[34,35], spectrophotometry[36], or multiple chromatographic techniques. Recent research in the Khaledi group has focused on developing LEKC as a tool for liposome/water partitioning studies.[14,15] These studies are very advantageous because they allow the rapid determination of the liposome/water partitioning behavior of multiple solutes in a very short run. Also, the liposomes used in LEKC are in free solution and therefore very similar to the fluid state that would be present in a biological system. LEKC also offers control over experimental lipid composition, pH, and temperature. There are two main drawbacks to LEKC studies. LEKC is limited by the presence of an elution window analogous to the elution window in MEKC. Therefore, extremely hydrophilic compounds may coelute with the hydrophilic t_{eo} marker and extremely hydrophobic compounds may coelute with the hydrophobic t_{lip} marker. Also, detection in LEKC is generally achieved by UV-Vis spectrophotometry. Therefore, the compounds that may be studied by LEKC are limited to those with a viable chromophore.

Presented Research

This dissertation presents several different studies of liposome/water partitioning using electrokinetic chromatography (EKC). Several of the chapters focus on the use of linear solvation energy relationships (LSER) models for the elucidation of the interactions responsible for liposome/water partitioning. One such study is focused on the effects of liposome cholesterol content on partitioning using LSER models. Liposome/water partitioning of a set of neutral drugs has also been determined by LSER models based on EKC experiments. A novel EKC pseudostationary phase that mimics the lipid composition of intestinal epithelial membranes has been characterized using LSER models. Finally, the retention properties of EKC pseudostationary phases comprised of vesicles spontaneously formed by short-chain lipids and long-chain lipids[37,38] have also been characterized by LSER models.

The driving force of partitioning of solutes between an aqueaous phase and hydrophobic phases such as bulk organic solvent, micelles, bilayer membranes and liquid chromatography phases is often described using classical hydrophobic effects or nonclassical hydrophobic effects. The classical hydrophobic effect, which is most often used to describe bulk organic solvent/water partitioning of nonpolar solutes, is characterized as entropically-driven at low temperatures and enthalpically driven at high temperatures with a negative heat capacity change at all temperatures. Conversely, the nonclassical hydrophobic effect, which is most often used to describe bilayer membrane/water

partitioning is characterized as enthalpically-driven at all temperatures. Moreover, many partitioning systems, such as bilayer membranes display nonlinear temperature dependence due to nonzero heat capacity changes. In this dissertation, a study of the temperature dependence and thermodynamic parameters of vesicle/water partitioning for a spontaneous vesicle system formed from short-chain lipids and long-chain lipids is presented.

The ultimate goal of many liposome/water partitioning experiments is the development of a predictive relationship between liposome/water partitioning data and permeability or bioavailability data. In this study, a quantitative structure-activity relationship (QSAR) was developed to predict skin permeability coefficients using three solute descriptors: LEKC retention factors, molecular weight, and a descriptor of hydrogen bonding determined from the solute structure. This model was generated using a set of 44 solutes including neutral aromatic solutes, ionizable aromatic solutes, and neutral aliphatic solutes and validated by the leave-one-out method. The model compared favorably with other models used for the prediction of skin permeability coefficients using similar descriptors.[39-42]

Works Cited

1. Harris, D.C. Chromatographic Methods and Capillary Electrophoresis. *Quantitative Chemical Analysis*, 4th ed.; W.H. Freeman and Company: New York, 1995; pp 699-733.
2. Terabe, S.; Otsuka, K.; Ichikawa, K.; Tsuchiya, A.; Ando, T. Electrokinetic separations with micellar solutions and open-tubular capillaries. *Anal. Chem.* **1984**, *56*, 111-113.
3. Terabe, S.; Otsuka, K.; Ando, T. Electrokinetic chromatography with micellar solution and open-tubular capillary. *Anal. Chem*. **1985**, *57*, 834-841.
4. Khaledi, M.G. Micellar Electrokinetic Chromatography. *High Performance Capillary Electrophoresis: Theory, Techniques, and Applications*; Wiley and Sons: New York, 1998; pp 77-131.
5. Trone, M.D.; Khaledi, M.G. Characterization of chemical selectivity in micellar electrokinetic chromatography. 4. Effect of surfactant headgroup. *Anal. Chem*. **1999**, *71* (7), 1270-1277.
6. Trone, M.D.; Leonard, M.S.; Khaledi, M.G. Congeneric behavior in estimations of octanol-water partition coefficients by micellar electrokinetic chromatography. *Anal. Chem*. **2000**, *72* (6), 1228-1235.
7. Trone, M.D.; Khaledi, M.G. Influence of ester and amide-containing surfactant headgroups on selectivity in micellar electrokinetic chromatography. *Electrophoresis*. **2000**, *21* (12), 2390-2396.
8. Trone, M.D.; Mack, J.P.; Goodell, H.P. Characterization of chemical selectivity in micellar electrokinetic chromatography VI. Effects of surfactant counter-ion. *J. Chrom. A*. **2000**, *888* (1-2), 229-240.
9. Trone, M.D.; Khaledi, M.G. Characterization of chemical selectivity in micellar electrokinetic chromatography: V. The effect of the surfactant hydrophobic chain. *J. Micro. Sep*. **2000**, *12* (8), 433-441.
10. Kelly, K.A.; Burns, S.T., Khaledi, M.G. Prediction of retention in micellar electrokinetic chromatography from solute structure. 1. Sodium dodecyl sulfate micelles. *Anal. Chem*. **2001**, *73* (24), 6057-6062.
11. Agbodjan, A.A.; Bui, H.; Khaledi, M.G. Study of solute partitioning in biomembrane-mimetic pseudophases by electrokinetic chromatography: Dihexadecyl phosphate small unilamellar vesicles. *Langmuir*. **2001**, *17* (10), 2893-2899.
12. Bui, H.H.; Khaledi, M.G. Determination of vesicle-water partition coefficients by electrokinetic chromatography: Study of temperature effect. *J. Colloid. Ineterf. Sci.* **2002**, *253* (2), 397-401.
13. Agbodjan, A.A.; Khaledi, M.G. Study of solute partitioning into cationic vesicles of dihexadecyldimethylammonium bromide using electrokinetic chromatography. *J. Chrom. A*. **2003**, *1004* (1-2), 145-153.

14. Burns, S.T.; Khaledi, M.G. Rapid determination of liposome-water partition coefficients (K-lw) using liposome electrokinetic chromatography (LEKC). *J. Pharm. Sci.* **2002**, *91* (7), 1601-1612.
15. Burns, S.T.; Agbodjan, A.A.; Khaledi, M.G. Characterization of solvation properties of lipid bilayer membranes in liposome electrokinetic chromatography. *J. Chrom. A*. **2002**, *973* (1-2), 167-176.
16. Kamlet, M.J.; Taft, R.W. The solvatochromic comparison method. I. The .beta.-scale of solvent hydrogen-bond acceptor (HBA) basicities. *J. Am. Chem. Soc*. **1976**, *98* (2), 377-383.
17. Taft, R.W.; Kamlet, M.J. The solvatochromic comparison method. 2. The .alpha.-scale of solvent hydrogen-bond donor (HBD) acidities. *J. Am. Chem. Soc*. **1976**, *98* (10), 2886-2894.
18. Yokoyama T.; Taft, R.W.; Kamlet, M.J. Solvatochromic comparison method .3. Hydrogen-bonding by some 2-nitroaniline derivatives. *J. Am. Chem. Soc*. **1976**, *98* (11), 3233-3237.
19. Kamlet M.J.; Abboud, J.L.; Taft, R.W. Solvatochromic Comparison Method .6. Pi-Star Scale Of Solvent Polarities. *J. Am. Chem. Soc*. **1977**, *99* (18), 6027-6038.
20. Tan, L.C.; Carr, P.W.; Abraham, M.H. Study of retention in reversed-phase liquid chromatography using linear solvation energy relationships .1. The stationary phase. *J. Chrom. A.* **1996**, 752 (1-2), 1-18.
21. Yang, S.Y.; Khaledi, M.G. chemical selectivity in micellar electrokinetic chromatography - characterization of solute micelle interactions for classification of surfactants. Anal. Chem. 1995, 67 (3), 499-510.
22. Yang, S.Y.; Bumgarner, J.G.; Kruk, L.F.R.; Khaledi, M.G. Quantitative structure-activity relationships studies with micellar electrokinetic chromatography – Influence of surfactant type and mixed micelles on estimation of hydrophobicity and bioavailability. *J. Chrom. A.* **1996**, *721* (2), 323-335.
23. Khaledi, M.G.; Bumgarner, J.G.; Hadjmohammadi, M. Characterization of mixed micellar pseudostationary phases in electrokinetic chromatography using linear solvation energy relationships. *J. Chrom. A.* **1998**, *802* (1), 35-47.
24. Muijselaar, P.G.; Claessens, H.A.; Cramers, C.A. Characterization of pseudostationary phases in micellar electrokinetic chromatography by applying linear solvation energy relationships and retention indexes. *Anal. Chem.* **1997**, *69* (6), 1184-1191.
25. Shi, W.; Zhang, J.; Wang, L.; Zou, H.F.; Zhang, Y.K. Effect of organic modifiers on the capacity factor in micellar electrokinetic chromatography. *Chin. J. Chem.* **1997**. *15* (2), 144-153.
26. Liu, Z. Zou, H.F.; Ye, M.L.; Ni, J.Y.; Zhang, Y.K. Effects of organic modifiers on retention mechanism and selectivity in micellar electrokinetic capillary chromatography studied by linear solvation energy relationships. *J. Chrom. A.* **1999**. *863* (1), 69-79.

27. Tellman, K.T.; Palmer, C.P. Polymers of sodium-N-undec-10-ene-1-oyl taurate and sodium-N-undec-10-ene-1-oyl aminoethyl-2-phosphate as pseudostationary phases for electrokinetic chromatography. *Electrophoresis.* **1999**, *20* (1), 152-161.
28. Fujimoto, C. Application of linear solvation energy relationships to polymeric pseudostationary phases in micellar electrokinetic chromatography. *Electrophoresis*. **2001**, *22* (7), 1322-1329.
29. Shi, W.; Peterson, D.S.; Palmer, C.P. Effect of pendant chain lengths and backbone functionalities on the chemical selectivity of sulfonated amphiphilic copolymers as pseudo-stationary phases in electrokinetic chromatography. *J. Chrom. A.* **2001**, *924* (1-2), 123-135.
30. Shi, W.; Palmer, C.P. Effect of pendent group structures on the chemical selectivity and performance of sulfonated copolymers as novel pseudophases in electrokinetic chromatography. *Electrophoresis*. **2002**, *23* (9), 1285-1295.
31. Akbay, C.; Shamsi, S.A. Polymeric sulfated surfactants with varied hydrocarbon tail: II. Chemical selectivity in micellar electrokinetic chromatography using linear solvation energy relationships study. *Electrophoresis.* **2003**, *25* (4-5), 635-644.
32. Tanford, C. The Hydrophobic Effect: Formation of Micelles and Biological Membranes; John Wiley and Sons: New York, 1973.
33. Pauletti, G.M.; Wunderli-Allenspach, H.; Partition coefficients in vitro: artificial membranes as a standardized distribution model. *Eur. J. Pharm. Sci.* **1994**, *1* (5), 273-282.
34. Zhang, F.; Rowe, E.S.; Titration Calorimetric and Differential Scanning Calorimetric Studies of the Interactions of n-Butanol with Several Phases of Dipalmitoylphosphatidylcholine. *Biochemistry*. **1992**, *31*, 2005-2011.
35. Rowe, E.S.; Zhang, F.; Leung, T.W.; Parr, J.S.; Guy, P.T.; Thermodynamics of Membrane Partitioning for a Series of n-Alcohols Determined by Titration Calorimetry: Role of Hydrophobic Effects. *Biochemistry*. **1998**, *37*, 2430-2440.
36. Pola, A.; Michalak, K.; Burliga, A.; Motohashi, N.; Kawase, M.; Determination of lipid bilayer/water partition coefficient of new phenothiazines using the second derivative of absorption spectra method. *Eur. J. Pharm. Sci.* **2004**, *21* (4), 421-427.
37. Gabriel, N.E.; Roberts, M.F. Spontaneous Formation of Unilamellar Vesicles. *Biochemistry.* **1984**, *23*, 4011-4015.
38. Gabriel, N.E.; Roberts, M.F. Interaction of Short-Chain Lecithin with Long-Chain Phospholipids: Characterization of Vesicles That Form Spontaneously. *Biochemistry.***1986**, *25*, 2812-2821.
39. Flynn, GL Physicochemical determinants of skin absorption. In *Principles of Route-to-Route Extrapolation for Risk Assessment*; Edited by T.R. Garrity and C.J. Henry, Elsevier: New York. 1990; 93-127.
40. Potts, R.O.; Guy, R. Predicting Skin Permeability. *Pharm. Res.* **1992**, *9*, 663-669.

41. Ren, S.; Das, A.; Lien, E.J. QSAR Analysis of Membrane Permeability to Organic Compounds. *J. Drug. Target.* **1996**, *4* (1), 103-107.

42. Martinez-Pla, J.J.; Martin-Biosca, Y.; Sagrado, S.; Villaneuva-Camanas, R.W.; Medina-Hernandez, M.J. Biopartitioning micellar chromatography to predict skin permeability. *Biomed. Chrom.* **2003,** *17*, 530-537.

Chapter 2

Experimental

Chemicals

1,2-Dihexanoyl-sn-Glycero-3-Phosphocholine (DHPC, 6:0), 1,2-Dipalmitoyl-*sn*-Glycero-3-[Phospho-*rac*-(1-glycerol)] (Sodium Salt) (DPPG, 16:0), 1,2-Dipalmitoyl-*sn*-Glycero-3-Phosphocholine (DPPC, 16:0), (2S,3R,4E)-2-acylaminooctadec-4-ene-3-hydroxy-1-Phosphocholine (Chicken Egg Sphingomyelin), 1,2-Dipalmitoyl-*sn*-Glycero-3-Phosphoethanolamine (DPPE, 16:0), 1,2-Dipalmitoyl-*sn*-Glycero-3-[Phospho-L-Serine] (Sodium Salt) (DPPS, 16:0), L-a-Phosphatidylinositol (Soybean PI), and cholesterol were all purchased from Avanti Polar Lipids, Inc. (Alabaster, Alabama). Structures of these lipids are included in **Appendix A-1**. Chloroform, methanol, and sodium hydroxide (NaOH) were purchased from Fisher Scientific (Fair Lawn, New Jersey). 4-(2-Hydroxyethyl)-1-piperazineethanesulfonic acid (HEPES Acid), 4-(2-Hydroxyethyl)-1-piperazineethanesulfonic acid, sodium salt (HEPES base), 2-(4-Morpholino)ethanesulfonic acid (MES acid), and 2-(4-Morpholino)ethanesulfonic acid, sodium salt (MES base) were purchased from Sigma Chemical Co. (St. Louis, Mo.). All aromatic solutes and neutral drugs were purchased from Aldrich (Milwaukee, Wi.). Structures, Abraham LSER descriptors, and properties of these solutes are included in **Appendix A-2**. Deionized water was obtained from a Milli-Q filtration system rated at 16 MΩ.

Preparation of Liposomes by Extrusion

Calculated amounts of the relevant lipids and cholesterol were weighed and transferred to an appropriate round-bottomed flask. The lipids were then completely dissolved in chloroform. After thorough mixing, chloroform was removed using rotary evaporation at 80 ^{o}C. The remaining lipid film was then rehydrated using buffer. This rehydration step was completed by mixing the solution using a vortexer and gently sonicating the solution using a bath sonicator. Complete rehydration of the dried lipids yields a milky solution of MLVs that is not optically clear. Finally, the solution was extruded using a LIPEX^{TM} thermobarrel extruder. This process involves repeatedly forcing the lipid solution through Nucleopore membrane filters (Whatman) using high-pressure nitrogen gas; the lipid solution was forced through 200 nm, 100 nm, and 50 nm filters eight times a piece. The extruder was maintained at 50 ^{o}C using a circulating water bath. This process yields an optically clear yet opalescent solution with a bluish tint.

Preparation of Liposomes by Probe Sonication

A milky solution of MLVs was prepared as described above. The solution was then sonicated using a Sonicator XL Ultrasonic Processor (Misonix). During sonication, the solution was maintained at 70 ^{o}C using a water bath heated in a 200 mL jacketed beaker (Ace Glass Co.) with an Model MT circulating oil bath (MGW Lauda). Lipid solutions were sonicated using an intermittent cycle of 3 seconds of sonication followed by a 2 second pause for a total on-time of 30 minutes (i.e, the entire program consisted of 600 3·second cycles of sonication followed immediately by a 2·second pause). This program is required because the sonication process can be vigorous enough to disrupt vesicle formation if pauses are not included. After sonication, the solution was nearly transparent with a slight bluish tint.

Preparation of Spontaneous Short-Chain/Long-Chain Liposomes

DPPG, DPPC, and DHPC were dissolved in chloroform and mixed as above. The chloroform was then removed using rotary evaporation at 80 ^{o}C. The remaining lipid film was then rehydrated in 25 mM HEPES buffer, pH=7.5. This rehydration step was completed by mixing the solution using a vortexer and gently sonicating the solution using a bath sonicator. Complete rehydration of the dried lipids yields an optically clear solution. By visual inspection, optical clarity of these liposome solutions increased with increasing composition of DHPC.

Dynamic Light Scattering

Sizing of lipid aggregates by dynamic light scattering was performed using a Zetasizer 1000 HAS (Malvern) particle sizer. Solutions were contained in disposable microcuvettes for the experiments. All experiments were performed at 36 ^{o}C. Data was acquired using PCS for Windows (Malvern) installed on a Dimension XPS P90 personal computer (Dell).

The dynamic light scattering instrument used in this study uses photon correlation to measure the frequency distribution of light scattered by particles in solution. Fluctuations in the time-resolved scattered light intensity occur due to Brownian motion. The time-resolved scattered light intensity is fit to an auto-correlation function from which the translational diffusion coefficient of the aggregate may be determined. The radius, and therefore the diameter, of spherical particles may be determined using the Stokes-Einstein relation:

$$D = \frac{k_B T}{6\pi\eta r} \qquad \textbf{Equation 2.1}$$

where k_B is Boltzmann's constant, T is the temperature, η is the viscosity of the solution, and r is the radius of the aggregate.[1] The results of a dynamic light scattering experiment include the average particle diameter and a polydispersity index. The polydispersity index is essentially a factor describing

the quality of fit of the intensity data to the auto-correlation function. For particles such as vesicles and micelles, it is often difficult to obtain statistically significant polydispersity indices because these particles are relatively polydisperse.[2] Therefore, the polydispersity index was excluded from this study. Instead, the standard deviation of the average diameter was used to evaluate the width of the size distribution.

Sample Preparation

Stock solutions of solid solutes were prepared by dissolving the solids in filtered methanol at a concentration of approximately 10 mg/mL. Some solid drug stock solutions were prepared differently in order to maximize solubility. Caffeine and tolnaftate were dissolved in 75% methanol/25% chloroform (v/v). Prednisone was dissolved in 75% methanol/25% acetone (v/v). Sample solutions were prepared by diluting approximately 10 µL of a stock solution and/or 1-10 µL of undiluted liquid solutes and 8 µL of octanophenone in 2 mL of filtered methanol. Each sample solution contained 3-5 solutes in order to minimize the number of experiments needed to generate data for the solute set. Stock solutions and sample solutions were prepared and stored in amber vials to minimize degradation of light-sensitive solutes. Additionally, stock solutions and sample solutions were stored at 4 ^{o}C when not in use.

Electrokinetic Chromatography

All EKC experiments were performed on a home-built instrument contained in a Plexiglass interlock box built by the North Carolina State University Department of Chemistry's Electronics Shop to minimize to hazard of electrical shock. Fused silica capillaries with an outer diameter of 360 µm and an inner diameter of 50 µm (Polymicro Technologies) were used for all experiments. Lipid phase solutions were contained in 5 mL capacity buffer reservoirs (Ace Glass Company). Tygon tubing and assorted fittings were plumbed in line with two 200 mL jacketed beakers (Ace Glass Company) and a Model 900 Isotemp Refridgerated Circulator (Fisher Scientific) to allow the immersion of the capillary in circulating and thermostatted light mineral oil (Fisher Scientific) to maintain the temperature of the capillary at a constant temperature. Buffer reservoirs were immersed in jacketed beakers containing water maintained at a constant temperature by the same circulating oil bath. The temperature of the lipid phase in the buffer reservoir was measured using a Fisher Scientific Digital Thermometer (Fisher Scientific). The temperature was measured several times over the course of a set of experiments to ensure relatively constant (± 0.2 ^{o}C) temperature. All experiments were performed at 36 ^{o}C unless otherwise noted. Voltage was supplied by a Series EH power supply (Glassman High Voltage). All experiments were performed with the voltage set at 25 kV. UV-Vis detection of solute migration through the detection window was performed using an SSI Model 500 Variable UV/Vis Detector

(Scientific Systems, Inc.) set at 214 nm. An analog-to-digital converter (National Instruments) connected the UV-Vis detector to a Dell OptiPlex GX100 personal computer. Data was collected and analyzed using a CE data acquisition program written in house using the LabView (National Instruments) software package.

Capillaries were prepared by cutting an appropriate length of capillary and burning off a small section of the polyimide coating to serve as a detection window. These experiments were conducted using capillaries with a total length (L_t) of 57 cm and a separation length (L_d) of 44 cm. Capillaries were then installed on the instrument, ensuring that the injection window was properly aligned in the UV-Vis detector. Before the first injection every day, capillaries were rinsed for 20 minutes each with methanol, water, 1 M sodium hydroxide, and the applicable lipid solution to ensure reproducible data. All sample solutions were prepared by dissolving solutes in methanol. Sample solutions were hydrodynamically injected for approximately three seconds. All samples were injected in triplicate.

Calculation of Retention Factors for Neutral Solutes

Retention factors for all neutral solutes were calculated using **Equation 2.2**:

$$k = \frac{t_r - t_{eo}}{t_{eo}\left[1 - \frac{t_r}{t_{lip}}\right]} \qquad \textbf{Equation 2.2}$$

Where t_r represents the migration time of the solute or marker (minutes), t_{eo} represents the migration time of the unretained EOF marker (minutes), and t_{lip} is the migration time of the hydrophobic marker. Please see **Chapter 1** for a full derivation of **Equation 2.2**.

Capillary Zone Electrophoresis of Ionizable Solutes

Capillary zone electrophoresis experiments were necessary to determine the electrophoretic mobility of some solutes that were determined to possibly be partially ionized at the buffer conditions used. All CZE experiments were conducted on the same instrument as the EKC experiments above with very similar experimental conditions. CZE experiments were performed using both 25 mM MES, pH=6.0 and 25 mM HEPES, pH=7.5. All samples were injected in triplicate.

Calculation of Retention Factors for Ionizable Solutes

Retention factors for ionizable solutes were calculated from the apparent mobility of the solute determined using an EKC system (μ), the apparent mobility of the solute while distributed to the lipid

phase (μ_{lip}), and the apparent mobility of the solute while distributed to the aqueous phase (μ_0) using **Equation 2.3**:

$$k = \frac{\mu - \mu_0}{\mu_{lip} - \mu} \quad \textbf{Equation 2.3}$$

μ was determined from the migration time of the solute determined using the EKC system, μ_{lip} was determined using the migration time of the hydrophobic lipid phase marker, and μ_0 was determined using CZE experiments described above. Please see **Chapter 1** for a full derivation of **Equation 2.3**.

Determination of Linear Solvation Energy Relationships Models

The LSER model used to describe retention in this study is:

$$\log k = vV + bB + aA + sS + eE + C \quad \textbf{Equation 2.4}$$

where lower case coefficients describe pseudostationary phase properties and upper case descriptors describe solute properties. Please see **Chapter 1** for a discussion of the interactions described by each of these descriptors. LSER models were determined for different EKC pseudostationary phases in this study using a multilinear regression of retention factors (expressed log k) and known solute descriptors from the literature.

Prediction of Retention Factors Using Linear Solvation Energy Relationships Models

Using LSER system coefficients determined using a training set of representative solutes as described above, retention factors may be predicted for solutes with known LSER solute descriptors without actually performing experiments using **Equation 2.4** above. This approach is very useful for compounds that are impossible to detect using a UV detector and very harzardous compounds.

Works Cited

1. *Photon Correlation Spectroscopy Size Theory*. Malvern Instruments.
2. Ford, N.C. Light Scattering Apparatus. In *Dynamic Light Scattering*; Pecora, R., Ed.; Plenum Press: New York, 1985; 7-58.

Chapter 3

General Applications of Linear Solvation Energy Relationships Models to Liposome/Water Partitioning Determined By Electrokinetic Chromatography

Abstract

In this two-part investigation, Linear Solvation Energy Relationship (LSER) models were applied to liposome/water partitioning data determined by liposome electrokinetic chromatography (LEKC). In the first part of the study, LEKC retention factors were determined for a set of 71 solutes including 50 neutral aromatic solutes and 21 neutral drugs using the liposome phases mM $DPPG_{20}DPPC_{80}$, 15 mM $DPPG_{20}DPPC_{80}$/3 mM cholesterol, and 15 mM $DPPG_{20}DPPC_{80}$/6 mM cholesterol. These retention factors were used to determine linear solvation energy relationships (LSER) models for each of the three lipid phases for the set of 50 neutral aromatic solutes and the entire set of 71 solutes. The predictive ability of the LSER model was tested by using the model generated for the set of 50 neutral aromatic solutes to predict retention factors for the 21 neutral drugs. The descriptive ability of the LSER model was tested and used to examine the interactions that control liposome/water partitioning for the set of 50 neutral aromatic solutes and the set of 71 solutes including 21 neutral drugs. In the second part of the study, two liposome electrokinetic chromatography (LEKC) lipid phases were introduced that approximate the lipid composition of the cell membrane of monkey intestinal epithelial cells. 15 mM $PI_{10}DPPS_{10}DPPC_{30}DPPE_{30}SPM_{20}$/9.75 mM cholesterol most nearly approximates the lipid composition of the cell membrane of monkey intestinal epithelial cells. 15 mM $DPPG_{20}DPPC_{80}$/9.75 mM cholesterol replaces the specific lipids contained in the monkey intestinal epithelial cell membranes with the zwitterioninc lipid DPPC and DPPG. The retention factors determined for a set of 50 neutral aromatic solutes using these two LEKC phases are highly correlated (r^2=0.99), with a slope near unity (m=0.91) and an intercept near zero (b=0.05). The normalized LSER system coefficients for these lipid phases are also very similar. The LSER system coefficients determined for 15 mM $PI_{10}DPPS_{10}DPPC_{30}DPPE_{30}SPM_{20}$/9.75 mM cholesterol and 15 mM $DPPG_{20}DPPC_{80}$/9.75 mM cholesterol were compared with an LSER model generated by Abraham, et al. for human intestinal absorption.

Introduction

Linear solvation energy relationships were first used by Kamlet and Taft to model various solvation systems.[1-4] This model was then revised by Abraham et al. to better describe selectivity chromatographic systems.[5] The LSER model has been extensively used by Khaledi et al. to characterize selectivity of micellar,[6-13] vesicular,[14-16] and lipid-based pseudostationary phases in electrokinetic chromatography systems.[17,18] Other groups have used the LSER model to characterize various micellar pseudostationary phases,[19] the effect of organic modifiers in MEKC,[20,21] and polymeric micellar pseudostationary phases.[22-26] Like any model, the LSER model can serve the dual purposes of description and prediction of solvation effects. First of all, when log k values are experimentally determined for a set of solutes with known descriptor values, system coefficients can be determined and used to characterize solvation effects of the given system. Also, known solute descriptors and system coefficients can be used to predict log k values for solutes without running additional experiments.

In the first part of the present study, both capabilities of the LSER model were tested. Retention factors were determined for a solute set comprised of 50 neutral aromatic solutes and 21 neutral drugs using three different liposome phases. LSER solute descriptors were available in the literature for the entire 71 solute set. The literature descriptors for the neutral aromatic solutes were determined experimentally[27] and the literature descriptors for the neutral drugs were calculated using the ABSOLV software.[28] The predictive ability of the LSER model was tested by determining an LSER model using LEKC retention factors for the set of 50 neutral aromatic solutes and predicting LEKC retention factors for the set of 21 neutral drugs. The predicted retention factors were then compared with experimental retention factors. LSER models were also determined for the entire 71 solute set. The LSER models determined using both solute sets were compared to elucidate the interactions responsible for liposome/water partitioning.

In the second part of the current study, two new biomimetic LEKC phases are introduced. The lipid composition of monkey intestinal epithelial membranes is 10% phosphatidylinositol, 10% phosphatidylserine, 30% phosphatidylcholine, 20% sphingomyelin, and 30% phosphatidylethanolamine with a lipid/cholesterol ratio of 0.65.[29] To approximate this lipid composition, liposomes were prepared with the composition 15 mM $PI_{10}DPPS_{10}DPPC_{30}DPPE_{30}SPM_{20}$/9.75 mM cholesterol. It should be noted that the PI and SPM used in these lipid mixtures were natural lipids and therefore contained a distribution of fatty acid chain lengths and saturation/unsaturations. DPPS, DPPC, and DPPE were synthetic 16:0 lipids. Natural cell membranes, including the monkey intestinal epithelial membranes approximated by these liposomes

also contain a distribution of fatty acid chain lengths and saturation/unsaturations. 15 mM $DPPG_{20}DPPC_{80}$/9.75 mM was a simpler lipid phase with the specific lipids used to approximate the intestinal epithelial membrane lipid structure replaced with a representative anionic lipid (DPPG) and a representative zwitterionic lipid (DPPC). LEKC retention factors were determined for a set of 50 neutral aromatic solutes using 15 mM $PI_{10}DPPS_{10}DPPC_{30}DPPE_{30}SPM_{20}$/9.75 mM and 15 mM $DPPG_{20}DPPC_{80}$/9.75 mM. These retention factors were used to determine linear solvation energy relationships (LSER) models to describe the interactions responsible for selectivity in these two LEKC phases. The LSER models and retention factors for these two lipid phases were first compared with each other and then compared with an LSER model for human intestinal absorption determined by Abraham, et al. using a set of 169 drugs.[30]

Experimental

Refer to **Chapter 2** for experimental procedures and details concerning chemicals, liposome and vesicle preparation, dynamic light scattering, sample preparation, electrokinetic chromatography, calculation of retention factors, and determination of linear solvation energy relationships (LSER) models.

Determination of Ionization of Neutral Drugs

The ionization of each of the drugs at the experimental pH was determined in order to verify that none of the drugs would have any ionization or electrophoretic mobility at the experimental conditions.

pK_a values for neutral drugs were obtained from a literature search and are included in **Appendix A-2**. From these pK_a values, the theoretical fraction ionized and percent ionized for each drug at pH=7.5 was calculated.

For acidic drugs, the fraction ionized was calculated using:

$$\frac{[A^-]}{[HA]} = 10^{pH-pK_a} \qquad \textbf{Equation 3.4}$$

and percent ionized was calculated using:

$$\%ionized = \frac{\frac{[A^-]}{[HA]}}{\frac{[A^-]}{[HA]}+1} \qquad \textbf{Equation 3.5}$$

For basic drugs, the fraction ionized was calculated using:

$$\frac{[BH^+]}{[B]} = 10^{pK_a - pH} \qquad \textbf{Equation 3.6}$$

and percent ionized was calculated using:

$$\%ionized = \frac{\frac{[BH^+]}{[B]}}{\frac{[BH^+]}{[B]} + 1} \qquad \textbf{Equation 3.7}$$

Results and Discussion

Determination of Ionization of Neutral Drugs

Calculated fraction ionized and percent ionized values for weakly acidic and basic neutral drugs at the operating pH are included in **Table 3.1**. All of these drugs are between 0.61% - 0.000013% ionized at pH=7.5. Therefore, they are all very weakly acidic or basic and not significantly ionized at the experimental pH.

Cross-correlation of LSER solute descriptors

In any model, unintentionally correlated descriptors can at least bias and significantly limit its predictive or descriptive abilities of the model.[31] Trone and Khaledi showed that a set of 36 neutral aromatic solutes with experimentally determined LSER descriptors did not show significant cross-correlation.[32]

Cross-correlation matrices for the set of 50 neutral aromatic solutes, 21 neutral drugs, and the combined set of 71 solutes used in the present study are included in **Tables 3.2**, **3.3**, and **3.4**.

For the set of 50 neutral aromatic solutes that are described by the cross-correlation matrix in **Table 3.2**, the R^2 values are relatively similar to those presented for the 36 solute set studied by Trone and Khaledi.[32] For the set of 21 neutral drugs and the combined set of 71 described by the cross-correlation matrices in **Tables 3.3** and **3.4,** the R^2 values are significantly higher which is indicative of higher cross correlation between these descriptors. From these matrices, the V descriptor is significantly correlated with the E, S, and B descriptors. Additionally, the S descriptor is significantly correlated with the E and B descriptors and the B descriptor is significantly correlated with the E descriptor. From these observations, there is apparently some inter-relationship between the

molecular volume and excess molar refraction, dipolarity/polarizability, and solute basicity; dipolarity/polarizability and excess molar refraction and solute basicity; and solute basicity and excess molar refraction. The cause of this error is likely the uncertainties in the additivity approach that was used to calculate LSER solute descriptors for the neutral drugs.

Determination of Retention Factors and Linear Solvation Energy Relationships Models

LEKC retention factors were determined for the set of 50 neutral aromatic solutes using 15 mM $DPPG_{20}DPPC_{80}$, 15 mM $DPPG_{20}DPPC_{80}$/3 mM cholesterol, 15 mM $DPPG_{20}DPPC_{80}$/6 mM cholesterol, 15 mM $DPPG_{20}DPPC_{80}$/9.75 mM cholesterol and 15 mM $PI_{10}DPPS_{10}DPPC_{30}DPPE_{30}SPM_{20}$/9.75 mM cholesterol. These retention factors are summarized in **Table 3.5**. LSER models were generated using these LEKC retention factors as a training set for each of these lipid phases as well. These models are summarized in **Table 3.6**.

Retention factors were determined experimentally for a test set of 21 neutral drugs with published LSER descriptors using 15 mM $DPPG_{20}DPPC_{80}$, 15 mM $DPPG_{20}DPPC_{80}$/3 mM cholesterol, 15 mM $DPPG_{20}DPPC_{80}$/6 mM cholesterol. For 15 mM $DPPG_{20}DPPC_{80}$, bifonazole, clotrimazole, diethylstilbestrol, and tolnaftate coeluted with the hydrophobic t_{mc} marker and therefore retention factors for those drugs could not be calculated. Likewise, tolnaftate coeluted with the hydrophobic t_{mc} marker for 15 mM $DPPG_{20}DPPC_{80}$/3 mM cholesterol as well. Experimental retention factors for the set of 21 neutral drugs are determined using 15 mM $DPPG_{20}DPPC_{80}$, 15 mM $DPPG_{20}DPPC_{80}$/3 mM cholesterol, and 15 mM $DPPG_{20}DPPC_{80}$/6 mM cholesterol are summarized in **Table 3.7**.

Finally, in addition to the LSER models generated using a training set of 50 neutral aromatic solutes, LSER models were also generated for 15 mM $DPPG_{20}DPPC_{80}$, 15 mM $DPPG_{20}DPPC_{80}$/3 mM cholesterol, and 15 mM $DPPG_{20}DPPC_{80}$/6 mM using LEKC retention factors for a training set of 71 neutral solutes representing 50 neutral aromatic solutes and 21 neutral drugs. These models are also summarized in **Table 3.6.**

Prediction of Liposome Electrokinetic Chromatography Retention Factors for Neutral Drugs Using Linear Solvation Energy Relationships

In order to evaluate the predictive ability of the LSER model using the set of 50 neutral aromatic solutes as a training set, retention factors were predicted for 15 mM $DPPG_{20}DPPC_{80}$, 15 mM $DPPG_{20}DPPC_{80}$/3 mM cholesterol, 15 mM $DPPG_{20}DPPC_{80}$/6 mM cholesterol for the test set of 21 neutral drugs with published LSER solute descriptors. Predicted retention factors are included in

Table 3.7. These values were then compared with the experimental retention factors determined for the neutral drugs as described above.

A scatter plots of predicted retention factors as a function of experimental retention factors for 15 mM $DPPG_{20}DPPC_{80}$ is included as **Figures 3.1**. The statistics of correlation between predicted and experimental retention factors are included in **Table 3.8**. The absolute difference between the experimental retention factors and the predicted values vary widely for the different neutral drugs. For example, the predicted and experimental retention factors for 3-bromoquinoline using 15 mM $DPPG_{20}DPPC_{80}$ differ by approximately 0.02 units. At the other extreme, the predicted and experimental retention factors for chloramphenicol using 15 mM $DPPG_{20}DPPC_{80}$ differ by approximately 1.67 units. The large differences between the experimental and predicted values is likely caused by the relatively high cross-correlation between the LSER solute descriptors calculated for the neutral drugs and/or flaws in the additivity algorithm used to calculate the LSER solute descriptors for the neutral drugs. In order to improve the predictive ability of the LSER model for neutral drugs, it may be necessary to revise the algorithm for calculationg the solute descriptors or to experimentally determine the solute descriptors for the neutral drugs. Also, the LSER solute descriptors calculated for the neutral drugs represent a much wider range of absolute values than those determined for the neutral aromatic solutes. While the set of 50 neutral aromatic compounds is comprised of a variety of compounds, a larger training set with more compound variability would likely provide somewhat improved predictive abilities.

Comparison of Linear Solvation Energy Relationships Model for Neutral Aromatic Solutes and Neutral Drugs

Similar general trends are found in all LSER models for liposome electrokinetic chromatography. All of the models contain relatively large and negative b coefficients and relatively large and positive v coefficients. The b coefficient describes the hydrogen bond donor ability of the liposome phase relative to the aqueous phase. Because this coefficient is large and negative, the liposome phase is generally a very weak hydrogen bond donor relative to the aqueous phase. Therefore, solutes that are strong hydrogen bond acceptors will be distributed preferentially to the aqueous phase compared to analogous solutes that are weak hydrogen bond donors; the solute hydrogen bond acceptor/aqueous phase hydrogen bond donor interaction is unfavorable to liposome/water partitioning. The v coefficient describes the cohesiveness of the liposome phase relative to the aqueous phase. The v coefficient is large and positive; therefore liposome phase is less cohesive and more “hydrocarbon-like” relative to the aqueous phase. This coefficient is generally used to describe the hydrophobic effect that favors distribution of hydrophobic solutes to a “hydrocarbon-like” phase rather than an aqueous phase. Because the b and v coefficients are larger in magnitude than the e, s,

and a coefficients, it may be concluded that the interactions described by the b an v coefficients dominate liposome/water partitioning for these lipid phases. The small negative *s* coefficients indicate that the lipid phase is moderately less dipolar than the bulk aqueous phase. Any dipolarity of the lipid phase is likely caused by polar lipid head groups and hydration of the lipid head group region.[18] The relatively small positive e coefficient is a polarizability correction factor that describes interactions not accounted for by the s coefficient. Finally, the small positive a coefficient indicates that the lipid phase is a moderately better hydrogen bond acceptor relative to the aqueous phase. Similar trends have previously been described for LSER models determined for other net anionic liposome phases[18], dihexadecylhydrogen phosphate (DHP) vesicles[15], and cationic dihexadecyldimethylammonium bromide (DHAB) vesicles.[16]

In order to evaluate the descriptive ability of LSER models, the models generated for the set of neutral aromatic solutes (n=50) were compared to the models generated using the neutral aromatic solutes and the neutral drugs (n=71). Cholesterol effects are apparent in the LSER models for lipid phases with increasing amounts of cholesterol. The main effects of cholesterol on the solvation properties of lipid bilayers, as described by LSER modes are increased cohesiveness and polarizability and decreased hydrogen bond acceptor ability and dipolarity. Please see **Chapter 4** for an in-depth discussion of the cholesterol effects. The addition of the neutral drugs to the LSER training set yields several noticeable effects. The same general trends described above occur in the LSER models generated for the 50 solute training set and the 71 solute training set with the almost insignificant exception that the a coefficient for the LSER model generated using the 71 solute training set is slightly negative. Also, for each of the models, the v coefficient becomes slightly larger in magnitude relative to the b coefficient upon the addition of the drugs to the solute set. This effect may be caused by the generally larger V descriptors of the neutral drugs relative to the neutral aromatic solutes. Because the same general trends are present in the models generated with and without the neutral drugs, the mechanism of liposome/water partitioning should be very similar for the simple neutral aromatic solutes and the more complicated neutral drugs.

In order to elucidate the trends in the LSER models generated with and without neutral drugs, the system coefficients were normalized by calculating the ratio of each system coefficient and the absolute value of the *b* term. These normalized LSER system coefficients are included in **Table 3.8**. The *v/b* term calculated for the models including the neutral drugs is greater than 1.00 because of the increased v coefficients relative to the b coefficients. In general, the same trends are apparent in the normalized and unnormalized models.

The addition of the drugs to the LSER training set adds a significant amount of error to the model generated. The models using the expanded training set have lower adjusted R^2 values and increased

error for the individual coefficients and standard error for the model. Three possible explanations likely explain this error. First, there may be uncertainties in the additivity algorithm used to calculate the solute descriptors for the neutral drugs, as discussed above. A comparison of experimental solute descriptors and solute descriptors calculated using the additivity approach would be helpful to evaluate the problems apparent in these LSER models. Also, the LSER solute descriptors for the training set including the drugs contain higher cross-correlation than the solute descriptors for the smaller training set. These two possible factors may be related; uncertainties in the additivity approach used to calculate these LSER descriptors may contribute to the cross-correlation noted above. Finally, there may be additional factors, such as the shape of a molecule, that influence liposome/water partitioning for the neutral drugs that are not explained by the coefficients of the currently proposed LSER model.

Comparison of 15 mM $DPPG_{20}DPPC_{80}$/9.75 mM cholesterol and 15 mM $PI_{10}DPPS_{10}DPPC_{30}DPPE_{30}SPM_{20}$/9.75 mM cholesterol

From the LSER system coefficients described in **Table 3.6**, the same general LSER trends are observed for both of these lipid phases; the relatively large and negative b coefficients and relatively large and positive v coefficients that are characteristic of most LEKC lipid phases are present here as well.

The magnitudes of the LSER system coefficients are very similar for both of these lipid phases. To facilitate the comparison of the models for these lipid phases, the terms were normalized by calculating the ratio of each system coefficient and the absolute value of the *b* term. These normalized LSER system coefficients are included in **Table 3.8**. Once normalized, the LSER system coefficients for these two lipid phases are nearly identical.

Given the statistical similarity of the LSER models generated for 15 mM $DPPG_{20}DPPC_{80}$/9.75 mM cholesterol and 15 mM $PI_{10}DPPS_{10}DPPC_{30}DPPE_{30}SPM_{20}$/9.75 mM cholesterol, it should be expected that the retention factors determined using each lipid phase should be well-correlated. A scatter plot for the retention factors determined using 15 mM $DPPG_{20}DPPC_{80}$/9.75 mM cholesterol and 15 mM $PI_{10}DPPS_{10}DPPC_{30}DPPE_{30}SPM_{20}$/9.75 mM cholesterol is included as **Figure 3.4**. From this plot, it is possible to see that the retention factors determined for the set of 50 neutral aromatic solutes using the two lipid phases are indeed highly correlated (r^2=0.99), with a slope near unity (m=0.91) and an intercept near zero (b=0.05).

Comparison of LSER models for LEKC Using Biomimetic Lipid Phases and Human Intestinal Absorption

Abraham et al. has determined an LSER model for human intestinal absorption using a set of 169 drugs that represents a wide variety of drug structures, bioavailability, ionization at physiological pH and pharmaceutical uses.[30] This model is summarized in **Table 3.6**.

It should be noted that this LSER model for human intestinal absorption was determined using drugs with LSER descriptors calculated using an additivity approach exclusively. Therefore, the errors and limitations that were noted in the LSER models for determined using the neutral drugs above apply to this model as well. In general, the range of the system coefficients determined for the LSER model of human intestinal absorption is much larger in magnitude than those of the LSER models determined for electrokinetic chromatography because the models are based on a percent value rather than a logarithmic value. The calculated LSER solute descriptors used to generate the model for intestinal absorption are much larger in magnitude than the experimental LSER solute descriptors for the neutral aromatic solutes used to generate the models for electrokinetic chromatography. Also, the human intestinal absorption data (expressed as % of drug absorbed) is much larger in magnitude than the retention factors used to determine the LSER models for the electrokinetic chromatography systems. This discrepancy likely explains the differences in the magnitudes of the system coefficients as well. For this reason, these LSER models may be judiciously compared in order to note general trends, but the inherent differences in the models may preclude in-depth analysis.

The Abraham LSER model for human intestinal absorption contains an additional solute descriptor, i, that is an indicator variable for strong acid drugs (pK_a<4.5) and strong base drugs (pK_a>8.5). For this model, i is assumed to be 1 for strong acids and strong bases and zero for all other compounds. The Abraham LSER model for human intestinal absorption is dominated by a large and negative b coefficient similar to the models for the biomimetic LEKC phases. Therefore, the hydrogen bonding interaction between a hydrogen bond accepting solute and the aqueous phase is unfavorable to both partitioning in an LEKC system and intestinal absorption. The a coefficient for the Abraham LSER model for human intestinal absorption is negative and of similar magnitude to the b coefficient. The hydrogen bonding interaction between a hydrogen bond donating drug and the aqueous phase is almost as unfavorable to intestinal absorption as the interaction described by the b coefficient. This observation is very different from the model for the biomimetic LEKC phases, where the a coefficient is statistically nearly zero. The v coefficients for the LSER models for the biomimetic LEKC phases and the Abraham LSER model for human intestinal absorption are positive and relatively large in magnitude. Therefore, the hydrophobic interactions described above favor human intestinal absorption. Similar to the LSER models for the biomimetic LEKC phases, the Abraham LSER model for human intestinal absorption contains e and s coefficients that are relatively small in magnitude. Like the LSER models for the biomimetic LEKC phases, the *e* coefficient for the Abraham LSER

model for human intestinal absorption is positive. In contrast to the LSER models for the biomimetic LSER phases, the e coefficient for the Abraham LSER model for human intestinal absorption is positive.

Conclusions

In conclusion, the current study tests the dual capabilities of the linear solvation energy relationships (LSER) model as applied to liposome/water partitioning studies conducted using liposome electrokinetic chromatography (LEKC). LEKC retention factors were determined for a set of 71 solutes including 50 neutral aromatic solutes and 21 neutral drugs using the liposome phases mM $DPPG_{20}DPPC_{80}$, 15 mM $DPPG_{20}DPPC_{80}$/3 mM cholesterol, and 15 mM $DPPG_{20}DPPC_{80}$/6 mM cholesterol. These retention factors are directly proportional to the liposome/water partition coefficient as described above. The predictive and descriptive abilities of the LSER model was tested using neutral aromatic solutes and neutral drugs. LSER models determined using neutral aromatic solutes were shown to have very poor predictive ability for neutral drugs. Addition of neutral drugs to the solute set was shown to decrease the descriptive ability of the LSER model by causing higher errors. Finally, two different lipid phases that approximate the composition of monket intestinal epitihelial cells were studied using LSER models. Both lipid phases were shown to display very similar retention properties. The LSER models determined for these two lipid phases were significantly different from an LSER model determined for intestinal absorption data.

Works Cited

1. Kamlet, M.J.; Taft, R.W. The solvatochromic comparison method. I. The .beta.-scale of solvent hydrogen-bond acceptor (HBA) basicities. *J. Am. Chem. Soc*. **1976**, *98* (2), 377-383.
2. Taft, R.W.; Kamlet, M.J. The solvatochromic comparison method. 2. The .alpha.-scale of solvent hydrogen-bond donor (HBD) acidities. *J. Am. Chem. Soc*. **1976**, *98* (10), 2886-2894.
3. Yokoyama T.; Taft, R.W.; Kamlet, M.J. Solvatochromic comparison method .3. Hydrogen-bonding by some 2-nitroaniline derivatives. *J. Am. Chem. Soc*. **1976**, *98* (11), 3233-3237.
4. Kamlet M.J.; Abboud, J.L.; Taft, R.W. Solvatochromic Comparison Method .6. Pi-Star Scale Of Solvent Polarities. *J. Am. Chem. Soc*. **1977**, *99* (18), 6027-6038.
5. Tan, L.C.; Carr, P.W.; Abraham, M.H. Study of retention in reversed-phase liquid chromatography using linear solvation energy relationships .1. The stationary phase. *J. Chrom. A.* **1996**, 752 (1-2), 1-18.
6. Yang, S.Y.; Khaledi, M.G. chemical selectivity in micellar electrokinetic chromatography - characterization of solute micelle interactions for classification of surfactants. Anal. Chem. 1995, 67 (3), 499-510.
7. Yang, S.Y.; Bumgarner, J.G.; Kruk, L.F.R.; Khaledi, M.G. Quantitative structure-activity relationships studies with micellar electrokinetic chromatography – Influence of surfactant type and mixed micelles on estimation of hydrophobicity and bioavailability. *J. Chrom. A.* **1996**, *721* (2), 323-335.
8. Khaledi, M.G.; Bumgarner, J.G.; Hadjmohammadi, M. Characterization of mixed micellar pseudostationary phases in electrokinetic chromatography using linear solvation energy relationships. *J. Chrom. A.* **1998**, *802* (1), 35-47.
9. Trone, M.D.; Khaledi, M.G. Characterization of chemical selectivity in micellar electrokinetic chromatography. 4. Effect of surfactant headgroup. *Anal. Chem*. **1999**, *71* (7), 1270-1277.
10. Trone, M.D.; Leonard, M.S.; Khaledi, M.G. Congeneric behavior in estimations of octanol-water partition coefficients by micellar electrokinetic chromatography. *Anal. Chem*. **2000**, *72* (6), 1228-1235.
11. Trone, M.D.; Khaledi, M.G. Influence of ester and amide-containing surfactant headgroups on selectivity in micellar electrokinetic chromatography. *Electrophoresis*. **2000**, *21* (12), 2390-2396.
12. Trone, M.D.; Mack, J.P.; Goodell, H.P. Characterization of chemical selectivity in micellar electrokinetic chromatography VI. Effects of surfactant counter-ion. *J. Chrom. A*. **2000**, *888* (1-2), 229-240.
13. Trone, M.D.; Khaledi, M.G. Characterization of chemical selectivity in micellar electrokinetic chromatography: V. The effect of the surfactant hydrophobic chain. *J. Micro. Sep*. **2000**, *12* (8), 433-441.

14. Agbodjan, A.A.; Bui, H.; Khaledi, M.G. Study of solute partitioning in biomembrane-mimetic pseudophases by electrokinetic chromatography: Dihexadecyl phosphate small unilamellar vesicles. *Langmuir*. **2001**, *17* (10), 2893-2899.
15. Bui, H.H.; Khaledi, M.G. Determination of vesicle-water partition coefficients by electrokinetic chromatography: Study of temperature effect. *J. Colloid. Ineterf. Sci.* **2002**, *253* (2), 397-401.
16. Agbodjan, A.A.; Khaledi, M.G. Study of solute partitioning into cationic vesicles of dihexadecyldimethylammonium bromide using electrokinetic chromatography. *J. Chrom. A*. **2003**, *1004* (1-2), 145-153.
17. Burns, S.T.; Khaledi, M.G. Rapid determination of liposome-water partition coefficients (K-lw) using liposome electrokinetic chromatography (LEKC). *J. Pharm. Sci*. **2002**, *91* (7), 1601-1612.
18. Burns, S.T.; Agbodjan, A.A.; Khaledi, M.G. Characterization of solvation properties of lipid bilayer membranes in liposome electrokinetic chromatography. *J. Chrom. A*. **2002**, *973* (1-2), 167-176.
19. Muijselaar, P.G.; Claessens, H.A.; Cramers, C.A. Characterization of pseudostationary phases in micellar electrokinetic chromatography by applying linear solvation energy relationships and retention indexes. *Anal. Chem.* **1997**, *69* (6), 1184-1191.
20. Shi, W.; Zhang, J.; Wang, L.; Zou, H.F.; Zhang, Y.K. Effect of organic modifiers on the capacity factor in micellar electrokinetic chromatography. *Chin. J. Chem.* **1997**. *15* (2), 144-153.
21. Liu, Z. Zou, H.F.; Ye, M.L.; Ni, J.Y.; Zhang, Y.K. Effects of organic modifiers on retention mechanism and selectivity in micellar electrokinetic capillary chromatography studied by linear solvation energy relationships. *J. Chrom. A.* **1999**. *863* (1), 69-79.
22. Tellman, K.T.; Palmer, C.P. Polymers of sodium-N-undec-10-ene-1-oyl taurate and sodium-N-undec-10-ene-1-oyl aminoethyl-2-phosphate as pseudostationary phases for electrokinetic chromatography. *Electrophoresis.* **1999**, *20* (1), 152-161.
23. Fujimoto, C. Application of linear solvation energy relationships to polymeric pseudostationary phases in micellar electrokinetic chromatography. *Electrophoresis*. **2001**, *22* (7), 1322-1329.
24. Shi, W.; Peterson, D.S.; Palmer, C.P. Effect of pendant chain lengths and backbone functionalities on the chemical selectivity of sulfonated amphiphilic copolymers as pseudo-stationary phases in electrokinetic chromatography. *J. Chrom. A.* **2001**, *924* (1-2), 123-135.
25. Shi, W.; Palmer, C.P. Effect of pendent group structures on the chemical selectivity and performance of sulfonated copolymers as novel pseudophases in electrokinetic chromatography. *Electrophoresis*. **2002**, *23* (9), 1285-1295.

26. Akbay, C.; Shamsi, S.A. Polymeric sulfated surfactants with varied hydrocarbon tail: II. Chemical selectivity in micellar electrokinetic chromatography using linear solvation energy relationships study. *Electrophoresis.* **2003**, *25* (4-5), 635-644.
27. Abraham, M.H.; Chadha, H.S.; Whiting,G.S.; Mitchell, R.C. Hydrogen Bonding.32. An analysis of water-octanol and water-alkane partitioning and the delta-log-P parameter of Seiler. *J. Pharm. Sci.* **1994**, *83* (8), 1085-1100.
28. Lombardo, F.; Shalaeva, M.Y.; Tupper, K.A.; Gao, F.; Abraham, M.H.; ElogP$_{oct}$: A Tool for Lipophilicity Determination in Drug Discovery. *J. Med. Chem.* **2000**, *43* (15), 2922-2928.
29. Ibrahim, S.A.; Balasubramanian, K.A.; Lipid-Composition and Membrane Fluidity Of Monkey Small-Intestinal Brush-Border Membrane - Regional Differences. *Indian J. Biochem. Biophys*., **1995,** *32*, 290-294.
30. Zhao, Y. H.; Le, J.; Abraham, M.H.; Hersey, A.; Eddershaw, P.J.; Luscombe, C.N.; Boutina, D.; Beck, G.; Sherborne, B.; Cooper, I.; Platts, J.A.; Evaluation of Human Intestinal Absorption Data and Subsequent Derivation of a Quantitative Structure-Activity Relationship (QSAR) with Abraham Descriptors. *J. Pharm. Sci.* **2001**, *90* (6), 749-784.
31. Poole, C.F.; Poole S.K.; Abraham M.H. Recommendations for the determination of selectivity in micellar electrokinetic chromatography. *J. Chrom. A*. **1998**, *798* (1-2), 207-222.
32. Trone, M.D.; Khaledi, M.G. Statistical evaluation of linear solvation energy relationship models used to characterize chemical selectivity in micellar electrokinetic chromatography. *J. Chrom. A.* **2000**, *886*, 245-257.

Table 3.1 – Calculated fraction ionized and percent ionized for potentially ionized drugs.

"Acidic" Solutes			
Solute Name	**[A-]/[HA] pH=7.5**	**fraction ionized pH=7.5**	**% ionized pH=7.5**
acetominophen	6.17E-03	6.13E-03	6.13E-01
chloramphenicol	2.95E-04	2.95E-04	2.95E-02

"Basic" Solutes			
Solute Name	**[BH+]/[B] pH=7.5**	**fraction ionized pH=7.5**	**% ionized pH=7.5**
3-bromoquinoline	1.55E-05	1.55E-05	1.55E-03
antipyrine	8.91E-07	8.91E-07	8.91E-05
caffeine	1.26E-07	1.26E-07	1.26E-05
metronidazole	1.00E-05	1.00E-05	1.00E-03
pentoxifylline	6.31E-08	6.31E-08	6.31E-06
quinoline	2.51E-03	2.51E-03	2.51E-01

Table 3.2 – Cross-correlation matrix for LSER descriptors representing the set 50 neutral aromatic solutes.

	E	***S***	***A***	***B***	***V***
E	1.000				
S	0.308	1.000			
A	0.021	0.089	1.000		
B	0.009	0.153	0.001	1.000	
V	0.035	0.047	0.102	0.208	1.000

Table 3.3 – Cross-correlation matrix for LSER descriptors representing the set of 21 neutral drugs.

	E	***S***	***A***	***B***	***V***
E	1.000				
S	0.326	1.000			
A	0.012	0.051	1.000		
B	0.103	0.390	0.014	1.000	
V	0.558	0.660	0.030	0.418	1.000

Table 3.4 – Cross-correlation matrix for LSER descriptors representing the combined set of 50 neutral aromatic solutes and 21 neutral drugs.

	E	***S***	***A***	***B***	***V***
E	1.000				
S	0.689	1.000			
A	0.075	0.157	1.000		
B	0.555	0.699	0.108	1.000	
V	0.748	0.789	0.079	0.728	1.000

Table 3.5 - LEKC retention factors (expressed as log k) determined for the set of 50 neutral aromatic solutes using 15 mM $DPPG_{20}DPPC_{80}$,15 mM $DPPG_{20}DPPC_{80}$/3 mM cholesterol, 15 mM $DPPG_{20}DPPC_{80}$/6 mM cholesterol, 15 mM $DPPG_{20}DPPC_{80}$/9.75 mM cholesterol, and 15 mM $PI_{10}DPPS_{10}DPPC_{30}DPPE_{30}SPM_{20}$/9.75 mM cholesterol (biomimetic phase).

Solute Name	**15 mM $DPPG_{20}DPPC_{80}$ 0 mM cholesterol**	**15 mM $DPPG_{20}DPPC_{80}$ 3 mM cholesterol**	**15 mM $DPPG_{20}DPPC_{80}$ 6 mM cholesterol**	**15 mM $DPPG_{20}DPPC_{80}$ 9.75 mM cholesterol**	**Biomimetic phase**
1-methylnaphthalene	1.30	1.39	1.30	1.33	1.62
2-methoxypyridine	-1.13	-1.11	-1.07	-1.07	-1.16
3,5 dimethyl phenol	0.17	-0.02	-0.32	-0.48	-0.47
3-bromophenol	0.66	0.57	0.33	0.13	0.05
3-chlorophenol	0.46	0.32	0.15	-0.07	-0.04
3-methyl benzyl alcohol	-0.71	-0.85	-1.01	-1.21	-1.15
3-phenyl-1-propanol	-0.52	-0.69	-0.85	-0.99	-0.89
4-bromophenol	0.68	0.62	0.43	0.22	0.26
4-chloroacetophenone	-0.14	-0.08	-0.27	-0.36	-0.27
4-chloroanisole	0.55	0.58	0.46	0.40	0.49
4-chlorophenol	0.49	0.40	0.22	0.04	0.04
4-chlorotoluene	0.83	0.85	0.78	0.74	0.93
4-ethylphenol	0.30	0.14	-0.15	-0.35	-0.29
4-fluoroacetohphenone	-0.70	-0.74	-0.84	-0.91	-0.92
4-fluorophenol	-0.19	-0.32	-0.50	-0.62	-0.70
4-methyl benzyl alcohol	-0.71	-0.83	-0.95	-0.97	-1.04
4-nitrotoluene	-0.05	-0.05	-0.13	-0.21	-0.17
acetophenone	-0.84	-0.84	-1.04	-1.00	-1.08
aniline	-1.00	-1.05	-1.10	-1.10	-1.24
benzaldehyde	-0.92	-0.93	-0.99	-0.86	-1.04

Solute Name	15 mM $DPPG_{20}DPPC_{80}$ 0 mM cholesterol	15 mM $DPPG_{20}DPPC_{80}$ 3 mM cholesterol	15 mM $DPPG_{20}DPPC_{80}$ 6 mM cholesterol	15 mM $DPPG_{20}DPPC_{80}$ 9.75 mM cholesterol	Biomimetic phase
benzene	-0.46	-0.41	-0.43	-0.42	-0.40
benzonitrile	-0.84	-0.91	-0.95	-0.96	-1.04
benzyl alcohol	-1.03	-1.11	-1.14	-1.14	-1.34
bromobenzene	0.49	0.40	0.33	0.30	0.51
butyl benzoate	1.06	1.17	1.01	0.77	0.88
butyrophenone	0.20	0.17	-0.08	-0.15	-0.03
chlorobenzene	0.19	0.18	0.15	0.11	0.21
ethyl benzoate	0.04	-0.01	-0.12	-0.27	-0.15
ethylbenzene	0.54	0.45	0.42	0.48	0.54
iodobenzene	0.77	0.71	0.61	0.57	0.78
m-cresol	-0.18	-0.31	-0.56	-0.74	-0.68
m-dichlorobenzene	0.94	0.91	0.85	0.74	0.92
methyl benzoate	-0.40	-0.35	-0.46	-0.62	-0.54
methyl-2-methyl benzoate	0.15	0.01	-0.09	-0.22	-0.01
naphthalene	0.82	0.83	0.83	0.75	0.87
nitrobenzene	-0.43	-0.49	-0.56	-0.60	-0.57
o-dichlorobenzene	0.83	0.81	0.74	0.75	0.84
o-xylene	0.44	0.60	0.46	0.44	0.51
p-cresol	-0.17	-0.25	-0.47	-0.64	-0.63
p-dichlorobenzene	0.71	0.76	0.72	0.83	0.75
Phenethyl alcohol	-0.87	-0.98	-1.07	-1.09	-1.22
phenol	-0.53	-0.67	-0.83	-0.93	-0.89
phenyl acetate	-0.82	-0.93	-1.01	-1.03	-1.15
phenyl benzoate	1.00	1.08	1.03	0.94	0.93

Solute Name	**15 mM $DPPG_{20}DPPC_{80}$ 0 mM cholesterol**	**15 mM $DPPG_{20}DPPC_{80}$ 3 mM cholesterol**	**15 mM $DPPG_{20}DPPC_{80}$ 6 mM cholesterol**	**15 mM $DPPG_{20}DPPC_{80}$ 9.75 mM cholesterol**	**Biomimetic phase**
propiophenone	-0.24	-0.32	-0.51	-0.58	-0.50
propyl benzoate	0.50	0.54	0.44	0.28	0.34
propylbenzene	1.13	0.99	0.96	1.01	1.13
p-xylene	0.54	0.63	0.64	0.65	0.76
toluene	0.04	0.06	0.03	0.05	0.09
valerophenone	0.77	0.75	0.58	0.46	0.48

Table 3.6 – Summary of LSER models. Standard errors for individual LSER system coefficients for the Abraham model for human absorption data were not published in Reference 30.

Lipid Composition	***v***	***b***	***a***	***s***	***e***	***C***	***I***	
15 mM $DPPG_{20}DPPC_{80}$	3.50 (0.09)	-3.60 (0.10)	0.66 (0.06)	-0.53 (0.10)	0.46 (0.10)	-2.41 (0.09)		R^2_{adj}=0.98 SE=0.09 n=50
15 mM $DPPG_{20}DPPC_{80}$	2.87 (0.15)	-2.55 (0.12)	0.33 (0.11)	-0.83 (0.10)	0.61 (0.13)	-1.89 (0.11)		R^2_{adj}=0.90 SE=0.23 n=67
15 mM $DPPG_{20}DPPC_{80}$ 3 mM cholesterol	3.58 (0.10)	-3.72 (0.11)	0.48 (0.07)	-0.50 (0.11)	0.50 (0.11)	-2.50 (0.11)		R^2_{adj}=0.98 SE=0.10 n=50
15 mM $DPPG_{20}DPPC_{80}$ 3 mM cholesterol	2.49 (0.16)	-2.38 (0.13)	0.03 (0.12)	-0.76 (0.11)	0.50 (0.15)	-1.52 (0.11)		R^2_{adj}=0.88 SE=0.28 n=70
15 mM $DPPG_{20}DPPC_{80}$ 6 mM cholesterol	3.38 (0.12)	-3.70 (0.13)	0.26 (0.07)	-0.59 (0.13)	0.58 (0.13)	-2.39 (0.12)		R^2_{adj}=0.97 SE=0.12 n=50
15 mM $DPPG_{20}DPPC_{80}$ 6 mM cholesterol	2.21 (0.18)	-2.15 (0.14)	-0.10 (0.13)	-0.69 (0.12)	0.43 (0.14)	-1.40 (0.11)		R^2_{adj}=0.85 SE=0.31 n=71
15 mM $DPPG_{20}DPPC_{80}$ 9.75 mM cholesterol	3.08 (0.13)	-3.61 (0.14)	-0.01 (0.08)	-0.67 (0.14)	0.68 (0.14)	-2.14 (0.14)		R^2_{adj}= 0.97 SE= 0.13 n=50

Lipid Composition	***v***	***b***	***a***	***s***	***e***	***C***	***I***	
15 mM $PI_{10}DPPS_{10}DPPC_{30}DPPE_{30}SPM_{20}$ 9.75 mM cholesterol	3.39 (0.12)	-3.85 (0.13)	-0.01 (0.08)	-0.91 (0.13)	0.85 (0.13)	-2.28 (0.12)		R^2_{adj}= 0.98 SE= 0.12 n= 50
% Absorbed, determined from human intestinal absorption data[14]	11.20	-20.90	-20.70	2.71	2.90	94.00	-3.14	R^2= 0.74 n=169

Table 3.7 – Summary of experimental retention factors and predicted retention factors (expressed as log k) of 21 neutral drugs for 15 mM $DPPG_{20}DPPC_{80}$,15 mM $DPPG_{20}DPPC_{80}$/3 mM cholesterol, and 15 mM $DPPG_{20}DPPC_{80}$/6 mM cholesterol. All experimental and predicted retention factors are expressed as log k.

	15 mM $DPPG_{20}DPPC_{80}$			**15 mM $DPPG_{20}DPPC_{80}$ 3 mM cholesterol**			**15 mM $DPPG_{20}DPPC_{80}$ 6 mM cholesterol**		
solute name	**experimental log *k***	**predicted log *k***	**difference**	**experimental log *k***	**predicted log *k***	**difference**	**experimental log *k***	**predicted log *k***	**difference**
3-bromoquinoline	0.48	0.46	0.02	0.31	0.49	-0.18	0.29	0.42	-0.13
acetominophen	-1.15	-1.07	-0.08	-1.23	-1.31	0.08	-1.14	-1.68	0.54
antipyrine	-1.33	-2.49	1.16	-1.36	-2.58	1.22	-1.33	-2.73	1.4
bifonazole	coelute with t_{mc}	2.25		1.73	2.33	-0.6	1.35	2.01	-0.66
caffeine	-1.34	-2.57	1.23	-1.37	-2.65	1.28	-1.33	-2.76	1.43
carbamazepine	-0.21	0.11	-0.32	-0.69	0.04	-0.73	-0.94	-0.27	-0.67
chloramphenicol	-0.31	-1.98	1.67	-0.67	-2.15	1.48	-0.75	-2.36	1.61
clotrimazole	coelute with t_{mc}	2.7		1.31	2.81	-1.5	0.9	2.45	-1.55
dexamethasone	0.33	0.46	-0.13	-0.4	0.34	-0.74	-0.8	-0.33	-0.47
diethylstilbestrol	coelute with t_{mc}	3.33		1.24	3.17	-1.93	0.67	2.58	-1.91
estradiol	1.02	1.8	-0.78	0.7	1.68	-0.98	0.54	1.21	-0.67
hydrocortisone	-0.28	0.13	-0.41	-0.8	0.01	-0.81	-0.92	-0.64	-0.28
metronidazole	-1.25	-2.18	0.93	-1.32	-2.28	0.96	-1.26	-2.45	1.19
nifedipine	1.06	0.67	0.39	0.66	0.63	0.03	0.46	0.18	0.28

	15 mM $DPPG_{20}DPPC_{80}$			15 mM $DPPG_{20}DPPC_{80}$ 3 mM cholesterol			15 mM $DPPG_{20}DPPC_{80}$ 6 mM cholesterol		
nifuroxime	-0.33	-0.72	0.39	-0.53	-0.88	0.35	-0.6	-1.08	0.48
pentoxifylline	-1.34	-2.18	0.84	-1.32	-2.25	0.93	-1.34	-2.53	1.19
prednisolone	-0.22	0.19	-0.41	-0.91	0.07	-0.98	-1.01	-0.52	-0.49
prednisone	-0.45	-0.36	-0.09	-0.92	-0.42	-0.5	-1.04	-0.97	-0.07
quinoline	-0.66	-0.62	-0.04	-0.85	-0.64	-0.21	-0.93	-0.68	-0.25
thiamphenicol	-1.53	-1.68	0.15	-1.68	-1.88	0.2	-1.6	-2.44	0.84
tolnaftate	coelute with t_{mc}	2.84		coelute with t_{mc}	2.96		1.41	2.71	-1.3

Table 3.8 – Statistics of correlation for experimental and predicted retention factors (expressed as log k) for neutral drugs.

Lipid Phase	Slope	Intercept	R^2	Standard Error
15 mM $DPPG_{20}DPPC_{80}$	1.40	-0.09	0.79	0.62
15 mM $DPPG_{20}DPPC_{80}$ 3 mM cholesterol	1.59	0.37	0.83	0.76
15 mM $DPPG_{20}DPPC_{80}$ 6 mM cholesterol	1.74	0.30	0.84	0.73

Table 3.9 - Normalized LSER models determined for 15 mM $DPPG_{20}DPPC_{80}$/9.75 mM cholesterol and 15 mM $PI_{10}DPPS_{10}DPPC_{30}DPPE_{30}SPM_{20}$/9.75 mM cholesterol using the training set of 50 neutral aromatic solutes. Also includes normalized LSER model for human intestinal absorption reported by Abraham et al. determined using a set of 169 diverse drugs.

System	***v/b***	***b/b***	***a/b***	***s/b***	***e/b***	***C/b***	***i/b***	
15 mM $DPPG_{20}DPPC_{80}$	0.97 (0.04)	-1.00 (0.04)	0.18 (0.01)	-0.14 (0.01)	0.13 (0.01)	-0.67 (0.02)		n=50
15 mM $DPPG_{20}DPPC_{80}$	1.13 (0.08)	-1.00 (0.07)	0.13 (0.04)	-0.33 (0.04)	0.24 (0.05)	-0.74 (0.06)		n=67
15 mM $DPPG_{20}DPPC_{80}$ 3 mM cholesterol	0.96 (0.04)	-1.00 (0.04)	0.13 (0.01)	-0.14 (0.01)	0.13 (0.01)	-0.67 (0.02)		n=50
15 mM $DPPG_{20}DPPC_{80}$ 3 mM cholesterol	1.05 (0.08)	-1.00 (0.07)	0.01 (0.05)	-0.32 (0.05)	0.21 (0.06)	-0.64 (0.06)		n=70
15 mM $DPPG_{20}DPPC_{80}$ 6 mM cholesterol	0.91 (0.04)	-1.00 (0.04)	0.07 (0.01)	-0.16 (0.01)	0.16 (0.01)	-0.65 (0.02)		n=50
15 mM $DPPG_{20}DPPC_{80}$ 6 mM cholesterol	1.03 (0.10)	-1.00 (0.08)	-0.05 (0.06)	-0.32 (0.06)	0.20 (0.07)	-0.65 (0.06)		n=71
15 mM $DPPG_{20}DPPC_{80}$ 9.75 mM cholesterol	0.85 (0.05)	-1.00 (0.06)	0.00 (0.02)	-0.19 (0.04)	0.19 (0.04)	-0.59 (0.04)		n=50
15 mM $PI_{10}DPPS_{10}DPPC_{30}DPPE_{30}SPM_{20}$ 9.75 mM cholesterol	0.88 (0.04)	-1.00 (0.05)	0.00 (0.02)	-0.24 (0.03)	0.22 (0.03)	-0.59 (0.04)		n=50
% Absorbed, determined from human intestinal absorption data[14]	0.54	-1.00	-0.99	0.13	0.14	4.50	-0.15	n=169

Figure 3.1 – Predicted retention factors as a function of experimental retention factors determined for a set of 21 neutral drugs using 15 mM $DPPG_{20}DPPC_{80}$.

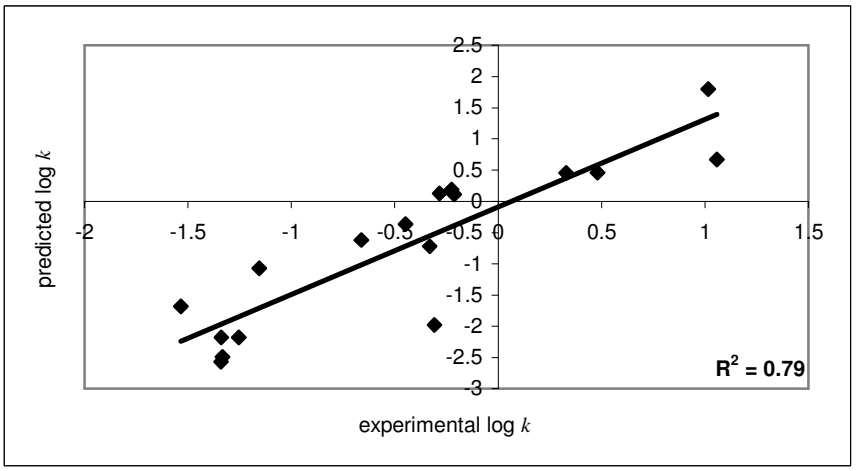

Figure 3.2 - Correlation plot for retention factors determined for the set of 50 neutral solutes using 15 mM $DPPG_{20}DPPC_{80}$/9.75 mM cholesterol and 15 mM $PI_{10}DPPS_{10}DPPC_{30}DPPE_{30}SPM_{20}$/9.75 mM cholesterol.

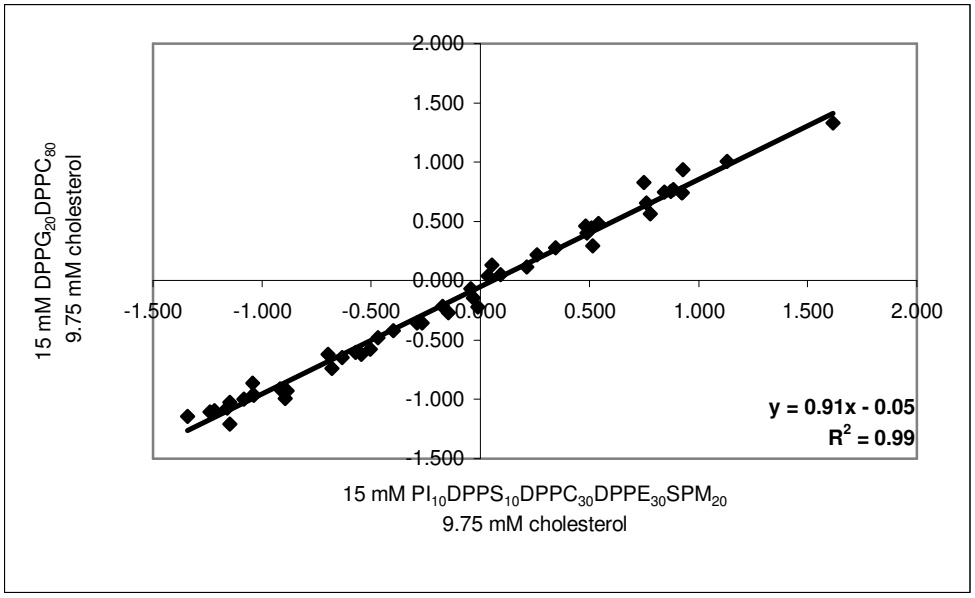

Chapter 4

Characterization of the Effects of Cholesterol on the Solvation Properties of Lipid Bilayer Membranes in Liposome Electrokinetic Chromatography (LEKC)

Abstract

The effect of cholesterol on liposome/water partitioning has been investigated using linear solvation energy relationship (LSER) models determined using liposome electrokinetic chromatography (LEKC) retention factors. LSER models were generated using LEKC retention factors determined for a set of 50 neutral aromatic solutes using lipid phases composed of 15 mM $DPPG_{20}DPPC_{80}$ with 0-15 mM cholesterol. LSER system coefficients describing the cohesiveness of the lipid phase and the hydrogen bonding and dipolar/polarizability interactions between the lipid phase and the solutes were studied. Increasing amounts of cholesterol was shown to decrease partitioning for most solutes studied. From the LSER models determined, increasing amounts of cholesterol in the lipid phase increases the cohesiveness and the polarizability of the lipid phase and decreases the hydrogen bond acceptor ability and dipolarity of the lipid phase. After a study of the contribution of each of the interactions described by the terms of the LSER model, it is apparent that the increased cohesiveness and decreased hydrogen bond acceptor ability of the lipid phase induced by the addition of increasing amounts of cholesterol are the most significant factors in the decreased liposome/water partitioning observed.

Introduction

The widely accepted fluid mosaic model describes the cell membrane as a spherical bilayer amalgamation of phospholipids with incorporated membrane proteins, glycolipids, glycoproteins and cholesterol. The most abundant constituent of these membranes, phospholipids, are characterized by a phosphate head group and a glycerol or sphingosine backbone attached to two long fatty acid chains. Membrane proteins of different structures and functions can be attached to the headgroups of phospholipids by electrostatic interactions or embedded in the phospholipid matrix by interactions between hydrophobic amino acid chains and the acyl chains of neighboring phospholipids. Glycolipids are essentially derivatives of phospholipids with a hydrophilic carbohydrate group attached to the lipid's phosphate group. Similarly, glycoproteins are proteins with attached monosachaccaride moieties. Cholesterol is comprised of a hydrophobic steroid ring linked to a

hydrophilic hydroxyl group.[1-3] In order to fully characterize biological membranes, the role of each of these membrane constituents must be well understood.

Cholesterol is a major component in biological membranes. The cholesterol content of different biological membranes varies wildly. Most bacterial membranes contain no cholesterol. *Bacillus licheniformis*, *micrococcus lysodiikticus*, *bacillus megaterium*, and *streptococcus faccalis* have all been shown to have cholesterol/phospholipid molar ratios of nearly zero.[4] The plasma membranes of various intracellular organelles such as the mitochondrial inner membrane also contain almost no cholesterol.[4] Intestinal epithelial cell membranes[5] and myelin[4] membranes have both been shown to contain significant amounts of cholesterol (cholesterol/phospholipid molar ratio= 0.65 and 0.70, respectively). Skin cells[6], red blood cells, and eukaryotic cells[4] have all been shown to contain cholesterol in nearly equimolar amounts to phospholipids (cholesterol/phospholipid molar ratio= 1.0).

The role of cholesterol in biological membranes has been characterized by various methods. The interfacial region of a lipid bilayer is comprised by the polar head groups of the phospholipids. The hydrophobic region of a lipid bilayer is formed by the very fluid phospholipid fatty acid chains. When cholesterol is incorporated in lipid bilayer membranes, the polar –OH group is aligned with the phospholipid polar head groups in the interfacial region and the hydrophobic steroid rings are incorporated into the hydrophobic region. The hydrophobic steroid rings that are inserted into this region when cholesterol is incorporated into a membrane are very rigid. Therefore, cholesterol is able to modulate the fluidity of the membrane.[7] Fluorescence studies have also shown that cholesterol decreases the polarity of lipid membranes because the dipole moment of the polar –OH group of cholesterol is lower than that of the polar head group of most phospholipids and because it partially dehydrates the interfacial region of the lipid membrane.[8] Incorporation of cholesterol in lipid membranes has also been shown to decrease liposome/water partitioning coefficients for various compounds using isothermal titration calorimetry,[9,10] immobilized liposome chromatography,[11] and surface plasmon resonance.[12]

The present study has used Linear Solvation Energy Relationships (LSER) models determined using LEKC retention factors determined for a set of 50 neutral aromatic solutes with known Abraham solute descriptors using 15 mM $DPPG_{20}DPPC_{80}$ with 0, 3, 6, 9, 12, and 15 mM cholesterol to investigate the effects of cholesterol on liposome/water partitioning. The linear solvation energy relationships (LSER) model was first used by Kamlet and Taft to model various solvation systems.[15-18] The model was then revised by Abraham et al. to better describe solvation effects in various physico-chemical and biological processes.[19] The LSER model has been extensively used by Khaledi et al. to characterize selectivity in electrokinetic chromatography systems.[14, 20-27]

Experimental

Refer to **Chapter 2** for experimental procedures and details concerning chemicals, liposome preparation, sample preparation, electrokinetic chromatography, calculation of retention factors, and determination of linear solvation energy relationships (LSER) models.

Results and Discussion

Determination of Linear Solvation Energy Relationships Models as a Function of Cholesterol Content

LEKC retention factors were determined for the set of 50 neutral aromatic solutes using lipid phases comprised of 15 mM $DPPG_{20}DPPC_{80}$ with 0, 3, 6, 9, 12, and 15 mM cholesterol. These retention factors are summarized in **Table 4.1**. LSER models were generated using the LEKC retention factors determined for these neutral aromatic solutes as a training set for each of these lipid phases. These models are summarized in **Table 4.2**.

Effect of Cholesterol on Liposome/Water Partitioning

The regression constant of the LSER model, C, is directly related to the chromatographic phase ratio (Φ) of the lipid phase, defined as the ratio of the volume of the liposomes to the volume of the aqueous phase. As shown in **Figure 4.1**, the C-constant increases significantly as the cholesterol content of the lipid phase is increased from 3 mM to 15 mM. This trend is due to the increase in the phase ratio with the addition of cholesterol.

For all EKC phases, the phase ratio may be calculated as:

$$\Phi = \frac{v(C_{lipid} - CAC)}{1 - v(C_{lipid} - CAC)} \qquad \textbf{Equation 4.5}$$

where v is the partial specific molar volume of the lipid phase, C_{lipid} is the total lipid concentration (including cholesterol) of the lipid phase, and CAC is the critical aggregation concentration of the lipid phase. The main effect of cholesterol on the phase ratio is the increase of the total lipid concentration; because there is "more" of the lipid phase present as cholesterol is added, the phase ratio increases. The critical aggregation concentrations of DPPG, DPPC, and cholesterol are in the micromolar range[29] and are therefore all insignificant relative to the total lipid concentration, C_{lipid}. Therefore, the effect of the lipid composition on the chromatographic phase ratio for these lipid phases depends only on the different partial specific molar volumes of the lipid phases. The magnitude of this increase is

not very large because the partial specific volume of cholesterol (0.3669 L/mole)[30] is smaller than that of DPPG (0.7524 L/mole) or DPPC (0.7002 L/mole).[31]

Retention factors determined by LEKC for a given solute depend on the solute's liposome/water partition coefficient and the chromatographic phase ratio of the LEKC system. Therefore, it is impossible to directly compare retention factors determined for separate lipid phases without correcting for the phase ratio. The regression constant of the LSER model, C, depends mainly on the chromatographic phase ratio, therefore it may be used to correct retention factors for the chromatographic phase ratio. In this study, corrected retention factors, log $k_{corrected}$, were calculated using:

$$\log k_{corrected} = \log k - C \qquad \textbf{Equation 4.4}$$

The corrected retention factors determined for the set of 50 neutral aromatic solutes are included in **Table 4.3**.

The solute set can be broken down into three groups: nonhydrogen bonding solutes, hydrogen bond acceptor solutes, and hydrogen bond donor solutes. Nonhydrogen bonding solutes are characterized by A descriptors of 0.000 and B descriptors less than 0.200. By these criteria, the homologous series of alkylbenzenes are all nonhydrogen bonding solutes. Plots of the corrected retention factors for these solutes as functions of cholesterol content are included in **Figure 4.2**. Hydrogen bond acceptor solutes are characterized by A descriptors of 0.000 and B descriptors greater than 0.200. By these criteria, the homologous series of alkylphenones are all hydrogen bond acceptor solutes. Plots of the corrected retention factors for these solutes as functions of cholesterol content are included in **Figure 4.3**. Finally, all solutes with A descriptors greater than 0.000 are hydrogen bond donor solutes. By these criteria, the homologous series of alkylphenols are all hydrogen bond donor solutes. Plots of the corrected retention factors for these solutes as functions of cholesterol content are included in **Figure 4.4**. From **Figures 4.2, 4.3**, and **4.4**, the extent of solute interactions with the lipid phase is reduced by the addition of cholesterol in concentrations from 3 mM to 12 mM to lipid phases comprised of DPPG and DPPC. Similar results have been shown for a variety of solutes including simple n-alkanols, drugs, and steroids using isothermal titration calorimetry,[9,10] immobilized liposome chromatography,[11] and surface plasmon resonance.[12]

Using LSER Models to Study the Effect of Cholesterol on the Solvation Properties of Lipid Bilayers

While the same general trends discussed in **Chapter 3** are present in all LSER models for lipid phases, the LSER models generated for 15 mM $DPPG_{20}DPPC_{80}$ with 0-15 mM cholesterol offer a good representation of the effect of cholesterol on the solvation properties of lipid bilayers. From the

LSER models summarized in **Table 4.2**, the large negative b coefficient is statistically constant with no easily discernable trend in variation, for each of the lipid phases studied. Therefore, the addition of cholesterol to an LEKC lipid phase has no significant effect on the hydrogen bond donating ability of the lipid phase relative to the aqueous phase.

The a coefficient that describes the hydrogen-bonding interaction between a solute as a hydrogen bond donor and the lipid phase as a hydrogen bond acceptor decreases significantly as the cholesterol content of the lipid phase is increased. This trend is shown in **Figure 4.5**. A similar effect was also noted in a previous study. In the previous study, the total lipid concentration (phospholipids and cholesterol) was maintained constant. Therefore, the decrease of the a coefficient was attributed to the replacement of phospholipid with cholesterol rather than the addition of cholesterol to the lipid bilayer.[14] In this study, the DPPG and DPPC compositions of the lipid phases studied were constant and independent of cholesterol content, therefore, the decrease in the hydrogen bond acceptor ability of the lipid phase is directly influenced by the incorporation of cholesterol. The hydrogen bond acceptor ability of lipid phases containing DPPC is generally attributed to the cationic center of the zwitterionic lipid.[14] The addition of cholesterol to the lipid phase causes these cationic centers to interact preferentially with the hydrogen atom contained in the hydroxyl group of the cholesterol molecule rather than hydrogen bond donor sites on solute molecules.

The v coefficient describes the hydrophobic effect that favors distribution of hydrophobic solutes to a "hydrocarbon-like" phase rather than an aqueous phase. This term decreases systematically with the addition of cholesterol to the lipid phase. This trend is shown in **Figure 4.6**. This effect likely occurs because the addition of cholesterol to a lipid membrane causes ordering/decreased motion of the lipid acyl chains and therefore causes the membrane to be more cohesive.[32] As a result of the lipid acyl chain ordering induced by cholesterol, the lipid molecules are not able to accommodate solute molecules partitioning from the aqueous phase as easily as membranes without cholesterol. This effect allows cholesterol to modulate the fluidity of biological membranes.

The s coefficient that describes the dipolarity/polarizability interactions between the solutes and lipid phase also decreases significantly as the cholesterol content of the lipid phase is increased. This trend is shown in **Figure 4.7**. The addition of cholesterol to liposomes prepared using DPPC and DPPG has been shown to reduce the polarity of the liposome interfacial region in two different ways.[8] First, the dipole moment of the polar –OH group of cholesterol (μ = 1.6 D)[33] is much smaller than that of the DPPG polar head group (μ = 11 D) or the DPPC polar head group (μ = 19 D).[34,35] Thus, the addition of cholesterol to a DPPG/DPPC membrane lowers the net dipole moment of the interfacial region of lipid bilayer membranes. Also, incorporation of cholesterol into lipid membranes has been shown to dehydrate the interfacial region.[8,32] As stated above, much of the polar character of lipid

membrane interfacial regions in caused by water molecules bound to the head groups of the lipid molecules. Therefore, dehydration of the head group region decreases the polarity of the interfacial region. The e coefficient that describes the polarizability of the lipid phase increases as a function of addition of cholesterol to the lipid phase. This trend is also shown in **Figure 4.7**. This term is essentially a correction factor for any dipolar interactions not described by the s coefficient above, therefore a similar trend, although opposite in sign, is not surprising.

LSER Contributions

The product of the LSER solute descriptor and the LSER system coefficient for a given interaction can be used to describe the contributions of each interaction described by the LSER model to the overall partitioning behavior of a given solute.

The contribution of hydrophobic interactions to liposome/water partitioning, described by the product vV, is the one of the dominant terms in each of the LSER models for each lipid phase. A plot of vV as a function of cholesterol content for benzene, acetophenone, and p-cresol is included in **Figure 4.8**. This plot follows nearly the same trend as the plots of log $k_{corrected}$ as a function of cholesterol content; vV decreases linearly from 3 mM cholesterol to 12 mM cholesterol. This trend is the same for all solutes, regardless of hydrogen bond donor or acceptor ability.

The dipolar and polarizability interactions between the solute and the lipid phase are described by the products eE and sS. Plots of eE, sS, and $eE+sS$ for benzene, acetophenone, and p-cresol are included in **Figures 4.9**, **4.10**, and 4.**11**. It is interesting to note that while the eE term increases and the sS term decreases for each of these solutes with the addition of cholesterol, the net dipolar and polarizability interactions described by the sum $eE+sS$ is quite small for each of these solutes. Therefore, these interactions play little role in the trends in liposome/water partitioning as a function of cholesterol content for these solutes. For highly polarizable solutes, such as substituted napthalenes or halogenated aromatics, the eE term is larger than the sS term and therefore by the sum $eE+sS$ is positive for these solutes. Plots of eE, sS, and $eE+sS$ for 1-methylnapthalene are included in Figure **4.12**. For highly polarizable solutes, the net dipolar and polarizability interactions described by the sum $eE+sS$ plays some role in the trends in liposome/water partitioning as a function of cholesterol content for these solutes.

The product aA describes the interactions between hydrogen bond donor solutes and the lipid phase as a hydrogen bond acceptor. Obviously, this term of the LSER model does not affect the liposome/water partitioning behavior of nonhydrogen bonding solutes or hydrogen bond acceptor solutes. Plots of aA for aniline, phenol, and 3-bromophenol are included in **Figure 4.13**. For all of

these solutes, the *aA* term decreases significantly from 0 mM cholesterol to 15 mM cholesterol. Therefore, these interactions play a significant role in the decreased liposome/water partitioning for hydrogen bond donor solutes with increasing cholesterol content.

Conclusions

In conclusion, liposome electrokinetic chromatography (LEKC) retention factors for 50 neutral aromatic solutes have been determined using six different lipid phases with increasing cholesterol content: 15 mM $DPPG_{20}DPPC_{80}$ with 0 mM cholesterol, 3 mM cholesterol, 6 mM cholesterol, 9 mM cholesterol, 12 mM cholesterol, and 15 mM cholesterol. Increasing amounts of cholesterol in the lipid phase was shown to decrease liposome/water partitioning for most solutes. Linear solvation energy relationships (LSER) models were generated for each lipid phase using the set of 50 neutral aromatic solutes. These LSER models were used to characterize the effects of cholesterol on the solvation properties of lipid bilayer membranes. LSER models determined for these lipid phases show that increasing amounts of cholesterol in the lipid phase increases the cohesiveness and the polarizability of the lipid phase and decreases the hydrogen bond acceptor ability and dipolarity of the lipid phase. Similar trends have also been noted in studies using various other methods for studying lipid bilayer membranes. The effects of cholesterol content on liposome/water partitioning may be explained by three possible mechanisms. First, the addition of cholesterol to lipid bilayers has been shown to induce partial ordering the acyl chain region of the membrane. Also, the dipole moment of the polar head group of cholesterol is significantly smaller than that of most lipid polar head groups. Therefore, the addition of cholesterol decreases the dipole moment of the lipid bilayer. Finally, spectroscopic methods have shown that cholesterol dehydrates the interfacial region of lipid bilayer membranes. After a study of the contribution of each of the interactions described by the terms of the LSER model, it is apparent that the increased cohesiveness and decreased hydrogen bond acceptor ability of the lipid phase induced by the addition of increasing amounts of cholesterol are the most significant factors in the decreased liposome/water partitioning observed.

Works Cited

1. Singer, S.J.; Nicolson, G.L. The Fluid Mosaic Model of Cell Membranes. *Science* **1972**, *175* (4023), 720-731.
2. Kleinsmith, L.J.; Kish, V.M. *Principles of Cell and Molecular Biology*, Harper Collins College Publishers: New York, **1995**.
3. Hansch, C., ed. *Comprehensive Medicinal Chemistry: Volume 3, Membranes and Receptors*, Pergamon Press: Oxford, **1990**.
4. Gomperts, B.D. The Plasma Membrane: Models For Structure and Function, Academic Press: London, **1977**.
5. Ibrahim, S.A.; Balasubramanian, K.A. Lipid-Composition and Membrane Fluidity of Monkey Small-Intestinal Brush-Border Membrane: Regional Differences. *Ind. J. Biochem Biophys.* **1995**, *32*, 290-294.
6. Velkova, V.; Lafleur, M. Influence of the lipid composition on the organization of skin lipid model mixtures: An infrared spectroscopy investigation. *Chemistry and Physics of Lipids.* **2002**, *117*, 63-74.
7. Yamamoto H.; Liljestrand H.M. Partitioning of selected estrogenic compounds between synthetic membrane vesicles and water: Effects of lipid components. *Environ. Sci. & Tech*. **2004**, *38* (4), 1139-1147.
8. Bernik, D.L.; Negri, R.M. Local Polarity at the Polar Head Level of Lipid Vesicles Using Dansyl Fluorescent Probes. *J. Coll. Inter. Sci.* **1998**, *203*, 97-105.
9. Rowe, E.S.; Zhang, F.L.; Leung, T.W.; Parr, J.S.; Guy, P.T.; Thermodynamics Of Membrane Partitioning For A Series Of N-Alcohols Determined By Titration Calorimetry: Role Of Hydrophobic Effects. *Biochemistry*. **1998**, *37* (8), 2430-2440.
10. Cantor, R.S.; Bilayer Partition Coefficients of Alkanols: Predicted Effects of Varying Lipid Composition. *J. Phys. Chem. B.* **2001**, 105, 7550-7553.
11. Liu, X.Y.; Yang, Q.; Kamo, N.; Miyake, J.; Effect of liposome type and membrane fluidity on drug-membrane partitioning analyzed by immobilized liposome chromatography. *J. Chrom. A.* **2001**, *913* (1-2), 123-131.
12. Baird, C.L.; Courtenay, E.S.; Myszka, D.G.; Surface plasmon resonance characterization of drug/liposome interactions. *Anal. Biochemistry*. **2002**, *310* (1), 93-99.
13. Burns, S.T.; Khaledi, M.G. Rapid determination of liposome-water partition coefficients (K-lw) using liposome electrokinetic chromatography (LEKC). *J. Pharm. Sci.* **2002**, *91* (7), 1601-1612.
14. Burns, S.T.; Agbodjan, A.A.; Khaledi, M.G.; Characterization of solvation properties of lipid bilayer membranes in liposome electrokinetic chromatography. *J. Chrom. A*. **2002**, *973* (1-2), 167-176.

15. Kamlet, M.J.; Taft, R.W. The solvatochromic comparison method. I. The .beta.-scale of solvent hydrogen-bond acceptor (HBA) basicities. *J. Am. Chem. Soc*. **1976**, *98* (2), 377-383.
16. Taft, R.W.; Kamlet, M.J. The solvatochromic comparison method. 2. The .alpha.-scale of solvent hydrogen-bond donor (HBD) acidities. *J. Am. Chem. Soc*. **1976**, *98* (10), 2886-2894.
17. Yokoyama T.; Taft, R.W.; Kamlet, M.J. Solvatochromic comparison method .3. Hydrogen-bonding by some 2-nitroaniline derivatives. *J. Am. Chem. Soc*. **1976**, *98* (11), 3233-3237.
18. Kamlet M.J.; Abboud, J.L.; Taft, R.W. Solvatochromic Comparison Method .6. Pi-Star Scale Of Solvent Polarities. *J. Am. Chem. Soc*. **1977**, *99* (18), 6027-6038.
19. Tan, L.C.; Carr, P.W.; Abraham, M.H. Study of retention in reversed-phase liquid chromatography using linear solvation energy relationships .1. The stationary phase. *J. Chrom. A.* **1996**, 752 (1-2), 1-18.
20. Trone, M.D.; Khaledi, M.G. Statistical evaluation of linear solvation energy relationship models used to characterize chemical selectivity in micellar electrokinetic chromatography. *J. Chrom. A.* **2000**, *886*, 245-257
21. Trone, M.D.; Khaledi, M.G. Characterization of chemical selectivity in micellar electrokinetic chromatography. 4. Effect of surfactant headgroup. *Anal. Chem*. **1999**, *71* (7), 1270-1277.
22. Trone, M.D.; Khaledi, M.G. Influence of ester and amide-containing surfactant headgroups on selectivity in micellar electrokinetic chromatography. *Electrophoresis*. **2000**, *21* (12), 2390-2396.
23. Trone, M.D.; Mack, J.P.; Goodell, H.P.; Khaledi, M.G. Characterization of chemical selectivity in micellar electrokinetic chromatography VI. Effects of surfactant counter-ion. *J. Chrom. A*. **2000**, *888* (1-2), 229-240.
24. Trone, M.D.; Khaledi, M.G. Characterization of chemical selectivity in micellar electrokinetic chromatography: V. The effect of the surfactant hydrophobic chain. *J. Micro. Sep*. **2000**, *12* (8), 433-441.
25. Agbodjan, A.A.; Bui, H.; Khaledi, M.G. Study of solute partitioning in biomembrane-mimetic pseudophases by electrokinetic chromatography: Dihexadecyl phosphate small unilamellar vesicles. *Langmuir*. **2001**, *17* (10), 2893-2899.
26. Bui, H.H.; Khaledi, M.G. Determination of vesicle-water partition coefficients by electrokinetic chromatography: Study of temperature effect. *J. Colloid. Ineterf. Sci.* **2002**, *253* (2), 397-401.
27. Agbodjan, A.A.; Khaledi, M.G. Study of solute partitioning into cationic vesicles of dihexadecyldimethylammonium bromide using electrokinetic chromatography *J. Chrom. A*. **2003**, *1004* (1-2), 145-153.
28. Kotz, J.C.; Purcell, K.F. *Chemistry and Chemical Reactivity*, Saunders College Publishing: Philadelphia, **1991**.

29. Pollegioni, L.; Gadda, G.; Ambrosius, D.; Ghisla, S.; Pilone, M.S. Cholesterol oxidase from Streptomyces hygroscopius and Brevibacterium sterolicum: effect of surfactants and organic solvents on activity. *Biotech. Appl. Biochem*. **1999**, *30*, 27-33.
30. Durchschlag, H. Specific Volumes of Biological Macromolecules and Some Other Molecules of Biological Interest. In *Thermodynamic Data for Biochemistry and Biotechnology*; Hinz, H.J., Ed.; Springer-Verlag: Berlin, **1986**.
31. Marsh, D. CRC *Handbook of Lipid Bilayers*, CRC Press: Boca Raton, **1990**; Section II.9.4.
32. Saito, H.; Araiso, T.; Shirahama, H.; Koyama, T. Dynamics of the Bilayer/Water Interface of Phospholipid-Vesicles and the Effect of Cholesterol: A Picosecond Fluorescence Anisotropy Study. *J. Biochem.* **1991**, *109* (4), 559-565.
33. Bechinger, B.; Seelig, J. Interaction of Electric Dipoles With Phospholipid Head Groups - A H-2 And P-31 Nmr-Study Of Phloretin And Phloretin Analogs In Phosphatidylcholine Membranes. *Biochemistry*. **1991**, *30* (16), 3923-3929.
34. Shepherd, J.C.W.; Buldt, G. Zwitterionic Dipoles as a Dielectric Probe For Investigating Head Group Mobility In Phospholipid Membranes. *Biochim. Biophys. Acta*. **1978**, *514* (1), 83-94.
35. MacDonald, P.M.; Leisen, J.; Marassi, F.M. Response of Phosphatidylcholine in the Gel and Liquid-Crystalline States to Membrane-Surface Charges. *Biochemistry*. **1991**, *30* (14), 3558-3566.

Table 4.1 – Retention factors, expressed as log k, determined for neutral aromatic solutes using 15 mM $DPPG_{20}DPPC_{80}$ with 0, 3, 6, 9, 12, and 15 mM cholesterol.

	Experimental log k 15 mM $DPPG_{20}DPPC_{80}$					
Solute Name	**0 mM cholesterol**	**3 mM cholesterol**	**6 mM cholesterol**	**9 mM cholesterol**	**12 mM cholesterol**	**15 mM cholesterol**
1-methylnaphthalene	1.299	1.392	1.303	1.283	1.101	1.329
2-methoxypyridine	-1.127	-1.106	-1.075	-1.082	-1.052	-1.024
3,5 dimethyl phenol	0.169	-0.018	-0.316	-0.480	-0.554	-0.592
3-bromophenol	0.656	0.574	0.325	0.151	-0.015	0.005
3-chlorophenol	0.456	0.321	0.149	-0.019	-0.179	-0.177
3-methyl benzyl alcohol	-0.708	-0.847	-1.009	-1.046	-0.964	-1.062
3-phenylpropanol	-0.525	-0.687	-0.845	-0.893	-1.009	-0.913
4-bromophenol	0.676	0.623	0.433	0.259	0.113	0.094
4-chloroacetophenone	-0.141	-0.077	-0.273	-0.350	-0.415	-0.351
4-chloroanisole	0.554	0.580	0.457	0.413	0.258	0.365
4-chlorophenol	0.493	0.401	0.217	0.064	-0.173	-0.094
4-chlorotoluene	0.834	0.855	0.784	0.809	0.723	0.841
4-ethylphenol	0.298	0.135	-0.149	-0.271	-0.290	-0.408
4-fluoroacetohphenone	-0.702	-0.736	-0.837	-0.910	-0.906	-0.894
4-fluorophenol	-0.195	-0.318	-0.497	-0.606	-0.689	-0.685
4-methyl benzyl alcohol	-0.713	-0.833	-0.949	-0.997	-0.949	-0.987
4-nitrotoluene	-0.046	-0.045	-0.135	-0.156	-0.265	-0.249
acetophenone	-0.841	-0.843	-1.039	-1.024	-0.956	-0.963

	Experimental log k 15 mM $DPPG_{20}DPPC_{80}$					
Solute Name	**0 mM cholesterol**	**3 mM cholesterol**	**6 mM cholesterol**	**9 mM cholesterol**	**12 mM cholesterol**	**15 mM cholesterol**
aniline	-1.002	-1.055	-1.097	-1.108	-1.087	-1.073
benzaldehyde	-0.919	-0.927	-0.992	-0.997	-1.006	-0.989
benzene	-0.459	-0.414	-0.434	-0.421	-0.315	-0.298
benzonitrile	-0.838	-0.912	-0.954	-1.001	-0.964	-0.968
benzyl alcohol	-1.031	-1.110	-1.143	-1.096	-1.122	-1.125
bromobenzene	0.489	0.402	0.329	0.299	0.397	0.415
butyl benzoate	1.059	1.169	1.015	0.825	0.802	0.795
butyrophenone	0.205	0.175	-0.081	-0.132	-0.108	-0.203
chlorobenzene	0.190	0.179	0.153	0.129	0.222	0.266
ethyl benzoate	0.042	-0.015	-0.124	-0.222	0.554	-0.177
ethylbenzene	0.536	0.446	0.418	0.439	-0.173	0.586
iodobenzene	0.775	0.710	0.611	0.581	0.653	0.680
m-cresol	-0.176	-0.315	-0.560	-0.670	-0.663	-0.750
m-dichlorobenzene	0.944	0.911	0.845	0.832	0.743	0.880
methyl benzoate	-0.402	-0.352	-0.461	-0.571	-0.538	-0.526
methyl-2-methyl benzoate	0.153	0.011	-0.094	-0.184	-0.226	-0.183
naphthalene	0.823	0.832	0.832	0.789	0.701	0.799
nitrobenzene	-0.431	-0.494	-0.565	-0.629	-0.612	-0.628
o-dichlorobenzene	0.833	0.813	0.745	0.778	0.696	0.817
o-xylene	0.439	0.600	0.462	0.473	0.437	0.553
p-cresol	-0.165	-0.250	-0.472	-0.597	-0.725	-0.659
p-dichlorobenzene	0.712	0.756	0.720	0.734	0.733	0.806

	Experimental log k 15 mM $DPPG_{20}DPPC_{80}$					
Solute Name	**0 mM cholesterol**	**3 mM cholesterol**	**6 mM cholesterol**	**9 mM cholesterol**	**12 mM cholesterol**	**15 mM cholesterol**
phenethyl alcohol	-0.868	-0.979	-1.075	-1.060	-1.104	-1.089
phenol	-0.525	-0.674	-0.828	-0.883	-0.880	-0.881
phenyl acetate	-0.820	-0.930	-1.015	-1.046	-1.026	-1.008
phenyl benzoate	1.000	1.085	1.028	0.943	0.654	0.779
propiophenone	-0.240	-0.322	-0.508	-0.560	-0.530	-0.590
propyl benzoate	0.502	0.541	0.443	0.326	1.023	0.345
propylbenzene	1.132	0.988	0.958	0.996	0.369	1.138
p-xylene	0.543	0.631	0.637	0.625	0.467	0.628
toluene	0.045	0.058	0.031	0.038	0.127	0.171
valerophenone	0.769	0.748	0.577	0.463	0.471	0.379

Table 4.2 - LSER models determined for 15 mM $DPPG_{20}DPPC_{80}$ with 0, 3, 6, 9, 12, and 15 mM cholesterol using the training set of 50 neutral aromatic solutes.

Lipid Composition	***v***	***b***	***a***	***s***	***e***	***C***	
15 mM $DPPG_{20}DPPC_{80}$	3.50 (0.09)	-3.60 (0.10)	0.66 (0.06)	-0.52 (0.10)	0.46 (0.10)	-2.41 (0.09)	R^2_{adj}=0.98 SE=0.09 n=50
15 mM $DPPG_{20}DPPC_{80}$ 3 mM cholesterol	3.58 (0.10)	-3.73 (0.11)	0.48 (0.07)	-0.50 (0.11)	0.50 (0.11)	-2.50 (0.11)	R^2_{adj}=0.98 SE=0.10 n=50
15 mM $DPPG_{20}DPPC_{80}$ 6 mM cholesterol	3.38 (0.12)	-3.70 (0.13)	0.26 (0.07)	-0.59 (0.13)	0.58 (0.13)	-2.39 (0.12)	R^2_{adj}=0.97 SE=0.12 n=50
15 mM $DPPG_{20}DPPC_{80}$ 9 mM cholesterol	3.16 (0.13)	-3.57 (0.13)	0.09 (0.08)	-0.74 (0.13)	0.69 (0.14)	-2.19 (0.13)	R^2_{adj}=0.97 SE=0.12 n=50
15 mM $DPPG_{20}DPPC_{80}$ 12 mM cholesterol	2.94 (0.11)	-3.34 (0.11)	-0.06 (0.07)	-0.89 (0.12)	0.61 (0.12)	-1.83 (0.11)	R^2_{adj}=0.98 SE=0.11 n=50
15 mM $DPPG_{20}DPPC_{80}$ 15 mM cholesterol	2.96 (0.12)	-3.49 (0.13)	-0.13 (0.08)	-0.98 (0.13)	0.76 (0.13)	-1.82 (0.12)	R^2_{adj}=0.97 SE=0.12 n=50

Table 4.3 – Corrected retention factors, expressed as log $k_{corrected}$, determined for neutral aromatic solutes using 15 mM $DPPG_{20}DPPC_{80}$ with 0, 3, 6, 9, 12, and 15 mM cholesterol.

	Experimental log $k_{corrected}$ 15 mM $DPPG_{20}DPPC_{80}$					
Solute Name	**0 mM cholesterol**	**3 mM cholesterol**	**6 mM cholesterol**	**9 mM cholesterol**	**12 mM cholesterol**	**15 mM cholesterol**
1-methylnaphthalene	3.706	3.896	3.692	3.473	2.935	3.164
2-methoxypyridine	1.280	1.397	1.314	1.108	0.783	0.811
3,5 dimethyl phenol	2.576	2.485	2.073	1.710	1.280	1.242
3-bromophenol	3.063	3.078	2.714	2.341	1.819	1.839
3-chlorophenol	2.863	2.824	2.537	2.171	1.656	1.657
3-methyl benzyl alcohol	1.699	1.656	1.379	1.144	0.870	0.773
3-phenylpropanol	1.882	1.816	1.544	1.297	0.826	0.922
4-bromophenol	3.083	3.127	2.822	2.449	1.948	1.929
4-chloroacetophenone	2.266	2.426	2.116	1.840	1.420	1.484
4-chloroanisole	2.961	3.084	2.845	2.603	2.093	2.199
4-chlorophenol	2.900	2.904	2.606	2.254	1.662	1.741
4-chlorotoluene	3.241	3.358	3.172	2.999	2.557	2.676
4-ethylphenol	2.705	2.638	2.240	1.919	1.545	1.426
4-fluoroacetohphenone	1.705	1.768	1.552	1.279	0.928	0.941
4-fluorophenol	2.212	2.186	1.891	1.584	1.145	1.150
4-methyl benzyl alcohol	1.694	1.670	1.439	1.193	0.885	0.847
4-nitrotoluene	2.361	2.458	2.254	2.034	1.569	1.586
acetophenone	1.566	1.661	1.350	1.166	0.878	0.872

aniline	1.405	1.449	1.291	1.082	0.748	0.761
benzaldehyde	1.488	1.576	1.396	1.193	0.829	0.845
benzene	1.948	2.089	1.954	1.769	1.520	1.536
benzonitrile	1.569	1.592	1.434	1.189	0.871	0.867
benzyl alcohol	1.376	1.393	1.246	1.094	0.713	0.710
bromobenzene	2.896	2.905	2.718	2.489	2.232	2.250
butyl benzoate	3.466	3.672	3.403	3.015	2.636	2.629
butyrophenone	2.612	2.678	2.308	2.058	1.726	1.632
chlorobenzene	2.597	2.682	2.542	2.319	2.056	2.100
ethyl benzoate	2.449	2.489	2.265	1.968	1.662	1.657
ethylbenzene	2.943	2.950	2.806	2.629	2.388	2.421
iodobenzene	3.182	3.214	3.000	2.771	2.487	2.515
m-cresol	2.231	2.189	1.829	1.520	1.171	1.085
m-dichlorobenzene	3.351	3.414	3.234	3.022	2.578	2.714
methyl benzoate	2.005	2.151	1.928	1.619	1.297	1.309
methyl-2-methyl benzoate	2.560	2.515	2.294	2.006	1.608	1.652
naphthalene	3.230	3.336	3.221	2.979	2.536	2.634
nitrobenzene	1.977	2.010	1.824	1.561	1.223	1.206
o-dichlorobenzene	3.240	3.316	3.133	2.968	2.531	2.651
o-xylene	2.846	3.104	2.850	2.663	2.271	2.387
p-cresol	2.242	2.253	1.916	1.593	1.109	1.176
p-dichlorobenzene	3.119	3.260	3.109	2.924	2.568	2.641
phenethyl alcohol	1.539	1.525	1.314	1.130	0.731	0.746
phenol	1.882	1.829	1.560	1.307	0.954	0.953
phenyl acetate	1.587	1.574	1.374	1.144	0.809	0.827
phenyl benzoate	3.407	3.588	3.417	3.133	2.489	2.614

propiophenone	2.167	2.181	1.881	1.630	1.305	1.245
propyl benzoate	2.909	3.044	2.832	2.516	2.204	2.179
propylbenzene	3.539	3.491	3.347	3.186	2.857	2.972
p-xylene	2.950	3.134	3.026	2.815	2.302	2.462
toluene	2.452	2.562	2.420	2.228	1.962	2.005
valerophenone	3.176	3.252	2.965	2.653	2.306	2.214

Figure 4.1 - LSER regression constant, C, as a function of cholesterol content determined for 15 mM $DPPG_{20}DPPC_{80}$ with 0, 3, 6, 9, 12, and 15 mM cholesterol using the training set of 50 neutral aromatic solutes.

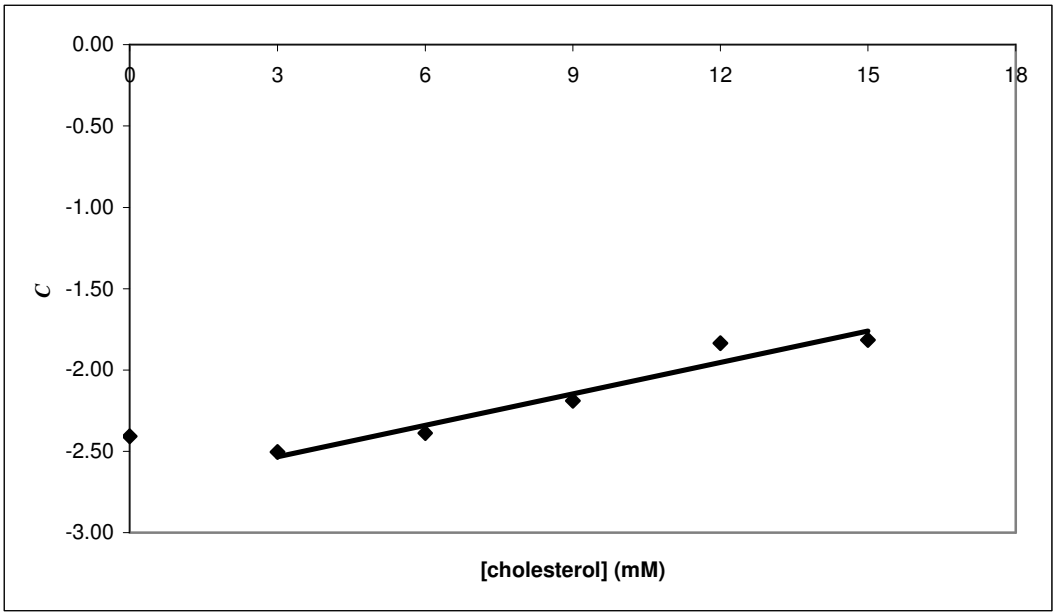

Figure 4.2 - Corrected retention factors, expressed as log $k_{corrected}$, as a function of cholesterol content determined for the homologous series of alkylbenzenes using 15 mM $DPPG_{20}DPPC_{80}$ with 0, 3, 6, 9, 12, and 15 mM cholesterol.

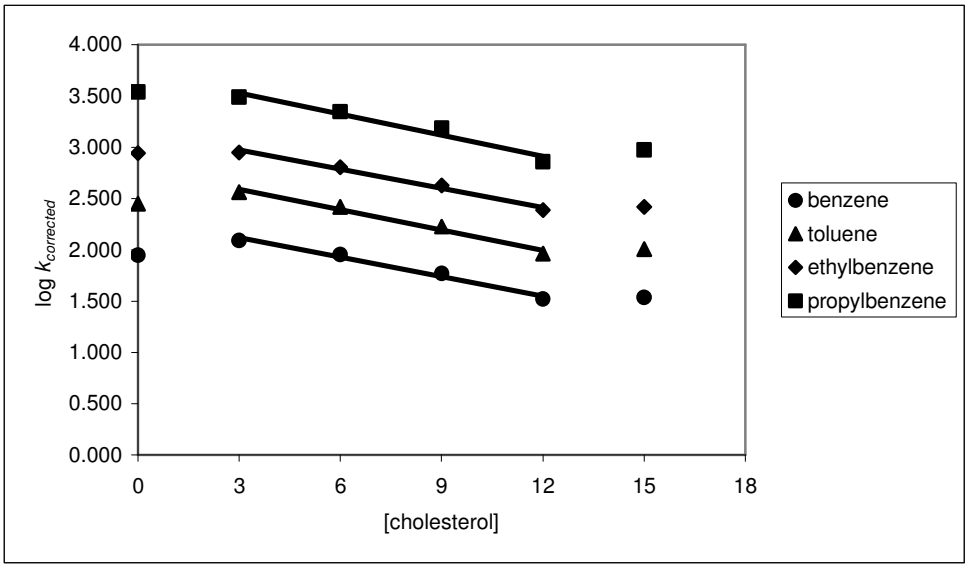

Figure 4.3 - Corrected retention factors, expressed as log $k_{corrected}$, as a function of cholesterol content determined for the homologous series of alkylphenones using 15 mM $DPPG_{20}DPPC_{80}$ with 0, 3, 6, 9, 12, and 15 mM cholesterol.

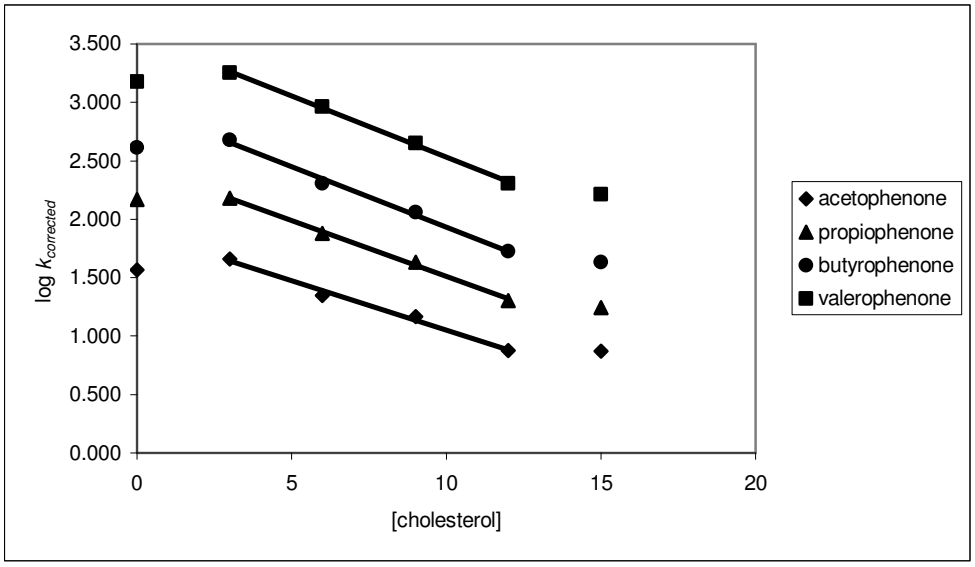

Figure 4.4 - Corrected retention factors, expressed as log $k_{corrected}$, as a function of cholesterol content determined for the homologous series of alkylphenols using 15 mM $DPPG_{20}DPPC_{80}$ with 0, 3, 6, 9, 12, and 15 mM cholesterol.

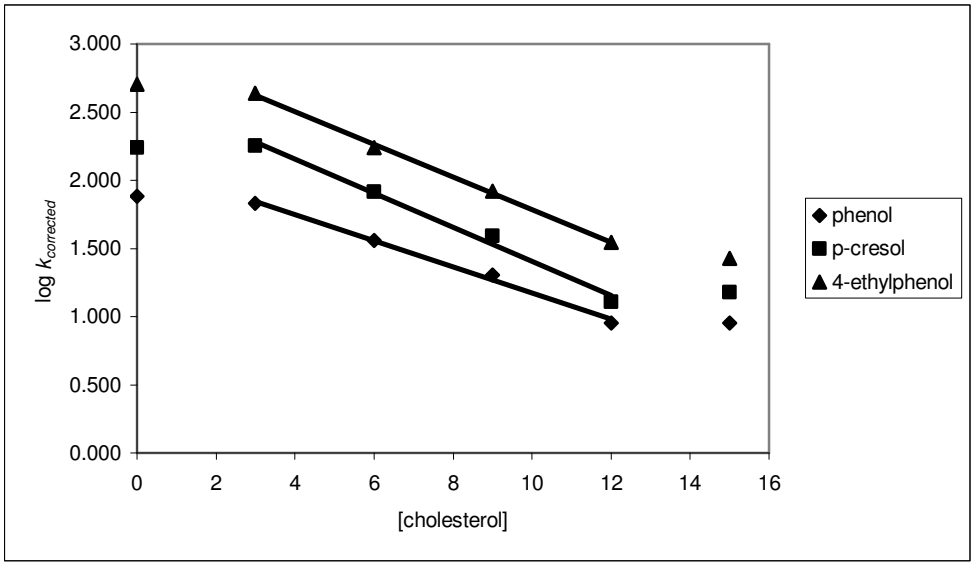

Figure 4.5 – Lipid phase hydrogen bond acceptor ability, described by the LSER system coefficient a, as a function of cholesterol content determined for 15 mM $DPPG_{20}DPPC_{80}$ with 0, 3, 6, 9, 12, and 15 mM cholesterol using the training set of 50 neutral aromatic solutes.

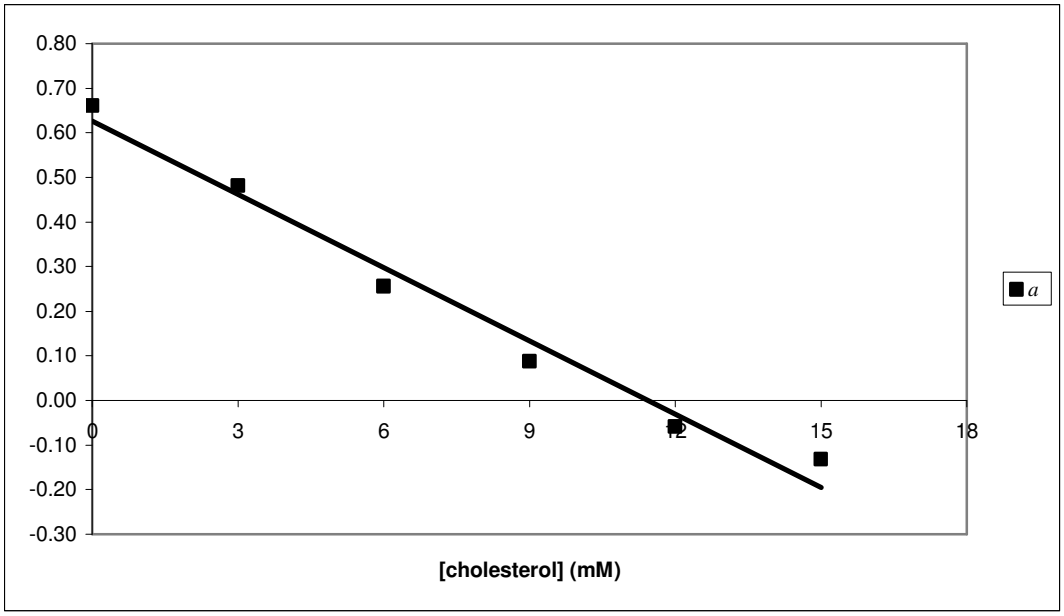

Figure 4.6 – Lipid phase cohesiveness, described by the LSER system coefficient v as a function of cholesterol content determined for 15 mM $DPPG_{20}DPPC_{80}$ with 0, 3, 6, 9, 12, and 15 mM cholesterol using the training set of 50 neutral aromatic solutes.

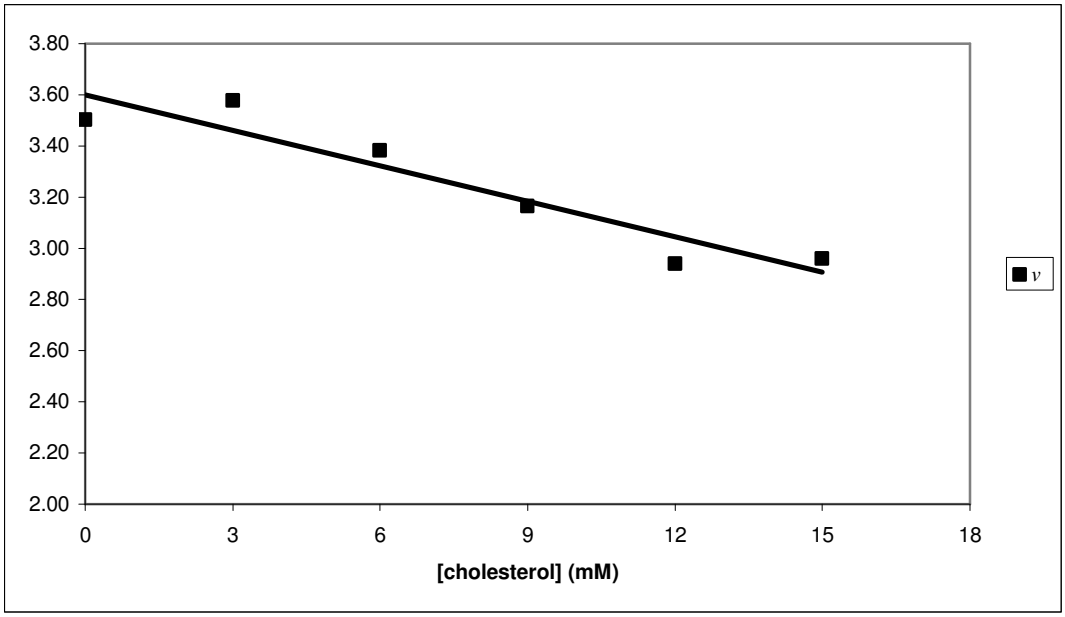

Figure 4.7 – Lipid phase dipolarity/polarizability, described by the LSER system coefficient s, and polarizability, described by e as a function of cholesterol content determined for 15 mM $DPPG_{20}DPPC_{80}$ with 0, 3, 6, 9, 12, and 15 mM cholesterol using the training set of 50 neutral aromatic solutes.

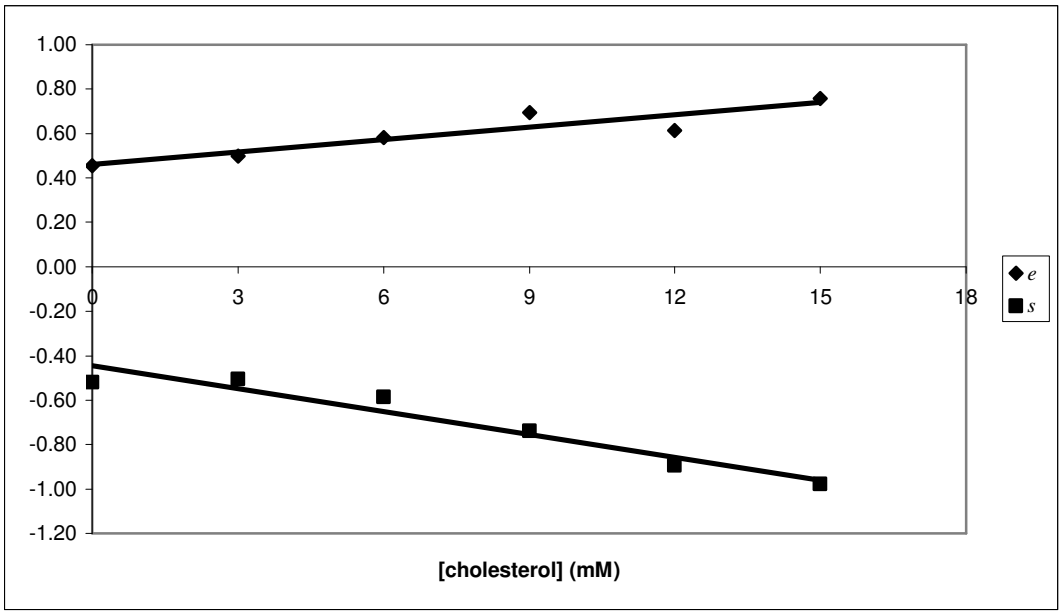

Figure 4.8 – Contribution of the lipid phase cohesiveness/solute volume term, vV, as a function of cholesterol content using 15 mM $DPPG_{20}DPPC_{80}$ with 0, 3, 6, 9, 12, and 15 mM cholesterol for benzene, acetophenone, and p-cresol.

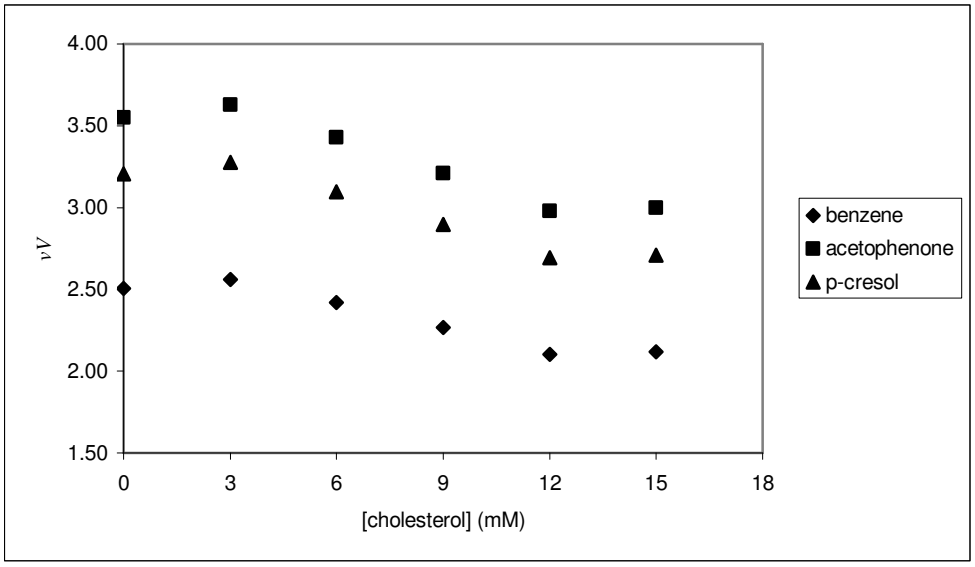

Figure 4.9 - Contribution of dipolar interactions term, sS, polarizability interactions term, eE, and net dipolar/polarizability interactions, $eE+sS$, as a function of cholesterol content using 15 mM $DPPG_{20}DPPC_{80}$ with 0, 3, 6, 9, 12, and 15 mM cholesterol for benzene.

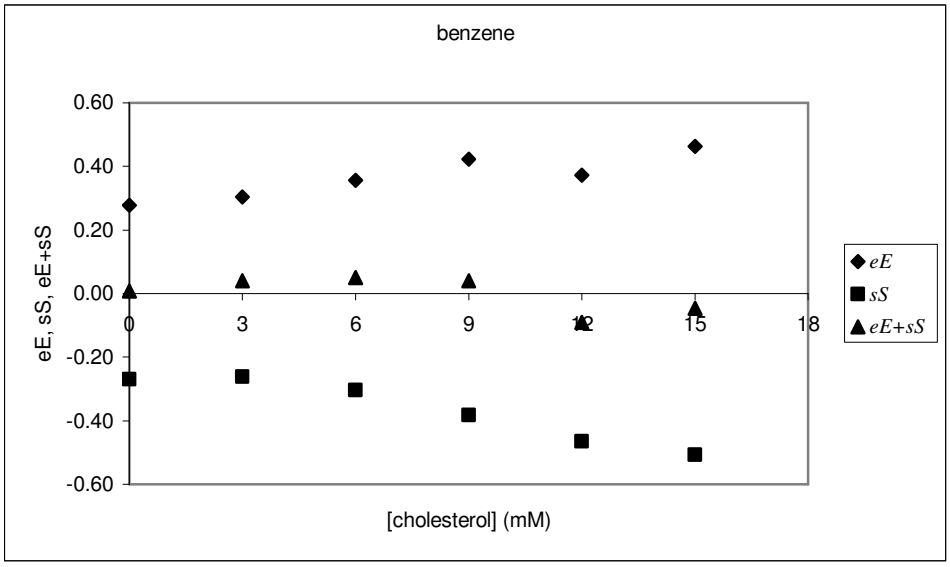

Figure 4.10 - Contribution of dipolar interactions term, sS, polarizability interactions term, eE, and net dipolar/polarizability interactions, $eE+sS$, as a function of cholesterol content using 15 mM $DPPG_{20}DPPC_{80}$ with 0, 3, 6, 9, 12, and 15 mM cholesterol for acetophenone.

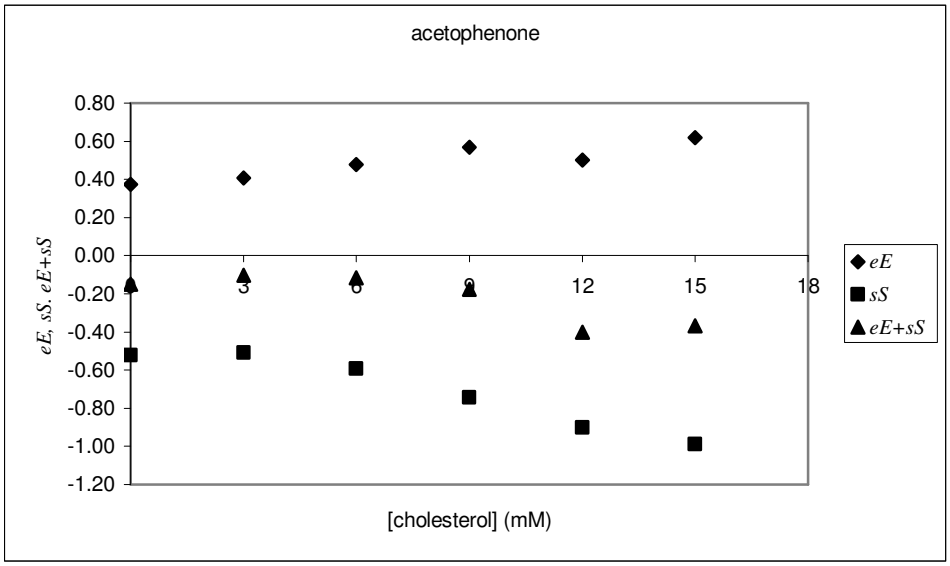

Figure 4.11 - Contribution of dipolar interactions term, sS, polarizability interactions term, eE, and net dipolar/polarizability interactions, $eE+sS$, as a function of cholesterol content using 15 mM $DPPG_{20}DPPC_{80}$ with 0, 3, 6, 9, 12, and 15 mM cholesterol for p-cresol.

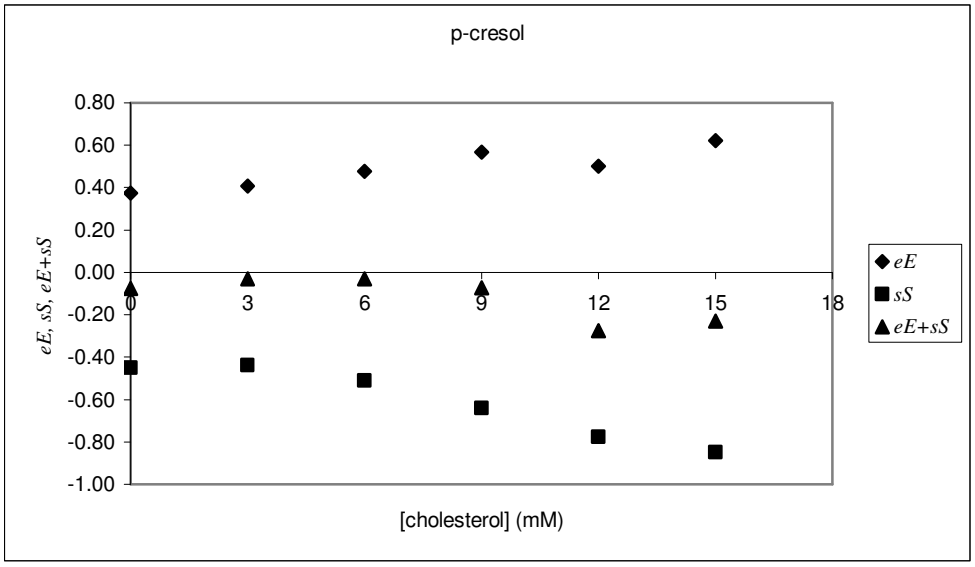

Figure 4.12 - Contribution of dipolar interactions term, sS, polarizability interactions term, eE, and net dipolar/polarizability interactions, $eE+sS$, as a function of cholesterol content using 15 mM $DPPG_{20}DPPC_{80}$ with 0, 3, 6, 9, 12, and 15 mM cholesterol for 1-methylnapthalene.

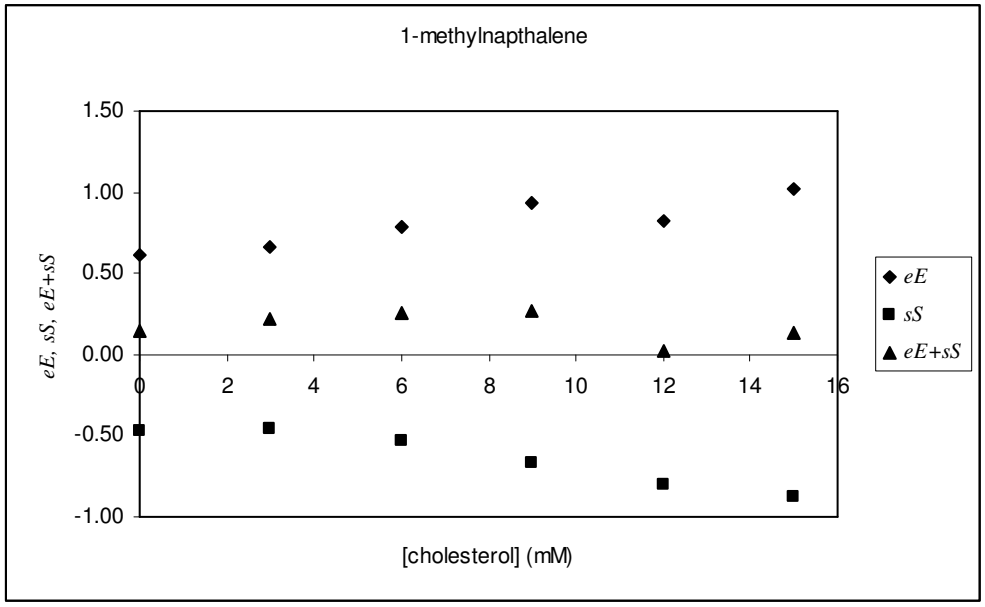

Figure 4.13 - Contribution of lipid phase hydrogen bond acceptor/solute hydrogen bond donor interactions term, aA, as a function of cholesterol content using 15 mM $DPPG_{20}DPPC_{80}$ with 0, 3, 6, 9, 12, and 15 mM cholesterol for aniline, phenol, and 3-bromophenol.

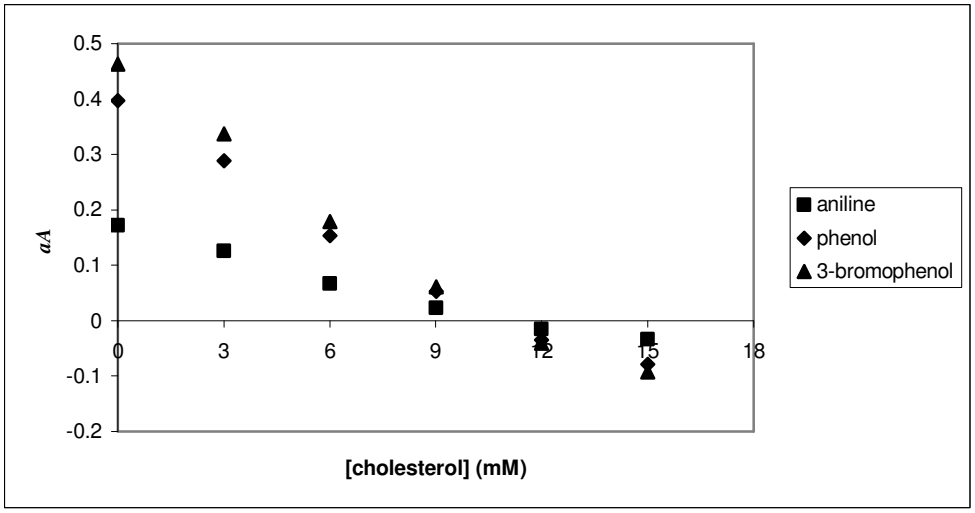

Chapter 5

Characterization of Novel Electrokinetic Chromatography Pseudostationary Phases Comprised of Vesicles Spontaneously Formed by Short-Chain and Long-Chain Lipids

Abstract

Aggregates formed spontaneously by mixing a short chain lipid (1,2-Dihexanoyl-*sn*-Glycero-3-Phosphocholine, DHPC, 6:0) and long chain lipids (1,2-Dipalmitoyl-*sn*-Glycero-3-[Phospho-*rac*-(1-glycerol)] (Sodium Salt), DPPG, 16:0 and 1,2-Dipalmitoyl-*sn*-Glycero-3-Phosphocholine, DPPC, 16:0) have been investigated as a pseudostationary phase for electrokinetic chromatography (EKC). The size of these vesicles as a function of the short-chain lipid, DHPC, content was determined by dynamic light scattering. As a general trend, the size of these aggregates decreased with the addition of higher mole fractions of DHPC. The electroosmotic mobilities in experiments using aggregates formed by the short-chain lipids and long-chain lipids were very similar to those observed when liposomes prepared by extrusion were used as a pseudostationary phase. Additionally, the electroosmotic mobilities observed in the presence of any lipid phase was generally smaller than those observed in the absence of a lipid phase; this effect is likely caused by partial modification of the capillary by the lipid phase. Electrophoretic mobilities of the lipid phases were generally similar as well. Retention of neutral solutes in an EKC system using these vesicles as a pseudostationary phase was determined as a function of the mole fraction of DHPC. Corrected retention factors for these solutes displayed a parabolic relationship with mole percent DHPC content. Using linear solvation energy relationships (LSER) models, this behavior is likely caused by changes in the lipid phase cohesiveness, hydrogen bond donor ability, and dipolarity that occur as a function of DHPC content. Finally, all of the retention factors determined using DPPG/DHPC/DPPC vesicle phases exhibit high correlation with those determined for 15 mM $DPPG_{20}DPPC_{80}$ liposomes prepared by extrusion.

Introduction

Amphiphilic molecules are comprised of a polar hydrophilic “head” group attached to a non-polar hydrophobic “tail” group. When such molecules are present above a specific concentration, referred to as the critical aggregation concentration (CAC) or the critical micelle concentration (CMC), they form colloidial aggregates. These aggregates arrange into a structure that allows the hydrophobic moieties to group together in order to minimize their unfavorable interactions with the surrounding

bulk aqueous medium while maximizing the interaction of the hydrophilic moieties with the surrounding bulk aqueous medium. As the hydrophilic head groups often possess a non-zero charge, the aggregates adopt a spherical structure to minimize electrostatic repulsion between like charged head groups. Israelachvili et al. correlated the formation of bilayers and micelles with the ratio of the volume of the hydrophobic chain group and the cross-sectional area of the head group; as this ratio increases, bilayer formation is favored over micelle formation.[1,2] As bilayer formation minimizes unfavorable interactions of the constituent hydrophobic tail groups with the bulk aqueous phase, the folding of flat bilayer sheets into spherical vesicles around an aqueous core completely eliminates the unfavorable interactions.

Naturally occurring and synthetic long-chain (chain length ≥ C_9) phospholipids spontaneously form multilamellar vesicles (MLVs) when dispersed in an aqueous solution. MLVs consist of five or more concentric phospholipid bilayers wrapped around an aqueous core and range from 100-1000 nm in diameter. Accordingly, MLVs are characterized by heterogenous size distributions. MLVs may be converted to small or large unilamellar vesicles (SUVs or LUVs) by processes such as extrusion or sonication. SUVs and LUVs are characterized by relatively homogenous size distributions. Conversely, synthetic short-chain (chain length < C_9) phospholipids spontaneously form micelles when dispersed in an aqueous solution. Micelles are generally between 3 nm and 10 nm in diameter with heterogenous size distributions.[3]

Gabriel and Roberts have shown that aqueous mixture of long-chain lipids with a chain length longer than C_{13} and short-chain lipids spontaneously form unilamellar vesicles.[4] These vesicles have been characterized by ^{1}H NMR[4], fluorescence microscopy[4], and electron microscopy[5]. They have been shown to be 10-100 nm in diameter with homogenous size distributions.[5] In a very narrow window of experimental conditions, mixtures of short-chain lipids and long-chain lipids form disc-shaped bilayered micelles, or “bicelles.” The main applications for bicelles are nuclear magnetic resonance (NMR) studies of membrane proteins that denature or change conformation outside of a lipid matrix. Traditional bilayered membranes, such as vesicles and liposomes, are not suitable for these studies because they produce broad NMR resonances that interfere with resonances from the protein. Bicelles, however, are aligned in magnetic fields due to their unique shape and therefore produce very high resolution NMR signals.[6,7] Sternin, Nizza, and Gawrisch determined by NMR that in DHPC/DMPC mixtures, bicelles only form in the temperature range of 34-36 ^{o}C. Outside of this range, mixed micelles and vesicles likely form.[8]

The current study investigates the use of vesicles formed from the short-chain lipid 1,2-Dihexanoyl-*sn*-Glycero-3-Phosphocholine (DHPC, 6:0) and the long-chain lipids 1,2-Dipalmitoyl-*sn*-Glycero-3-[Phospho-*rac*-(1-glycerol)] (Sodium Salt) (DPPG, 16:0) and 1,2-Dipalmitoyl-*sn*-Glycero-3-

Phosphocholine (DPPC, 16:0) as a pseudostationary phase for electrokinetic chromatography (EKC). Previous studies in the Khaledi research group have focused on other membrane-based pseudostationary phases for EKC including dihexadecyldimethylammonium bromide (DHAB) vesicles[9], dihexadecylphosphate (DHP) vesicles[10,11] and phospholipid liposomes.[12,13] Other groups have also investigated membrane-based pseudostationary phases. Foley et al. have demonstrated separations and octanol/water partition coefficient predictions using vesicles spontaneously formed from a pair of oppositely charged, single-tailed surfactants such as sodium dodecyl sulfate (SDS) and n-dodecyltrimethylammonium bromide (DTAB).[14,15] Foley et al. have also compared this system with micelles and liposomes using linear solvation energy relationships models.[16] Wiedmer et al. have reported the use of liposomes containing various zwitterionic and anionic lipids, as well as cholesterol, as pseudostationary phases.[17,18] Vesicles formed from (1R,2S)-(-)-N-dodecyl-N-methyl-ephedrinium bromide, a chiral cationic surfactant, have been used for enantioseparations of various nonsteroidal anti-inflammatory drugs.[19] Although bicelles seem to have no advantages over other bilayer-based pseudostationary phases, studies using bicellar pseudostationary phases have been published. Holland and Leigh have demonstrated separations of a homologous series of beta blockers and a set of cationic peptides using bicelles formed from DMPC and DHPC.[20] Holland and Mills have reported a study of the lipophilicity of three cationic peptides using a similar pseudostationary phase.[21]

In the current study, electrokinetic chromatography lipid phases comprised of DHPC, DPPG, and DPPC have been characterized using a variety of approaches. The average diameter of DPPG/ DHPC/DPPC vesicles has been studied using dynamic light scattering (DLS). The electroosmotic mobilities and electrophoretic mobilities of each lipid phase was also determined and compared to other systems. Retention properties of EKC pseudostationary phases comprised of DPPG/ DHPC/DPPC vesicles have been studied as a function of total lipid concentration and DHPC content. Finally, the retention properties of DPPG/DHPC/DPPC vesicles have been compared with analogous liposome EKC pseudostationary phases prepared by extrusion.

Experimental

Refer to **Chapter 2** for experimental procedures and details concerning chemicals, liposome and vesicle preparation, dynamic light scattering, sample preparation, electrokinetic chromatography, calculation of retention factors, and determination of linear solvation energy relationships (LSER) models.

Results and Discussion

Visual Observations

As mentioned previously, the dispersion of long-chain lipids such as DPPC and DPPG in an aqueous medium results in a milky solution that is characteristic of solutions of MLVs. Such solutions are not optically clear. Mixing of DPPG, DHPC, and DPPC in an aqueous medium result in a spontaneously optically clear solution. Optical clarity suggests that this solution consists of lipid mixed micelles or vesicles.

Determination of Aggregate Size by Dynamic Light Scattering

The average diameter of aggregates formed using DPPG, DHPC, and DPPC was determined by dynamic light scattering. Summaries of this data as well as the average diameter of 15 mM $DPPG_{20}DPPC_{80}$ liposomes formed by both sonication and extrusion are included in **Table 5.1**.

The general trend of the data presented in **Table 5.1** is different for aggregates with a total lipid concentration of 15 mM and a total lipid concentration of 25 mM. The size of the aggregates with a total lipid concentration of 15 mM decreases with the mole fraction of DHPC from 0.30 to 0.60 and then increases from 0.60 to 0.70. For aggregates formed using a total lipid concentration of 25 mM, the average diameter decreases dramatically from mole fractions of DHPC from 0.30 to 0.40 and then remains fairly consistent from 0.40 to 0.70. All of these aggregates are smaller than the liposomes prepared by sonication and extrusion. These trends are also shown in **Figure 5.1**.

The width of the size distribution, as determined by the standard deviation of the average diameter, describes the homogeneity of the population of aggregates. The standard deviations of the average diameters of the aggregates with DHPC mole fraction of 0.70 are much larger than the standard deviations of the measurements of aggregates with DHPC mole fractions of 0.30 to 0.60 for total lipid concentrations of both 15 mM and 25 mM. Dynamic light scattering experiments of heterogenous populations generally contain very large errors.[22] Therefore, these solutions are likely mixtures of heterogenous mixed micelles and multilamellar vesicles rather than homogenous unilamellar vesicles.

The size distribution for 15 mM $DPPG_{20}DHPC_{30}DPPC_{50}$ is characterized by a larger average diameter than any of the other measurements for DHPC mole fractions from 0.40 to 0.60. From this observation, this composition likely does not include enough DHPC to form unilamellar structures with all of the DPPG and DPPC. Therefore, this population likely consists of a mixture of mixed micelles and vesicles.

These size distributions indicate that most of these aggregates are likely vesicles. Spherical micelles are usually much smaller than these aggregates, with a diameter on the order of 3-10 nm.[23] The size distributions determined for most of these aggregates are on a similar order as the similarly formed vesicles investigated by Gabriel et al. using electron microscopy. In the same study, Gabriel et al. also observed decreasing vesicle diameter with increasing amount of short-chain lipid.[5]

Determination of Electroosmotic Mobility and Electrophoretic Mobility of Aggregates

The electroosmotic mobility and electrophoretic mobility of the aggregates studied were determined for vesicles prepared by extrusion and spontaneous aggregates of short-chain and long-chain lipids using the migration times of the unretained electroosmotic flow marker (methanol) and the hydrophobic lipid phase marker (octanophenone). Additionally, the electroosmotic mobility of a capillary zone electrophoresis system using 25 mM HEPES, pH=7.5 without liposomes was determined in a similar fashion. These values are included in **Table 5.2**.

The electroosmotic mobility determined in experiments using the different lipid phases were statistically the same for liposomes prepared by extrusion and aggregates of short-chain lipids and long-chain lipids. The electroosmotic mobilities determined for the different lipid phase systems is consistently smaller than that determined for the capillary zone electrophoresis system. This difference may be caused by differences in the ionic strength of the separation buffer with and without lipid phases and/or by modification of the capillary walls by the lipid phase. Modification of fused silica capillaries used for capillary electrophoresis has been previously demonstrated. Lucy et al. used capillaries coated with zwitterionic lipids in order to prevent protein adsorption in capillary electrophoresis studies and allow separation of anionic and cationic proteins in one run.[24] Riekkola et al. have reported separations of neutral compounds using fused silica capillaries coated with anionic lipids.[25] In both of these studies, reduced electroosmotic flow was noted for the coated capillaries relative to bare capillaries.

The electrophoretic mobilities determined for the liposomes prepared by extrusion and the aggregates formed by short-chain lipids and long-chain lipids are also very statistically similar. The aggregates with the larger average diameters, such as the liposomes formed by extrusion and 15 mM $DPPG_{20}DHPC_{30}DPPC_{50}$, generally displayed slightly lower electrophoretic mobilities. The electrophoretic mobility of any particle, including liposomes and other aggregates, is directly related to the charge-to-size ratio (q/r) of the particle.[26] Therefore, the charge-to-size ratio of these lipid phases is generally very similar, most likely because they all include the same mole fraction of anionic lipid,

ie. X_{DPPG}=0.20. Variability in this data may indicate differential interactions of aggregates with the capillary wall.

Study of Retention as a Function of Total Lipid Concentration

The retention factors of the homologous series of alkylphenones 5 mM, 10 mM, 15 mM, 20 mM, 30 mM and 40 mM $DPPG_{20}DHPC_{50}DPPC_{30}$. A plot of these retention factors as a function of total lipid concentration is included in **Figure 5.2**. From this plot, the linear relationship between the retention factors and total lipid concentration for each solute intersects the x-axis near total lipid concentration of 0 mM.

Similar linear relationships have been shown for EKC experiments micelles (SDS)[27], DHP vesicles[11], and phospholipid liposomes[13] as pseudostationary phases. In the case of SDS micelles, the linear relationship between the retention factors and total lipid concentration intersects the x-axis at approximately 10 mM, which is taken to be the CMC of SDS at the given conditions.[27] For DHP vesicles and phospholipid liposomes, this relationship intersects the x-axis at approximately 0 mM which is an approximation of the very small CAC of DHP and phospholipids. All of these observations can be explained using the definition of the retention factor:

$$k = K\Phi = K\left(\frac{\nu(C_{lipid} - CAC)}{1 - \nu(C_{lipid} - CAC)}\right) \qquad \textbf{Equation 5.7}$$

When the total lipid concentration is equal to the CAC, the phase ratio, and therefore the retention factor approaches zero.

In the case of $DPPG_{20}DHPC_{50}DPPC_{30}$, it is questionable that this method can provide an accurate estimation of the CAC of the lipid phase. Gabriel and Roberts showed that very dilute solutions of short-chain lipids and long-chain lipids can result in short-chain lipid monomers and multilamellar vesicles.[4] Therefore, it is possible that retention could occur at a lipid concentration where spontaneous vesicles were not formed due to the formation of multilamellar vesicles consisting of only DPPG and DPPC. For this reason, a different method should be used to determine the CAC of these lipid phases.

Electrokinetic chromatography experiments were conducted using lipid phases with mole fractions of DHPC from 0.30 to 0.70 and a total lipid concentration of 25 mM in order to approximate the solutions used by Gabriel, et al. to form stable vesicles from short-chain lipids and long-chain lipids.[4-5] These preliminary experiments were performed using 20 test solutes that represented a subset of the solutes used to generate LSER models. Reproducible chromatographic performance and retention

factors were obtained for each of these different lipid solutions. Retention factors obtained for these preliminary experiments are included in **Table 5.3**.

In a second set of experiments, retention factors were generated for the same 20 test solutes using lipid phases with mole fractions of DHPC from 0.30 to 0.70 and a total lipid concentration of 15 mM. Reproducible chromatographic performance and retention factors were obtained for each of these different lipid solutions as well. Retention factors obtained for these preliminary experiments, as well as retention factors for an additional set of solutes used to generated LSER models, are included in **Table 5.4**.

As would be expected for EKC experiments, very high correlation (>0.994) was observed between retention factors measured for 15 mM and 25 mM solutions with the same DHPC content. Therefore, the only difference in retention factors for 15 mM and 25 mM solutions with the same DHPC content is the phase ratio. A plot displaying this high correlation for 15 mM $DPPG_{20}DHPC_{50}DPPC_{30}$ and 25 mM $DPPG_{20}DHPC_{50}DPPC_{30}$ are included as **Figure 5.3**. Values of the slopes, intercepts, and correlation coefficients for the comparison of the other lipid phases are included in **Table 5.5**.

Study of Retention as a Function of DHPC Content

LSER models were generated using the entire set of 50 solutes. The LEKC retention factors used to determine LSER models for all of these lipid phases are included in **Table 5.4**. The LSER system coefficients determined for each of these lipid phases are included in **Table 5.6.**

The LSER system coefficients determined for these lipid systems are statistically very similar. The most significant system coefficients in each of these models are b and v. For all of these models, the b coefficient is negative and large in magnitude. Therefore, all of these lipid systems are very poor hydrogen bond donors relative to the aqueous phase. Any lipid phase hydrogen bond donor ability is due to the hydration of the lipid interfacial region.[28] The water molecules that hydrate the lipid interfacial region are bound to the polar headgroup moieties. Therefore, these water molecules do not have the same properties as bulk water and cannot act as hydrogen bond donors like those in bulk aqueous phase. The v coefficients are all large and positive; the lipid phases are all less cohesive and more “hydrocarbon-like” than the aqueous phase. The regression constant, C, is also large and negative. This term contains information about the phase ratio of the lipid pseudostationary phase.

In order to compare the partitioning of solutes as a function of DHPC content, corrected retention factors, log $k_{corrected}$, were calculated for the 20 test solutes used for preliminary EKC studies as described in **Chapter 4**. These values are included in **Table 5.7**. The corrected retention factors of

the 20 test solutes used for preliminary EKC studies were plotted as a function of DHPC content (**Figures 5.4-5.8**). For all 20 solutes, the same general parabolic trend was noted. Retention factors increase from the mole fraction of DHPC of 0.30 to a maximum at the mole fraction of DHPC of 0.50 and then decrease from 0.50 to 0.70.

The rest of the LSER system coefficients, e, s, and a, are relatively small, but still statistically significant. The small and positive a term signifies that these lipid phases are marginally better hydrogen bond acceptors than the aqueous phase. The hydrogen bond accepting ability of these lipid phases may be attributed to the cationic center of the zwitterionic lipids DHPC and DPPC.[12] The s coefficient is small and negative. Any lipid phase dipolar character is caused by the same water molecules that are responsible for the lipid phase hydrogen bond donor ability. Similarly, this water is less dipolar than bulk water due to their attachment to the polar lipid headgroup moieties. Finally, the small and positive e term denotes that the lipid phases have a slightly greater ability to interact with solute *n*- and *π*- electrons relative to the aqueous phase. This term is generally considered to be a polarizability correction term that accounts for any polarizability not considered by the s term.

The v, b, and s coefficients all exhibit a roughly parabolic relationship with mole percent DHPC. These trends are shown in **Figures 5.9-5.11**. The b and s coefficients both decrease from 30% DHPC to 50% DHPC and increase from 50% DHPC to 70% DHPC. The v term increases from 30% DHPC to 50% DHPC and decreases from 50% DHPC to 70% DHPC. These three terms cause the parabolic behavior of the corrected retention factors as a function of mole percent DHPC content. Neither the e or a terms show obvious trends with mole percent DHPC composition.

Despite the subtle differences in the LSER models of the lipid phases with different mole percent DHPC content, there is very little difference in the selectivity of the different lipid phases. A cross-correlation matrix, included in **Table 5.8**, shows very high correlation ($R^2 \geq 0.99$) between the retention factors of all 50 LSER solutes determined using liposomes prepared by extrusion and lipid phases with X_{DHPC}=0.30 to 0.70.

Comparison with Liposomes Prepared by Extrusion

Selectivity in all of the lipid phases composed of DPPG, DHPC, and DPPC is also very similar to that of 15 mM $DPPG_{20}DPPC_{80}$ liposomes prepared by extrusion. LSER system coefficients for 15 mM $DPPG_{20}DPPC_{80}$ liposomes prepared by extrusion determined using the same solute set (n=50) are included in **Table 5.6**. The same general trends are apparent in the LSER models for all of these lipid phases; the LSER models for all of these phases are dominated by a large positive v coefficient and large negative b and c coefficients. The magnitude of the positive v coefficient for the extruded

liposome system is significantly larger than those for the DPPG, DHPC, and DPPC phases. Therefore, the DPPG, DHPC, and DPPC phases are significantly more cohesive than the extruded liposome phase. Likewise, the magnitude of the negative b coefficient for the extruded liposome system is significantly larger than those for the DPPG, DHPC, and DPPC phases. The extruded liposome phase has less hydrogen bond donor ability than the DPPG, DHPC, and DPPC phases. Finally, the magnitude of the negative C constant for the extruded liposome system is significantly larger than those for the DPPG, DHPC, and DPPC phases. Therefore, the chromatographic phase ratios of the DPPG, DHPC, and DPPC phases are larger than that of the extruded liposome phase.

Even though the LSER models for these two sets of pseudostationary phases have subtle differences, the retention factors determined using the lipid phases composed of DPPG, DHPC, and DPPC and extruded liposomes are highly correlated. **Table 5.9** contains correlation coefficients (R^2) for the retention factors (expressed as log k) determined for of DPPG, DHPC, and DPPC and extruded liposomes for the entire LSER solute set. All of the retention factors display high correlation ($R^2 \geq 0.98$).

Conclusions

In conclusion, the current study explores the use of vesicles spontaneously formed from DPPG, DHPC, and DPPC as a pseudostationary phase for electrokinetic chromatography. Dynamic light scattering studies have shown that that average diameter of these vesicles depends on both total lipid concentration and the mole percentage of DHPC included. The electroosmotic mobilities in experiments using aggregates formed by the short-chain lipids and long-chain lipids were very similar to those observed when liposomes prepared by extrusion were used as a pseudostationary phase. Additionally, the electroosmotic mobilities observed in the presence of any lipid phase was generally smaller than those observed in the absence of a lipid phase; this effect is likely caused by partial modification of the capillary by the lipid phase. Electrophoretic mobilities of the lipid phases were generally similar as well. The retention properties of these lipid phases have been investigated as a function of total lipid concentration and DHPC content. Retention factors determined for $DHPC_{50}DPPG_{20}DPPC_{30}$ vesicle systems displayed a linear relationship with total lipid concentration over a range from 5 mM-40 mM. These relationships intersected with the x-axis at 0 mM, but this may not represent an accurate estimation of the CAC of this lipid phase. Retention factors determined for 15 mM $DPPG_{20}DHPC_{30}DPPC_{50}$, 15 mM $DPPG_{20}DHPC_{40}DPPC_{40}$, 15 mM $DPPG_{20}DHPC_{50}DPPC_{30}$, 15 mM $DPPG_{20}DHPC_{60}DPPC_{20}$, and 15 mM $DPPG_{20}DHPC_{70}DPPC_{10}$ display a parabolic relationship with mole percent DHPC content. From LSER studies, this behavior is likely caused by changes in the lipid phase cohesiveness, hydrogen bond donor ability, and dipolarity that occur as a function of DHPC content. Finally, the retention behavior of all of the retention factors determined using

DPPG/DHPC/ DPPC vesicle phases exhibit high correlation with retention factors determined for 15 mM $DPPG_{20}DPPC_{80}$ liposomes prepared by extrusion.

Works Cited

1. Israelachvili, J.; Mitchell, D.; Ninham, B.E. Theory Of Self-Assembly Of Hydrocarbon Amphiphiles Into Micelles And Bilayers. *J. Chem. Soc., Faraday Trans.* **1976**, *72*, 1525-1568.
2. Israelachvili J.N.; Mitchell D.J.; Ninham B.W. Theory Of Self-Assembly Of Lipid Bilayers And Vesicles. *Biochim. Biophys. Acta.* **1977,** *470* (2), 185-201.
3. Tausk, R.J.M.; Overbeek, J.T. Physical-Chemical Studies Of Short-Chain Lecithin Homologs .4. Simple Model For Influence Of Salt And Alkyl Chain-Length On Micellar Size. *Biophys. Chem*. **1974**, *2* (2), 175-179.
4. Gabriel, N.E.; Roberts, M.F. Spontaneous Formation of Unilamellar Vesicles. *Biochemistry.* **1984**, *23*, 4011-4015.
5. Gabriel, N.E.; Roberts, M.F. Interaction of Short-Chain Lecithin with Long-Chain Phospholipids: Characterization of Vesicles That Form Spontaneously. *Biochemistry.* **1986**, *25*, 2812-2821.
6. Sanders, C.R.; Prosser, R.S. Bicelles: a model membrane system for all seasons? *Structure*, **1998**, *6*, 1227-1234.
7. Luchette, P.A.; Vetman, T.N.; Prosser, R.S.; Hancock, R.E.W.; Nieh, M.P.; Glinka, C.J.; Krueger, S.; Katsaras, J. Morphology of fast-tumbling bicelles: a small angle neutron scattering and NMR study. *Biochim. Biophys. Acta*. **2001**, *1513*, 83-94.
8. Sternin, E.; Nizza, D.; Gawrisch, K. Temperature Dependence of DMPC/DHPC Mixing in a Bicellar Solution and Its Structural Implications. *Langmuir*. **2001**, *17*, 2610-2616.
9. Agbodjan, A.A.; Khaledi, M.G. Study of solute partitioning into cationic vesicles of dihexadecyldimethylammonium bromide using electrokinetic chromatography. *J. Chrom. A.* **2003**, *1004* (1-2), 145-153
10. Agbodjan, A.A.; Bui, H.H.; Khaledi, M.G. Study of solute partitioning in biomembrane-mimetic pseudophases by electrokinetic chromatography: Dihexadecyl phosphate small unilamellar vesicles. *Langmuir*. **2001**, *17* (10), 2893-2899.
11. Bui, H.H. Determination of vesicle-water partition coefficients by electrokinetic chromatography: Study of temperature effect. *J. Colloid. Interf. Sci.* **2002**, *253* (2), 397-401.
12. Burns, S.T.; Agbodjan, A.A.; Khaledi, M.G. Characterization of solvation properties of lipid bilayers membranes in liposome electrokinetic chromatography. *J. Chrom. A*. **2002**, *973*, 167-176.
13. Burns, S.T.; Khaledi, M.E. Rapid Determination of Liposome-Water Partition Coefficients (K_{lw}) Using Liposome Electrokinetic Chromatography (LEKC). *J. Pharm. Sci.* **2002,** *91* (7), 1601-1612.

14. Hong, M.; Weekley, B.S.; Grieb, S.J.; Foley, J.P. Electrokinetic chromatography using thermodynamically stable vesicles and mixed micelles formed from oppositely charged surfactants. *Anal. Chem.* **1998**, *70* (7), 1394-1403.
15. Klotz, W.L.; Schure, M.R. Foley, J.P. Rapid estimation of octanol-water partition coefficients using synthesized vesicles in electrokinetic chromatography. *J. Chrom. A*. **2002**, *962* (1-2), 207-219.
16. Pascoe, R.J.; Foley, J.P. Characterization of surfactant and phospholipid vesicles for use as pseudostationary phases in electrokinetic chromatography. *Electrophoresis*. **2003**, *24*, 4227-4240.
17. Wiedmer, S.K.; Holopainen, J.M.; Mustakangas, P.; Kinnunen, P.K.J.; Riekkola, M.L. Liposomes as carriers in electrokinetic chromatography. *Electrophoresis*. **2000**, *21* (15), 3191-3198.
18. Wiedmer, S.K.; Jussila, M.S.; Holopainen, J.M.; Alakoskela, J.M.; Kinnunen, P.K.J.; Riekkola, M.L. Cholesterol-containing phosphatidylcholine liposomes: Characterization and use as dispersed phase in electrokinetic capillary chromatography. *J. Sep. Sci.* **2002**, *25* (7), 427-437.
19. Dey, J.; Mohanty, A.; Roy, S.; Khatua, D. Cationic vesicles as chiral selector for enantioseparations of nonsteroidal anti-inflammatory drugs by micellar electrokinetic chromatography. *J. Chrom. A.* **2004**, *1048* (1), 127-132.
20. Holland, L.A.; Leigh, A.M. Bilayered phospholipid micelles and capillary electrophoresis: A new additive for electrokinetic chromatography. *Electrophoresis*. **2003**, *24*, 2935-2939.
21. Mills, L.O.; Holland, L.A. Membrane-mediated capillary electrophoresis: Interaction of cationic peptides with bicelles. *Electrophoresis*. **2004**, *25*, 1237-1242.
22. Hauser, H. Phospholipid Vesicles. In *Phospholipids Handbook*; Cevc, G.; Marcel Dekker, Inc.: New York, 1993; p 623.
23. The Guelph Biophysics Light Scattering Lab website
24. http://www.physics.uoguelph.ca/GBLL/
25. (accessed June 2004)
26. Cunliffe, J.M.; Baryla, N.E.; Lucy, C.A. Phospholipid Bilayer Coatings for the Separation of Proteins in Capillary eletrophoresis. *Anal. Chem*. **2002**, *74*, 776-783.
27. Hautala, J.T.; Linden, M.V.; Wiedmer, S.K.; Ryhanen, S.J.; Saily, M.J.; Kinnunen, P.K.J.; Riekkola, M.L. Simple coating of capillaries with anionic liposomes in capillary electrophoresis. *J. Chrom. A.* **2003**, *1004*, 81-90.
28. Roberts, M.A.; Locascio-Brown, L.; MacCrehan, W.A.; Durst, R.A. Liposome Behavior in Capillary Electrophoresis. *Anal. Chem.* **1996**, *68*, 3434-3440.

Table 5.1 – Dynamic light scattering data for DPPG/DHPC/DPPC lipid phases at 35 ^{o}C.

Lipid Composition	**X_{DHPC}**	**Average Diameter (nm)**
15 mM $DPPG_{20}DPPC_{80}$ (sonicated)	0	45.1±2.5
15 mM $DPPG_{20}DPPC_{80}$ (extruded)	0	68.9±2.0
15 mM $DPPG_{20}DHPC_{30}DPPC_{50}$	.30	35.0±2.0
15 mM $DPPG_{20}DHPC_{40}DPPC_{40}$	.40	16.0±1.1
15 mM $DPPG_{20}DHPC_{50}DPPC_{30}$	.50	13.3±0.3
15 mM $DPPG_{20}DHPC_{60}DPPC_{20}$	.60	8.3±0.3
15 mM $DPPG_{20}DHPC_{70}DPPC_{10}$	.70	196.9±12.1
25 mM $DPPG_{20}DHPC_{30}DPPC_{50}$	.30	14.1±0.8
25 mM $DPPG_{20}DHPC_{40}DPPC_{40}$	.40	7.7±1.1
25 mM $DPPG_{20}DHPC_{50}DPPC_{30}$	.50	8.3±0.2
25 mM $DPPG_{20}DHPC_{60}DPPC_{20}$	.60	9.9±1.3
25 mM $DPPG_{20}DHPC_{70}DPPC_{10}$	.70	31.5±14.0

Table 5.2 – Electroosmotic mobilities and electrophoretic mobilities determined in the presence of and absence of lipid phases. The capillary electrophoresis system used the same buffer system as the systems with lipid phases, 25 mM HEPES, pH=7.5.

Lipid Composition	**X_{DHPC}**	**Electroosmotic Mobility (μ_{eo}, 10^{-4} $cm^2/(V \cdot s)$)**	**Lipid Phase Electrophoretic Mobility (μ_{ep}, 10^{-4} $cm^2/(V \cdot s)$)**
Capillary Zone Electrophoresis		9.5±0.1	
15 mM $DPPG_{20}DPPC_{80}$ (extruded)	0	7.3±0.1	-4.12±0.01
15 mM $DPPG_{20}DHPC_{30}DPPC_{50}$	.30	8.5±0.1	-4.18±0.07
15 mM $DPPG_{20}DHPC_{40}DPPC_{40}$	.40	8.6±0.1	-3.71±0.03
15 mM $DPPG_{20}DHPC_{50}DPPC_{30}$	.50	8.7±0.1	-3.61±0.07
15 mM $DPPG_{20}DHPC_{60}DPPC_{20}$	.60	8.9±0.1	-3.81±0.05
15 mM $DPPG_{20}DHPC_{70}DPPC_{10}$	.70	8.7±0.1	-3.65±0.07
25 mM $DPPG_{20}DHPC_{30}DPPC_{50}$	.30	8.6±0.1	-3.78±0.03
25 mM $DPPG_{20}DHPC_{40}DPPC_{40}$	.40	7.4±0.3	-3.72±0.03
25 mM $DPPG_{20}DHPC_{50}DPPC_{30}$	.50	7.8±0.1	-3.47±0.04
25 mM $DPPG_{20}DHPC_{60}DPPC_{20}$	.60	9.0±0.1	-3.61±0.07
25 mM $DPPG_{20}DHPC_{70}DPPC_{10}$	.70	8.6±0.1	-3.51±0.05

Table 5.3 - EKC retention factors (expressed as log *k*) for 25 mM DPPG/DHPC/DPPC aggregates generated in preliminary experiments.

	Experimental log k 25 mM Total Lipid Concentration, 20 % DPPG				
Solute Name	**$DHPC_{30}DPPC_{50}$**	**$DHPC_{40}DPPC_{40}$**	**$DHPC_{50}DPPC_{30}$**	**$DHPC_{60}DPPC_{20}$**	**$DHPC_{70}DPPC_{10}$**
acetophenone	-0.47	-0.64	-0.67	-0.43	-0.45
benzene	-0.12	-0.28	-0.32	-0.10	-0.11
bromobenzene	0.70	0.59	0.50	0.74	0.68
butyl benzoate	1.35	1.13	1.17	1.31	1.23
butyrophenone	0.33	0.20	0.15	0.34	0.32
chlorobenzene	0.54	0.40	0.31	0.57	0.53
ethyl benzoate	0.30	0.14	0.12	0.32	0.30
ethylbenzene	0.77	0.66	0.53	0.81	0.79
hexanophenone	1.29	1.23	1.19	1.36	1.28
iodobenzene	0.94	0.85	0.76	1.02	0.93
m-cresol	0.04	-0.12	-0.11	0.05	0.00
methyl benzoate	-0.06	-0.22	-0.25	-0.04	-0.07
naphthalene	1.09	0.95	0.85	1.16	1.08
phenol	-0.28	-0.44	-0.44	-0.26	-0.31
propiophenone	-0.06	-0.24	-0.26	-0.04	-0.07
propyl benzoate	0.75	0.69	0.63	0.80	0.75
propylbenzene	1.27	1.13	1.01	1.35	1.30
p-xylene	0.82	0.70	0.59	0.86	0.82
toluene	0.37	0.20	0.15	0.38	0.37
valerophenone	0.80	0.75	0.67	0.81	0.78

Table 5.4 - EKC retention factors (expressed as log k) for 15 mM DPPG/DHPC/DPPC aggregates.

	Experimental log k **15 mM Total Lipid Concentration, 20 % DPPG**				
solute name	**$DHPC_{30}DPPC_{50}$**	**$DHPC_{40}DPPC_{40}$**	**$DHPC_{50}DPPC_{30}$**	**$DHPC_{60}DPPC_{20}$**	**$DHPC_{70}DPPC_{10}$**
1-methylnaphthalene	0.97	1.08	1.36	1.35	1.26
2-methoxypyridine	-1.14	-1.05	-1.04	-0.99	-0.94
3,5 dimethyl phenol	-0.02	0.01	0.04	0.08	0.07
3-bromophenol	0.39	0.48	0.51	0.49	0.46
3-chlorophenol	0.23	0.31	0.38	0.37	0.31
3-methyl benzyl alcohol	-0.79	-0.75	-0.70	-0.66	-0.62
3-phenylpropanol	-0.60	-0.56	-0.52	-0.46	-0.43
4-bromophenol	0.41	0.54	0.58	0.54	0.46
4-chloroacetophenone	-0.24	-0.14	-0.14	-0.07	-0.06
4-chloroanisole	0.27	0.38	0.38	0.46	0.45
4-chlorophenol	0.27	0.29	0.36	0.36	0.34
4-chlorotoluene	0.53	0.69	0.76	0.82	0.80
4-ethylphenol	0.09	0.12	0.16	0.16	0.16
4-fluoroacetohphenone	-0.74	-0.71	-0.67	-0.61	-0.56
4-fluorophenol	-0.37	-0.34	-0.31	-0.29	-0.31
4-methyl benzyl alcohol	-0.78	-0.75	-0.71	-0.66	-0.60
4-nitrotoluene	-0.20	-0.11	-0.11	-0.03	-0.03
acetophenone	-0.89	-0.85	-0.68	-0.68	-0.68
aniline	-1.06	-1.02	-1.01	-0.95	-0.91
benzaldehyde	-0.97	-0.91	-0.89	-0.81	-0.77

	Experimental log k 15 mM Total Lipid Concentration, 20 % DPPG				
benzene	-0.52	-0.48	-0.32	-0.36	-0.37
benzonitrile	-0.90	-0.85	-0.82	-0.76	-0.73
benzyl alcohol	-1.08	-1.01	-1.00	-0.97	-0.94
bromobenzene	0.21	0.31	0.50	0.46	0.44
butyl benzoate	0.76	0.91	1.10	1.08	0.99
butyrophenone	-0.09	-0.04	0.12	0.08	0.07
chlorobenzene	0.05	0.12	0.32	0.29	0.28
ethyl benzoate	-0.16	-0.11	0.08	0.07	0.03
ethylbenzene	0.26	0.39	0.59	0.54	0.52
hexanophenone	0.89	1.10	1.14	1.08	1.02
iodobenzene	0.46	0.61	0.78	0.72	0.70
m-cresol	-0.32	-0.35	-0.18	-0.22	-0.24
m-dichlorobenzene	0.60	0.78	0.89	0.94	0.88
methyl benzoate	-0.51	-0.46	-0.28	-0.28	-0.32
methyl-2-methyl benzoate	-0.13	-0.02	-0.03	0.07	0.07
naphthalene	0.62	0.70	0.90	0.87	0.82
nitrobenzene	-0.58	-0.50	-0.47	-0.43	-0.43
o-dichlorobenzene	0.61	0.75	0.80	0.83	0.85
o-xylene	0.30	0.40	0.43	0.54	0.51
p-cresol	-0.33	-0.30	-0.28	-0.22	-0.22
p-dichlorobenzene	0.47	0.68	0.76	0.78	0.71
phenethyl alcohol	-0.93	-0.88	-0.86	-0.79	-0.73
phenol	-0.66	-0.67	-0.49	-0.54	-0.55
phenyl acetate	-0.89	-0.84	-0.83	-0.74	-0.70

	Experimental log k 15 mM Total Lipid Concentration, 20 % DPPG				
phenyl benzoate	0.74	0.90	0.92	0.97	0.95
propiophenone	-0.49	-0.45	-0.28	-0.29	-0.31
propyl benzoate	0.30	0.38	0.56	0.55	0.48
propylbenzene	0.70	0.96	1.15	1.07	1.02
p-xylene	0.37	0.43	0.59	0.60	0.57
toluene	-0.12	-0.02	0.16	0.12	0.11
valerophenone	0.40	0.49	0.62	0.55	0.51

Table 5.5 – Correlation of retention factors for 20 solutes using 15 mM and 25 mM DPPG/DHPC/DPPC aggregates.

Lipid Composition	**Slope**	**Y-intercept**	**R^2**
$DPPG_{20}DHPC_{30}DPPC_{50}$	0.9349	-0.421	0.991
$DPPG_{20}DHPC_{40}DPPC_{40}$	1.003	-0.237	0.995
$DPPG_{20}DHPC_{50}DPPC_{30}$	1.021	-0.015	0.992
$DPPG_{20}DHPC_{60}DPPC_{20}$	0.986	-0.257	0.999
$DPPG_{20}DHPC_{70}DPPC_{10}$	0.988	-0.247	0.999

Table 5.6 – LSER system coefficients determined for 15 mM $DPPG_{20}DHPC_{30}DPPC_{50}$, 15 mM $DPPG_{20}DHPC_{40}DPPC_{40}$, 15 mM $DPPG_{20}DHPC_{50}DPPC_{30}$, 15 mM $DPPG_{20}DHPC_{60}DPPC_{20}$, and 15 mM $DPPG_{20}DHPC_{70}DPPC_{10}$.

Lipid Composition	***v***	***b***	***a***	***s***	***e***	***C***	
15 mM $DPPG_{20}DHPC_{30}DPPC_{50}$	3.00 (0.08)	-3.13 (0.08)	0.56 (0.05)	-0.47 (0.08)	0.46 (0.08)	-2.25 (0.08)	R^2_{adj}=0.98 SE=0.07 n=50
15 mM $DPPG_{20}DHPC_{40}DPPC_{40}$	3.14 (0.09)	-3.33 (0.09)	0.50 (0.05)	-0.48 (0.09)	0.46 (0.09)	-2.24 (0.09)	R^2_{adj}=0.98 SE=0.08 n=50
15 mM $DPPG_{20}DHPC_{50}DPPC_{30}$	3.26 (0.09)	-3.38 (0.09)	0.49 (0.06)	-0.73 (0.09)	0.59 (0.10)	-2.13 (0.09)	R^2_{adj}=0.98 SE=0.09 n=50
15 mM $DPPG_{20}DHPC_{60}DPPC_{20}$	3.18 (0.08)	-3.31 (0.08)	0.43 (0.05)	-0.62 (0.08)	0.54 (0.08)	-2.11 (0.08)	R^2_{adj}=0.99 SE=0.08 n=50
15 mM $DPPG_{20}DHPC_{70}DPPC_{10}$	3.01 (0.08)	-3.13 (0.08)	0.39 (0.05)	-0.61 (0.08)	0.55 (0.08)	-2.00 (0.08)	R^2_{adj}=0.98 SE=0.08 n=50
15 mM $DPPG_{20}DPPC_{80}$	3.50 (0.09)	-3.60 (0.10)	0.66 (0.06)	-0.52 (0.10)	0.46 (0.10)	-2.41 (0.09)	R^2_{adj}=0.98 SE=0.09 n=50

Table 5.7-Corrected retention factors, expressed as log $k_{corrected}$, determined for 20 neutral aromatic solutes used for preliminary studies with 15 mM $DPPG_{20}DHPC_{30}DPPC_{50}$, 15 mM $DPPG_{20}DHPC_{40}DPPC_{40}$, 15 mM $DPPG_{20}DHPC_{50}DPPC_{30}$, 15 mM $DPPG_{20}DHPC_{60}DPPC_{20}$, and 15 mM $DPPG_{20}DHPC_{70}DPPC_{10}$.

	Corrected log $k_{corrected}$ 15 mM Total Lipid Concentration				
Solute Name	**$DHPC_{30}DPPC_{50}$**	**$DHPC_{40}DPPC_{40}$**	**$DHPC_{50}DPPC_{30}$**	**$DHPC_{60}DPPC_{20}$**	**$DHPC_{70}DPPC_{10}$**
acetophenone	1.36	1.39	1.45	1.43	1.32
benzene	1.73	1.76	1.81	1.75	1.63
benzonitrile	1.35	1.39	1.31	1.35	1.27
bromobenzene	2.46	2.55	2.63	2.57	2.44
butyl benzoate	3.01	3.15	3.23	3.19	2.99
butyrophenone	2.16	2.20	2.25	2.19	2.07
chlorobenzene	2.30	2.36	2.45	2.40	2.28
ethyl benzoate	2.09	2.13	2.21	2.18	2.03
ethylbenzene	2.51	2.63	2.72	2.65	2.52
iodobenzene	2.71	2.85	2.91	2.83	2.70
m-cresol	1.93	1.89	1.95	1.89	1.76
methyl benzoate	1.74	1.78	1.85	1.83	1.68
naphthalene	2.87	2.94	3.03	2.98	2.82
phenol	1.59	1.57	1.64	1.57	1.45
propiophenone	1.76	1.79	1.85	1.82	1.69
propyl benzoate	2.55	2.62	2.69	2.66	2.48
propylbenzene	2.95	3.20	3.28	3.18	3.02
p-xylene	2.62	2.67	2.72	2.71	2.57

	Corrected log $k_{corrected}$ 15 mM Total Lipid Concentration				
Solute Name	**$DHPC_{30}DPPC_{50}$**	**$DHPC_{40}DPPC_{40}$**	**$DHPC_{50}DPPC_{30}$**	**$DHPC_{60}DPPC_{20}$**	**$DHPC_{70}DPPC_{10}$**
toluene	2.13	2.22	2.29	2.23	2.11
valerophenone	2.65	2.73	2.75	2.66	2.51

Table 5.8 – Cross-correlation matrix for retention factors determined using 15 mM $DPPG_{20}DHPC_{30}DPPC_{50}$, 15 mM $DPPG_{20}DHPC_{40}DPPC_{40}$, 15 mM $DPPG_{20}DHPC_{50}DPPC_{30}$, 15 mM $DPPG_{20}DHPC_{60}DPPC_{20}$, and 15 mM $DPPG_{20}DHPC_{70}DPPC_{10}$

	$DHPC_{30}DPPC_{50}$	**$DHPC_{40}DPPC_{50}$**	**$DHPC_{50}DPPC_{50}$**	**$DHPC_{60}DPPC_{50}$**	**$DHPC_{70}DPPC_{50}$**
$DHPC_{30}DPPC_{50}$	1.000				
$DHPC_{40}DPPC_{50}$	0.995	1.000			
$DHPC_{50}DPPC_{50}$	0.986	0.987	1.000		
$DHPC_{60}DPPC_{50}$	0.991	0.994	0.995	1.000	
$DHPC_{70}DPPC_{50}$	0.990	0.994	0.992	0.999	1.000

Table 5.9 – Correlation between 15 mM $DPPG_{20}DPPC_{80}$ liposomes prepared by extrusion and 15 mM $DPPG_{20}DHPC_{30}DPPC_{50}$, 15 mM $DPPG_{20}DHPC_{40}DPPC_{40}$, 15 mM $DPPG_{20}DHPC_{50}DPPC_{30}$, 15 mM $DPPG_{20}DHPC_{60}DPPC_{20}$, and 15 mM $DPPG_{20}DHPC_{70}DPPC_{10}$

	15 mM $DPPG_{20}DPPC_{80}$
15 mM $DPPG_{20}DHPC_{30}DPPC_{50}$	0.994
15 mM $DPPG_{20}DHPC_{40}DPPC_{40}$	0.992
15 mM $DPPG_{20}DHPC_{50}DPPC_{30}$	0.984
15 mM $DPPG_{20}DHPC_{60}DPPC_{20}$	0.986
15 mM $DPPG_{20}DHPC_{70}DPPC_{10}$	0.984

Figure 5.1 – Average diameters of DPPG/DHPC/DPPC lipid phases at 35 ^{o}C.

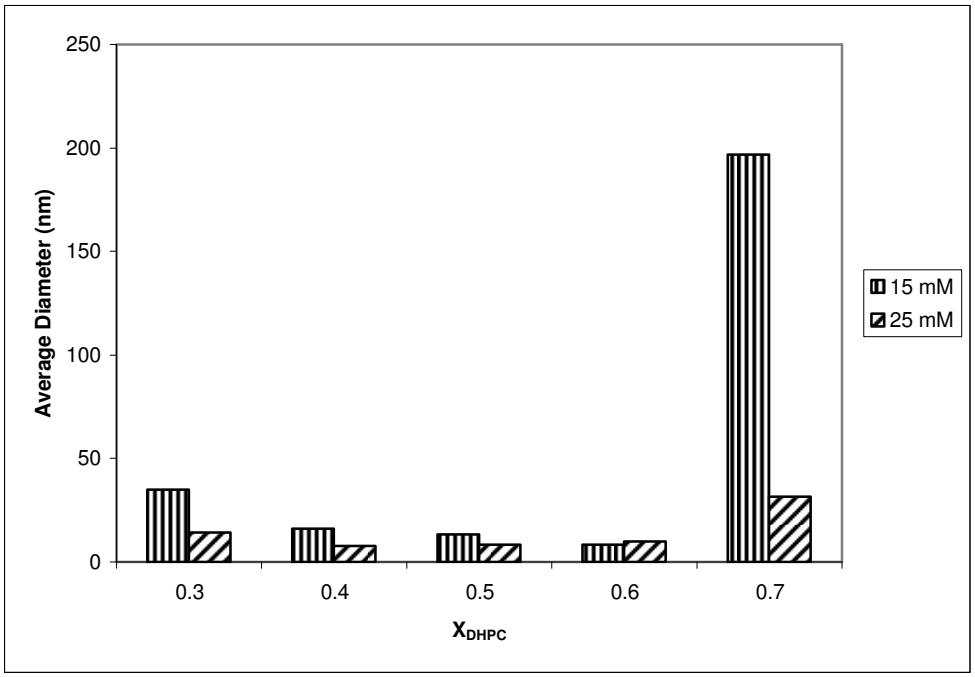

Figure 5.2 – Retention factors of acetophenone, propiophenone, and butyrophenone as a function of total lipid concentration for 5 mM, 10 mM, 15 mM, 20 mM, 30 mM and 40 mM $DPPG_{20}DHPC_{50}DPPC_{30}$

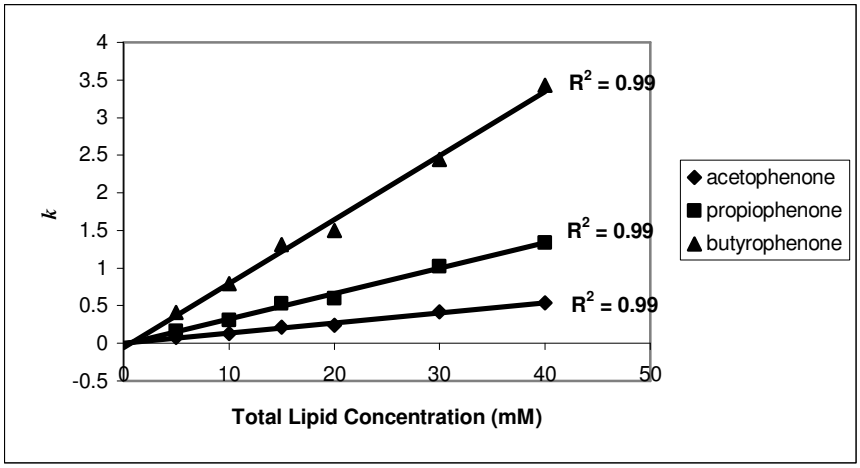

Figure 5.3 – Correlation of retention factors for 20 test solutes for 15 mM and 25 mM $DPPG_{20}DHPC_{50}DPPC_{30}$.

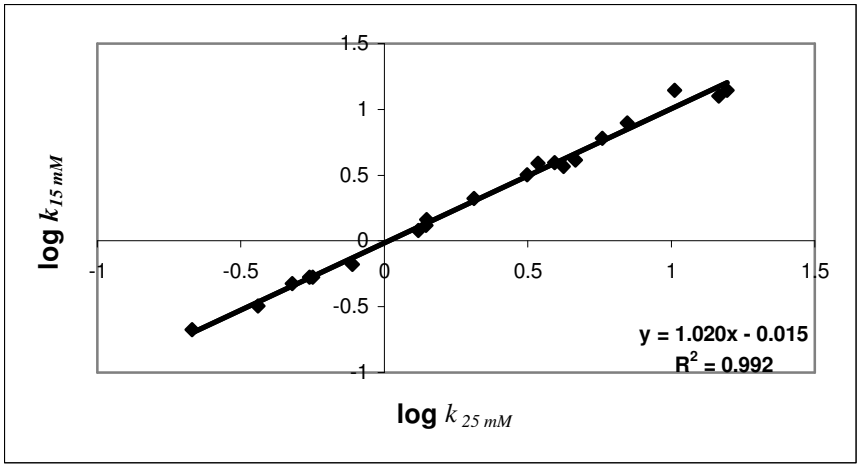

Figure 5.4 – Corrected retention factors (log $k_{corrected}$) for benzene, toluene, ethylbenzene, and propylbenzene as a function of mole fraction of DHPC.

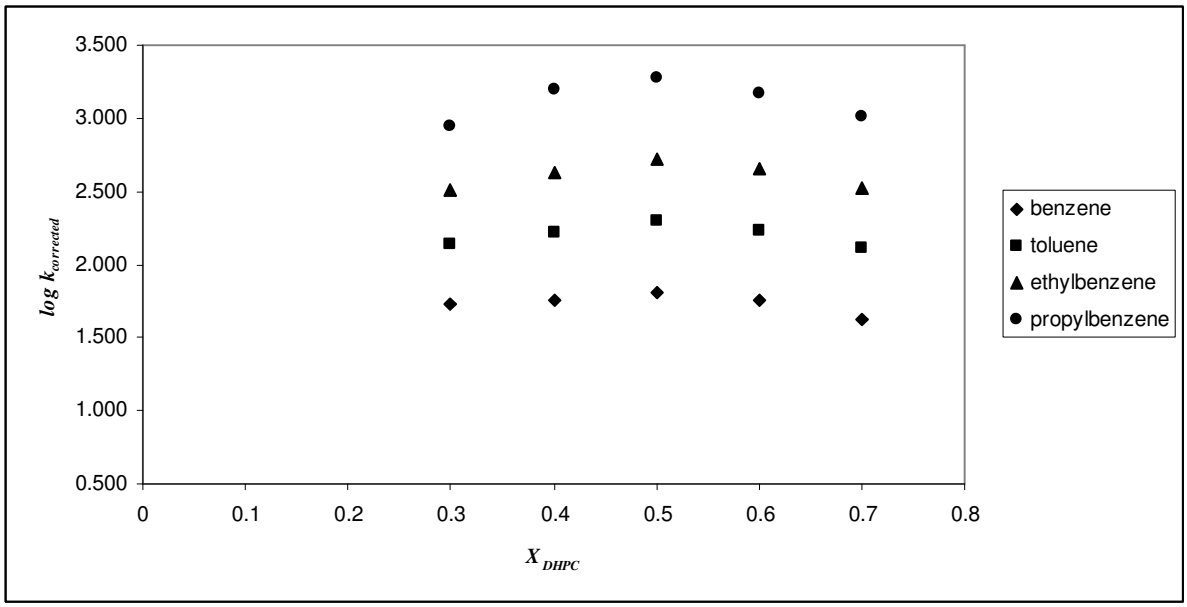

Figure 5.5 – Corrected retention factors (log $k_{corrected}$) for acetophenone, propiophenone, butyrophenone, valerophenone, and hexanophenone as a function of mole fraction of DHPC.

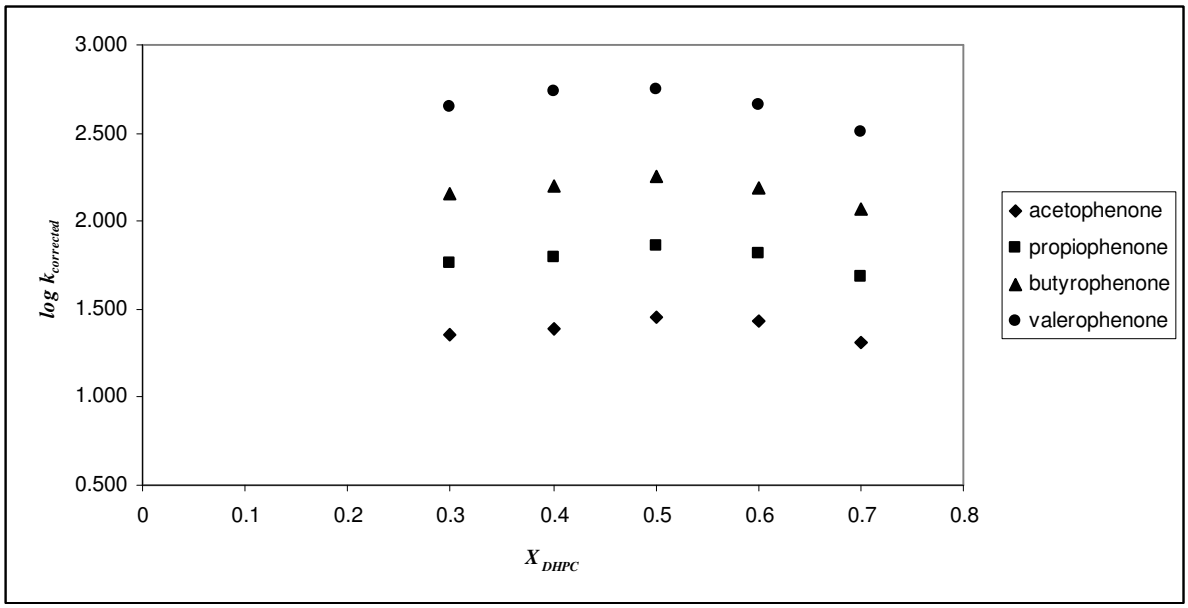

Figure 5.6 – Corrected retention factors (log $k_{corrected}$) for methyl benzoate, ethyl benzoate, propyl benzoate, and butyl benzoate as a function of mole fraction of DHPC.

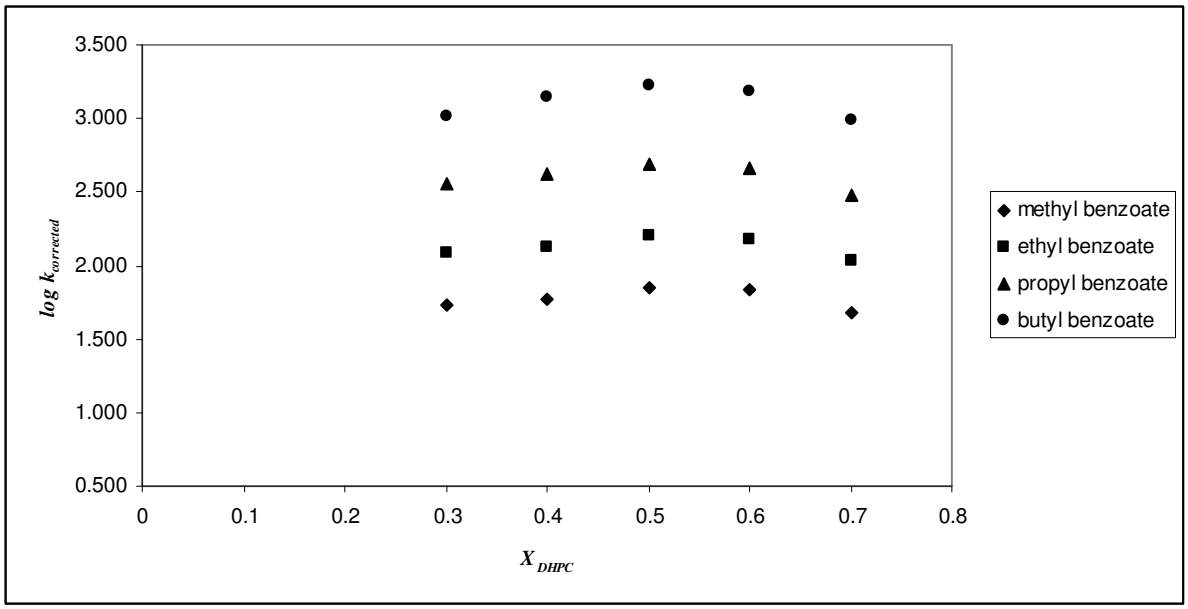

Figure 5.7 – Corrected retention factors (log $k_{corrected}$) for bromobenzene, chlorobenzene, and iodobenzene as a function of mole fraction of DHPC.

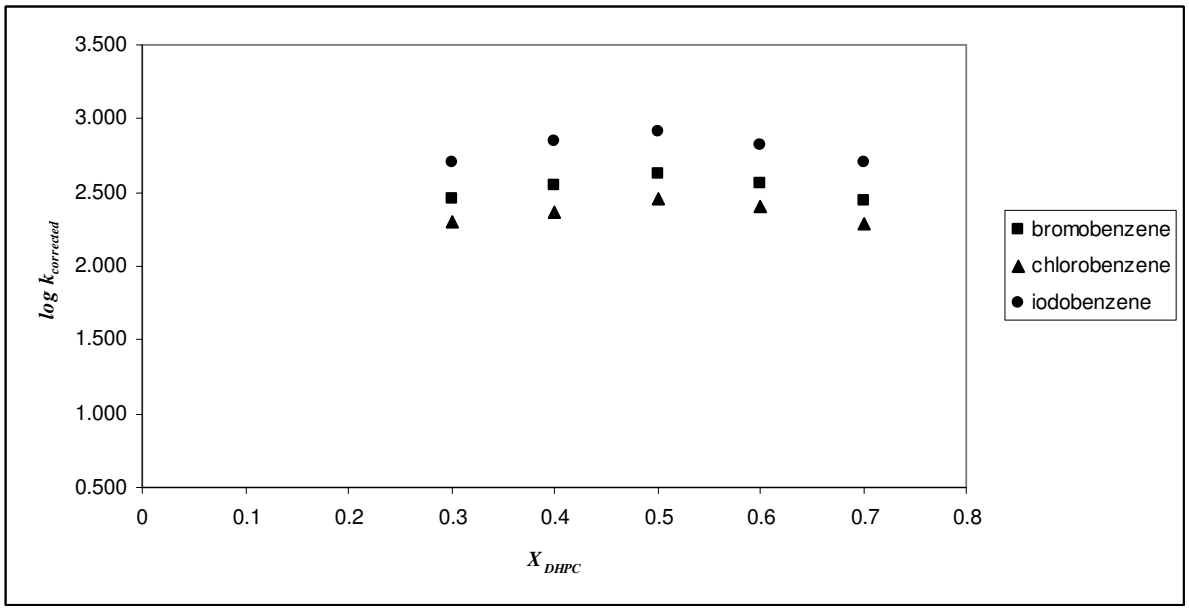

Figure 5.8 – Corrected retention factors (log $k_{corrected}$) for m-cresol, naphthalene, phenol, and p-xylene as a function of mole fraction of DHPC.

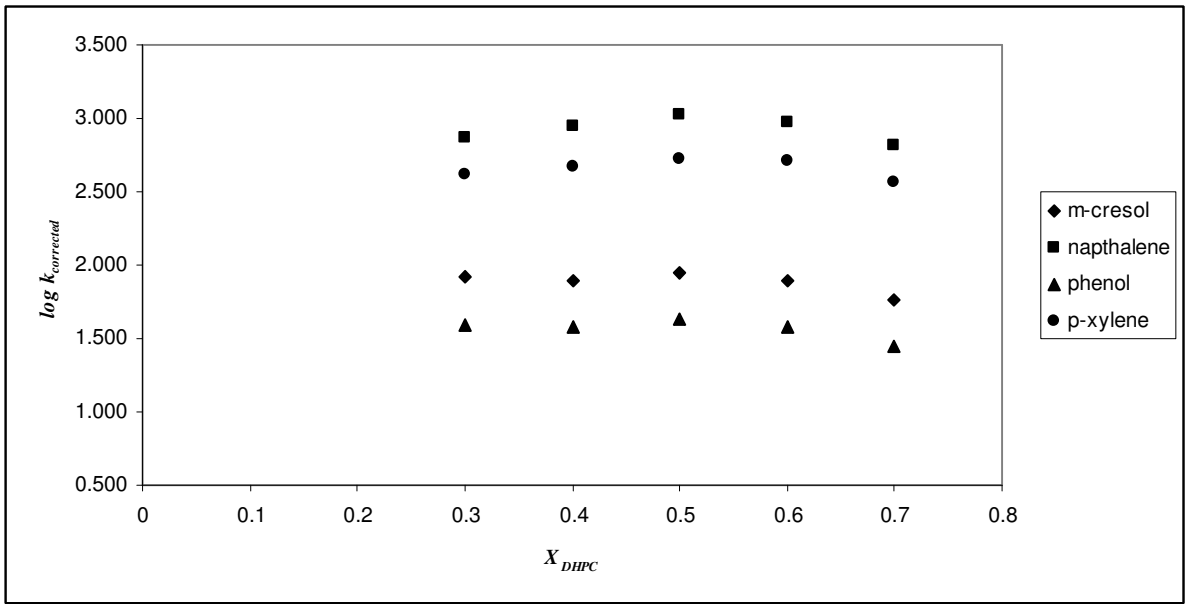

Figure 5.9 – LSER cohesiveness coefficient, v, as a function of mole fraction of DHPC.

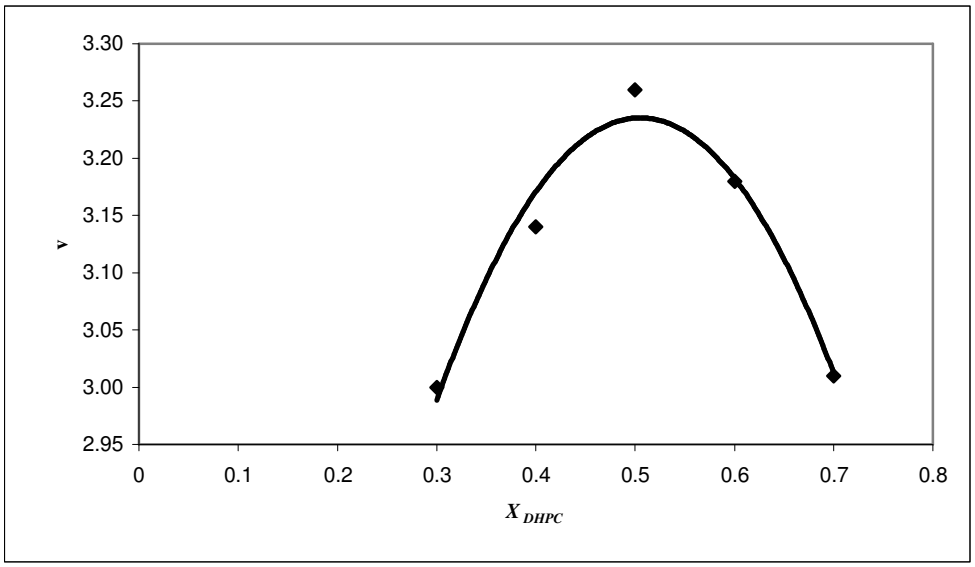

Figure 5.10 – LSER lipid phase hydrogen bond donating ability coefficient, b, as a function of mole fraction of DHPC.

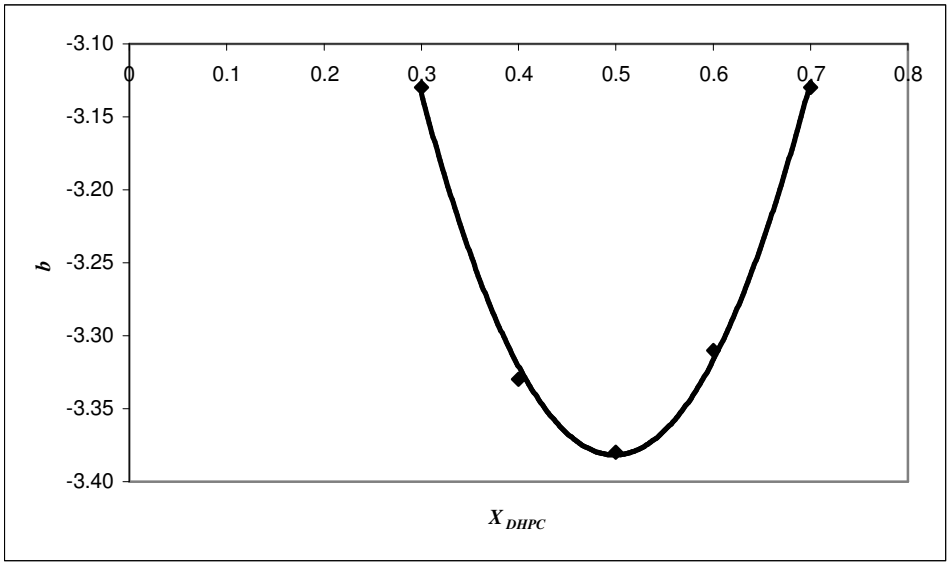

Figure 5.11 – LSER lipid phase dipolarizability/polarizability coefficient, s, as a function of mole fraction of DHPC.

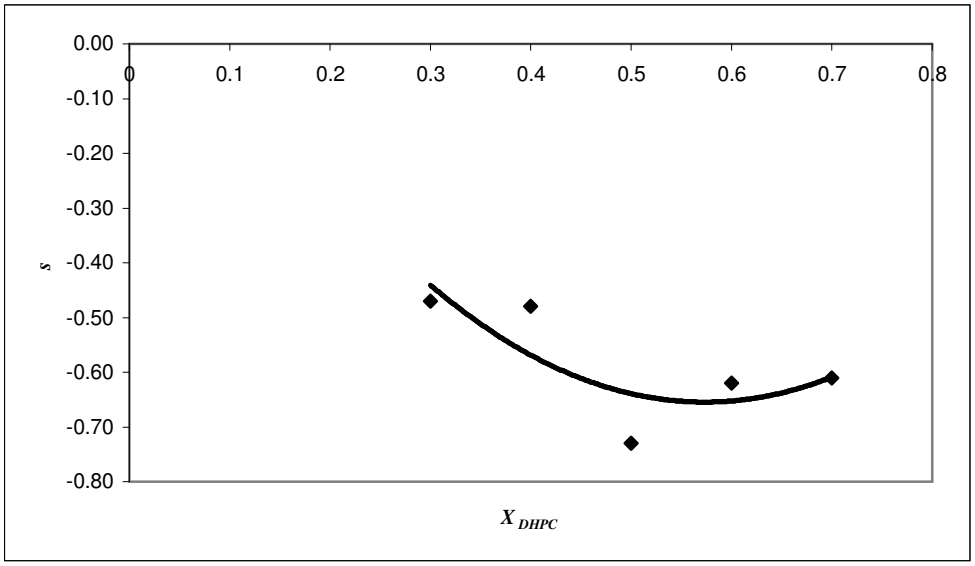

Chapter 6

Temperature Dependence and Thermodynamic Parameters of Vesicle/Water Partitioning for Lipid Phases Formed By Short-Chain and Long-Chain Lipids

Abstract

A study of the temperature dependence and thermodynamic parameters of vesicle/water partitioning for lipid phases comprised of spontaneous vesicles formed by short-chain and long-chain lipids has been conducted using electrokinetic chromatography (EKC). EKC retention factors were determined for a set of 20 neutral aromatic solutes from 15 ^{o}C to 70 ^{o}C. Vesicle/water partition coefficients were determined from these retention factors and chromatographic phase ratios estimated for 15 mM $DPPG_{20}DHPC_{50}DPPC_{30}$ and 15 mM $DPPG_{20}DHPC_{70}DPPC_{10}$. Thermodynamic parameters including the free energy change (ΔG), the enthalpy change (ΔH), the entropy change (ΔS), and the heat capacity change (ΔC_p) associated with vesicle/water partitioning were determined using non-linear van't Hoff plots for both of these lipid phases. Comparisons of this thermodynamic data and thermodynamic data from similar partitioning systems were made in an effort to elucidate the mechanism and the driving force of the partitioning system.

Introduction

The distribution of a solute between an aqueous phase and a hydrophobic phase such as a nonpolar solvent or aggregates such as micelles or lipid membranes has been studied by a diverse array of partitioning experiments. The driving force behind the preferential distribution of nonpolar molecules from aqueous phases to hydrophobic phases is widely assumed to be the hydrophobic effect. The hydrophobic effect is describes the unfavorable interactions between nonpolar molecules with polar molecules. Hydrophobic interactions caused by this effect are responsible for the low solubility of nonpolar solutes in water, retention in some modes of chromatography, protein folding, and the association of phospholipids to form biological membranes.[1]

While conventional wisdom would relate the hydrophobic effect and hydrophobic interactions with the "like dissolves like" paradigm that predicts the immiscibility of oil and water, they are more closely related to the strong attractive forces between water molecules than repulsion between polar molecules and nonpolar molecules. The attractive forces between water molecules are caused by

intermolecular hydrogen bonding. The network of hydrogen-bonded water molecules that these attractive forces form must be disrupted in order to solvate any solute in an aqueous medium. Strongly polar or ionic solutes are able to interact strongly with water molecules. These interactions compensate for the disruption of intermolecular water bonds that occurs during the solvation process. Nonpolar solutes are not able to interact with water molecules in this manner. Instead, the water molecules are ordered around the solute molecules in order to maintain their intermolecular hydrogen bonding interactions.[2]

The thermodynamic parameters that govern hydrophobic interactions are of great interest due to the importance of the hydrophobic effect in biological systems. The free energy (ΔG), entropy (ΔS), enthalpy (ΔH), and heat capacity (ΔC_p) changes associated with various hydrophobic interactions have been assessed by a wide assortment of experimental methods. Classical hydrophobic interactions have been observed in bulk organic solvent/water partitioning[3,4], hydrophobic interaction chromatography[5], and protein folding[6] systems. These hydrophobic effects are characterized by large positive entropy changes due to the disordering of the water molecules necessary to solvate the nonpolar solute that occurs when the solute is transferred to a nonpolar environment and large negative heat capacity changes related to the decrease in nonpolar surface area accessible to water at room temperature.[1] The enthalpy change associated with the classical model of hydrophobic interactions is considered to be negligible compared to the entropy change at room temperature.[7] Studies of the temperature dependency of the classical hydrophobic effect have shown that the favorable free energy change associated with the classical hydrophobic effect is dominated by the entropy term ($T\Delta S$) at low temperatures and the enthalpy change at higher temperatures, with a large negative heat capacity change over the entire temperature range.[8]

A “nonclassical” hydrophobic effect, driven by favorable enthalpic contributions and positive heat capacity changes has been noted for several systems, especially systems that involve distribution of a solute between an aqueous phase and an ordered hydrophobic phase. Phospholipid bilayer membrane/water partitioning of small organic molecules[9,10,11], fatty-acids[12], polyene antibiotics[13], and peptides[14,15] as well as amino acid retention on high density bonded phase liquid chromatography systems[16] and lysophospholipid micelle/water partitioning of peptides[17] all display thermodynamic parameters concordant with the nonclassical hydrophobic effect. Studies of these systems conclude that “bilayer effects” due to the phase transition behavior of lipid membranes cause deviation from classical hydrophobic effect behavior.

In the current study, the temperature dependence and thermodynamic parameters of vesicle-water partitioning has been investigated using electrokinetic chromatography with a lipid phase consisting of vesicles spontaneously formed from the long-chain lipids 1,2-Dipalmitoyl-*sn*-Glycero-3-[Phospho-*rac*-

(1-glycerol)] (DPPG, 16:0) and 1,2-Dipalmitoyl-*sn*-Glycero-3-Phosphocholine (DPPC, 16:0) and the short-chain lipid 1,2-Dihexanoyl-*sn*-Glycero-3-Phosphocholine (DHPC, 6:0). Gabriel and Roberts have shown that aqueous mixture of long-chain lipids with a chain length longer than C_{13} and short-chain lipids spontaneously form unilamellar vesicles. These vesicles have been characterized by ^{1}H NMR, fluorescence microscopy, and electron microscopy. They have been shown to be 10-100 nm in diameter with homogenous size distributions.[18,19]

Experimental

Refer to **Chapter 2** for experimental procedures and details concerning chemicals, liposome and vesicle preparation, dynamic light scattering, sample preparation, and electrokinetic chromatography, calculation of retention factors.

Theory

Estimation of Chromatographic Phase Ratio

The chromatographic phase ratio, Φ, may be determined for LEKC methods using:

$$\Phi = \frac{\nu(C_{lipid} - CAC)}{1 - \nu(C_{lipid} - CAC)} \qquad \textbf{Equation 6.1}$$

where ν is the partial specific molar volume of the lipid phase and *CAC* is the critical aggragation concentration of the lipid phase.

The partial specific molar volume of a compound is volume increase caused by the addition of one mole of that compound to a large excess of a solution; in this case the compound would be said to be at infinite dilution.[20] For a thermodynamics study of this nature, the partial specific molar volume should ideally be determined experimentally at each unique temperature used in the study. In general, the partial specific molar volume is determined using the method of intercepts. The densities of a series of lipid solutions of different concentrations, including the density of the buffer solution with no lipids, would be measured at each applicable temperature. The apparent partial specific volume at each concentration would then be calculated using:

$$\nu_{apparent} = \frac{1}{\rho_{buffer}}\left(1 - \frac{\rho_{lipid} - \rho_{buffer}}{C}\right) \qquad \textbf{Equation 6.2}$$

where ρ_{buffer} and ρ_{lipid} are the measured densities of the buffer and the lipid solution in mL/g and *C* is the concentration of the lipid solution in g/mL. A plot of the apparent partial specific volumes as a function of the lipid concentration should yield a linear relationship with the y-intercept at the partial

specific volume at infinite dilution.[21] The partial specific molar volume may then be calculated using the molar mass of the compound.

Densities were measured for 5 mM, 10 mM, 15 mM, 20 mM and 25 mM $DPPG_{20}DHPC_{50}DPPC_{30}$ using a Mettler Toledo DE40 Density Meter. A plot of the apparent partial specific volumes calculated using these densities was not linear. This behavior is likely explained by the dynamic nature of these vesicles relative to total lipid concentration. The formation of spontaneous unilamellar vesicles depends upon the concentration of DHPC in the solution. Therefore, at very low concentrations, it is likely that the solution includes a mixture of mixed micelles and multilamellar vesicles rather than the unilamellar vesicles that are found at higher concentrations. The method of intercepts is not applicable to this data.

Instead, the partial specific molar volume of this vesicle system was estimated using literature values of the partial specific volume for DPPG, DHPC, and DPPC. These values are included in **Appendix A-1**. Using the molar mass for each of these lipids, the partial specific molar volumes of DPPG, DHPC, and DPPC were calculated to be 0.7532 L/mole, 0.3946 L/mole, and 0.7003 L/mole, respectively. Using an additivity approach:

$$\nu = X_{DPPG}\nu_{DPPG} + X_{DHPC}\nu_{DHPC} + X_{DPPC}\nu_{DPPC} \qquad \textbf{Equation 6.3}$$

where X_{DPPG}, X_{DHPC}, and X_{DPPC} are the mole fractions of each of the lipids and v_{DPPG}, v_{DHPC}, and v_{DPPG} are the individual partial specific molar volumes of each of the lipids. Using **Equation 6.3** above, the partial specific volume of 15 mM $DPPG_{20}DHPC_{50}DPPC_{30}$ was calculated to be 0.5580 L/mole and the partial specific volume of 15 mM $DPPG_{20}DHPC_{70}DPPC_{10}$ was calculated to be 0.4969 at 25 °C.

The $(C_{lipid}\text{-}CAC)$ term in **Equation 6.1** above estimates the concentration of lipids that are aggregated into vesicles. The critical aggregation concentration used in this term has been determined as the x-intercept of a plot of the retention factors for a series of solutes using a series of lipid phases with different concentrations as a function of the lipid phase concentration. For this study, the retention factors of the homologous series of alkylphenones was determined using 5 mM, 10 mM, 15 mM, 20 mM, and 25 mM $DPPG_{20}DHPC_{50}DPPC_{30}$ and $DPPG_{20}DHPC_{50}DPPC_{30}$. A plot of this data is included as **Figure 6.1** and **Figure 6.2**. From these plots, the critical aggregation concentration for these vesicles is very near zero. This is similar to the critical aggregation concentration determined for other liposome[22] and vesicle[23] systems.

Estimation of Vesicle-Water Partition Coefficients

Using the retention factors determined above and the chromatographic phase ratios estimated above, vesicle-water partition coefficients representing the distribution of the solute between the aqueous

phase and 15 mM $DPPG_{20}DHPC_{50}DPPC_{30}$ and 15 mM $DPPG_{20}DHPC_{70}DPPC_{10}$ were determined for each of the solutes using:

$$K = \frac{k}{\Phi} \qquad \textbf{Equation 6.4}$$

Estimation of Thermodynamic Quantities

The van't Hoff equation describes the temperature dependence of the partition coefficient that is relative to the distribution of a solute between two phases. The linearity of the van't Hoff plots for a given partitioning system is directly related to the heat capacity change associated with the system. For systems where the heat capacity change is temperature independent and equal to zero, linear van't Hoff plots should be expected. For systems where the heat capacity is temperature independent and nonzero or linearly dependant on the temperature, nonlinear van't Hoff plots should be expected.[24] A summary of the effects of the heat capacity change on the van't Hoff plots and enthalpy, entropy, and free energy changes for partitioning systems is included in **Table 6.1**.

The free energy change (ΔG) associated with any partitioning system may be calculated using:

$$\Delta G = -RT \ln K \qquad \textbf{Equation 6.5}$$

where R is the gas constant, T is the temperature, and K is the partition coefficient.

When the heat capacity change of a partitioning system is temperature independent and equal to zero, the relationship between the partition coefficient and the absolute temperature is described by a linear equation:

$$\ln K = -\frac{\Delta H}{RT} + \frac{\Delta S}{R} \qquad \textbf{Equation 6.6}$$

where ΔH is the enthalpy change due to the transfer of the solute between phases, ΔS is the entropy change due to the transfer of the solute between phases, R is the gas constant, and T is the temperature.[25,26] In this case, the enthalpy change and the entropy change are both temperature independent as well. For systems characterized by linear van't Hoff plots, the enthalpy and entropy changes of the system can be determined using a set of partition coefficients determined for different temperatures using **Equation 6.6**.

If the heat capacity change associated with a partitioning system is temperature independent and nonzero or linearly dependent on temperature, nonlinear van't Hoff plots should be expected. For both of these cases, the enthalpy and entropy changes associated with the system should also be temperature dependant. For the first case, the enthalpy change should show a linear relationship with temperature and the entropy change should show a nonlinear relationship with temperature. For the

second case, both the enthalpy change and the entropy change should display nonlinear relationships with temperature.[24]

A second-order nonlinear equation has been used to describe the retention processes in hydrophobic interaction chromatography (HIC).[1] While most reversed phase liquid chromatography (RPLC) systems display linear van't Hoff plots, second-order van't Hoff plots have also been reported for some RPLC systems.[27] Other studies have shown that the temperature dependency of systems such as the interaction of polypeptides with n-octyl ligands,[28,29] vesicle-water partitioning, and liposome-water partitioning[30] are better described by a third-order nonlinear equation of the form:

$$\ln K = \frac{a}{T^3} + \frac{b}{T^2} + \frac{c}{T} + d \qquad \textbf{Equation 6.7}$$

The enthalpy change, entropy change, and heat capacity change may be calculated using a series of equations obtained from the integrated form of Kirchoff's law[29,31]:

$$\Delta H = -R\left(\frac{3a}{T^2} + \frac{2b}{T} + c\right) \qquad \textbf{Equation 6.8}$$

$$\Delta S = R\left(d - \frac{2a}{T^3} - \frac{b}{T^2}\right) \qquad \textbf{Equation 6.9}$$

$$\Delta C_p = \frac{R}{T^2}\left(\frac{6a}{T} + 2b\right) \qquad \textbf{Equation 6.10}$$

In this study, the enthalpy change, entropy change, and heat capacity change associated with the partition coefficients estimated above were calculated for each solute at each temperature using **Equations 6.8**, **6.9**, and **6.10** above.

Results and Discussion

Average Vesicle Diameter as a Function of Temperature

The average vesicle diameter of 15 mM $DPPG_{20}DHPC_{50}DPPC_{30}$ and 15 mM $DPPG_{20}DHPC_{70}DPPC_{10}$ lipid phases were determined using dynamic light scattering from 15 ^{o}C-75 ^{o}C in 10 ^{o}C increments. Average vesicle diameters for these lipid phases are included in **Tables 6.2** and **6.3**.

The average vesicle diameters of 15 mM $DPPG_{20}DHPC_{50}DPPC_{30}$ were statistically very similar from 15-35 ^{o}C. From 35 ^{o}C-75 ^{o}C, the average vesicle diameter increased in an almost exponential fashion. This trend is shown in **Figure 6.3**. Trends of increasing average diameter as a function of temperature has been previously noted for DHP vesicles and liposomes formed from DPPG, DPPC, and cholesterol.[32] Standard errors associated with the size distributions also increased significantly

from 35 °C-75 °C. From this observation, the heterogeneity of the size distribution also increases with temperature.

The average vesicle diameters of 15 mM $DPPG_{20}DHPC_{70}DPPC_{10}$ displayed no dependence on temperature over the entire temperature range investigated. The average diameters, the standard errors of the average diameters determined for this lipid phase much larger than should be expected for a homogenous population of unilamellar vesicles over this entire temperature range. This lipid phase is likely a mixture of mixed micelles and multilamellar vesicles rather than unilamellar vesicles.

Estimation of the Chromatographic Phase Ratio

The chromatographic phase ratios for the lipid phases composed of 15 mM $DPPG_{20}DHPC_{50}DPPC_{30}$ and 15 mM $DPPG_{20}DHPC_{70}DPPC_{10}$ were estimated using the partial specific molar volumes and critical aggregation concentrations calculated above and **Equation 6.1**. The chromatographic phase ratio for 15 mM $DPPG_{20}DHPC_{50}DPPC_{30}$ was estimated to be 0.008844 and the chromatographic phase ratio for 15 mM $DPPG_{20}DHPC_{70}DPPC_{10}$ was estimated to be 0.007509.

These values represent an estimation of the chromatographic phase ratio and may not be entirely accurate. In order to make these estimations, the partial specific molar volume was assumed to be constant over the temperature range investigated and equivalent to the weighted sum of partial specific molar volumes of the lipid monomers. As described above, the procedure generally used to experimentally determine the partial specific molar volume for aggregates such as micelles and vesicles was invalid for these aggregates because of their dynamic nature relative to concentration. Previously, the partial specific molar volume and the chromatographic phase ratio for DHP vesicles has been shown to increase 9% over the range of 15 °C to 70 °C and the partial specific molar volume and the chromatographic phase ratio for DPPG/DPPC/Cholesterol vesicles has been shown to increase 2% over the range of 15 °C to 70 °C.[32] Given that the size of 15 mM $DPPG_{20}DHPC_{50}DPPC_{30}$ increases over this temperature range it is reasonable to expect that the chromatographic phase ratio would also increase over this temperature range.

Van't Hoff Plots

Electrokinetic chromatography experiments were conducted for a set of 20 neutral aromatic compounds using 15 mM $DPPG_{20}DHPC_{50}DPPC_{30}$ and 15 mM $DPPG_{20}DHPC_{70}DPPC_{10}$ lipid phases from 15 °C-70 °C. At temperatures above 50 °C, reproducible chromatography was not possible using 15 mM $DPPG_{20}DHPC_{50}DPPC_{30}$. Therefore, retention factors for this lipid phase were only determined from 15 °C-50 °C. These retention factors are summarized in **Table 6.4**. Retention factors were

determined for 15 mM $DPPG_{20}DHPC_{70}DPPC_{10}$ over the entire temperature range. These retention factors are summarized in **Table 6.5**. Partition coefficients, K, were calculated for each retention factor using the chromatographic phase ratio determined above. Summaries of ln K for each solute at each experimental temperature for 15 mM $DPPG_{20}DHPC_{50}DPPC_{30}$ and 15 mM $DPPG_{20}DHPC_{70}DPPC_{10}$ are included in **Table 6.6** and **Table 6.7**.

Van't Hoff plots were constructed by plotting ln K as a function of the inverse absolute temperature ($1/T$, in Kelvin). Van't Hoff plots for 15 mM $DPPG_{20}DHPC_{50}DPPC_{30}$ are included in **Figures 6.4-6.8**. Van't Hoff plots for 15 mM $DPPG_{20}DHPC_{70}DPPC_{10}$ are included in **Figures 6.9-6.13**.

The van't Hoff plots generated for 15 mM $DPPG_{20}DHPC_{50}DPPC_{30}$ all fit the third-order trend lines reasonably well (R^2>0.97) over the temperature range 15 ^oC-50 ^oC. As described above, chromatography experiments above 50 ^oC were not reproducible and any data from these experiments did not fit the third-order trend lines. From the dynamic light scattering data, the size of these vesicles increased dramatically from 45 ^oC- 55 ^oC. It is likely that these vesicles are simply unstable above 50 ^oC. Many of the van't Hoff plots generated for 15 mM $DPPG_{20}DHPC_{70}DPPC_{10}$ do not fit the third-order trend lines well over the experimental temperature range. From the size distributions determined for these aggregates by dynamic light scattering, it is likely that these dispersions include a heterogeneous mixture of mixed micelles and multilamellar vesicles. Therefore, this lipid phase probably does not provide the stability and batch-to-batch reproducibility that would be necessary to generate good van't Hoff plots.

Estimation of Thermodynamic Quantities

The free energy changes (ΔG) associated with vesicle/water partitioning of the 20 neutral aromatic solutes in the 15 mM $DPPG_{20}DHPC_{50}DPPC_{30}$ and 15 mM $DPPG_{20}DHPC_{50}DPPC_{30}$ lipid phases were calculated using the partition coefficients determined as described above. The associated entropy changes (ΔS), enthalpy changes (ΔH), and heat capacity changes (ΔC_p) were determined from the regression coefficients and constants of the nonlinear van't Hoff plots using **Equations 6.8**, **6.9**, and **6.10**. Summaries of the regression coefficients and constants for 15 mM $DPPG_{20}DHPC_{50}DPPC_{30}$ and 15 mM $DPPG_{20}DHPC_{70}DPPC_{10}$ are included in **Table 6.8** and **Table 6.9**, respectively. Summaries of these thermodynamic quantities for 15 mM $DPPG_{20}DHPC_{50}DPPC_{30}$ are included in **Tables 6.10**, **6.11**, **6.12**, and **6.13**. Summaries of these thermodynamic quantities for 15 mM $DPPG_{20}DHPC_{70}DPPC_{10}$ are included in **Tables 6.14**, **6.15**, **6.16**, and **6.17**.

It is important to note that the van't Hoff plots determined for several of the solutes using 15 mM $DPPG_{20}DHPC_{70}DPPC_{10}$ do not exhibit very good correlation between temperature and ln K. The van't

Hoff plots for benzene, toluene, ethylbenzene, propylbenzene and butyl benzoate all display R^2 < 0.90. Therefore, the thermodynamic quantities determined for these five compounds likely include error due to the poor correlations of the van't Hoff plots.

Temperature Dependency of Thermodynamic Quantities For 15 mM $DPPG_{20}DHPC_{50}DPPC_{30}$

Plots of the free energy changes (ΔG), enthalpy changes (ΔH), entropy changes (ΔS), and heat capacity changes (ΔC_p) associated with vesicle/water partitioning of benzene, acetophenone, chlorobenzene, methyl benzoate, and phenol in the 15 mM $DPPG_{20}DHPC_{50}DPPC_{30}$ lipid phase as a function of temperature are included in **Figures 6.14**, **6.15**, **6.16**, **6.17**, and **6.18**.

For 15 mM $DPPG_{20}DHPC_{50}DPPC_{30}$, the entropy changes and the enthalpy changes both decrease from a large positive value at 15 ^oC to a minimum value at approximately 30 ^oC. From 30 ^oC the entropy changes and the enthalpy changes both increase to a maximum positive value. The entropy changes are all positive over the entire temperature range studied. The minimum enthalpy change for some compounds is negative, but the enthalpy changes determined are also positive for the most part. The magnitude of the entropic contribution to the free energy change, $-T\Delta S$, is larger than the magnitude of the enthalpic contribution, ΔH, over the entire experimental temperature range. Therefore, the partitioning of these solutes between the lipid phase 15 mM $DPPG_{20}DHPC_{50}DPPC_{30}$ and water appears to be entropy driven from 15 ^oC to 50 ^oC. The heat capacity changes increase from a negative value at 15 ^oC to a positive value at 50 ^oC. The plot of the heat capacity change as a function of temperature intersects the x-axis at approximately 30 ^oC for all of the solutes studied.

From 15 ^oC to 30 ^oC, this partitioning system displays behavior consistent with the classical hydrophobic effect. The distribution of solutes from the aqueous phase to the lipid phase is entropically-driven because the magnitude of the entropic contribution to the free energy change, $-T\Delta S$, is larger than the magnitude of the enthalpic contribution to the free energy change, ΔH, and the system displays negative heat capacity changes over this temperature range. The partitioning behavior is enthalpically hindered for most of the compounds over this temperature range. Hexanophenone, benzene, propylbenzene, butyl benzoate, phenol, and 4-propyl phenol all display negative enthalpies of distribution around the minimum at 30 ^oC. At this temperature, the partitioning system is *enthalpically-favored* rather than *enthalpically-driven* because the magnitude of the entropic contribution to the free energy change, $-T\Delta S$, is still larger than the magnitude of the enthalpic contribution to the free energy change, ΔH. From 30 ^oC to 50 ^oC, the partitioning system deviates from behavior associated with the classical hydrophobic effect. The distribution of solutes from the aqueous phase to the lipid phase is still entropically-driven, but the system displays a positive heat capacity change. The negative heat capacity change, theoretically associated with the dehydration of

a nonpolar solute that occurs when the solute is transferred from an aqueous phase to a hydrophobic phase, is considered to be "the true hallmark of the (classical) hydrophobic effect."[37] This behavior is not completely analogous to the classical hydrophobic effect due to the positive heat capacity change, but the entropic and enthalpic contributions to the free energy change of partitioning are similar to those associated with classical hydrophobic effect.

In systems associated with the classical hydrophobic effect, the favorable free energy change associated with distribution of a solute from an aqueous phase to a hydrophobic phase is dominated by the entropy term ($T\Delta S$) at low temperatures and the enthalpy change at higher temperatures, with a large negative heat capacity change over the entire temperature range. This effect is caused by the higher entropy of water molecules at higher temperatures; as their entropy increases, they are more able to arrange themselves in order to solvate a nonpolar solute with less of an unfavorable entropy change. If a similar effect does not occur in the hydrophobic phase, the overall entropic contribution to the distribution system then decreases in magnitude.[8] In this vesicle system, this behavior is mimicked from 15 ^{o}C to 30 ^{o}C. Above 30 ^{o}C, the lipid phase likely undergoes a gel to liquid crystalline phase transition that is accompanied by a "melting" of the lipid hydrocarbon chains. This is supported by the particle size data; the average diameter of the vesicles increases at temperatures higher than 30 ^{o}C. This transition is likely accompanied by an increase in the entropy of the lipid phase. Therefore, the entropy change associated with the distribution of solute molecules from the aqueous phase to the lipid phase increases as the hydrocarbon chains become more able to arrange around solutes.

Temperature Dependency of Thermodynamic Quantities For 15 mM $DPPG_{20}DHPC_{70}DPPC_{10}$

Plots of the free energy changes (ΔG), enthalpy changes (ΔH), entropy changes (ΔS), and heat capacity changes (ΔC_p) associated with vesicle/water partitioning of benzene, acetophenone, chlorobenzene, methyl benzoate, and phenol in the 15 mM $DPPG_{20}DHPC_{70}DPPC_{10}$ lipid phase as a function of temperature are included in **Figures 6.19**, **6.20**, **6.21**, **6.22**, and **6.23**.

From these plots, the entropy changes and enthalpy show a roughly parabolic relationship with temperature. Both the entropy and enthalpy changes determined for this lipid phase display slight increases from 15 ^{o}C to 30 ^{o}C and then show large decreases from 30 ^{o}C to 70 ^{o}C. At higher temperatures (between 45 ^{o}C and 55 ^{o}C), both the enthalpy change associated with partitioning intersects the x-axis and becomes negative. Similarly, above approximately 60 ^{o}C, the entropy change associated with partitioning intersects the x-axis and becomes negative. Therefore, from 15 ^{o}C to approximately 45 ^{o}C to 55 ^{o}C, partitioning is *entropically-driven* and *enthalpically-hindered* for 15 mM $DPPG_{20}DHPC_{70}DPPC_{10}$. From approximately 45 ^{o}C to 55 ^{o}C to approximately 60 ^{o}C, partitioning

is *entropically-driven* and *enthalpically-favored*. Finally, at temperatures higher than approximately 60 ^{o}C, partitioning is *entropically-hindered* and *enthalpically-driven* for this lipid phase. The heat capacity changes associated with partitioning in the system are negative for most of the solutes over the entire temperature range. Therefore, from 15 ^{o}C to approximately 60 ^{o}C, this system displays behavior consistent with the classical hydrophobic effect. Above 60 ^{o}C, the behavior is similar to the nonclassical hydrophobic effect that has been shown for several systems, but the heat capacity changes are negative rather than positive.

Comparison with of Thermodynamic Quantities with Literature Data

In a similar, but separate, study of the thermodynamic parameters associated with the partitioning of neutral aromatic solutes between sodium dodecylsulfate (SDS) micelles, dihexadecyl hydrogen phosphate (DHP) vesicles, and phospholipid liposomes and water by Khaledi and Bui, very different behavior was found. The SDS micelle/water partitioning system was shown to be *enthalpically-driven* and *entropically-favored* from 15 ^{o}C to 70 ^{o}C; enthalpic contributions accounted for approximately 70% of the free energy change in that study. The vesicle/water and liposome/water systems were shown to be *entropically-driven* from 20 ^{o}C to 55 ^{o}C and *enthalpically-driven* above 57 ^{o}C. A summary of the free energy changes and the entropy and enthalpy changes determined in this study are included in **Table 6.18** and **Table 6.19**, respectively. Two other interesting trends were noted from this study. First, both the enthalpy and entropy changes associated with vesicle/water and liposome/water partitioning were shown to increase from 15 ^{o}C to a maximum value at approximately 45 ^{o}C and the decrease from 45 ^{o}C to 70 ^{o}C. Also, the heat capacity change was shown to decrease from a positive value at 15 ^{o}C to a negative value at 70 ^{o}C. [30] Effectively, an opposite trend was observed relative to the current study for 15 mM $DPPG_{20}DHPC_{50}DPPC_{30}$. Converesely, this trend is very similar to the behavior noted for 15 mM $DPPG_{20}DHPC_{50}DPPC_{30}$. An extensive literature search failed to find a partitioning system with similar thermodynamic effects to the effects observed for the partitioning of neutral aromatic solutes to 15 mM $DPPG_{20}DHPC_{50}DPPC_{30}$.

Unfortunately, conflicting conclusions regarding the thermodynamic nature of partitioning processes involving bilayer membrane or membrane-like hydrophobic phases seem to be widespread throughout the literature. For example, the study cited above found SDS micelle/water partitioning of neutral aromatic solutes determined by micellar electrokinetic chromatography to be enthalpically driven over the entire experimental temperature range. A similar study by Woodrow and Dorsey, using a similar micellar phase and similar solute set, found SDS micelle/water partitioning to be entropically driven at 25 ^{o}C.[38] Most studies of bilayer membrane/water partitioning have been performed using calorimetric, sedimentation, or spectroscopic, rather than chromatographic, methods. Enthalpically-driven nonclassical hydrophobic effects in bilayer/water partitioning of small

organic molecules have been shown using sedimentation methods[36], nuclear magnetic resonance[10,17], and calorimetric methods.[11,33] Calorimetric studies have demonstrated nonclassical hydrophobic effects associated with bilayers/water partitioning of fatty acids[12], polyene antibiotics[13], and peptides.[14,15] Conflicting studies have found that bilayer membrane/water partitioning is entropically-driven and therefore likely governed by classical hydrophobic effects. In the electrokinetic chromatography study discussed above, Khaledi and Bui found liposome/water and vesicle/water partitioning to be entropically-driven at relatively low temperatures and enthalpically-driven at high temperatures. In an isothermal titration calorimetry study, Zhang and Rowe reported that the liposome/water partitioning of butanol is entropically-driven over the entire temperature range of 15 ^{o}C to 55 ^{o}C.[34] In an additional study, Zhang and Rowe reported that liposome/water partitioning of hexanol, heptanol, octanol, and nonanol is entropically-driven, with significant unfavorable enthalpic effects, at 45 ^{o}C. This study also reported negative heat capacity changes for liposome/water partitioning of these alcohols that should be attributed to the classical hydrophobic effect.[35] Finally, Martinez and Gomez reported that the liposome/water partitioning of a series of sulfonamides determined by a sedimentation method was entropically-driven from 20 ^{o}C to 50 ^{o}C. It should be noted that this study was conducted using multilamellar vesicles rather than unilamellar vesicles.[36]

The discrepancies in the thermodynamic parameters determined in separate studies for bilayer membrane/water partitioning is likely rooted in “bilayer effects” caused by the unique architecture of bilayer membranes. Wimley and White have proposed that the bilayer membrane/water partitioning behavior observed in most studies is driven by forces similar to the classical description of the hydrophobic effect and also modified by enthalpic effects caused by solute-induced changes in lipid-lipid interactions or dipolar interactions.[37] A titration calorimetry study by Beschiaschivili and Seelig has shown that the enthalpic contribution to liposome/water partitioning of peptides varies with the size of the liposome. This study showed that partitioning was enthalpically-driven for systems comprised of smaller liposomes (diameter = 30 nm) and entropically-driven for systems comprised of larger liposomes (diameter = 100 nm). This difference was related to differences in the lipid packing of the two different liposome populations. The surface of the liposome is more highly curved and therefore the lipids are tightly packed and highly ordered in populations of small liposomes relative to large liposomes. Interestingly, the free energy change of partitioning was the same, regardless of liposome size, in this study.[33] Similarly, Dill et al. have shown that the thermodynamic parameters associated with retention of amino acids on reverse-phase liquid chromatography stationary phases depends distinctly on the bonding density of the stationary phase.[16] The common denominator of these studies is the possibility that the thermodynamic parameters associated with bilayers/water partitioning is keenly dependant on the lipid-lipid interactions, lipid packing and order of the lipids that form the bilayer. Therefore, lipid bilayers aggregates formed using different lipid formulations or different preparation methods could display widely different behavior.

Conclusions

In conclusion, a study of the temperature dependence and thermodynamic parameters associated with the distribution of neutral aromatic solutes between water and bilayered vesicles spontaneously formed using mixtures of short-chain lipids (DHPC) and long-chain lipids (DPPG and DPPC) has been conducted using electrokinetic chromatography. Retention factors were determined for a set of 20 neutral aromatic solutes using 15 mM $DPPG_{20}DHPC_{50}DPPC_{30}$ and 15 mM $DPPG_{20}DHPC_{70}DPPC_{10}$ as electrokinetic chromatography pseudostationary phases from 15 ^{o}C to 70 ^{o}C. Partition coefficients were calculated for each of these retention factors using chromatographic phase ratios calculated for each lipid phase. Van't Hoff plots of the natural logarithm of the partition coefficient as a function of the inverse absolute temperature were nonlinear for both lipid phases. Van't Hoff plots for 15 mM $DPPG_{20}DHPC_{50}DPPC_{30}$ fit the third-order equation relatively well (R^2>0.97) over the temperature range 15 ^{o}C-50 ^{o}C. Van't Hoff plots for 15 mM $DPPG_{20}DHPC_{70}DPPC_{10}$ did not fit this equation as well; van't Hoff plots for benzene, toluene, ethylbenzene, propylbenzene and butyl benzoate all display R^2 < 0.90. The free energy changes (ΔG) associated with vesicle/water partitioning of the 20 neutral aromatic solutes in the 15 mM $DPPG_{20}DHPC_{50}DPPC_{30}$ and 15 mM $DPPG_{20}DHPC_{70}DPPC_{10}$ lipid phases were calculated using the partition coefficients and the associated entropy changes (ΔS), enthalpy changes (ΔH), and heat capacity changes (ΔC_p) were determined from the nonlinear van't Hoff plots using the integrated forms of Kirchoff's law. The thermodynamic parameters determined for 15 mM $DPPG_{20}DHPC_{50}DPPC_{30}$ were not comparable to the behavior associated with the classical hydrophobic effect that is often associated with bulk organic solvent/water partitioning systems or the nonclassical hydrophobic effect that is often associated with biliayer membrane/water partitioning systems. The thermodynamic parameters determined for 15 mM $DPPG_{20}DHPC_{70}DPPC_{10}$ displayed similar trends to those reported by Bui and Khaledi for phospholipid liposomes and DHP vesicles.

Chromatographic studies offer a very fast method for determining thermodynamic parameters for partitioning systems using linear and nonlinear van't Hoff plots. Also, chromatographic studies require very small sample amounts and do not require high-purity samples. The lipid phases studied in these experiments may be an example of a system that would be better studied by a direct method for determining the thermodynamic parameters associated with partitioning, such as calorimetry, for multiple reasons. First, the phase ratios could not be experimentally determined for either of the lipid phases. The phase ratios were estimated using literature partial specific molar volume values that may not be accurate over the entire temperature range. Second, the 15 mM $DPPG_{20}DHPC_{70}DPPC_{10}$ lipid phase did not fit the nonlinear van't Hoff equation sufficiently. In order to generate enough chromatography data to properly determine the thermodynamic parameters, very high reproducibility is essential. Some lipid phases, such as 15 mM $DPPG_{20}DHPC_{70}DPPC_{10}$, may be too heterogenous or

not stable enough to provide the required reproducibility. Finally, the use of third-order polynomial equations risks the introduction of statistical artifacts to the data set. Therefore, thermodynamic parameters determined using chromatography experiments may not agree well with thermodynamic parameters determined using calorimetry. Such differences have already been shown for the retention of various different proteins in hydrophobic interaction chromatography.[39] For these reasons, it is likely necessary to perform parallel chromatography and calorimetry experiments in order to validate the use of chromatographic methods for the determination of thermodynamic parameters of different partitioning systems.

Works Cited

1. Vailaya, A.; Horvath, C. Retention thermodynamics in hydrophobic interaction chromatography. *Ind. Eng Chem. Res.* **1996**, 35, 2964-2981.
2. Tanford, C. The Hydrophobic Effect: Formation of Micelles and Biological Membranes; John Wiley and Sons: New York, 1973; p 1-36.
3. Bahadur, N.P.; Shiu, W.Y.; Boocock, D.G.; Mackay, D. Temperature Dependence of Octanol-Water Partition Coefficient for Selected Chlorobenzenes. *J. Chem. Eng. Data.* **1997**, *42*, 685-688.
4. Martinez, F.; Gomez, A. Thermodynamics of partitioning of some sulfonamides in 1-octanol-buffer and liposome systems. *J. Phys Org. Chem*. **2002**, *15*, 874-880.
5. Haidacher, D.; Vailaya, A.; Horvath, C. Temperature effects in hydrophobic interaction chromatography. *Proc. Natl. Acad. Sci. USA*. **1996**, *93*, 2290-2295.
6. Baldwin, R.L. Temperature dependence of the hydrophobic interaction in protein folding. *Proc. Natl. Acad. Sci. USA*. **1986**, *83*, 8069-8072.
7. Russell, C.J.; Thorgeirsson, T.E.; Shin, Y.K. Temperature Dependence of Polypeptide Partitioning between Water and Phospholipid Bilayers. *Biochemistry*. **1996**, *35*, 9526-9532.
8. Southall, N.T.; Dill, K.A.; Haymet, A.D.J. A View of the Hydrophobic Effect. *J. Phys. Chem. B.* **2002**, *106*, 521-533.
9. Huang, C.H.; Charlton, J.P. Interactions of Phostatidylcholine Vesicles with 2-p-Toluidinylnapthalene-6-sulfonate. *Biochemistry*. **1972**, *11* (5), 735-740.
10. De Young, L.R.; Dill, K.A. Solute Partitioning into Lipid Bilayer Membranes. *Biochemistry*. **1988**, *27*, 5281-5289.
11. Seelig, J.; Ganz, P. Nonclassical Hydrophobic Effect in Membrane Binding Equilibria. *Biochemistry*. **1991**, *30*, 9354-9359.
12. Richieri, G.V.; Ogata, R.T. Kleinfeld, A.M. Thermodynamics of Fatty Acid Binding to Fatty Acid-binding Proteins and Fatty Acid Partition between Water and Membranes Measured Using the Fluorescent Probe ADIFAB. *J. Biol. Chem*. **1995**, *270* (25), 15076-15084.
13. Milhaud, J.; Lancelin, J.M.; Michels, B.; Blume, A. Association of polyene antibiotics with sterol-free lipid membranes: I. Hydrophobic binding of filipin to dimyristoylphosphatidylcholine bilayers. *Biochim. Biophys. Acta*. **1996**, *1278*, 223-232.
14. Wieprecht, T.; Beyermann, M.; Seelig, J. Binding of Antibacterial Magainin Peptides to Electrically Neutral Membranes: Thermodynamics and Structure. *Biochemistry*. **1999**, *38*, 10377-10387.
15. Binder, H. Lindblom, G. Interaction of the Trojan peptide penetratin with anionic lipid membranes-a calorimetric study. *Phys. Chem. Chem. Phys.* **2003**, *5*, 5108-5117.

16. DeVido, D.R.; Dorsey, J.G.; Chan, H.S.; Dill, K.A. Oil/Water Partitioning Has a Different Thermodynamic Signature When the Oil Solvent Chains Are Aligned Than When They Are Amorphous. *J. Phys. Chem. B.* **1998**, *102*, 7272-7279.
17. Wong, T. C.; Gao, X. the Temperature Dependence and Thermodynamic Functions of Partitioning of Substance P Peptides in Dodecylphosphocholine Micelles. *Biopolymers*. **1998**, *45*, 395-403.
18. Gabriel, N.E.; Roberts, M.F. Spontaneous Formation of Unilamellar Vesicles. *Biochemistry.* **1984**, *23*, 4011-4015.
19. Gabriel, N.E.; Roberts, M.F. Interaction of Short-Chain Lecithin with Long-Chain Phospholipids: Characterization of Vesicles That Form Spontaneously. *Biochemistry.* **1986**, *25*, 2812-2821.
20. Atkins, P. Chapter 7: The Properties of Simple Mixtures. *Physical Chemistry*, 5th Edition; W.H. Freeman and Company: Oxford, 1994; p. 208.
21. Epand, R.M.; Epand, R.F. Studies of Thermotropic Phospholipid Phase Transitions Using Scanning Densitometry. *Chem. Phys. Lipids.* **1980**, *27*, 139-150.
22. Burns, S.T.; Khaledi, M.G. Rapid determination of liposome-water partition coefficients (K-lw) using liposome electrokinetic chromatography (LEKC). *J. Pharm. Sci*. **2002**, *91*(7), 1601-1612.
23. Bui, H.H.; Khaledi, M.G. Determination of vesicle-water partition coefficients by electrokinetic chromatography: Study of temperature effect. *J. Colloid. Interf. Sci.* **2002**, *253*(2), 397-401.
24. Vailaya, A.; Horvath, C. Enthalpy-Entropy Compensation in Hydrophobic Interaction Chromatography. *J. Phys. Chem.* **1996**, *100*, 2447-2455.
25. Terabe, S.; Katsura, T.; Okada, Y.; Ishihama, Y. Measurement of thermodynamic quantities of micellar solubilization by micellar electrokinetic chromatography with sodium dodecyl sulfate. *J. Microcolumn. Sep.* **1993**, *23* (5), 23-33.
26. Foley, J.P.; Peterson, A.G. Determining thermodynamic quantities of micellar solubilization of chiral pharmaceutical compounds in aqueous solutions of N-deoxycarbonylvaline using micellar electrokinetic chromatography. *J. Microcolumn. Sep.* **1996**, *8* (6), 427-437.
27. Cole, L.A.; Dorsey, J.G. Temperature dependence of retention in reversed-phase liquid chromatography. 1. Stationary phase considerations. *Anal. Chem.* **1992**, *64* (13), 1324-1327.
28. Chowhury, M.A.; Boysen, R.I.; Ihara, H.; Hearn, M.T.W. Binding behavior of crystalline and noncrystalline phases: Evaluation of the enthalpic and entropic contributions to the separation selectivity of nonpolar solutes with a novel chromatographic sorbent. *J. Phys. Chem. B.* **2002**, *106* (46), 11936-11950.
29. Boysen, R.I.; Jong, A.J.O.; Wilce, J.A.; King, G.F.; Hearn, M.T.W. Role of interfacial hydrophobic residues in the stabilization of leucine zipper structure of the transcription factors c-Fos and c-Jun. *J. Biol. Chem*. **2002**, *277* (1), 23-31.

30. Bui, H.H. Thermodynamic Study and Prediction of Solute Partitioning Into Micelles and Liposomes Using Electrokinetic Chromatography. Ph. D. Dissertation, North Carolina State University, Raleigh, N.C., August 2003, Chapter 4. Thermodynamic Study of Homologous Series in Micellar, Vesicular, and Liposome Electrokinetic Chromatography.
31. Alberty, R.A.; Daniels, F. *Physical Chemistry*, 4th ed.; Wiley: Hoboken, N.J., 1993.
32. Bui, H.H. Thermodynamic Study and Prediction of Solute Partitioning Into Micelles and Liposomes Using Electrokinetic Chromatography. Ph. D. Dissertation, North Carolina State University, Raleigh, N.C., August 2003, Chapter 2. Properties of Micelles and Liposomes.
33. Beschiaschvili, G.; Seelig, J. Peptide Binding to Lipid Bilayers. Nonclassical Hydrophobic Effect and Membrane-Induced pK Shifts. *Biochemistry*. **1992**, *31*, 10044-10053.
34. Zhang, F.; Rowe, E.S. Titration Calorimetric and Differential Scanning Calorimetric Studies of the Interactions of n-Butanol with Several Phases of Dipalmitoylphosphatidylcholine. *Biochemistry*. **1992**, *31*, 2005-2011.
35. Rowe, E.S.; Zhang, F.; Leung, T.W.; Parr, J.S.; Guy, P.T. Thermodynamics of Membrane Partitioning for a Series of n-Alcohols Determined by Titration Calorimetry: Role of Hydrophobic Effects. *Biochemistry*. **1998**, *37*, 2430-2440.
36. Martinez, F.; Gomez, A. Thermodynamics of partitioning of some sulfonamides in 1-octanol-buffer and liposome systems. *J. Phys. Org. Chem*. **2002**, *15*, 874-880.
37. Wimley, W.C.; White, S.H. Membrane Partitioning: Distinguishing Bilayer Effects from the Hydrophobic Effect. *Biochemistry*. **1993**, *32*(25), 6307-6312.
38. Woodrow, B.N.; Dorsey, J.G. Thermodynamics of Micelle-Water Partitioning in Micellar Electrokinetic Chromatography: Comparisons with 1-Octanol-Water Partitioning and Biopartitioning. *Environ. Sci. Technol.* **1997**, *31*, 2812-2820.
39. Chen, W.Y.; Huang, H.M.; Lin, C.C.; Lin, F.Y.; Chan, Y.C. Effect of Temperature on Hydrophobic Interaction between Proteins and Hydrophobic Adsorbents: Studies by Isothermal Titration Calorimetry and the van't Hoff Equation. *Langmuir*. **2003**, *19*, 9395-9403.

Table 6.1 - A summary of the effects of the temperature dependency of heat capacity change on van't Hoff plots and enthalpy, entropy, and free energy changes for partitioning systems. Adapted from Reference 26.

Case	ΔC_p	ΔH	ΔS	ΔG	van't Hoff plots
1	$\Delta C_p=0$	temperature independant	temperature independant	temperature dependent, linear	linear
2	$\Delta C_p\neq0$, temperature independant	temperature dependent, linear	temperature dependent, nonlinear	temperature dependent, nonlinear	nonlinear
3	ΔC_p is a linear function of temperature	temperature dependent, nonlinear	temperature dependent, nonlinear	temperature dependent, nonlinear	nonlinear

Table 6.2 – Average diameter for 15 mM $DPPG_{20}DHPC_{50}DPPC_{30}$ at 15 ^{o}C - 75 ^{o}C.

Temperature (^{o}C)	**Average Diameter (nm)**
15	10.8±0.3
25	11.4±0.8
35	11.1±0.1
45	13.0±1.2
55	23.7±2.8
65	29.5±3.0
75	53.7±10.2

Table 6.3 – Average diameter for 15 mM $DPPG_{20}DHPC_{70}DPPC_{10}$ from 15 ^{o}C - 75 ^{o}C.

Temperature (^{o}C)	**Average Diameter (nm)**
15	194.3±4.5
25	194.6±11.5
35	196.9±12.1
45	210.4±15.9
55	215.9±15.7
65	212.0±11.2
75	206.3±10.4

Table 6.4 - Retention factors for 15 mM $DPPG_{20}DHPC_{50}DPPC_{30}$ from 15 °C-50 °C.

	Retention Factor, k						
Solute	**15.7 °C**	**20.7 °C**	**24.1 °C**	**30.5 °C**	**41.5 °C**	**45.3 °C**	**51.2 °C**
acetophenone	0.13	0.14	0.15	0.15	0.17	0.20	0.24
propiophenone	0.35	0.37	0.39	0.38	0.44	0.50	0.62
butyrophenone	0.76	0.87	0.94	0.95	1.13	1.27	1.55
valerophenone	2.34	2.73	3.15	2.98	3.48	3.72	4.37
hexanophenone	8.57	10.09	12.53	10.55	11.42	11.35	13.13
benzene	0.32	0.35	0.39	0.37	0.41	0.48	0.66
toluene	0.78	0.88	0.98	0.97	1.14	1.54	1.99
ethylbenzene	2.00	2.32	2.61	2.61	2.89	3.41	4.43
propylbenzene	6.65	7.65	9.08	7.65	7.68	9.72	12.55
chlorobenzene	1.21	1.38	1.48	1.58	1.72	1.99	2.48
bromobenzene	1.82	2.09	2.25	2.37	2.56	2.83	3.42
iodobenzene	3.42	3.99	4.29	4.30	4.63	4.87	5.99
methyl benzoate	0.34	0.37	0.37	0.37	0.46	0.50	0.63
ethyl benzoate	0.70	0.82	0.87	0.87	1.08	1.19	1.48
propyl benzoate	2.13	2.55	2.67	2.71	3.32	3.25	4.26
butyl benzoate	6.36	7.77	8.20	7.93	8.73	8.59	12.75
phenol	0.22	0.24	0.24	0.24	0.26	0.27	0.33
p-cresol	0.48	0.53	0.54	0.55	0.60	0.60	0.73
4-ethylphenol	1.26	1.40	1.42	1.47	1.58	1.59	1.90
4-propylphenol	3.80	4.63	4.81	4.56	4.87	4.77	5.82

Table 6.5 - Retention factors for 15 mM $DPPG_{20}DHPC_{70}DPPC_{10}$ from 15 °C-70 °C.

	Retention Factor, k										
Solute	**16.3 °C**	**21.3 °C**	**25.8 °C**	**30.5 °C**	**36.1 °C**	**40.0 °C**	**44.9 °C**	**50.7 °C**	**60.2 °C**	**65.7 °C**	**70.5 °C**
acetophenone	0.18	0.19	0.21	0.21	0.23	0.22	0.23	0.22	0.21	0.18	0.18
propiophenone	0.44	0.45	0.49	0.50	0.51	0.50	0.53	0.51	0.47	0.41	0.41
butyrophenone	1.08	1.11	1.24	1.19	1.26	1.23	1.29	1.25	1.14	1.01	0.95
valerophenone	3.36	3.43	3.86	3.51	3.93	3.78	3.82	3.68	3.28	2.92	2.83
hexanophenone	10.96	11.74	14.00	13.19	14.30	13.36	13.94	12.48	10.79	9.72	8.94
benzene	0.39	0.41	0.43	0.46	0.47	0.47	0.51	0.53	0.47	0.41	0.43
toluene	1.18	1.18	1.33	1.37	1.31	1.34	1.40	1.40	1.24	1.14	1.09
ethylbenzene	3.36	3.18	3.72	3.75	3.51	3.55	3.82	3.95	3.43	3.23	3.07
propylbenzene	10.05	10.21	11.74	11.80	11.70	11.86	12.37	12.87	10.91	9.99	9.39
chlorobenzene	1.96	2.02	2.18	1.97	1.97	2.06	2.08	2.07	1.76	1.46	1.39
bromobenzene	3.07	3.09	3.36	3.06	2.91	3.03	3.05	2.97	2.50	2.19	1.98
iodobenzene	6.04	6.24	6.60	6.02	5.29	5.48	5.43	5.20	4.30	3.76	3.33
methyl benzoate	0.44	0.45	0.47	0.49	0.50	0.50	0.53	0.52	0.49	0.42	0.40
ethyl benzoate	1.03	1.03	1.13	1.15	1.16	1.17	1.22	1.19	1.12	0.96	0.95
propyl benzoate	3.16	3.11	3.44	3.40	3.40	3.42	3.61	3.44	3.28	2.83	2.71
butyl benzoate	9.15	9.48	10.93	11.15	10.83	10.41	11.03	10.34	9.99	7.93	7.83
phenol	0.28	0.28	0.30	0.30	0.29	0.28	0.29	0.26	0.24	0.21	0.18
p-cresol	0.60	0.62	0.64	0.64	0.58	0.59	0.59	0.53	0.49	0.43	0.39
4-ethylphenol	1.58	1.61	1.63	1.60	1.41	1.42	1.41	1.25	1.13	0.99	0.86
4-propylphenol	5.28	5.39	5.46	4.93	4.11	4.23	4.13	3.64	3.31	2.76	2.45

Table 6.6 – Partition coefficients, expressed as ln K, for 15 mM $DPPG_{20}DHPC_{50}DPPC_{30}$ from 15 °C-50 °C.

	ln K						
Solute	**15.7 °C**	**20.7 °C**	**24.1 °C**	**30.5 °C**	**41.5 °C**	**45.3 °C**	**51.2 °C**
acetophenone	2.66	2.79	2.84	2.83	2.97	3.10	3.31
propiophenone	3.67	3.73	3.77	3.77	3.92	4.04	4.25
butyrophenone	4.46	4.59	4.67	4.67	4.85	4.97	5.16
valerophenone	5.58	5.73	5.87	5.82	5.97	6.04	6.20
hexanophenone	6.88	7.04	7.26	7.08	7.16	7.16	7.30
benzene	3.58	3.68	3.78	3.75	3.85	3.99	4.31
toluene	4.48	4.61	4.71	4.69	4.86	5.16	5.42
ethylbenzene	5.42	5.57	5.69	5.69	5.79	5.96	6.22
propylbenzene	6.62	6.76	6.93	6.76	6.77	7.00	7.26
chlorobenzene	4.92	5.05	5.12	5.18	5.27	5.42	5.64
bromobenzene	5.32	5.46	5.54	5.59	5.67	5.77	5.96
iodobenzene	5.96	6.11	6.18	6.19	6.26	6.31	6.52
methyl benzoate	3.64	3.73	3.74	3.74	3.95	4.03	4.26
ethyl benzoate	4.38	4.53	4.59	4.59	4.81	4.90	5.12
propyl benzoate	5.49	5.66	5.71	5.72	5.93	5.91	6.18
butyl benzoate	6.58	6.78	6.83	6.80	6.89	6.88	7.27
phenol	3.20	3.30	3.32	3.31	3.37	3.42	3.60
p-cresol	4.00	4.08	4.12	4.14	4.22	4.21	4.41
4-ethylphenol	4.96	5.06	5.08	5.11	5.19	5.19	5.37
4-propylphenol	6.06	6.26	6.30	6.25	6.31	6.29	6.49

Table 6.7 – Partition coefficients, expressed as ln K, for 15 mM $DPPG_{20}DHPC_{70}DPPC_{10}$ from 15 °C-70 °C.

	ln K										
Solute	**16.3 °C**	**21.3 °C**	**25.8 °C**	**30.5 °C**	**36.1 °C**	**40.0 °C**	**44.9 °C**	**50.7 °C**	**60.2 °C**	**65.7 °C**	**70.5 °C**
acetophenone	3.20	3.24	3.31	3.35	3.41	3.36	3.41	3.39	3.32	3.18	3.16
propiophenone	4.08	4.10	4.18	4.19	4.22	4.21	4.26	4.22	4.15	4.01	4.00
butyrophenone	4.97	5.00	5.10	5.07	5.13	5.10	5.14	5.11	5.02	4.90	4.84
valerophenone	6.10	6.12	6.24	6.15	6.26	6.22	6.23	6.20	6.08	5.96	5.93
hexanophenone	7.29	7.35	7.53	7.47	7.55	7.48	7.53	7.42	7.27	7.17	7.08
benzene	3.94	3.99	4.05	4.10	4.15	4.13	4.21	4.25	4.14	4.00	4.04
toluene	5.05	5.05	5.18	5.20	5.16	5.18	5.22	5.23	5.11	5.03	4.97
ethylbenzene	6.10	6.05	6.21	6.21	6.15	6.16	6.23	6.26	6.12	6.07	6.01
propylbenzene	7.20	7.22	7.35	7.36	7.35	7.36	7.41	7.45	7.28	7.19	7.13
chlorobenzene	5.56	5.60	5.67	5.57	5.57	5.61	5.62	5.62	5.46	5.27	5.22
bromobenzene	6.01	6.02	6.10	6.01	5.96	6.00	6.01	5.98	5.81	5.68	5.58
iodobenzene	6.69	6.72	6.78	6.69	6.56	6.59	6.58	6.54	6.35	6.22	6.10
methyl benzoate	4.06	4.09	4.14	4.19	4.19	4.20	4.26	4.24	4.17	4.03	3.98
ethyl benzoate	4.92	4.93	5.01	5.03	5.04	5.05	5.09	5.06	5.00	4.86	4.84
propyl benzoate	6.04	6.02	6.13	6.11	6.11	6.12	6.18	6.13	6.08	5.93	5.89
butyl benzoate	7.11	7.14	7.28	7.30	7.27	7.23	7.29	7.23	7.19	6.96	6.95
phenol	3.61	3.63	3.68	3.67	3.64	3.63	3.67	3.55	3.46	3.35	3.18
p-cresol	4.39	4.41	4.45	4.45	4.35	4.37	4.37	4.26	4.18	4.04	3.95
4-ethylphenol	5.35	5.37	5.38	5.36	5.23	5.24	5.23	5.12	5.02	4.88	4.75
4-propylphenol	6.56	6.58	6.59	6.49	6.31	6.33	6.31	6.18	6.09	5.91	5.79

Table 6.8 - Regression coefficients and constants for 15 mM $DPPG_{20}DHPC_{50}DPPC_{30}$ determined using **Equations 6.7-6.10** for 15 ^{o}C-50 ^{o}C.

Solute	***a***	***b***	***c***	***d***	R^2	***SE***
acetophenone	-3.310E+10	3.287E+08	-1.088E+06	1.205E+03	0.99	0.02
propiophenone	-2.334E+10	2.339E+08	-7.819E+05	8.754E+02	1.00	0.02
butyrophenone	-2.694E+10	2.673E+08	-8.853E+05	9.827E+02	0.99	0.03
valerophenone	-3.195E+10	3.143E+08	-1.031E+06	1.134E+03	0.97	0.05
hexanophenone	-4.649E+10	4.551E+08	-1.484E+06	1.620E+03	0.82	0.09
benzene	-5.021E+10	4.984E+08	-1.649E+06	1.823E+03	0.99	0.03
toluene	-4.432E+10	4.418E+08	-1.469E+06	1.633E+03	0.98	0.07
ethylbenzene	-4.777E+10	4.725E+08	-1.558E+06	1.719E+03	0.99	0.03
propylbenzene	-7.072E+10	6.993E+08	-2.304E+06	2.536E+03	0.93	0.08
chlorobenzene	-3.520E+10	3.485E+08	-1.151E+06	1.273E+03	1.00	0.02
bromobenzene	-3.293E+10	3.247E+08	-1.068E+06	1.177E+03	1.00	0.01
iodobenzene	-3.833E+10	3.776E+08	-1.240E+06	1.364E+03	1.00	0.01
methyl benzoate	-2.133E+10	2.142E+08	-7.179E+05	8.062E+02	0.99	0.03
ethyl benzoate	-2.751E+10	2.732E+08	-9.056E+05	1.006E+03	0.99	0.03
propyl benzoate	-3.202E+10	3.164E+08	-1.043E+06	1.152E+03	0.98	0.05
butyl benzoate	-6.411E+10	6.330E+08	-2.083E+06	2.291E+03	0.97	0.05
phenol	-3.016E+10	2.986E+08	-9.855E+05	1.087E+03	1.00	0.01
p-cresol	-2.500E+10	2.471E+08	-8.146E+05	8.993E+02	0.98	0.03
4-ethylphenol	-2.377E+10	2.348E+08	-7.735E+05	8.545E+02	0.98	0.02
4-propylphenol	-4.465E+10	4.386E+08	-1.436E+06	1.573E+03	0.97	0.04

Table 6.9 - Regression coefficients and constants for 15 mM $DPPG_{20}DHPC_{70}DPPC_{10}$ determined using **Equations 6.7-6.10** for 15 °C-70 °C.

Solute	***a***	***b***	***c***	***d***	R^2	***SE***
acetophenone	3.338E+09	-3.502E+07	1.214E+05	-1.357E+02	0.94	0.03
propiophenone	3.790E+09	-3.904E+07	1.332E+05	-1.465E+02	0.93	0.03
butyrophenone	3.889E+09	-4.024E+07	1.379E+05	-1.516E+02	0.95	0.03
valerophenone	2.464E+09	-2.664E+07	9.484E+04	-1.052E+02	0.91	0.04
hexanophenone	-1.687E+09	1.157E+07	-2.187E+04	1.430E+01	0.95	0.04
benzene	5.250E+09	-5.303E+07	1.775E+05	-1.929E+02	0.86	0.04
toluene	3.427E+09	-3.555E+07	1.221E+05	-1.336E+02	0.88	0.04
ethylbenzene	4.472E+09	-4.496E+07	1.502E+05	-1.604E+02	0.71	0.05
propylbenzene	4.901E+09	-5.013E+07	1.700E+05	-1.838E+02	0.89	0.04
chlorobenzene	7.403E+09	-7.382E+07	2.451E+05	-2.653E+02	0.92	0.05
bromobenzene	5.888E+09	-5.906E+07	1.974E+05	-2.138E+02	0.95	0.04
iodobenzene	2.627E+09	-2.769E+07	9.737E+04	-1.075E+02	0.96	0.05
methyl benzoate	6.653E+09	-6.650E+07	2.208E+05	-2.394E+02	0.95	0.02
ethyl benzoate	4.605E+09	-4.672E+07	1.573E+05	-1.707E+02	0.93	0.03
propyl benzoate	5.950E+09	-5.943E+07	1.974E+05	-2.118E+02	0.89	0.03
butyl benzoate	1.434E+09	-1.728E+07	6.664E+04	-7.600E+01	0.88	0.05
phenol	5.085E+09	-5.181E+07	1.757E+05	-1.946E+02	0.98	0.03
p-cresol	1.278E+09	-1.485E+07	5.639E+04	-6.590E+01	0.98	0.03
4-ethylphenol	1.900E+09	-2.056E+07	7.410E+04	-8.357E+01	0.98	0.04
4-propylphenol	8.269E+08	-9.695E+06	3.796E+04	-4.290E+01	0.97	0.06

Table 6.10 – Free energy changes (ΔG, kJ/mole) determined for vesicle/water partitioning of 20 neutral aromatic solutes using 15 mM $DPPG_{20}DHPC_{50}DPPC_{30}$.

	ΔG (kJ/mole)						
Solute	**15.7 °C**	**20.7 °C**	**24.1 °C**	**30.5 °C**	**41.5 °C**	**45.3 °C**	**51.2 °C**
acetophenone	-6.39	-6.81	-7.02	-7.13	-7.77	-8.20	-8.93
propiophenone	-8.81	-9.10	-9.32	-9.51	-10.24	-10.69	-11.45
butyrophenone	-10.69	-11.20	-11.53	-11.79	-12.68	-13.15	-13.92
valerophenone	-13.39	-14.00	-14.51	-14.69	-15.62	-15.99	-16.72
hexanophenone	-16.51	-17.19	-17.92	-17.87	-18.73	-18.94	-19.69
benzene	-8.59	-8.98	-9.34	-9.45	-10.06	-10.56	-11.61
toluene	-10.76	-11.24	-11.64	-11.85	-12.71	-13.65	-14.60
ethylbenzene	-13.02	-13.60	-14.05	-14.35	-15.13	-15.76	-16.76
propylbenzene	-15.90	-16.51	-17.13	-17.07	-17.69	-18.53	-19.56
chlorobenzene	-11.81	-12.33	-12.65	-13.08	-13.78	-14.33	-15.19
bromobenzene	-12.78	-13.34	-13.69	-14.11	-14.82	-15.27	-16.06
iodobenzene	-14.30	-14.93	-15.28	-15.61	-16.37	-16.70	-17.57
methyl benzoate	-8.75	-9.11	-9.23	-9.44	-10.34	-10.67	-11.48
ethyl benzoate	-10.51	-11.05	-11.33	-11.58	-12.57	-12.98	-13.79
propyl benzoate	-13.17	-13.83	-14.11	-14.44	-15.50	-15.63	-16.65
butyl benzoate	-15.79	-16.55	-16.87	-17.16	-18.03	-18.20	-19.60
phenol	-7.67	-8.05	-8.20	-8.35	-8.81	-9.06	-9.72
p-cresol	-9.60	-9.97	-10.17	-10.44	-11.03	-11.14	-11.89
4-ethylphenol	-11.91	-12.37	-12.55	-12.90	-13.57	-13.73	-14.47
4-propylphenol	-14.55	-15.29	-15.56	-15.76	-16.50	-16.65	-17.49

Table 6.11 – Enthalpy changes (ΔH, kJ/mole) determined for vesicle/water partitioning of 20 neutral aromatic solutes using 15 mM $DPPG_{20}DHPC_{50}DPPC_{30}$.

	ΔH (kJ/mole)						
Solute	**15.7 °C**	**20.7 °C**	**24.1 °C**	**30.5 °C**	**41.5 °C**	**45.3 °C**	**51.2 °C**
acetophenone	23.00	10.89	6.04	3.64	17.47	26.83	45.41
propiophenone	12.10	5.68	3.66	4.52	18.41	26.37	41.53
butyrophenone	23.01	13.03	8.99	6.89	17.89	25.42	40.41
valerophenone	31.39	16.82	10.23	4.45	12.17	19.35	34.49
hexanophenone	42.22	18.78	7.71	-3.39	3.46	12.46	32.32
benzene	29.71	11.17	3.70	-0.13	20.52	34.61	62.64
toluene	27.27	12.76	7.39	6.24	28.09	41.72	68.25
ethylbenzene	36.15	16.86	8.66	3.02	19.44	31.77	56.83
propylbenzene	42.39	13.59	1.28	-7.36	16.45	34.56	71.42
chlorobenzene	28.07	14.25	8.46	4.78	17.63	26.97	45.81
bromobenzene	29.89	15.61	9.30	4.23	13.62	21.48	37.80
iodobenzene	31.55	14.62	7.08	0.80	11.13	20.09	38.78
methyl benzoate	11.14	5.77	4.24	5.62	19.27	26.86	41.19
ethyl benzoate	22.87	12.92	8.95	7.09	18.79	26.63	42.18
propyl benzoate	27.83	14.63	8.95	4.84	15.30	23.40	39.93
butyl benzoate	42.72	15.75	4.03	-4.84	15.08	30.94	63.52
phenol	19.42	7.52	2.53	-0.70	10.22	18.19	34.28
p-cresol	18.63	8.43	4.07	0.99	9.36	15.75	28.76
4-ethylphenol	18.92	9.03	4.76	1.60	9.20	15.15	27.34
4-propylphenol	35.62	14.69	5.12	-3.64	6.04	15.70	36.31

Table 6.12 – Entropy change term ($T\Delta S$, kJ/mole) determined for vesicle/water partitioning of 20 neutral aromatic solutes using 15 mM $DPPG_{20}DHPC_{50}DPPC_{30}$.

	$T\Delta S$ (kJ/mole)						
Solute	**15.7 °C**	**20.7 °C**	**24.1 °C**	**30.5 °C**	**41.5 °C**	**45.3 °C**	**51.2 °C**
acetophenone	29.32	17.60	12.93	10.77	25.17	34.89	54.28
propiophenone	20.93	14.81	12.95	14.09	28.70	37.05	53.03
butyrophenone	33.62	24.13	20.35	18.64	30.46	38.41	54.25
valerophenone	44.77	30.84	24.57	19.24	27.73	35.29	51.22
hexanophenone	58.68	36.04	25.32	14.62	22.04	31.35	51.97
benzene	38.41	20.37	13.09	9.47	30.74	45.28	74.40
toluene	38.04	24.05	18.93	18.15	40.97	55.17	82.96
ethylbenzene	49.08	30.46	22.56	17.32	34.57	47.39	73.55
propylbenzene	58.41	30.35	18.32	9.94	34.41	53.03	91.20
chlorobenzene	39.94	26.68	21.17	17.89	31.55	41.32	61.10
bromobenzene	42.59	28.91	22.90	18.25	28.41	36.66	53.80
iodobenzene	45.89	29.60	22.35	16.47	27.51	36.85	56.39
methyl benzoate	20.01	14.93	13.57	15.24	29.65	37.64	52.79
ethyl benzoate	33.50	24.03	20.33	18.87	31.41	39.68	56.09
propyl benzoate	41.10	28.49	23.10	19.43	30.73	39.24	56.64
butyl benzoate	58.57	32.36	20.95	12.41	33.00	49.35	83.14
phenol	27.08	15.54	10.69	7.65	18.98	27.22	43.97
p-cresol	28.38	18.57	14.40	11.58	20.48	27.15	40.78
4-ethylphenol	30.78	21.33	17.27	14.44	22.66	28.92	41.75
4-propylphenol	50.20	29.95	20.66	12.24	22.44	32.43	53.83

Table 6.13 – Heat capacity change (ΔC_p, kJ/mole) determined for vesicle/water partitioning of 20 neutral aromatic solutes using 15 mM $DPPG_{20}DHPC_{50}DPPC_{30}$.

	ΔC_p (kJ/mole)						
Solute	**15.7 °C**	**20.7 °C**	**24.1 °C**	**30.5 °C**	**41.5 °C**	**45.3 °C**	**51.2 °C**
acetophenone	-3.05	-1.82	-1.05	0.27	2.18	2.74	3.54
propiophenone	-1.72	-0.86	-0.33	0.58	1.90	2.29	2.84
butyrophenone	-2.51	-1.50	-0.88	0.20	1.75	2.21	2.86
valerophenone	-3.53	-2.32	-1.56	-0.27	1.61	2.16	2.95
hexanophenone	-5.59	-3.82	-2.71	-0.81	1.95	2.77	3.94
benzene	-4.66	-2.79	-1.62	0.38	3.27	4.13	5.35
toluene	-3.73	-2.10	-1.07	0.68	3.21	3.96	5.02
ethylbenzene	-4.77	-2.98	-1.86	0.06	2.83	3.65	4.82
propylbenzene	-7.11	-4.46	-2.80	0.04	4.14	5.37	7.09
chlorobenzene	-3.43	-2.12	-1.29	0.11	2.15	2.76	3.61
bromobenzene	-3.49	-2.25	-1.47	-0.14	1.78	2.35	3.16
iodobenzene	-4.12	-2.68	-1.77	-0.22	2.02	2.69	3.63
methyl benzoate	-1.47	-0.69	-0.21	0.62	1.82	2.17	2.67
ethyl benzoate	-2.51	-1.49	-0.85	0.24	1.83	2.30	2.96
propyl benzoate	-3.25	-2.05	-1.30	-0.01	1.85	2.40	3.19
butyl benzoate	-6.62	-4.21	-2.70	-0.12	3.61	4.72	6.29
phenol	-2.95	-1.83	-1.12	0.09	1.83	2.35	3.09
p-cresol	-2.52	-1.58	-0.99	0.01	1.46	1.89	2.50
4-ethylphenol	-2.43	-1.54	-0.98	-0.03	1.36	1.77	2.35
4-propylphenol	-5.05	-3.35	-2.29	-0.48	2.15	2.93	4.04

Table 6.14 – Free energy changes (ΔG, kJ/mole) determined for vesicle/water partitioning of 20 neutral aromatic solutes using 15 mM $DPPG_{20}DHPC_{70}DPPC_{10}$.

	ΔG (kJ/mole)										
Solute	**16.3 °C**	**21.3 °C**	**25.8 °C**	**30.5 °C**	**36.1 °C**	**40.0 °C**	**44.9 °C**	**50.7 °C**	**60.2 °C**	**65.7 °C**	**70.5 °C**
acetophenone	-7.69	-7.93	-8.23	-8.46	-8.75	-8.75	-9.01	-9.13	-9.19	-8.95	-9.03
propiophenone	-9.81	-10.02	-10.39	-10.57	-10.83	-10.95	-11.27	-11.37	-11.49	-11.29	-11.43
butyrophenone	-11.96	-12.23	-12.68	-12.79	-13.17	-13.26	-13.60	-13.76	-13.91	-13.80	-13.82
valerophenone	-14.68	-14.98	-15.50	-15.51	-16.09	-16.19	-16.47	-16.67	-16.84	-16.79	-16.94
hexanophenone	-17.52	-18.00	-18.71	-18.85	-19.41	-19.48	-19.89	-19.96	-20.14	-20.18	-20.22
benzene	-9.48	-9.76	-10.07	-10.36	-10.66	-10.75	-11.14	-11.44	-11.46	-11.28	-11.55
toluene	-12.16	-12.37	-12.87	-13.13	-13.26	-13.49	-13.81	-14.07	-14.14	-14.16	-14.20
ethylbenzene	-14.68	-14.80	-15.42	-15.68	-15.80	-16.03	-16.47	-16.86	-16.97	-17.08	-17.17
propylbenzene	-17.32	-17.65	-18.27	-18.57	-18.89	-19.17	-19.58	-20.04	-20.17	-20.26	-20.36
chlorobenzene	-13.38	-13.69	-14.09	-14.06	-14.31	-14.61	-14.86	-15.13	-15.11	-14.84	-14.91
bromobenzene	-14.46	-14.73	-15.16	-15.17	-15.31	-15.61	-15.87	-16.10	-16.09	-15.98	-15.93
iodobenzene	-16.09	-16.45	-16.84	-16.87	-16.85	-17.16	-17.40	-17.60	-17.59	-17.50	-17.41
methyl benzoate	-9.77	-10.00	-10.28	-10.56	-10.78	-10.92	-11.27	-11.42	-11.56	-11.35	-11.37
ethyl benzoate	-11.84	-12.05	-12.45	-12.69	-12.95	-13.14	-13.45	-13.63	-13.86	-13.67	-13.83
propyl benzoate	-14.53	-14.74	-15.22	-15.43	-15.71	-15.93	-16.32	-16.49	-16.84	-16.71	-16.82
butyl benzoate	-17.09	-17.47	-18.09	-18.43	-18.69	-18.83	-19.27	-19.45	-19.93	-19.61	-19.85
phenol	-8.68	-8.87	-9.14	-9.26	-9.35	-9.45	-9.70	-9.56	-9.58	-9.42	-9.09
p-cresol	-10.55	-10.79	-11.04	-11.22	-11.19	-11.37	-11.54	-11.47	-11.57	-11.39	-11.28
4-ethylphenol	-12.87	-13.14	-13.37	-13.53	-13.45	-13.63	-13.83	-13.77	-13.90	-13.75	-13.55
4-propylphenol	-15.77	-16.09	-16.37	-16.37	-16.21	-16.48	-16.67	-16.64	-16.86	-16.63	-16.53

Table 6.15 – Enthalpy changes (ΔH, kJ/mole) determined for vesicle/water partitioning of 20 neutral aromatic solutes using 15 mM $DPPG_{20}DHPC_{70}DPPC_{10}$.

	ΔH (kJ/mole)										
Solute	**16.3 °C**	**21.3 °C**	**25.8 °C**	**30.5 °C**	**36.1 °C**	**40.0 °C**	**44.9 °C**	**50.7 °C**	**60.2 °C**	**65.7 °C**	**70.5 °C**
acetophenone	9.29	8.60	7.54	6.01	3.70	1.81	-0.88	-4.44	-11.07	-15.30	-19.18
propiophenone	6.67	6.60	6.01	4.90	3.00	1.34	-1.11	-4.48	-10.94	-15.15	-19.06
butyrophenone	7.09	6.85	6.09	4.80	2.67	0.84	-1.82	-5.45	-12.34	-16.81	-20.94
valerophenone	8.17	6.90	5.44	3.64	1.16	-0.77	-3.39	-6.76	-12.80	-16.56	-19.97
hexanophenone	19.56	13.92	9.25	4.73	-0.18	-3.33	-7.00	-10.94	-16.56	-19.40	-21.64
benzene	7.44	8.37	8.44	7.82	6.22	4.62	2.08	-1.60	-9.02	-14.00	-18.71
toluene	7.33	7.02	6.27	5.06	3.09	1.41	-1.01	-4.29	-10.50	-14.51	-18.22
ethylbenzene	3.41	4.40	4.63	4.27	3.12	1.89	-0.11	-3.06	-9.08	-13.16	-17.02
propylbenzene	7.73	7.98	7.52	6.39	4.28	2.36	-0.52	-4.54	-12.39	-17.55	-22.37
chlorobenzene	-0.93	1.31	2.22	2.16	0.86	-0.76	-3.55	-7.85	-16.92	-23.16	-29.14
bromobenzene	-1.37	0.07	0.51	0.17	-1.21	-2.73	-5.23	-8.97	-16.68	-21.93	-26.92
iodobenzene	-0.69	-1.36	-2.31	-3.63	-5.58	-7.16	-9.37	-12.30	-17.72	-21.15	-24.29
methyl benzoate	3.66	5.53	6.22	6.04	4.72	3.16	0.53	-3.47	-11.84	-17.58	-23.05
ethyl benzoate	5.24	5.85	5.75	5.03	3.43	1.89	-0.50	-3.92	-10.72	-15.25	-19.51
propyl benzoate	2.01	3.71	4.36	4.23	3.08	1.71	-0.61	-4.16	-11.59	-16.70	-21.57
butyl benzoate	11.84	9.36	7.00	4.43	1.22	-1.09	-4.07	-7.70	-13.82	-17.44	-20.64
phenol	2.12	2.57	2.26	1.26	-0.74	-2.60	-5.43	-9.42	-17.27	-22.47	-27.33
p-cresol	3.68	2.01	0.38	-1.44	-3.75	-5.44	-7.64	-10.36	-15.00	-17.78	-20.26
4-ethylphenol	-0.52	-1.52	-2.66	-4.06	-6.00	-7.50	-9.54	-12.15	-16.84	-19.75	-22.40

	ΔH (kJ/mole)										
Solute	**16.3 °C**	**21.3 °C**	**25.8 °C**	**30.5 °C**	**36.1 °C**	**40.0 °C**	**44.9 °C**	**50.7 °C**	**60.2 °C**	**65.7 °C**	**70.5 °C**
4-propylphenol	-4.76	-5.93	-7.06	-8.32	-9.90	-11.05	-12.55	-14.39	-17.52	-19.40	-21.06

Table 6.16 – Entropy change term ($T\Delta S$, kJ/mole) determined for vesicle/water partitioning of 20 neutral aromatic solutes using 15 mM $DPPG_{20}DHPC_{50}DPPC_{30}$.

	$T\Delta S$ (kJ/mole)										
Solute	**16.3 °C**	**21.3 °C**	**25.8 °C**	**30.5 °C**	**36.1 °C**	**40.0 °C**	**44.9 °C**	**50.7 °C**	**60.2 °C**	**65.7 °C**	**70.5 °C**
acetophenone	16.96	16.56	15.74	14.45	12.39	10.64	8.10	4.65	-1.94	-6.23	-10.23
propiophenone	16.47	16.68	16.34	15.49	13.86	12.36	10.08	6.87	0.51	-3.72	-7.71
butyrophenone	19.05	19.13	18.65	17.65	15.83	14.19	11.73	8.29	1.54	-2.94	-7.15
valerophenone	22.95	22.06	20.93	19.45	17.30	15.58	13.18	10.02	4.18	0.47	-2.96
hexanophenone	37.03	31.99	27.76	23.65	19.12	16.20	12.76	9.01	3.57	0.77	-1.48
benzene	16.98	18.21	18.56	18.22	16.95	15.55	13.23	9.76	2.52	-2.46	-7.23
toluene	19.45	19.48	19.02	18.10	16.45	14.97	12.76	9.69	3.67	-0.31	-4.05
ethylbenzene	18.02	19.33	19.86	19.81	19.01	18.01	16.28	13.60	7.90	3.92	0.08
propylbenzene	24.93	25.61	25.54	24.80	23.13	21.50	18.93	15.21	7.70	2.63	-2.19
chlorobenzene	12.58	15.05	16.21	16.40	15.40	13.96	11.36	7.23	-1.74	-8.07	-14.20
bromobenzene	13.16	14.85	15.51	15.41	14.31	12.96	10.64	7.07	-0.55	-5.84	-10.95
iodobenzene	15.39	14.98	14.26	13.16	11.43	9.99	7.91	5.10	-0.24	-3.70	-6.93
methyl benzoate	13.43	15.55	16.49	16.56	15.54	14.17	11.74	7.92	-0.33	-6.12	-11.72
ethyl benzoate	17.05	17.97	18.14	17.70	16.42	15.07	12.90	9.69	3.08	-1.44	-5.75
propyl benzoate	16.51	18.51	19.45	19.62	18.83	17.69	15.62	12.33	5.16	0.10	-4.80
butyl benzoate	28.88	26.88	24.92	22.71	19.89	17.82	15.10	11.71	5.85	2.29	-0.90
phenol	10.81	11.46	11.31	10.48	8.66	6.90	4.16	0.21	-7.75	-13.11	-18.20
p-cresol	14.26	12.83	11.38	9.72	7.57	5.97	3.84	1.17	-3.50	-6.37	-8.95
4-ethylphenol	12.40	11.61	10.64	9.39	7.61	6.20	4.24	1.68	-3.03	-6.02	-8.76
4-propylphenol	11.15	10.16	9.18	8.06	6.61	5.53	4.11	2.33	-0.78	-2.68	-4.39

Table 6.17 – Heat capacity change (ΔC_p, kJ/mole) determined for vesicle/water partitioning of 20 neutral aromatic solutes using 15 mM $DPPG_{20}DHPC_{70}DPPC_{10}$.

	ΔC_p (kJ/mole)										
Solute	**16.3 °C**	**21.3 °C**	**25.8 °C**	**30.5 °C**	**36.1 °C**	**40.0 °C**	**44.9 °C**	**50.7 °C**	**60.2 °C**	**65.7 °C**	**70.5 °C**
acetophenone	-0.08	-0.19	-0.28	-0.37	-0.46	-0.51	-0.58	-0.65	-0.74	-0.79	-0.83
propiophenone	0.05	-0.08	-0.18	-0.28	-0.39	-0.46	-0.54	-0.62	-0.74	-0.79	-0.84
butyrophenone	0.02	-0.11	-0.22	-0.32	-0.43	-0.50	-0.58	-0.67	-0.78	-0.84	-0.88
valerophenone	-0.22	-0.29	-0.35	-0.41	-0.47	-0.51	-0.56	-0.60	-0.67	-0.70	-0.72
hexanophenone	-1.18	-1.08	-1.00	-0.92	-0.84	-0.78	-0.72	-0.64	-0.54	-0.49	-0.45
benzene	0.28	0.09	-0.06	-0.20	-0.36	-0.46	-0.57	-0.69	-0.86	-0.95	-1.01
toluene	0.00	-0.12	-0.21	-0.30	-0.40	-0.46	-0.53	-0.60	-0.70	-0.75	-0.79
ethylbenzene	0.28	0.12	-0.01	-0.14	-0.27	-0.36	-0.46	-0.56	-0.70	-0.78	-0.83
propylbenzene	0.14	-0.03	-0.17	-0.30	-0.45	-0.54	-0.64	-0.75	-0.90	-0.97	-1.03
chlorobenzene	0.59	0.32	0.09	-0.12	-0.34	-0.49	-0.65	-0.83	-1.07	-1.20	-1.29
bromobenzene	0.40	0.18	0.01	-0.15	-0.33	-0.45	-0.57	-0.71	-0.91	-1.00	-1.08
iodobenzene	-0.09	-0.18	-0.25	-0.31	-0.38	-0.43	-0.48	-0.53	-0.61	-0.64	-0.67
methyl benzoate	0.50	0.25	0.06	-0.13	-0.33	-0.46	-0.61	-0.77	-0.99	-1.10	-1.18
ethyl benzoate	0.21	0.04	-0.09	-0.22	-0.35	-0.44	-0.54	-0.64	-0.79	-0.86	-0.92
propyl benzoate	0.45	0.23	0.06	-0.11	-0.29	-0.41	-0.54	-0.68	-0.88	-0.98	-1.05
butyl benzoate	-0.48	-0.51	-0.54	-0.56	-0.58	-0.60	-0.62	-0.63	-0.65	-0.66	-0.67
phenol	0.18	0.00	-0.14	-0.28	-0.43	-0.52	-0.63	-0.74	-0.90	-0.98	-1.04
p-cresol	-0.32	-0.35	-0.38	-0.40	-0.43	-0.44	-0.46	-0.48	-0.50	-0.51	-0.52
4-ethylphenol	-0.17	-0.23	-0.28	-0.32	-0.37	-0.40	-0.43	-0.47	-0.52	-0.54	-0.56
4-propylphenol	-0.22	-0.24	-0.26	-0.27	-0.29	-0.30	-0.31	-0.32	-0.34	-0.34	-0.35

Table 6.18 – Free energy changes (ΔG, kJ/mole) determined for SDS micelle/water partitioning of 20 neutral aromatic solutes using 40 mM SDS.

	ΔG (kJ/mole)						
Solute	**15 °C**	**20 °C**	**30 °C**	**40 °C**	**50 °C**	**60 °C**	**70 °C**
benzene	-11.33	-11.41	-11.40	-11.57	-11.76	-12.05	-11.76
toluene	-14.19	-13.82	-13.92	-14.15	-14.36	-14.61	-14.74
ethylbenzene	-16.34	-16.05	-16.18	-16.44	-16.65	-16.94	-17.01
propylbenzene	-18.66	-18.51	-18.93	-19.18	-19.39	-19.62	-19.54
methylbenzoate		-13.90	-14.23	-14.41	-14.46	-14.34	-14.34
ethylbenzoate		-16.09	-16.41	-16.63	-16.72	-16.64	-16.60
propylbenzoate		-18.37	-18.84	-19.06	-19.18	-19.08	-19.00
butylbenzoate		-20.98	-21.35	-21.61	-21.77	-21.61	-21.73
iodobenzene		-17.26	-17.65	-17.81	-17.81	-17.48	-17.61

Table 6.19 – Enthalpy changes (ΔH, kJ/mole) and entropy changes ($T\Delta S$, kJ/mole) determined for SDS micelle/water partitioning of 20 neutral aromatic solutes using 40 mM SDS.

	ΔH (kJ/mole)	**$T\Delta S$ (kJ/mole)**						
Solute		**15 °C**	**20 °C**	**30 °C**	**40 °C**	**50 °C**	**60 °C**	**70 °C**
benzene	-8.09	3.24	3.29	3.41	3.52	3.63	3.74	3.86
toluene	-9.88	4.01	4.08	4.22	4.36	4.50	4.64	4.78
ethylbenzene	-11.46	4.64	4.72	4.88	5.04	5.20	5.37	5.53
propylbenzene	-12.70	5.89	5.99	6.20	6.40	6.60	6.81	7.01
methylbenzoate	-11.74	2.31	2.35	2.43	2.51	2.59	2.67	2.75
ethylbenzoate	-13.30	2.91	2.96	3.06	3.17	3.27	3.37	3.47
propylbenzoate	-14.98	3.57	3.63	3.76	3.88	4.00	4.13	4.25
butylbenzoate	-16.99	4.10	4.17	4.31	4.45	4.59	4.74	4.88
iodobenzene	-16.25	1.22	1.24	1.29	1.33	1.37	1.41	1.45

Figure 6.1 – Retention factors of acetophenone, propiophenone, and butyrophenone as a function of total lipid concentration for 5 mM, 10 mM, 15 mM, 20 mM, 30 mM and 40 mM $DPPG_{20}DHPC_{50}DPPC_{30}$ at 35 °C.

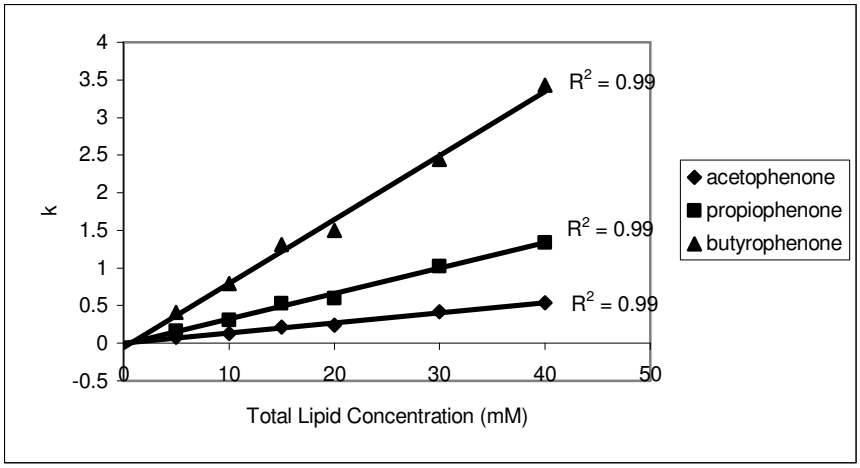

Figure 6.2 – Retention factors of acetophenone, propiophenone, and butyrophenone as a function of total lipid concentration for 5 mM, 10 mM, 15 mM, 20 mM, 30 mM and 40 mM $DPPG_{20}DHPC_{70}DPPC_{10}$ at 35 °C.

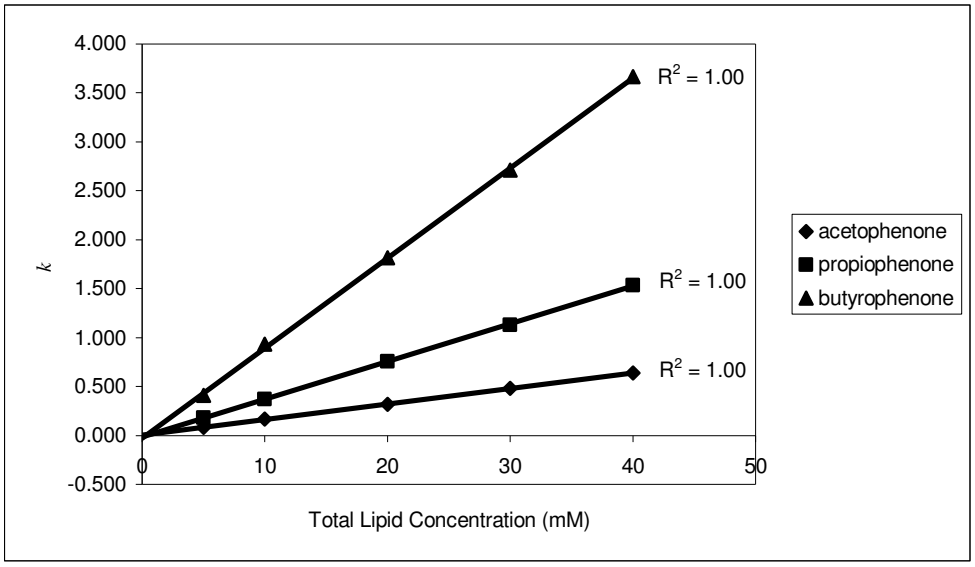

Figure 6.3 – Average diameter of 15 mM $DPPG_{20}DHPC_{50}DPPC_{30}$ as a function of temperature from 15 °C - 75 °C.

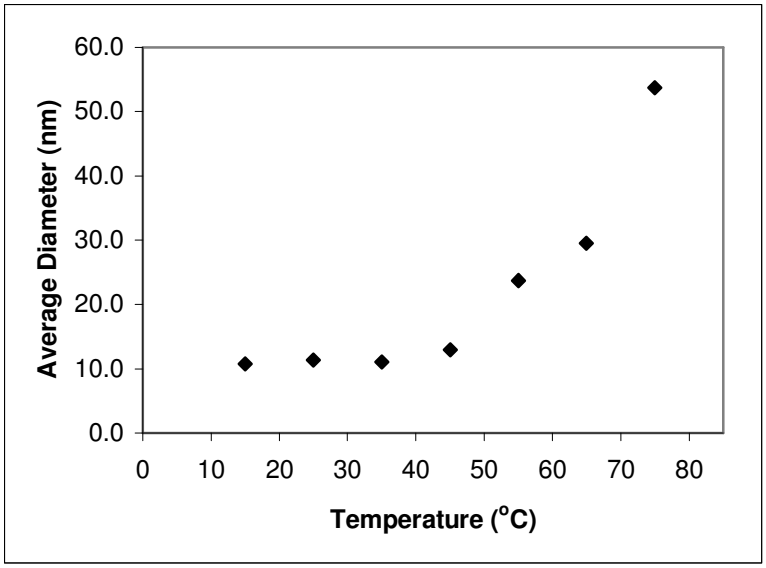

Figure 6.4 – Third-order polynomial Van't Hoff plots for acetophenone, propiophenone, butyrophenone, and valerophenone using 15 mM $DPPG_{20}DHPC_{50}DPPC_{30}$ from 15 °C-50 °C.

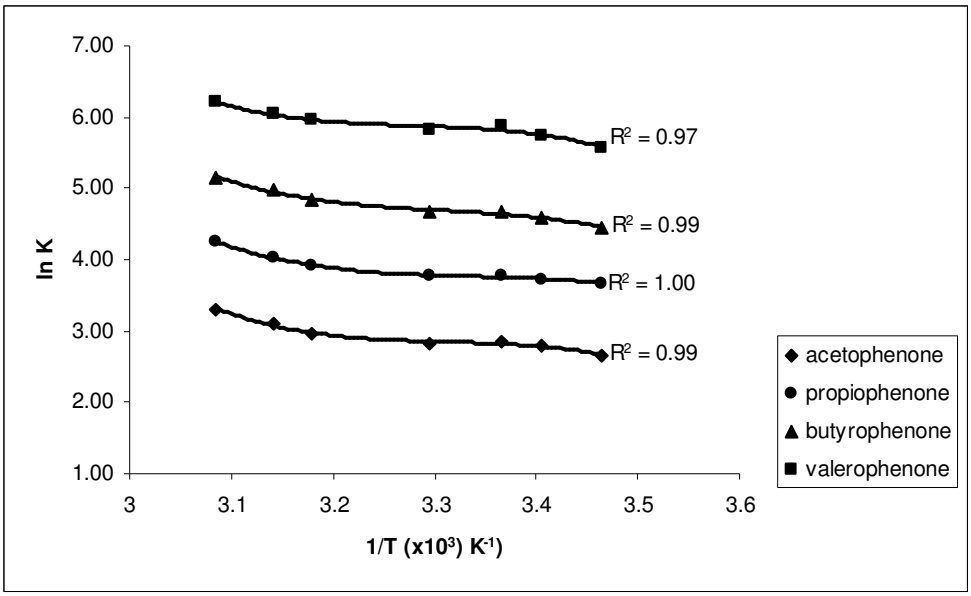

Figure 6.5 – Third-order polynomial Van't Hoff plots for benzene, toluene, ethylbenzene, and propylbenzene using 15 mM $DPPG_{20}DHPC_{50}DPPC_{30}$ from 15 °C-50 °C.

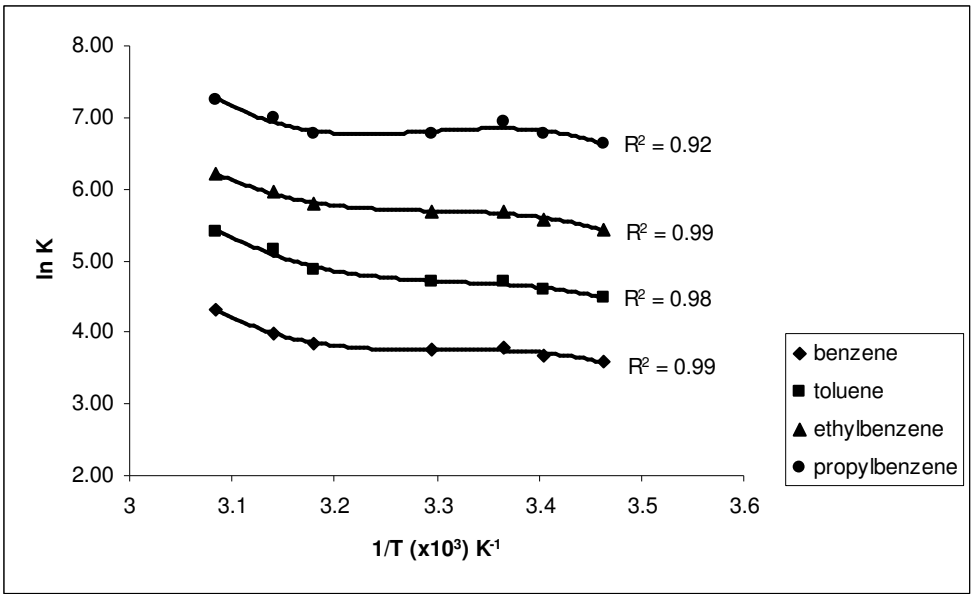

Figure 6.6 – Third-order polynomial Van't Hoff plots for chlorobenzene, bromobenzene, and iodobenzene using 15 mM $DPPG_{20}DHPC_{50}DPPC_{30}$ from 15 ^{o}C-50 ^{o}C.

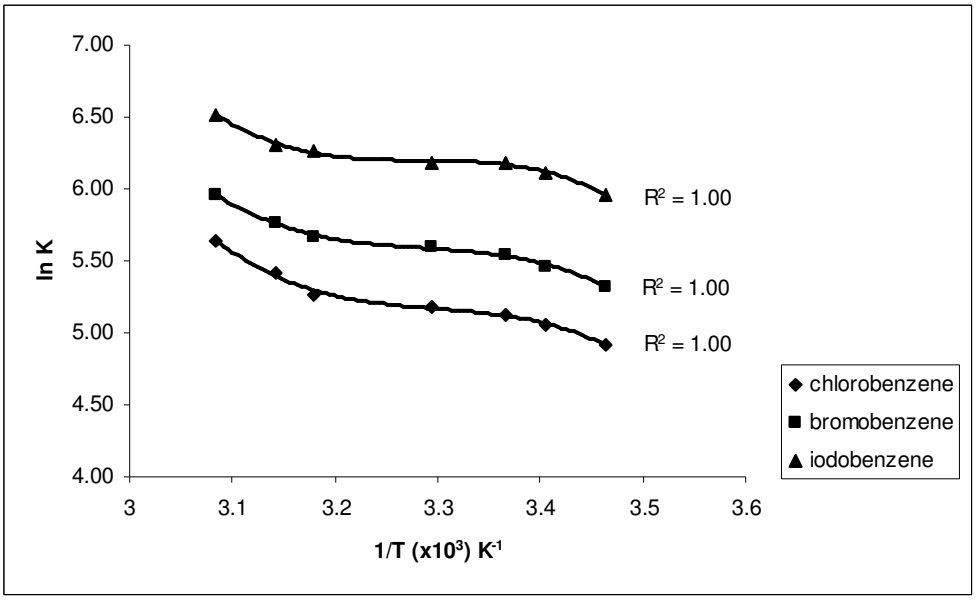

Figure 6.7 – Third-order polynomial Van't Hoff plots for methyl benzoate, ethyl benzoate, propyl benzoate and butyl benzoate using 15 mM $DPPG_{20}DHPC_{50}DPPC_{30}$ from 15 ^{o}C-50 ^{o}C.

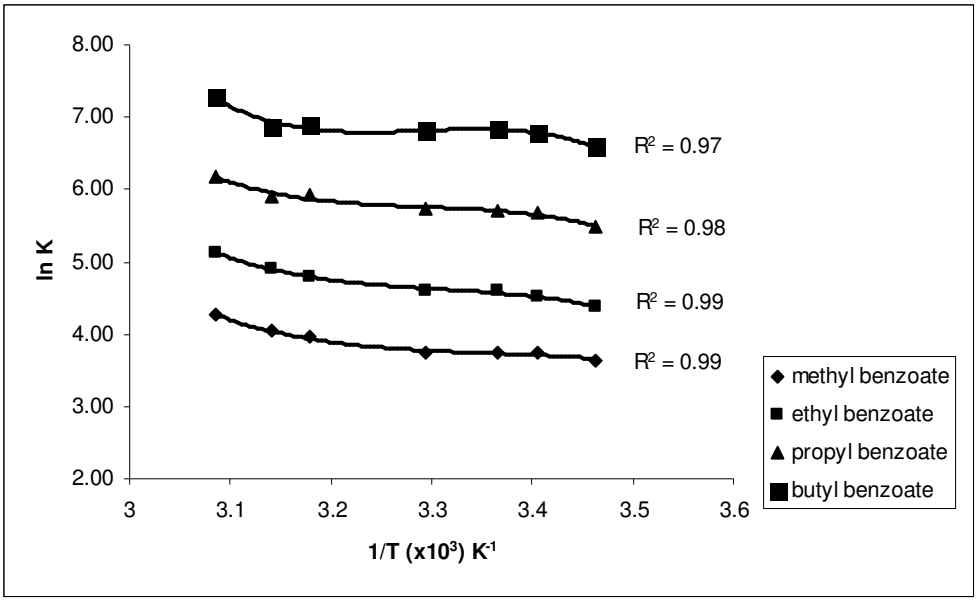

Figure 6.8 – Third-order polynomial Van't Hoff plots for phenol, p-cresol, 4-ethyl phenol and 4-propyl phenol using 15 mM $DPPG_{20}DHPC_{50}DPPC_{30}$ from 15 ^{o}C-50 ^{o}C.

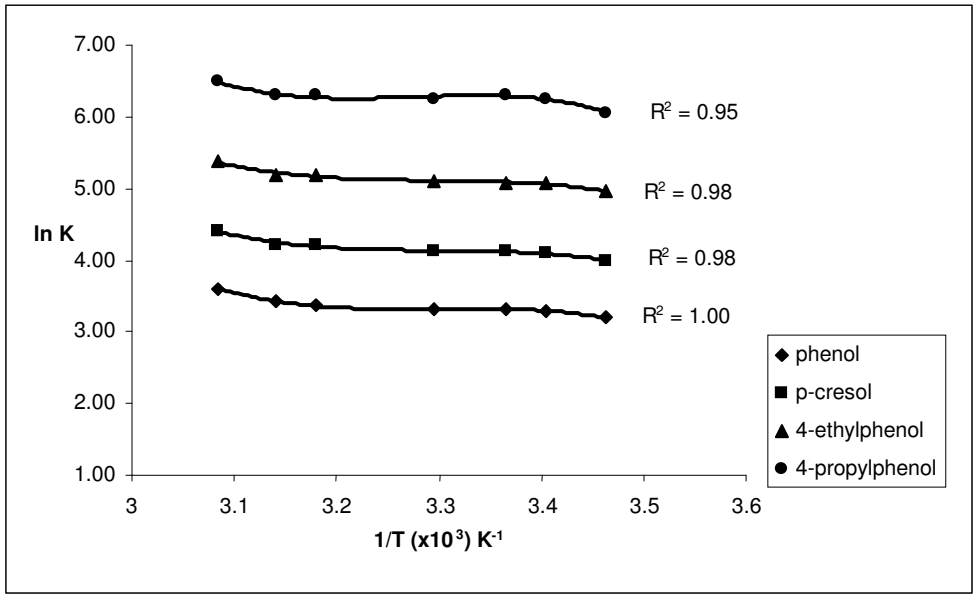

Figure 6.9 – Third-order polynomial Van't Hoff plots for acetophenone, propiophenone, butyrophenone, and valerophenone using 15 mM $DPPG_{20}DHPC_{70}DPPC_{10}$ from 15 °C-70 °C.

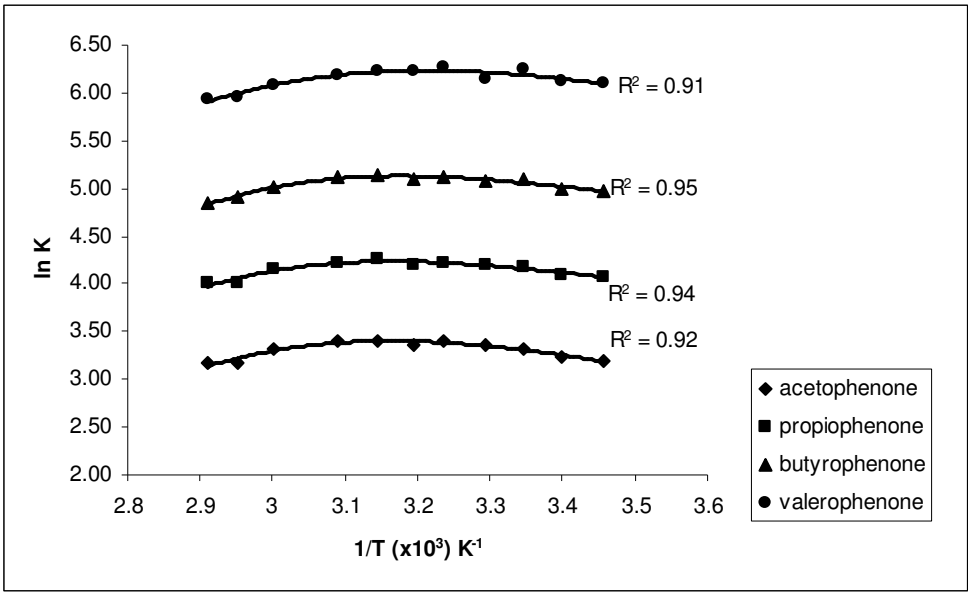

Figure 6.10 – Third-order polynomial Van't Hoff plots for benzene, toluene, ethylbenzene, propylbenzene using 15 mM $DPPG_{20}DHPC_{70}DPPC_{10}$ from 15 ^{o}C-70 ^{o}C.

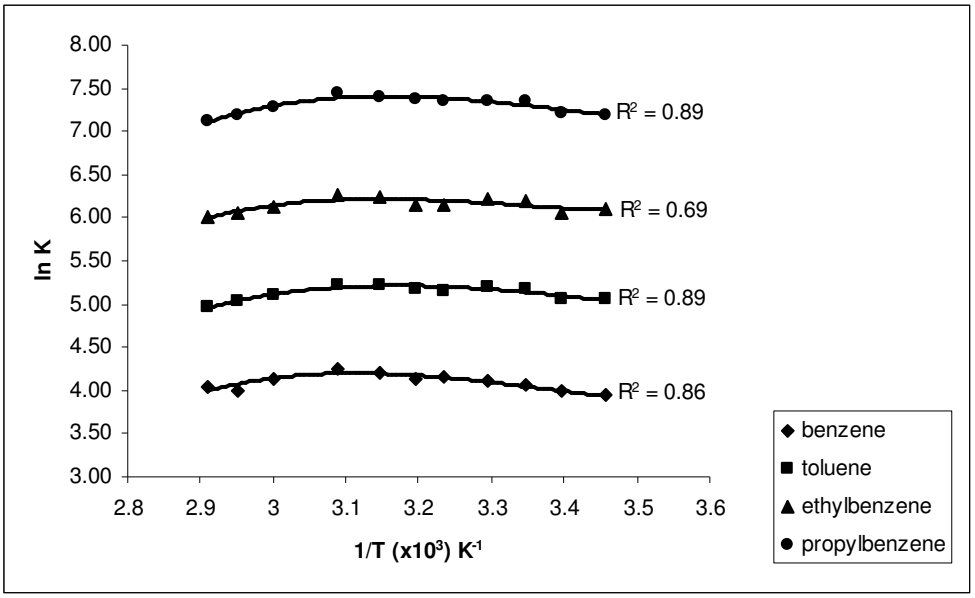

Figure 6.11 – Third-order polynomial Van't Hoff plots for chlorobenzene, bromobenzene, and iodobenzene using 15 mM $DPPG_{20}DHPC_{70}DPPC_{10}$ from 15 °C-70 °C.

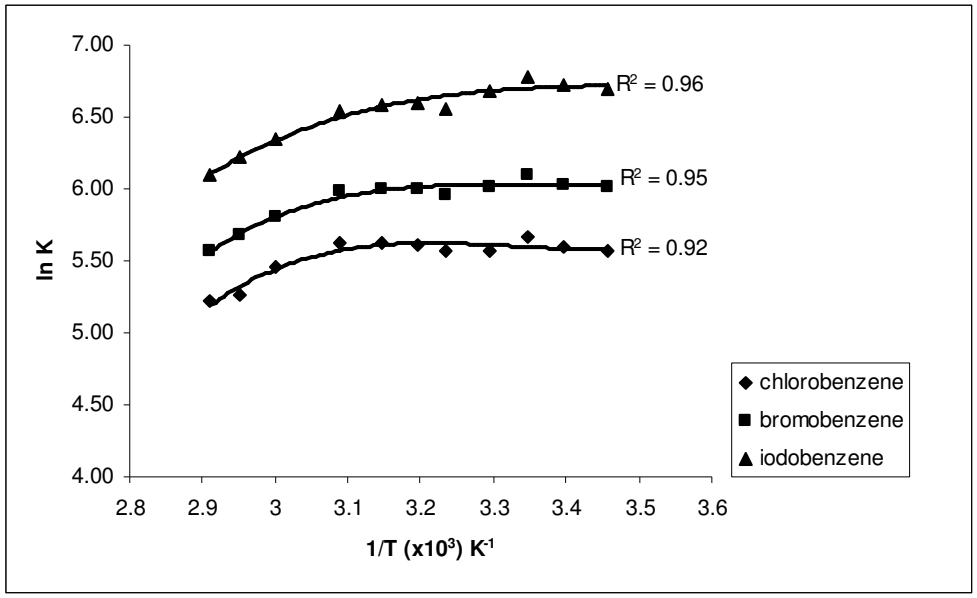

Figure 6.12 – Third-order polynomial Van't Hoff plots for methyl benzoate, ethyl benzoate, propyl benzoate, and butyl benzoate using 15 mM $DPPG_{20}DHPC_{70}DPPC_{10}$ from 15 °C-70 °C.

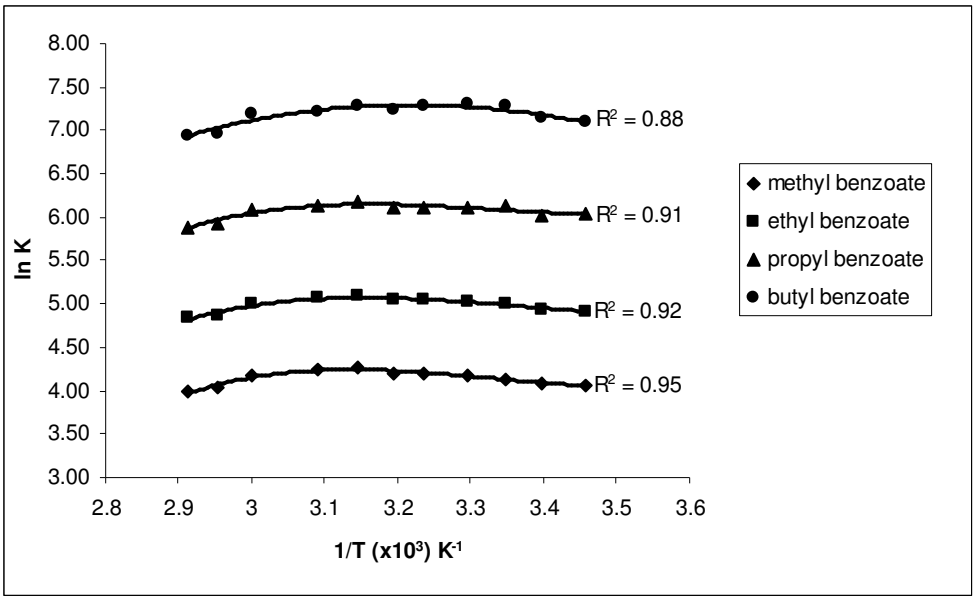

Figure 6.13 – Third-order polynomial Van't Hoff plots for phenol, p-cresol, 4-ethylphenol, 4-propylphenol using 15 mM $DPPG_{20}DHPC_{70}DPPC_{10}$ from 15 °C-70 °C.

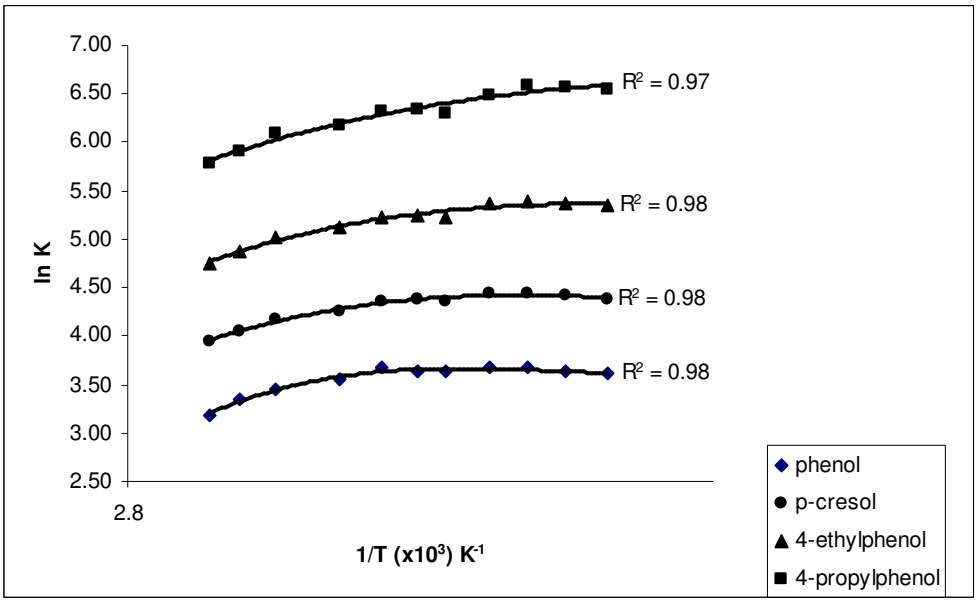

Figure 6.14 - Free energy change (ΔG), enthalpy change (ΔH), entropy change (ΔS), and heat capacity change (ΔC_p) associated with vesicle/water partitioning of benzene in the 15 mM $DPPG_{20}DHPC_{50}DPPC_{30}$ as a function of temperature.

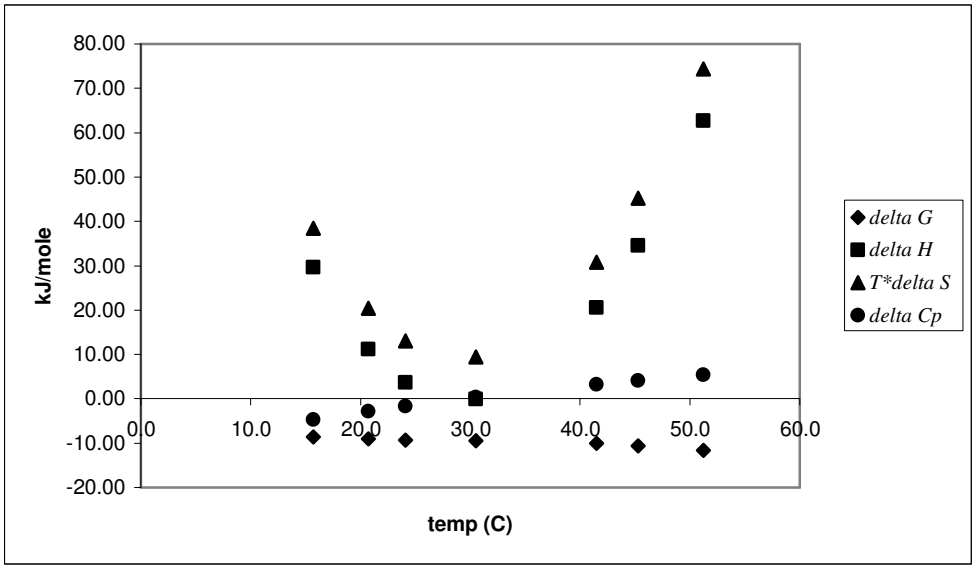

Figure 6.15 - Free energy change (ΔG), enthalpy change (ΔH), entropy change (ΔS), and heat capacity change (ΔC_p) associated with vesicle/water partitioning of acetophenone in the 15 mM $DPPG_{20}DHPC_{50}DPPC_{30}$ as a function of temperature.

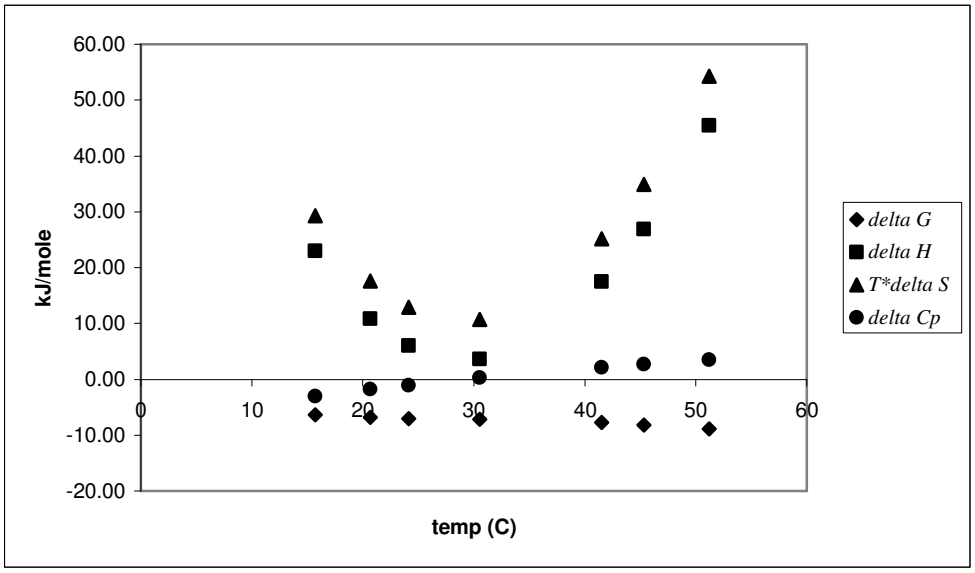

Figure 6.16 - Free energy change (ΔG), enthalpy change (ΔH), entropy change (ΔS), and heat capacity change (ΔC_p) associated with vesicle/water partitioning of chlorobenzene in the 15 mM $DPPG_{20}DHPC_{50}DPPC_{30}$ as a function of temperature.

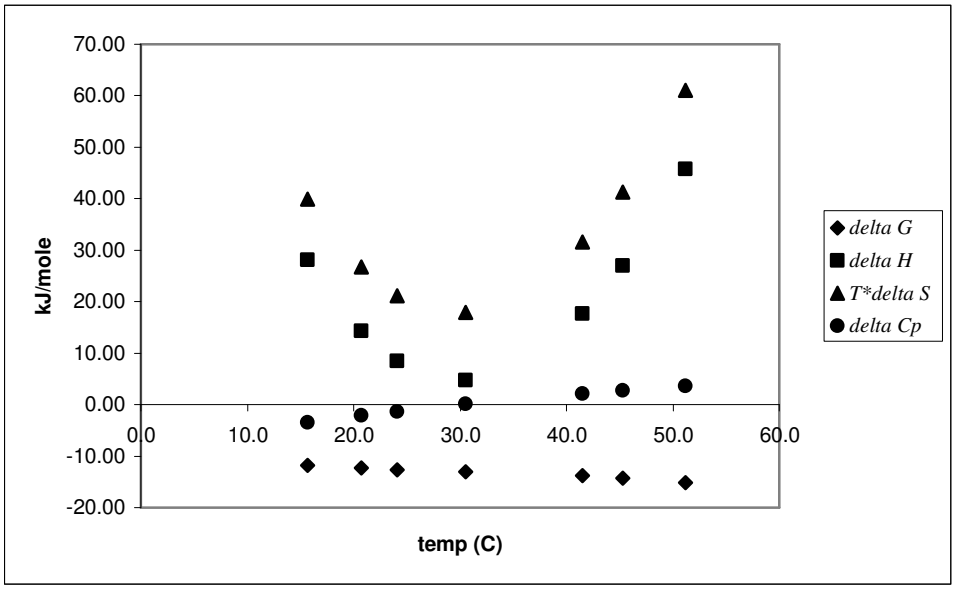

Figure 6.17 - Free energy change (ΔG), enthalpy change (ΔH), entropy change (ΔS), and heat capacity change (ΔC_p) associated with vesicle/water partitioning of methyl benzoate in the 15 mM $DPPG_{20}DHPC_{50}DPPC_{30}$ as a function of temperature.

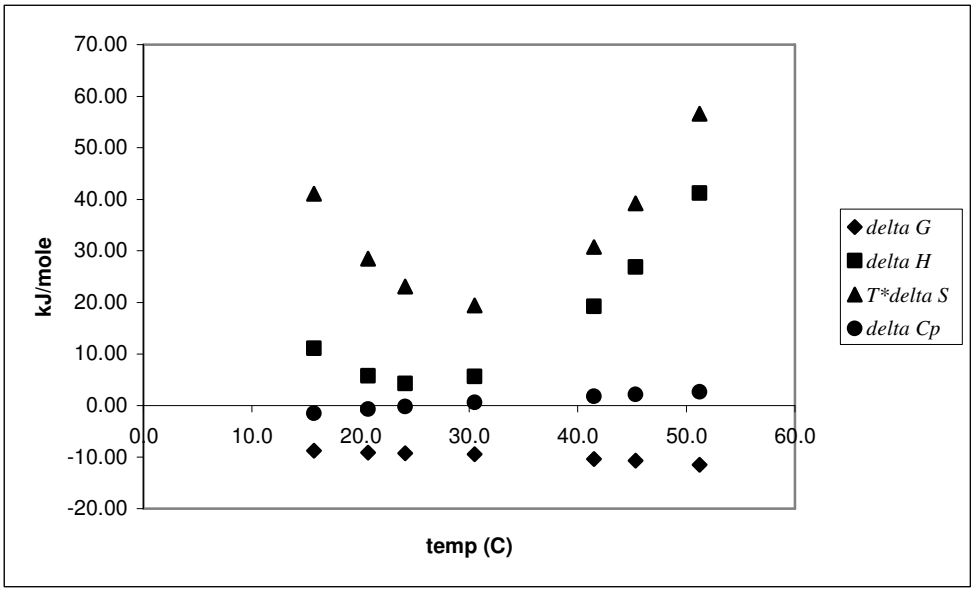

Figure 6.18 - Free energy change (ΔG), enthalpy change (ΔH), entropy change (ΔS), and heat capacity change (ΔC_p) associated with vesicle/water partitioning of phenol in the 15 mM $DPPG_{20}DHPC_{50}DPPC_{30}$ as a function of temperature.

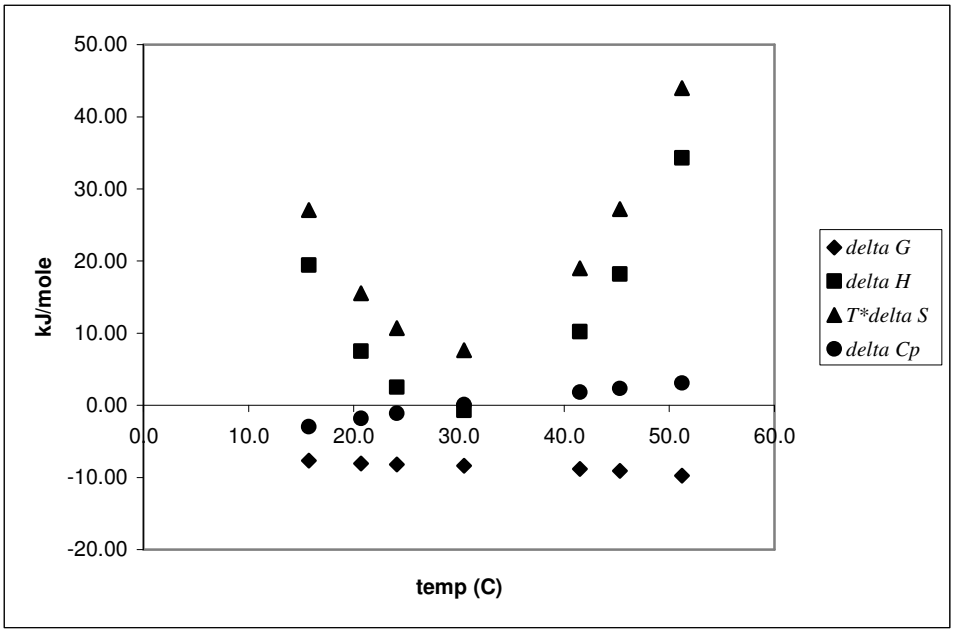

Figure 6.19 - Free energy change (ΔG), enthalpy change (ΔH), entropy change (ΔS), and heat capacity change (ΔC_p) associated with vesicle/water partitioning of benzene in the 15 mM $DPPG_{20}DHPC_{70}DPPC_{10}$ as a function of temperature.

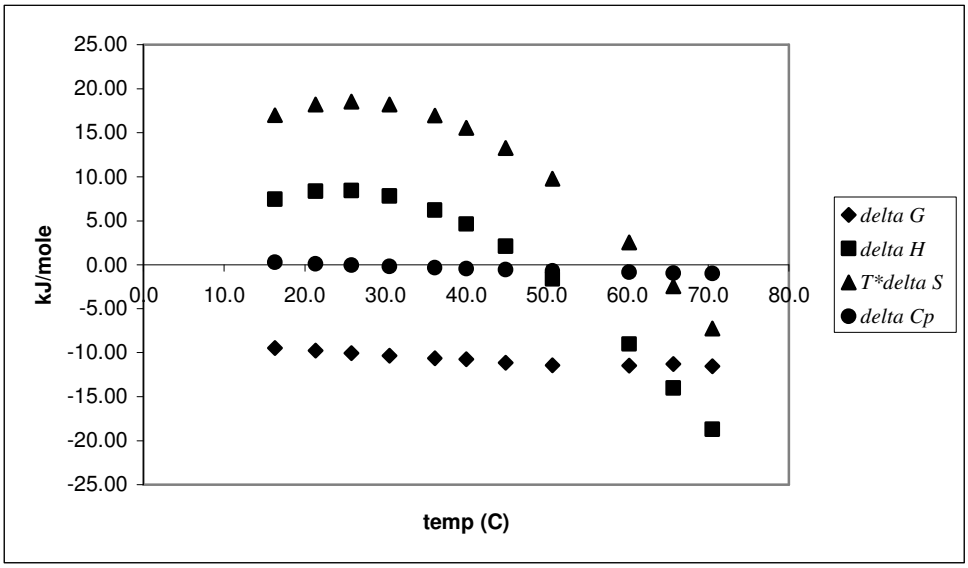

Figure 6.20 - Free energy change (ΔG), enthalpy change (ΔH), entropy change (ΔS), and heat capacity change (ΔC_p) associated with vesicle/water partitioning of acetophenone in the 15 mM $DPPG_{20}DHPC_{70}DPPC_{10}$ as a function of temperature.

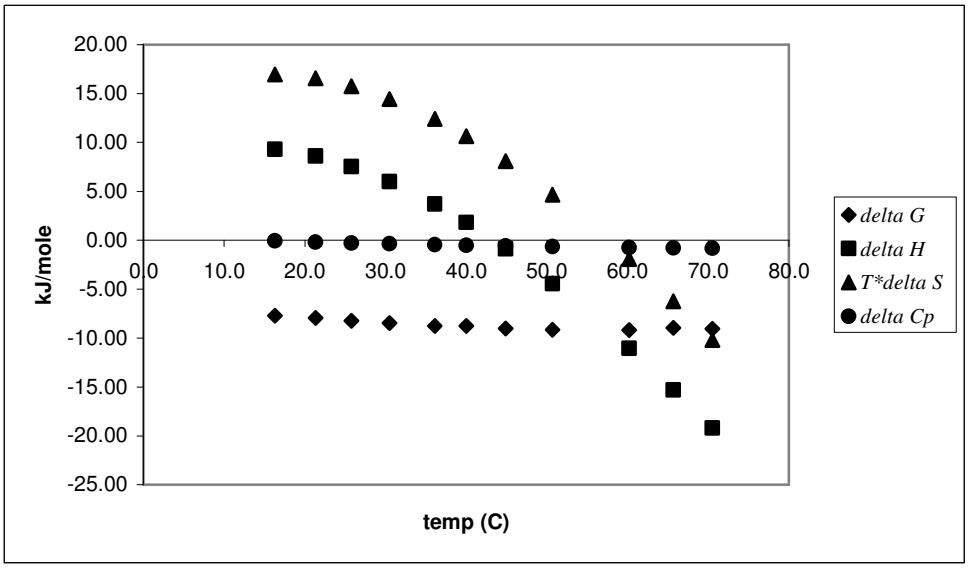

Figure 6.21 - Free energy change (ΔG), enthalpy change (ΔH), entropy change (ΔS), and heat capacity change (ΔC_p) associated with vesicle/water partitioning of chlorobenzene in the 15 mM $DPPG_{20}DHPC_{70}DPPC_{10}$ as a function of temperature.

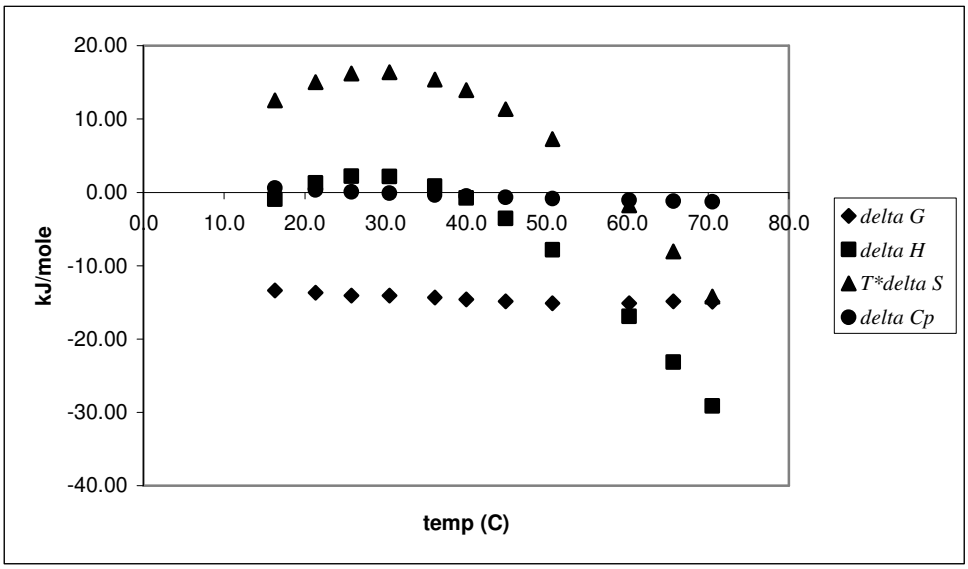

Figure 6.22 - Free energy change (ΔG), enthalpy change (ΔH), entropy change (ΔS), and heat capacity change (ΔC_p) associated with vesicle/water partitioning of methyl benzoate in the 15 mM $DPPG_{20}DHPC_{70}DPPC_{10}$ as a function of temperature.

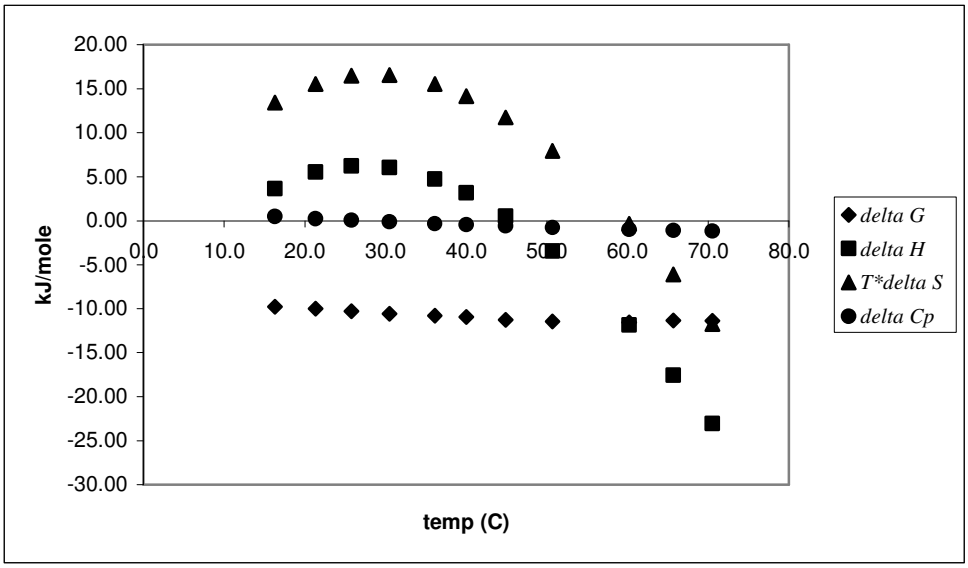

Figure 6.23 - Free energy change (ΔG), enthalpy change (ΔH), entropy change (ΔS), and heat capacity change (ΔC_p) associated with vesicle/water partitioning of phenol in the 15 mM $DPPG_{20}DHPC_{70}DPPC_{10}$ as a function of temperature.

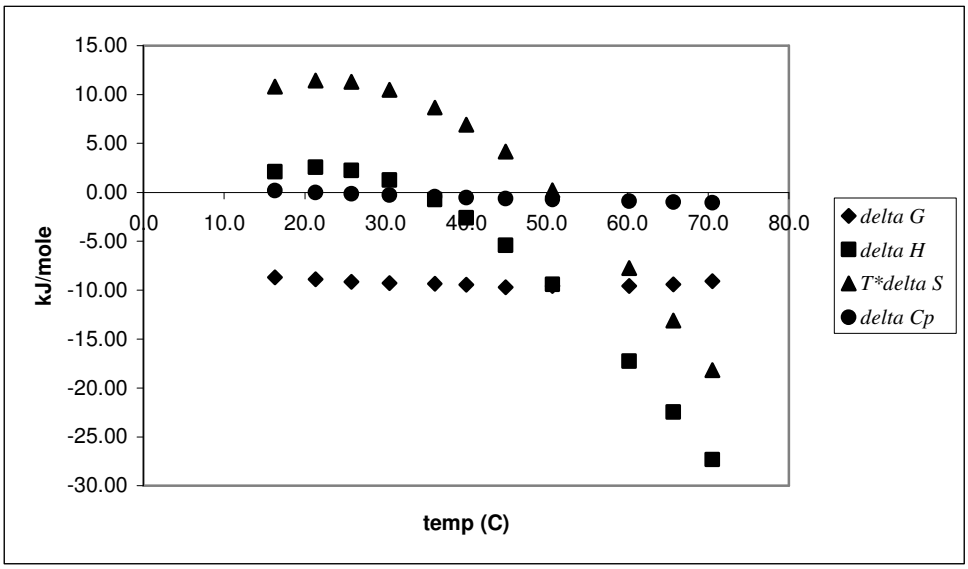

Chapter 7

Prediction of Human Epidermal Permeability Using Liposome Electrokinetic Chromatography (LEKC)

Abstract

A quantitative structure activity relationship (QSAR) was developed to predict skin permeability coefficients from three solute descriptors: liposome electrokinetic chromatography (LEKC) retention factors, molecular weight, and a descriptor of hydrogen bonding determined using the solute structure. Retention factors determined by LEKC are directly related to liposome/water partition coefficients and are therefore an excellent measure of a molecule's lipophilicity. This model was generated using a set of 44 solutes including neutral aromatic solutes, ionizable aromatic solutes, and neutral aliphatic solutes. The model was validated using the same set of solutes by the leave-one-out approach and favorably compared with other models used for the prediction of skin permeability coefficients using similar descriptors. Finally, skin permeability and the liposome/water partitioning system were compared using linear solvation energy relationships.

Introduction

Most organisms, including humans, have barrier membranes that serve as physical protection against the entrance of bacteria, viruses, and xenobiotic compounds. The most notable barrier membranes of the human body are the epithelial tissue and mucous membranes that line the digestive, respiratory, and genitourinary tracts, as well as the skin.[1] The skin is often considered to be the largest human organ. An average human weighing 65 kg will have approximately 18,000 cm^2 of skin surface area that weighs approximately 7 kg.[2] The skin serves multiple functions such as protection against microbes and xenobiotics, temperature control, metabolic functions and sensation. Numerous studies have focused on understanding the function of the skin as a barrier membrane and the determination or prediction of permeability of different compounds across the skin. Such studies are important for the development of pharmaceutical products and the assessment of the exposure risks for environmental pollutants. Good absorption of topically applied anti-inflammatory drugs has been shown to provide direct, localized, and immediate pain relief. Transdermal delivery of other pharmaceutical products allows minimized patient-to-patient absorption variability relative to oral delivery and easy termination of drug input.[3]

The outermost layer of the skin is the epidermis. The epidermis is subdivided into five layers or strata, the stratum germinativum, the stratum spinosum, the stratum granulosum, the stratum lucidum, and the stratum corneum.[4] The outermost stratum of the epidermis, the stratum corneum, is comprised of cells filled with a dense, crystalline protein called keratin packed in a lipid matrix. This lipid matrix includes phospholipids, sphingolipid, cholesterol, and free fatty acids arranged in lamellar sheets. In the stratum corneum, cholesterol is often found in equimolar amounts with other lipids. These keratocytes and the intercellular lipid matrix compose the main barriers for the exclusion of xenobiotics and microbes from the interior of the human body. The lower four strata of the epidermis are collectively referred to as the viable epidermis. The viable epidermis is comprised of live epithelial cells, melanocytes responsible for skin pigmentation, and nerve cells.[2]

Beneath the epidermis lies the papillary dermis, a layer of tissue that contains blood vessels and nerves.[5] The thickness of these three regions vary across the different regions of the body. In general, the stratum corneum is on the order of 10 μm thick, the viable epidermis is on the order of 100 μm thick, and the papillary dermis is on the order of 100-200 μm thick.[6]

Experiments have shown that the densely packed keratocytes and intercellular lipids that comprise the stratum corneum form the major barrier for permeation of xenobiotics across the entirety of the skin. As early as 1919, H.W. Smith et al. demonstrated that dichloroethyl sulfide, the blistering agent in mustard gas, can be washed away with solvents up to 15 minutes after application. From this data, Smith hypothesized that the compound was trapped in the outermost layers of the skin and therefore those layers must provide a barrier to permeants of the skin. In 1953, Blank et al. found that skin remains relatively impermeable to water unless the stratum corneum layer is selectively removed. Later studies used isotopic markers to show that the majority of compounds that an excised skin membrane is exposed to end up in the stratum corneum. From this data, it has been proposed that the mechanism for permeation of a xenobiotic compound across the skin is: 1. distribution of the compound from the outside medium into the stratum corneum, 2. diffusion of the compound across the stratum corneum, 3. diffusion of the compound across the viable epidermis, and 4. diffusion of the compound through the papillary dermis and into it blood vessels and capillaries. Permeability of compounds into the blood vessels and capillaries in the papillary dermis has been shown to be very high, therefore the wall of these vessels and capillaries provides no barrier for these compounds.[6]

The stratum corneum merely provides a passive barrier for permeability; no active modes of transport have been demonstrated. Therefore, it is reasonable to hypothesize that the permeability of a given compound across the stratum corneum is likely related to the lipophilicity or lipid solubility of the compound. Such relationships have been explored since Meyer and Overton noticed a strong correlation between the olive oil/water partitioning behavior and the narcotic activity of simple organic

compounds in the late nineteenth century.[7] In the early twentieth century, Schwenkenbacker noted greater skin permeability of lipid-soluble substances and relative impermeability of skin to water and electrolytes.[8] Correlation of skin permeability with properties of a compound that can be measured or determined independently of a permeability experiment allow the development of quantitative structure activity relationships (QSARs) that can be used to predict skin permeability. Such models are useful because direct determination of skin permeability requires reproducible tissue samples and long experiment times; such experiments are not suitable for the high-throughput screening that is generally performed to determine physicochemical properties of new pharmaceutical candidates.

Flynn, *et al.* generated one of the first QSARs by demonstrating the relationship between octanol/water partition coefficients ($P_{o/w}$) and skin permeability coefficients for a set of 90 compounds. In this work, Flynn noticed better correlations when the compound set was subdivided into sets of molecules with similar sizes.[9] Potts and Guy refined the work of Flynn by modeling skin permeability coefficients for the set of 90 compounds using $P_{o/w}$ and molecular weight.[10] Based on this work, Lien *et al*. improved upon the model built by Potts and Guy by adding a descriptor of hydrogen bonding ability. Specifically, Lien et al. proposed a model for predicting skin permeability coefficients (K_p) based on $P_{o/w}$, molecular weight (MW), and a measure of maximum hydrogen bonding ability determined by the structure of the molecule (H_b). This model can be described using:[3,11-12]

$$\log K_p = k_1 \log P_{o/w} + k_2 MW + k_3 H_b + k_4 \qquad \textbf{Equation 7.1}$$

where k_1, k_2, and k_3 are regression coefficients and k_4 is the regression constant.

The validity of the QSARs described above relies on the assumption that octanol/water partitioning adequately models the partitioning of compounds to the corneocytes and intercellular lipid matrix of the stratum corneum. This assumption may not be accurate because the octanol/water "bulk solvent" system does not necessarily mimic the interfacial system present in the lipid bilayer membranes that comprise most biological barrier membranes. The interfacial system present in biological membranes is characterized by significantly different membrane properties in different regions of the bilayers. This characteristic of biological membranes is not accurately modeled by octanol in the octanol/water system. Octanol/water partitioning experiments also have some inherent disadvantages. The shake-flask method that is traditionally used to determine $P_{o/w}$ is very time-consuming. Also, high lab-to-lab deviations have been reported for $P_{o/w}$ determinations.

Studies of liposome/water partitioning offer an alternative to octanol/water experiments in terms of studying lipophilicity to predict absorption or permeability of compounds. Liposome/water partition coefficients (K_{lw}) can be determined by equilibrium dialysis[13], potentiometry[13], calorimetry[14-15], spectrophotometry[16], immobilized liposome chromatography[17], or immobilized artificial membrane chromatography[18]. Khaledi, Burns, and Agbodjan have recently introduced liposome electrokinetic

chromatography (LEKC) as a tool for rapidly determining K_{lw}[19-20]. LEKC offers several advantages over other methods of determining K_{lw}, as well as studies of octanol/water partitioning. LEKC experiments are very fast and offer the possibility of determining K_{lw} values for multiple compounds at the same time. Preparation of a batch of liposomes normally requires approximately two hours and preparation of a capillary has similar time requirements. Individual LEKC runs last approximately 5-12 minutes, depending on the pH and buffers used. Using a single capillary, liposome/water partitioning behavior has been determined for up to six compounds in a single run. Use of a multiplexed instrument could significantly increase throughput. LEKC also allows the determination of K_{lw} using liposome phases that estimate the lipid and cholesterol composition of biologically significant membranes.

Retention factors determined from LEKC data are related to K_{lw} by **Equation 7.2** below:

$$k = \frac{n_{lip}}{n_{aq}} = \frac{[solute]_{lip}}{[solute]_{aq}} * \frac{V_{lip}}{V_{aq}} = K_{lw} * \Phi \quad \textbf{Equation 7.2}$$

where n_{lip} is the number of moles of a given solute in the lipid phase, n_{aq} is the number of moles of the solute in the aqueous phase, $[solute]_{lip}$ is the concentration of the solute in the lipid phase, $[solute]_{aq}$ is the concentration of the solute in the aqueous phase, V_{lip} is the volume of the lipid phase, V_{aq} is the volume of the aqueous phase, and Φ is the volume phase ratio of the chromatographic system.

In the present study, a new QSAR based on the model built by Lien et al. for the prediction of skin permeability of a set of aromatic and aliphatic compounds with permeability data published by the United States Environmental Protection Agency (EPA)[21] using LEKC retention factor, molecular weights, and maximum hydrogen bond ability was built.

Experimental

Refer to **Chapter 2** for experimental procedures and details concerning chemicals, liposome preparation, sample preparation, electrokinetic chromatography, calculation of retention factors for neutral and ionizable solutes, determination of linear solvation energy relationships (LSER) models, and prediction of retention factors of aliphatic solutes using linear solvation energy relationships models.

Determination of Maximum Hydrogen Bonding Ability

H_b was determined from each solute's structure using the rules described by Lien, et al.[3,11-12] Briefly, the number of hydrogen bond donors was determined by counting the number of hydrogen atoms capable of forming a hydrogen bond as a donor, mainly –OH and –NH. The number of hydrogen

bond acceptors was determined by counting the number of lone electron pairs capable of forming a hydrogen bond as an acceptor. H_b was therefore calculated as the sum of the number of hydrogen bond donors and the number of hydrogen bond acceptors.

Examples of determination of H_b for different common functional groups are included in **Figures 7.1-7.4**.

Results and Discussion

Preliminary Experiments

The first step in this project was to establish a preliminary relationship between LEKC retention data and skin permeability data. In 1992, the EPA published a survey of skin permeability data published in several papers by several different labs in *Dermal Exposure Assessment: Principles and Applications.*[21] Each skin permeability coefficient presented in this survey was graded on a scale of 0-100 using a scoring system based on the methodology used to determine the data in an effort to quantify the quality of the data. For the purposes of this study, only skin permeability data scored higher than 40 was used.

LSER models were generated for 15 mM $DPPG_{20}DPPC_{80}$, 15 mM $DPPG_{20}DPPC_{80}$/3 mM cholesterol, 15 mM $DPPG_{20}DPPC_{80}$/6 mM cholesterol, 15 mM $DPPG_{20}DPPC_{80}$/9 mM cholesterol, 15 mM $DPPG_{20}DPPC_{80}$/12 mM cholesterol, and 15 mM $DPPG_{20}DPPC_{80}$/15 mM cholesterol in 25 mM HEPES buffer, pH=7.5 using retention factors determined for a training set of 50 neutral aromatic compounds with known Abraham solute descriptors using each liposome phase studied**.** The retention factors generated using the lipid phases listed above for the training set of 50 neutral aromatic solutes were previously listed in **Table 4.1**. The system coefficients determined for the liposome phases were previously included in **Table 4.2**.

To establish a preliminary relationship between skin permeability coefficients and LEKC retention factors, a set of solutes was chosen with LEKC retention factors that had been determined for a set of liposome phases in previous studies or could be predicted using Abraham solute descriptors and LSERs for liposome phases determined in previous studies. The set of liposome phases used for this preliminary study included 15 mM $DPPG_{20}DPPC_{80}$, 15 mM $DPPG_{20}DPPC_{80}$/3 mM cholesterol, 15 mM $DPPG_{20}DPPC_{80}$/6 mM cholesterol, 15 mM $DPPG_{20}DPPC_{80}$/9 mM cholesterol, 15 mM $DPPG_{20}DPPC_{80}$/12 mM cholesterol, and 15 mM $DPPG_{20}DPPC_{80}$/15 mM cholesterol in 25 mM HEPES buffer, pH=7.5. A summary of the retention factors and r-squared values for this preliminary

experiment are included as **Table 7.1**. From this experiment, it was noted that the correlation between log K_p and log k improved for liposome phases with higher cholesterol content.

In response to the observation that the best correlation between LEKC retention factors and skin permeability coefficients occurred using 15 mM $DPPG_{20}DPPC_{80}$/15 mM cholesterol, retention factors for an expanded solute set were experimentally determined using this liposome phase.

Preliminary experiments were conducted using 25 mM HEPES buffer with pH=7.5 because that buffer condition had been used in previous LEKC experiments. The EPA literature contains no details about experimental buffer or pH conditions for the skin permeability experiments, but it was learned after the completion of these preliminary experiments that most of the skin permeability experiments had been performed using unbuffered water with a pH near 6.[22] Therefore, all subsequent LEKC experiments were conducted using both 25 mM HEPES at pH=7.5 and 25 mM MES at pH=6.0.

Comparison of Skin Permeability and Liposome/Water Partitioning Using Linear Solvation Energy Relationships

As discussed above, LEKC retention factors are directly proportional to liposome/water partition coefficients. Therefore, LSER models generated using these retention factors and skin permeability coefficients for solutes with known Abraham solute descriptors may be used to compare the interactions responsible for liposome/water partitioning and skin permeability.

The LSER models determined for 15 mM $DPPG_{20}DPPC_{80}$, 15 mM cholesterol at pH 6.0 using a set of 50 neutral aromatic solutes as well as an LSER model determined for skin permeability by Abraham, et al. are included in **Table 7.2**. The LSER model determined for 15 mM $DPPG_{20}DPPC_{80}$, 15 mM cholesterol at pH 7.5 was previously listed in **Table 4.2**. It is important to note that the Abraham LSER model for skin permeability includes several steroids with LSER descriptors that were determined by theoretical calculations while the LSER models based on LEKC retention factors were based on solute sets with experimentally determined descriptors.[23]

General trends for LSER models determined for liposome/water partitioning as described by LEKC retention factors have been discussed elsewhere in this dissertation. The dominant system coefficient in the LSER model for the skin permeability system is the b coefficient. The relatively large and negative b coefficient indicates that solute basicity strongly hinders permeability across dermal membranes. Smaller negative s and a coefficients indicate that solute dipolarity/polarizability and acidity also do not favor permeability across dermal membranes. The positive v coefficient indicates

that increased solute size improves permeability across dermal membranes. Finally, the small positive e coefficient indicates that interactions with n- or π- electrons improve skin permeability.

The b coefficient in the LSER models for skin permeability and liposome/water partitioning are both similarly large in magnitude and negative. The unfavorable effect of solute basicity is similar for both systems. The a coefficient in the LSER model for the skin permeability system is negative and significantly larger in magnitude than the same term in either LEKC model. This observation indicated that solute hydrogen bond acidity hinders permeability of a given solute across skin membranes more than it hinders distribution of the solute to a liposome phase or octanol phase. The increased magnitude of the a coefficient likely reflects the composition of the stratum corneum membranes that form the barrier to skin permeability. The interfacial regions of these membranes are hydrated and contain significant amounts of the protein keratin.[24]

The *v* term in the LSER model for the skin permeability system is positive and significantly smaller in magnitude than the same term in the LEKC models. This observation indicated that solute size favors permeability of a given solute across skin membranes less than it favors distribution of the solute to a liposome phase or octanol phase. Abraham, et al. proposed that the decreased v coefficient observed in LSER models of skin permeability relative to bulk solvent/water partitioning systems indicates that the skin is less "hydrocarbon-like" and more organized and cohesive than most organic solvents.[24] Another possible contribution to the relatively small magnitude of the v coefficient in the skin permeability model may be the nature of the kinetic phenomenon of diffusion as opposed to the equilibrium phenomenon of partitioning. From the mechanism proposed by Blank et al. the diffusion of a molecule across the stratum corneum is an important step in permeability of a molecule across epidermal membranes; this step depends upon the diffusion coefficient of the molecule in the given membrane, D_m. From the Stokes-Einstein equation, the diffusion coefficient of a molecule in any system is inversely proportional to the solute's volume. Therefore, while a solute's size contributes *favorably* to the equilibrium distribution of the solute to the membrane interfacial region and contributes *unfavorably* to the kinetic diffusion of the solute across the membrane.

Capillary Zone Electrophoresis of Ionizable Aromatic Solutes

CZE experiments were conducted using 25 mM MES pH 6.0 and 25 mM HEPES pH 7.5 for all solutes that could be ionizable at the experimental conditions. Apparent mobilities determined by CZE for these solutes are included in **Table 7.3**. Injections of several of the potentially ionized solutes resulted in peaks not resolved from the methanol peak used to mark the EOF. These solutes were assumed to be neutral at the given pH.

Retention Factors for Neutral Aromatic Solutes

Retention factors for all neutral aromatic solutes were determined for 15 mM $DPPG_{20}DPPC_{80}$, 15 mM Cholesterol prepared in 25 mM MES, pH=6.0 and 25 mM HEPES, pH=7.5 using the LEKC method described in **Chapter 2**. Included in this list are ionizable solutes, such as various phenols, shown to be neutral at the experimental conditions. These retention factors are included in **Table 7.4**.

Retention Factors for Ionizable Aromatic Solutes

Retention factors for ionizable aromatic solutes were determined for 15 mM $DPPG_{20}DPPC_{80}$, 15 mM Cholesterol prepared in 25 mM MES, pH=6.0 and 25 mM HEPES, pH=7.5 using LEKC and CZE data as described in **Chapter 2**. These retention factors are also included in **Table 7.4**.

Predicted Retention Factors for Neutral Aliphatic Solutes

Retention factors for neutral aliphatic solutes that could not be determined using LEKC were predicted for 15 mM $DPPG_{20}DPPC_{80}$, 15 mM Cholesterol using Abraham solute descriptors and the LSER model described in **Chapter 2**. The LSER system coefficients used to represent 15 mM $DPPG_{20}DPPC_{80}$, 15 mM Cholesterol in 25 mM MES pH 6.0 and 25 mM HEPES pH 7.5 are included in **Table 2**. The predicted retention factors are also included in **Table 7.4**.

Determining Maximum Hydrogen Bond Forming Ability

Maximum hydrogen bond forming ability was assessed for each solute as described above. These values are included as **Table 7.4**.

Building the Models by Stepwise Regression

The retention factors determined for the combined set of neutral aromatic solutes, partially ionized aromatic solutes, and neutral aliphatic solutes were used to build a model for skin permeability coefficients determined using multiple assays based on measurements of the flux of a compound across an actual skin sample[21] as discussed above. This skin permeability data is summarized in **Table 7.5**.

Models to predict skin permeability coefficients using retention factors from LEKC using 15 mM $DPPG_{20}DPPC_{80}$, 15 mM cholesterol at pH 6.0 and pH 7.5, molecular weights, and maximum hydrogen bonding ability was adapted from the Lien model for the combined set of neutral aromatic

solutes, partially ionized aromatic solutes, and neutral aliphatic solutes.[3,11-12] Molecular weight was divided by 100 to scale it with retention factors and maximum hydrogen bonding abilities. For comparison, a model was also built using octanol/water partition coefficients using the same solute set. Each of the three models was built using a stepwise regression procedure published by Massart et al.[25] The stepwise regression for each model is detailed in **Appendices A-4**, **A-5**, and **A-6**.

From the stepwise regression results, log k, MW/100, and H_b were all significant for the model built using retention factors for 15 mM $DPPG_{20}DPPC_{80}$, 15 mM cholesterol at pH 6.0. This model is described by:

$$\log K_p = 0.81(\pm 0.09)\log k - 0.75(\pm 0.25)\frac{MW}{100} - 0.12(\pm 0.03)H_b + 0.11(\pm 0.29) \quad \textbf{Equation 7.3}$$

R^2_{adj}=0.89, Standard Error=0.29, n=44

For the model built using retention factors for 15 mM $DPPG_{20}DPPC_{80}$, 15 mM cholesterol at pH 7.5, only log k and H_b were found to be significant. This model is described by:

$$\log K_p = 0.64(\pm 0.05)\log k - 0.15(\pm 0.02)H_b - 0.73(\pm 0.08) \quad \textbf{Equation 7.4}$$

R^2_{adj}=0.87, Standard Error=0.33, n=44

Similarly, for the model built using octanol/water partition coefficients, only log P_{ow} and H_b were found to be significant. This model is described by:

$$\log K_p = 0.43(\pm 0.05)\log P_{o/w} - 0.18(\pm 0.03)H_b - 1.94(\pm 0.16) \quad \textbf{Equation 7.5}$$

R^2_{adj}=0.80, Standard Error=0.40, n=44

From **Equations 7.3-7.5,** the model built using retention factors for 15 mM $DPPG_{20}DPPC_{80}$, 15 mM cholesterol at pH 6.0 (**Equation 7.3**) has the lowest standard error (SE=0.29) and highest adjusted R^2 value (R^2_{adj}=0.89). The models built using retention factors from 15 mM $DPPG_{20}DPPC_{80}$, 15 mM cholesterol at pH 7.5 (**Equation 7.4**, SE=0.33, R^2_{adj}=0.87) and octanol/water partition coefficients (**Equation 7.5**, SE=0.40, R^2_{adj}=0.80) both have higher standard errors and lower adjusted R^2 values. From these observations, the model described by **Equation 7.3** provides the best correlation between experimental skin permeability coefficients, LEKC retention factors, molecular weight, and hydrogen bond forming ability.

From the coefficients determined for these models, it is evident that log k and log $P_{o/w}$ both have a positive effect on log K_p while MW/100 and H_b have a negative effect on log K_p. Therefore, compounds with increasing lipophilicity as estimated by LEKC retention factors or octanol/water partitioning will have increased permeability across skin membranes. This observation is easily reconciled with the mechanism for permeability across skin membranes described above. Compounds with low lipophilicity will not enter the stratum corneum layer of cells and will not permeate across the rest of the membrane. Compounds with increased lipophilicity will readily enter

the stratum corneum layer of cells and will permeate across the rest of the membrane. The negative molecular weight-based correction for solute size included in **Equation 7.3** describes the discrepancy in the effect of a molecule's size on the distribution to the membrane from the aqueous phase and the kinetic diffusion of the molecule across the membrane. The negative hydrogen bonding correction included in all three of the models above indicates that compounds with increasing hydrogen bonding ability will also have decreased permeability across skin membranes. Such compounds are relatively hydrophilic; a molecule with excessive hydrogen bonding ability will remain in the aqueous phase rather than entering the stratum corneum. The necessity of these negative correction factors correlates well with the differences in the LSER models for the LEKC system and the skin permeability system as discussed above.

Validating the Models Using the Leave-One-Out Approach

The set of solutes with relevant retention factors, octanol/water partition coefficients, and skin permeability coefficients for this study only included 44 compounds. Therefore, there was not enough data available to build a suitable training set and separate test set for cross-validation. Instead, the models were validated using a leave-one out approach. By the leave-one-out approach to model validation, one data point is removed from the data set (with n total data points) and the model is generated using the remaining $n-1$ data points. This model is then used to predict a value for the removed data point. After n iterations, values for each data point in the data set are predicted. A plot of predicted values against experimental values is used to determine the accuracy of the model's predictive ability.[25]

A comparison of the predicted skin permeability coefficients determined using the models described by **Equation 7.3**, **Equation 7.4**, and **Equation 7.5** are included in **Table 7.5**. Scatter plots of predicted skin permeability coefficients determined using the models described by **Equation 7.3**, **Equation 7.4**, and **Equation 7.5** and experimental skin permeability coefficients are included as **Figure 7.5**, **Figure 7.6**, and **Figure 7.7**, respectively.

From **Figures 7.5**, **7.6**, and **7.7**, the best correlation between predicted skin permeability coefficients and experimental skin permeability coefficients is obtained using the model based on retention factors obtained using 15 mM $DPPG_{20}DPPC_{80}$, 15 mM cholesterol at pH 6.0 (R^2=0.87), closely followed by the model based on retention factors obtained using 15 mM $DPPG_{20}DPPC_{80}$, 15 mM cholesterol at pH 7.5 (R^2=0.85). Both of these models based on LEKC data offer better correlations than the model based on octanol/water partition coefficients (R^2=0.76). Much of the difference in these R^2 values can likely be explained by the difference in experimental conditions for skin permeability assays, LEKC experiments, and octanol/water experiments. LEKC experiments at pH 6.0 are closest to the

experimental conditions of the permeability experiments and LEKC experiments. Conversely, literature octanol/water partition coefficients describe the distribution of the solutes between octanol and water in their uncharged state. Varying dissociation/ionization of acidic and basic solutes strongly affect their skin permeability. Therefore, octanol/water partition coefficients are likely to not be very good predictors of skin permeability.

Comparison of the LEKC-Based Model with Literature Models of Skin Permeability

A summary of the model based on 15 mM $DPPG_{20}DPPC_{80}$, 15 mM cholesterol at pH 6.0 and pH 7.5 in comparison with several literature models is included in **Table 7.6.** While it is difficult to draw direct conclusions about the relative quality of two models unless the solute sets are exactly the same, some comparison is still worthwhile.

Flynn et al. proposed the first correlation between skin permeability coefficients and octanol/water partition coefficients.[9] They presented a very poor correlation (R^2=0.26) for a set of 90 solutes with molecular weights between 18 and greater than 750 and log $P_{o/w}$ between -3 and 6.[10] Better correlations were obtained for small sets of solutes of similar size.[38] These observations emphasize the importance of a term relating molecular size in models of skin permeability.

Potts and Guy added a molecular weight term to the model proposed by Flynn.[10] For a set of 42 compounds including water and assorted n-alkanols, n-alkanoic acids, alkanediols, and phenols, this model displayed better correlation (R^2=0.82).

Lien and Gao further refined the model proposed by Potts and Guy by adding a hydrogen bonding term, H_b. For a reduced set of 23 assorted n-alkanols, n-alkanoic acids, alkanediols, and phenols and water, this model displayed very good correlation (R^2=0.93). The weakeness of this model is the reduced size of the solute set.

Medina-Hernandez et al. proposed a chromatography-based model for skin permeability coefficients. This model used retention factors obtained from a biopartitioning micellar chromatography (BMC) method in place of octanol/water partition coefficients and the melting point of each solute. This model displayed good correlation (R^2=0.79) for a training set of 43 solutes including assorted n-alkanols, alkanediols, phenols, and steroids and water. This model was tested by predicting skin permeability coefficients for a set of 12 non-steroidal anti-inflammatories and opioid analgesics with reasonable success.[26]

The LEKC-based model presented in the current study compares favorably with all of these models. The best comparisons are drawn between the octanol/water-based model of Potts and Guy and the BMC-based model of Medina-Hernandez due to the similarity in sizes of the solute sets. All three models display similar correlation coefficients; the LEKC-based model displays a slightly better correlation than the other two. The LEKC-based method has some less tangible advantages relative to the other two models. First, this model is based on measurement of solute partitioning in a liposome/water system. This measurement removes the assumption that partitioning in a free solution interfacial biological lipid environment is the same as partitioning between two bulk solvents (octanol/water) or a between a bonded stationary phase and micellar mobile phase in liquid chromatography column (BMC). LEKC is also a much faster method than BMC or any method for experimentally determining octanol/water partition coefficients.

Conclusions

In conclusion, liposome water electrokinetic chromatography (LEKC) offers a very fast and reproducible method of determining liposome/water partitioning behavior. LEKC retention factors may be used as a descriptor of lipophilicity that avoids some of the assumptions inherent in lipophilicity estimation using octanol/water partition coefficients or other chromatographic methods. The current study introduces a quantitative structure-activity relationship (QSAR) model built and validated using a set of 44 neutral aromatic, ionizable aromatic, and neutral aliphatic solutes. This model compares favorably with other models in the literature based on octanol/water partition coefficients and other chromatographic methods. Finally, the LSER models determined for the skin permeability and LEKC systems highlight the differences between the two systems and the effect that these differences have on the QSAR introduced.

Works Cited

1. Campbell, N.A.; Reece, J.B.; Mitchell, L.G. *Biology*; Addison, Wesley, Longman, Inc.: Menlo Park, Ca., 1999; Fifth Edition.
2. Schaefer, H.; Redelmeier, T.E. *Skin Barrier: Principles of Percutaneous Absorption*; Karger: Basel, 1996.
3. Lien E.J.; Gao, H. QSAR Analysis of Skin Permeability of Various Drugs in Man as Compared to in Vivo and in Vitro Studies in Rodents. *Pharm. Res.* **1995**, *12* (4), 583-587.
4. Loyola University Medical Education Network Website: Introduction to the Skin. http://www.meddean.luc.edu/lumen/MedEd/medicine/dermatology/skinlsn/skini.htm (accessed May 2004).
5. Houk, J.; Guy, R.H. Membrane Models for Skin Penetration Studies. *Chem. Rev*. **1988**, *88* (3), 455-471.
6. Scheuplein, R.J.; Blank, I.H. Permeability of the Skin. *Physio. Rev*. **1971**, *51* (4), 702-747.
7. Meyer, H.H. Zur Theorie der Alkoholnarkose. Erste Mittheliung. Welche Eigenschaft der Anasethetica bedingt ihre narkotische Wirkung? *Arch. Exper. Path*. **1899**, *42*, 109-118.
8. Schwenkenbecker, A. Das Absorptionverniogen der haut. *Arch. Anat. Physiol*. **1904**, 121-164.
9. Flynn, GL Physicochemical determinants of skin absorption. In *Principles of Route-to-Route Extrapolation for Risk Assessment*; Edited by T.R. Garrity and C.J. Henry, Elsevier: New York. 1990; 93-127.
10. Potts, R.O.; Guy, R. Predicting Skin Permeability. *Pharm. Res.* **1992**, *9*, 663-669.
11. Lien, E.J.; Koda, R.T.; Tong, G.L. Buccal and Percutaneous Absorptions. *Drug Int. and Clin. Pharm.* **1971**, *5* (2), 38-41.
12. Ren, S.; Das, A.; Lien, E.J. QSAR Analysis of Membrane Permeability to Organic Compounds. *J. Drug. Target.* **1996**, *4* (1), 103-107.
13. Van Balen, G.P.; Martinet, C.A.M.; Caron, G.; Bouchard, G.; Reist, M.; Carrupt, P.A.; Fruttero, R.; Gasco, A.; Testa, B. Liposome/Water Lipophilicity: Methods, Information Content, and Pharmaceutical Applications. *Med. Res. Rev.* **2004**, *24* (3), 299-324.
14. Zhang, F.; Rowe, E.S. Titration Calorimetric and Differential Scanning Calorimetric Studies of the Interactions of n-Butanol with Several Phases of Dipalitoylphosphatidylcholine. *Biochemistry*. **1992**, *31*, 2005-2011.
15. Guy, P.T.; Parr, J.S.; Leung, T.W.; Zhang, F.; Rowe, E.S. Thermodynamics of Membrane Partitioning for a Series of n-Alcohols Determine by Titration Calorimetry: Role of Hydrophobic Effects. *Biochemistry*. **1998**, *37*, 2430-2440.

16. Pola, A.; Michalak, K.; Burliga, A.; Motohashi, N.; Kawase, M. Determination of lipid bilayers/water partition coefficient of new phenothiazines using the second derivative of absorption spectra method. *Eur. J. Pharm. Sci*. **2004**, *21*, 421-427.
17. Beigi, F.; Yang, Q.; Lundahl, P. Immobilized-Liposome Chromatographic Analysis of Drug Partitioning into Lipid Bilayers. *J. Chrom. A.* **1995**, *704* (2), 315-321.
18. Ong, S.W.; Liu, H.L.; Qiu, X.X.; Bhat, G.; Pidgeon, C. Membrane Partition-Coefficients Chromatographically Measured Using Immobilized Artificial Membrane Surfaces. *Anal. Chem*. **1995**, *67* (4), 755-762.
19. Burns, S.T.; Khaledi, M.G. Rapid determination of liposome-water partition coefficients (K-lw) using liposome electrokinetic chromatography (LEKC). *J. Pharm. Sci.* **2002**, *91* (7), 1601-1612.
20. Burns, S.T.; Agbodjan A.A.; Khaledi M.G. Characterization of solvation properties of lipid bilayer membranes in liposome electrokinetic chromatography. *J. Chrom. A*. **2002**, *973* (1-2), 167-176.
21. Exposure Assessment Group. *Dermal Exposure Assessment: Principle and Applications*; EPA/600/8-91/011B; U.S. Environmental Protection Agency, Office of Health and Environmental Assessment, U.S. Government Printing Office: Washington, DC, 1992.
22. Roberts, M.S. Personal Email; University of Queensland, Department of Medicine; 2004.
23. Abraham, M.H.; Martins, F.; Mitchell, R.C. Algorithms for Skin Permeability Using Hydrogen Bond Descriptors: the Problem of Steroids. *J. Pharm. Pharmacol*. **1997**, *49*, 858-865.
24. Abraham, M.H.; Chadha, H.S.; Mitchell, R.C. The Factors that Influence Skin Penetration of Solutes. *J. Pharm. Pharmacol*. **1995**, *47*, 8-16.
25. Massart, D.L.; Vandeginiste, B.G.M.; Buydens, L.M.C.; De Jong, S.; Lewi, P.J.; Smeyers-Verbeke, J. *Handbook of Chemometrics and Qualitmetrics: Part A;* Elsevier: Amsterdam, 1997.
26. Martinez-Pla, J.J.; Martin-Biosca, Y.; Sagrado, S.; Villaneuva-Camanas, R.W.; Medina-Hernandez, M.J. Biopartitioning micellar chromatography to predict skin permeability. *Biomed. Chrom.* **2003,** *17*, 530-537.

Table 7.1 – Demonstration of preliminary relationship between skin permeability coefficients (expressed as log K_p) and LEKC retention factors (expressed as log k) for 15 mM $DPPG_{20}DPPC_{80}$, 15 mM $DPPG_{20}DPPC_{80}$/3 mM cholesterol, 15 mM $DPPG_{20}DPPC_{80}$/6 mM cholesterol, 15 mM $DPPG_{20}DPPC_{80}$/9 mM cholesterol, 15 mM $DPPG_{20}DPPC_{80}$/12 mM cholesterol, and 15 mM $DPPG_{20}DPPC_{80}$/15 mM cholesterol in 25 mM HEPES buffer, pH=7.5. All skin permeability coefficients taken from reference 21. R^2 represents the correlation coefficient for log K_p as a function of log k.

		Experimental and Predicted log k 15 mM $DPPG_{20}DPPC_{80}$					
Solute Name	**log K_p**	**0 mM cholesterol**	**3 mM cholesterol**	**6 mM cholesterol**	**9 mM cholesterol**	**12 mM cholesterol**	**15 mM cholesterol**
1,4-dioxane*	-3.37	-2.57	-2.67	-2.70	-2.65	-2.85	-2.52
2,4-dimethylphenol*	-0.96	0.21	0.09	-0.10	-0.20	-0.31	-0.26
2-chlorophenol*	-1.48	-0.23	-0.31	-0.44	-0.49	-0.62	-0.50
2-ethoxyethanol*	-3.52	-2.58	-2.76	-2.87	-2.83	-3.02	-2.72
2-napthol*	-1.55	0.69	0.60	0.41	0.31	0.13	0.19
3,4-xylenol*	-1.44	0.19	0.07	-0.13	-0.25	-0.38	-0.33
4-bromophenol	-1.44	0.67	0.60	0.42	0.26	0.09	0.09
4-chloro-3-methyl phenol*	-1.26	0.76	0.65	0.41	0.25	0.11	0.10
4-chlorophenol	-1.44	0.49	0.37	0.22	0.06	-0.11	-0.09
4-ethylphenol	-1.46	0.30	0.18	-0.15	-0.27	-0.41	-0.41
aniline	-1.39	-1.00	-1.08	-1.10	-1.11	-1.36	-1.07
benzene	-0.95	-0.47	0.02	-0.49	-0.42	-0.35	-0.30
benzyl alcohol	-2.22	-1.02	-1.09	-1.15	-1.10	-1.29	-1.12
butanol*	-2.60	-1.45	-1.60	-1.72	-1.72	-1.81	-1.62
carbon disulfide*	-0.27	-0.65	-0.68	-0.60	-0.43	-0.38	-0.15
chloroform*	-0.89	-0.28	-0.33	-0.38	-0.36	-0.36	-0.24
decanol*	-1.10	1.50	1.41	1.12	0.94	1.02	0.86
ethanol*	-3.10	-2.43	-2.60	-2.65	-2.59	-2.74	-2.43
ethylbenzene	0.14	0.54	0.72	0.40	0.44	0.54	0.59
heptanol*	-1.42	0.03	-0.09	-0.29	-0.38	-0.39	-0.37
hexanol*	-1.56	-0.47	-0.60	-0.77	-0.83	-0.86	-0.79
m-cresol	-1.82	-0.17	-0.26	-0.60	-0.67	-0.79	-0.75
methanol*	-2.80	-2.84	-3.03	-3.07	-2.99	-3.17	-2.82

		Experimental and Predicted log k 15 mM $DPPG_{20}DPPC_{80}$					
Solute Name	**log K_p**	**0 mM cholesterol**	**3 mM cholesterol**	**6 mM cholesterol**	**9 mM cholesterol**	**12 mM cholesterol**	**15 mM cholesterol**
nonanol*	-1.22	1.00	0.90	0.65	0.49	0.55	0.44
o-cresol*	-1.80	0.00	-0.11	-0.28	-0.37	-0.51	-0.42
octanol*	-1.21	0.52	0.41	0.18	0.05	0.08	0.03
p-cresol	-1.76	-0.17	-0.30	-0.47	-0.60	-0.71	-0.66
pentanol*	-2.22	-0.96	-1.10	-1.24	-1.27	-1.33	-1.20
phenol	-2.09	-0.52	-0.69	-0.90	-0.88	-1.00	-0.88
propanol*	-2.77	-1.94	-2.10	-2.18	-2.15	-2.27	-2.02
styrene*	-0.17	0.41	0.41	0.36	0.37	0.38	0.46
tetrachloroethylene*	-0.43	0.59	0.59	0.56	0.58	0.66	0.71
toluene	0.00	0.05	0.40	0.01	0.04	0.13	0.17
trichloroethylene*	-0.64	0.09	0.05	0.03	0.06	0.12	0.22
water*	-2.81	-2.77	-3.04	-3.17	-3.17	-3.39	-3.09
	R^2	0.60	0.67	0.68	0.73	0.76	0.79

*solutes with log k predicted using Abraham solute descriptors and LSER models for given lipid phases.

Table 7.2 – LSER models for LEKC using 15 mM cholesterol in 25 mM MES, pH 6.0 and skin permeability coefficients (calculated as log K_p). The LSER model for skin permeability coefficients was determined by Abraham et al. and published in reference 23.

Liposome Composition	***v***	***b***	***a***	***s***	***e***	***C***	
15 mM $DPPG_{20}DPPC_{80}$ 15 mM Cholesterol 25 mM MES pH=6.0	3.25 (0.12)	-3.72 (0.13)	-0.12 (0.08)	-0.96 (0.13)	0.70 (0.13)	-2.01 (0.12)	R^2_{adj}=0.98 SE=0.12 n=50
skin permeability (determined by Abraham, et al.[40])	1.94 (0.11)	-3.44 (0.16)	-1.48 (0.13)	-0.49 (0.12)	0.44 (0.13)	-5.13 (0.10)	R^2_{adj}=0.96 SE=0.21 n=53

Table 7.3 - Apparent mobilities determined for potentially ionized aromatic solutes using CZE with 25 mM MES pH 6.0 and 25 mM HEPES pH 7.5. Solutes marked *coelute with* t_{eo} are result in peaks not resolved from the peak representing the unretained marker used to mark the mobility of the EOF.

	Average μ_0	
Solute Name	**25 mM MES pH 6.0**	**25 mM HEPES pH 7.5**
2,4,6-trichlorophenol	-1.082E-02	-1.995E-02
2,4-dichlorophenol	coelute with t_{eo}	-6.514E-03
2,4-dimethylphenol	coelute with t_{eo}	coelute with t_{eo}
2-amino-4-nitrophenol	-3.617E-03	-1.706E-02
2-chlorophenol	coelute with t_{eo}	-2.864E-03
2-napthol	coelute with t_{eo}	coelute with t_{eo}
3,4-dimethylphenol	coelute with t_{eo}	coelute with t_{eo}
3-nitrophenol	coelute with t_{eo}	-3.339E-03
4-amino-2-nitrophenol	-8.594E-04	-6.449E-03
4-bromophenol	coelute with t_{eo}	coelute with t_{eo}
4-chloro-3,5-dimethylphenol	coelute with t_{eo}	coelute with t_{eo}
4-chlorophenol	coelute with t_{eo}	coelute with t_{eo}
4-ethylphenol	coelute with t_{eo}	coelute with t_{eo}
4-fluorophenol	coelute with t_{eo}	coelute with t_{eo}
4-nitrophenol	-3.337E-03	-1.606E-02
aniline	1.493E-03	coelute with t_{eo}
m-cresol	coelute with t_{eo}	coelute with t_{eo}
methyl hydroxybenzoate	coelute with t_{eo}	coelute with t_{eo}
o-cresol	coelute with t_{eo}	coelute with t_{eo}
p-cresol	coelute with t_{eo}	coelute with t_{eo}
phenol	coelute with t_{eo}	coelute with t_{eo}
thymol	coelute with t_{eo}	coelute with t_{eo}

Table 7.4 – LEKC retention factors (expressed as log k) and hydrogen bonding data used to build skin permeability models. log k values marked with the superscript n were neutral at experimental conditions and were therefore determined using LEKC retention data alone. log k values marked with the superscript i were partially ionized at experimental conditions and were therefore determined using both LEKC and CZE retention data. log k values marked with the superscript p were correspond to aliphatic solutes. log k values for these solutes were predicted using the LSER models.

Solute Name	25 mM MES pH 6.0	25 mM HEPES pH 7.5	Number Of Hydrogen Bond Donors	Number Of Hydrogen Bond Acceptors	H_b
1,4-dioxane	-2.67^{p}	-2.52^{p}	0	4	4
2,4,6-trichlorophenol	0.42^{i}	-0.68^{i}	1	2	3
2,4-dichlorophenol	0.48^{n}	0.20^{i}	1	2	3
2,4-dimethylphenol	-0.47^{n}	-0.52^{n}	1	2	3
2-amino-4-nitrophenol	-0.61^{i}	-1.08^{i}	3	8	11
2-chlorophenol	-0.56^{n}	-0.71^{i}	1	2	3
2-ethoxyethanol	-2.88^{p}	-2.72^{p}	1	4	5
2-napthol	0.39^{n}	0.24^{n}	1	2	3
3,4-dimethylphenol	-0.55^{n}	-0.64^{n}	1	2	3
3-nitrophenol	-0.34^{n}	-0.46^{i}	1	7	8
4-amino-2-nitrophenol	-1.01^{i}	-1.09^{i}	3	8	11
4-bromophenol	0.09^{n}	0.09^{n}	1	2	3
4-chloro-3,5-dimethylphenol	0.51^{n}	0.38^{n}	1	2	3
4-chloro-3-methyl phenol	0.18^{n}	0.16^{n}	1	2	3
4-chlorophenol	-0.11^{n}	-0.09^{n}	1	2	3
4-ethylphenol	-0.41^{n}	-0.41^{n}	1	2	3

Solute Name	25 mM MES pH 6.0	25 mM HEPES pH 7.5	Number Of Hydrogen Bond Donors	Number Of Hydrogen Bond Acceptors	H_b
4-nitrophenol	-0.40[i]	-0.84[i]	1	7	8
aniline	-0.92[i]	-1.07[n]	2	1	3
benzene	-0.30[n]	-0.30[n]	0	0	0
benzyl alcohol	-1.21[n]	-1.13[n]	1	2	3
butanol	-1.71[p]	-1.62[p]	1	2	3
carbon disulfide	-0.26[p]	-0.15[p]	0	0	0
chloroform	-0.27[p]	-0.24[p]	0	0	0
decanol	1.01[p]	0.86[p]	1	2	3
ethanol	-2.61[p]	-2.43[p]	1	2	3
ethylbenzene	0.61[n]	0.59[n]	0	0	0
heptanol	-0.35[p]	-0.37[p]	1	2	3
hexanol	-0.80[p]	-0.79[p]	1	2	3
m-cresol	-0.73[n]	-0.75[n]	1	2	3
methanol	-3.04[p]	-2.82[p]	1	2	3
methyl hydroxybenzoate	-0.59[n]	-0.47[n]	1	6	7
nonanol	0.56[p]	0.44[p]	1	2	3
o-cresol	-0.81[n]	-0.79[n]	1	2	3
octanol	0.10[p]	0.03[p]	1	2	3
p-cresol	-0.70[n]	-0.66[n]	1	2	3
pentanol	-1.26[p]	-1.20[p]	1	2	3
phenol	-0.97[n]	-0.88[n]	1	2	3

Solute Name	25 mM MES pH 6.0	25 mM HEPES pH 7.5	Number Of Hydrogen Bond Donors	Number Of Hydrogen Bond Acceptors	H_b
propanol	-2.16[p]	-2.02[p]	1	2	3
styrene	0.41[n]	0.32[n]	0	0	0
tetrachloroethylene	0.73[p]	0.71[p]	0	0	0
thymol	-0.20[n]	-0.34[n]	1	2	3
toluene	0.19[n]	0.17[n]	0	0	0
trichloroethylene	0.20[p]	0.22[p]	0	0	0
water	-3.30[p]	-3.09[p]	2	2	4

Table 7.5 – Experimental skin permeability data used to build the model. K_p, log K_p, and score values taken from reference 21 and predicted log K_p values determined using **Equations 7.3**, **7.4**, and **7.5**.

Solute Name	Experimental K_p (cm/h)	Experimental log K_p	Score	Predicted log K_p Equation 7.3	Predicted log K_p Equation 7.4	Predicted log K_p Equation 7.5
1,4-dioxane	4.30E-04	-3.37	70	-3.17	-2.91	-2.72
2,4,6-trichlorophenol	5.90E-02	-1.23	70	-1.45	-1.64	-0.84
2,4-dichlorophenol	6.01E-02	-1.22	70	-1.08	-1.05	-1.14
2,4-dimethylphenol	1.10E-01	-0.96	45	-1.56	-1.54	-1.49
2-amino-4-nitrophenol	6.60E-04	-3.18	70	-2.78	-3.10	-3.25
2-chlorophenol	3.31E-02	-1.48	70	-1.68	-1.65	-1.54
2-ethoxyethanol	3.00E-04	-3.52	70	-3.51	-3.21	-2.92
2-napthol	2.79E-02	-1.55	70	-1.00	-1.02	-1.29
3,4-dimethylphenol	3.60E-02	-1.44	70	-1.62	-1.61	-1.51
3-nitrophenol	5.64E-03	-2.25	70	-2.18	-2.26	-2.53
4-amino-2-nitrophenol	2.80E-03	-2.55	70	-3.43	-3.32	-3.79
4-bromophenol	3.61E-02	-1.44	70	-1.48	-1.12	-1.34
4-chloro-3,5-dimethylphenol	5.90E-02	-1.23	70	-0.97	-0.94	-0.98
4-chloro-3-methyl phenol	5.50E-02	-1.26	70	-1.17	-1.08	-1.12
4-chlorophenol	3.63E-02	-1.44	70	-1.30	-1.25	-1.43
4-ethylphenol	3.49E-02	-1.46	70	-1.51	-1.45	-1.43
4-nitrophenol	5.58E-03	-2.25	70	-2.23	-2.51	-2.57
aniline	4.10E-02	-1.39	55	-1.71	-1.90	-2.15
benzene	1.11E-01	-0.95	70	-0.69	-0.92	-1.02
benzyl alcohol	6.00E-03	-2.22	70	-2.04	-1.90	-2.03
butanol	2.50E-03	-2.60	70	-2.18	-2.21	-2.13
carbon disulfide	5.40E-01	-0.27	55	-0.73	-0.86	-1.16
chloroform	1.30E-01	-0.89	55	-1.01	-0.88	-1.10
decanol	8.00E-02	-1.10	70	-0.58	-0.60	-0.39
ethanol	8.00E-04	-3.10	70	-2.67	-2.71	-2.59
ethylbenzene	1.38E+00	0.14	70	-0.23	-0.39	-0.62
heptanol	3.76E-02	-1.42	70	-1.41	-1.43	-1.29
hexanol	2.77E-02	-1.56	80	-1.68	-1.70	-1.59

Solute Name	Experimental K_p (cm/h)	Experimental log K_p	Score	Predicted log K_p Equation 7.3	Predicted log K_p Equation 7.4	Predicted log K_p Equation 7.5
m-cresol	1.52E-02	-1.82	70	-1.65	-1.67	-1.62
methanol	1.60E-03	-2.80	70	-2.99	-2.56	-2.69
methyl hydroxybenzoate	9.12E-03	-2.04	70	-2.40	-2.12	-2.18
nonanol	6.00E-02	-1.22	70	-0.87	-0.89	-0.55
o-cresol	1.57E-02	-1.80	70	-1.72	-1.69	-1.62
octanol	6.10E-02	-1.21	70	-1.14	-1.17	-1.16
p-cresol	1.75E-02	-1.76	70	-1.63	-1.61	-1.63
pentanol	6.00E-03	-2.22	70	-1.93	-1.96	-1.90
phenol	8.22E-03	-2.09	70	-1.73	-1.75	-1.84
propanol	1.70E-03	-2.77	70	-2.43	-2.47	-2.34
styrene	6.70E-01	-0.17	70	-0.36	-0.55	-0.69
tetrachloroethylene	3.70E-01	-0.43	55	-0.55	-0.25	-0.46
thymol	5.28E-02	-1.28	70	-1.56	-1.41	-1.02
toluene	1.01E+00	0.00	55	-0.48	-0.66	-0.80
trichloroethylene	2.30E-01	-0.64	55	-0.71	-0.58	-0.82
water	1.55E-03	-2.81	80	-3.29	-3.44	-3.24

Table 7.6 - Comparison of the model presented in this study with models presented in literature.

Author	Date	Model	Solute Set	Reference
Flynn	1990	$\log K_p = fn(\log P_{o/w})$ R^2=0.26	n=90 MW=18-750+ log $P_{o/w}$=-3-+6	9, 10
Potts and Guy	1992	$\log K_p = 0.70(\pm 0.09)\log P_{o/w} - 5.0(\pm 0.3)\frac{MW}{1000} - 6.0(\pm 0.2)$ R^2=0.82	n=42 water, n-alkanols, n-alkanoic acids, alkanediols, and phenols	9
Lien and Gao	1995	$\log K_p = -0.096(\log P_{o/w})^2 + 1.027\log P_{o/w} - 0.201H_b - 2.633\log MW + 5.597$ R^2=0.93, Standard Error=0.36	n=23 water, n-alkanols, alkanediols, and phenols	12
Medina-Hernandez	2003	$\log K_p = 1.3(\pm 0.2)\log k_{BMC} - 0.0080(\pm 0.0016)MP - 3.2(\pm 0.3)$ log k_{BMC} generated from biopartitioning micellar chromatography using a C_{18} LC column and 40 mM Brij35 in 50 mM sodium citrate, pH 5.5. R^2=0.79, Standard Error=0.55 MP=melting point	n=43 water, n-alkanols, alkanediols, phenols, and steroids	26
Barker and Khaledi	2004	$\log K_p = 0.81(\pm 0.09)\log k - 0.75(\pm 0.25)\frac{MW}{100} - 0.12(\pm 0.03)H_b + 0.11(\pm 0.29)$ log k generated from LEKC using 15 mM $DPPG_{20}DPPC_{80}$, 15 mM cholesterol in 25 mM MES, pH 6.0 R^2_{adj}=0.89, Standard Error=0.29	n=44	Current study

Figure 7.1 – Determination of maximum hydrogen bonding ability, H_b, for a functional group.

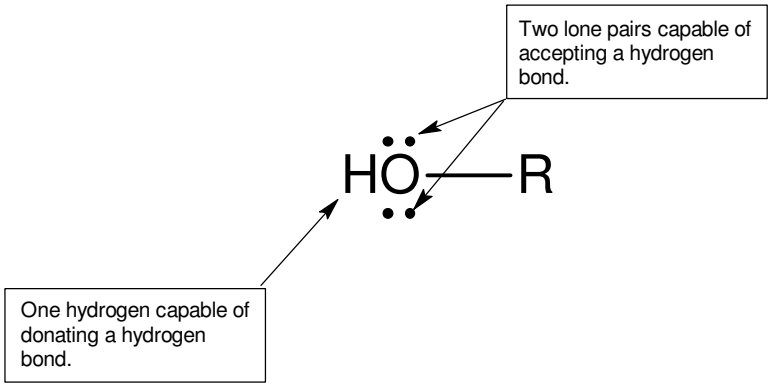

One hydrogen capable of donating a hydrogen bond and **two** lone pairs capable of accepting a hydrogen bond, therefore, H_b=3.

Figure 7.2 – Determination of maximum hydrogen bonding ability, H_b, for a functional group.

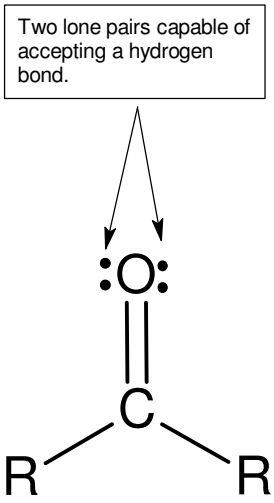

Zero hydrogens capable of donating a hydrogen bond and **two** lone pairs capable of accepting a hydrogen bond, therefore, H_b=2.

Figure 7.3 – Determination of maximum hydrogen bonding ability, H_b, for a functional group.

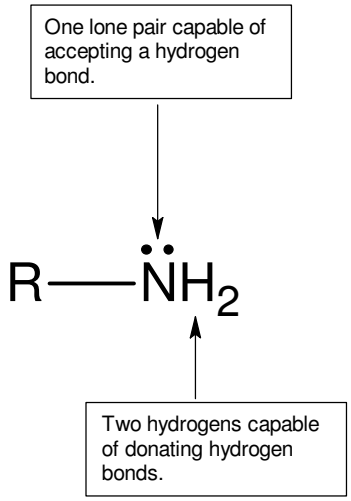

Two hydrogens capable of donating hydrogen bonds and **one** lone pair capable of accepting a hydrogen bond, therefore, H_b=3.

Figure 7.4 – Determination of maximum hydrogen bonding ability, H_b, for a functional group.

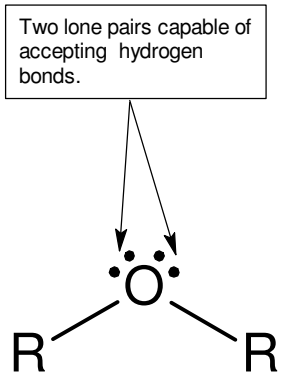

Zero hydrogens capable of donating hydrogen bonds and **two** lone pairs capable of accepting a hydrogen bond, therefore, H_b=2.

Figure 7.5 - Scatter plot of the predicted skin permeability coefficients using log k from 15 mM $DPPG_{20}DPPC_{80}$, 15 mM cholesterol at pH 6.0, $MW/100$, and H_b and experimental skin permeability coefficients

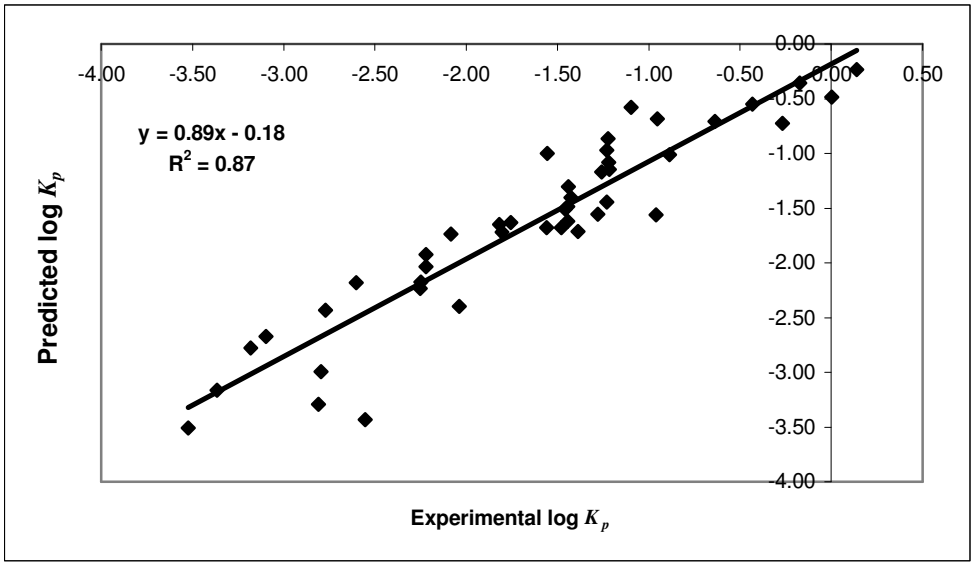

Figure 7.6 - Scatter plot of the predicted skin permeability coefficients using log k from 15 mM $DPPG_{20}DPPC_{80}$, 15 mM cholesterol at pH 7.5 and H_b and experimental skin permeability coefficients

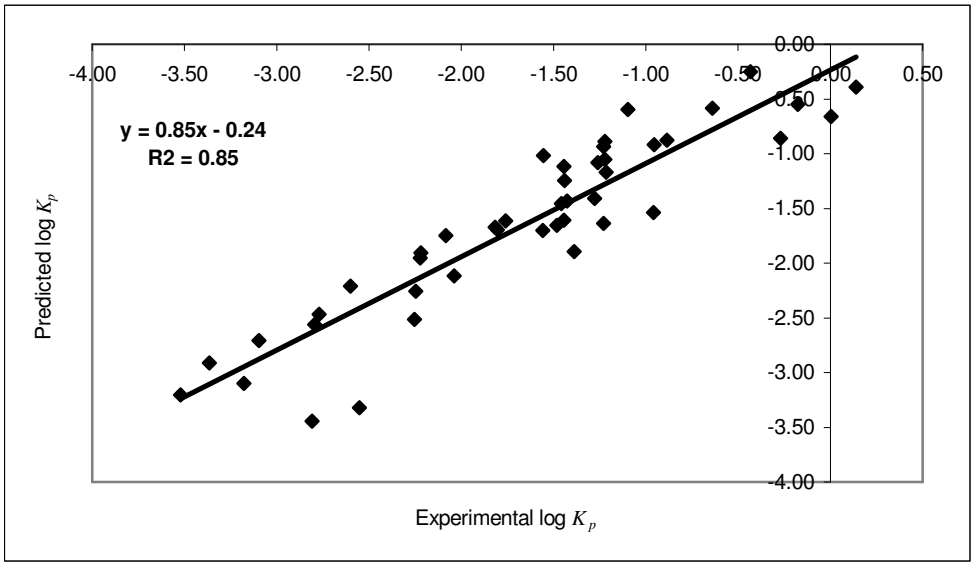

Figure 7.7 - Scatter plot of the predicted skin permeability coefficients using log $P_{o/w}$ and H_b and experimental skin permeability coefficients

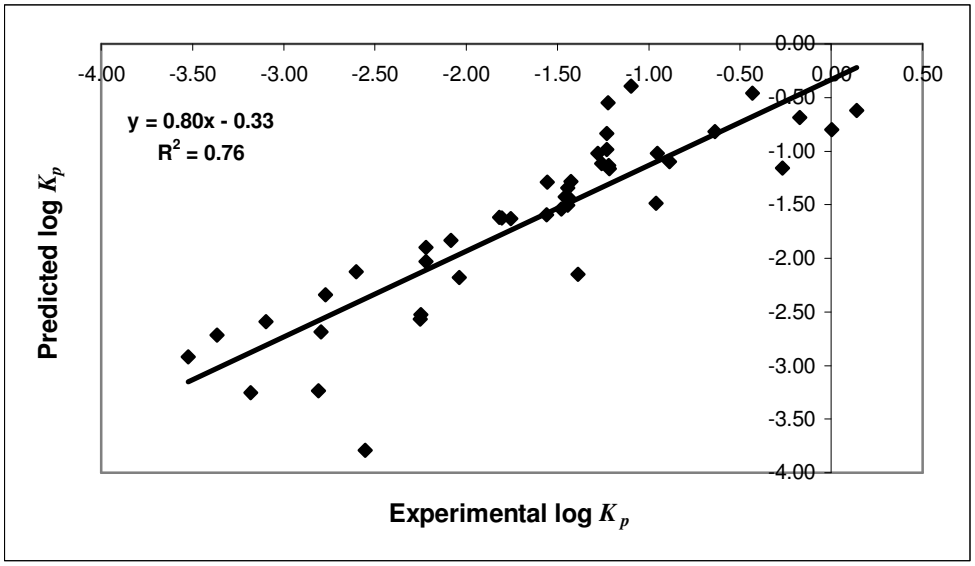

Chapter 8

Future Trends

Linear Solvation Energy Relationships Studies

The studies presented in this dissertation have investigated several different aspects of liposome/water partitioning using electrokinetic chromatography (EKC) with various lipid-based pseudostationary phases. Several of these presented studies have used linear solvation energy relationship (LSER) models to characterize the interactions responsible for liposome/water partitioning. For these experiments, EKC experiments were conducted using a set of 50 neutral aromatic solutes with known LSER descriptors. System coefficients that describe the interactions that influence retention, and therefore, partitioning in the given system were then determined by multilinear regression of the retention data as a function of the solute descriptors. The addition of 3-15 mM cholesterol to 15 mM $DPPG_{20}DPPC_{80}$ liposomes was shown to decrease partitioning for most of the solutes analyzed. From the LSER models generated for these lipid phases, the addition of cholesterol was shown to increase the cohesiveness and the polarizability of the liposomes while decreasing the hydrogen bond acceptor ability and the dipolarity of the liposomes. These effects are likely caused by the ability of cholesterol to order lipid acyl chains[1], decrease the polarity of the lipid membrane interfacial region[2], and dehydrate the lipid membrane interfacial region.[1,2]

Another LSER-based study investigate the liposome/water partitioning behavior of 21 neutral drugs with LSER solute descriptors calculated by Abraham et al.[3] This study tested the predictive ability of the LSER model by using the LSER system coefficients determined using the set of 50 neutral aromatic solutes to predict EKC retention factors for the 21 neutral drugs. The correlation between the predicted and experimental retention factors was reasonable ($0.79 \leq R^2 \leq 0.85$) for the lipid phases studied. The descriptive ability of the LSER model was tested and used to examine the interactions that control liposome/water partitioning for the set of 50 neutral aromatic solutes and the set of 71 solutes including 21 neutral drugs. The same general trends were observed for both solute sets. Therefore, the partitioning mechanism is likely very similar for the simple neutral aromatic solutes and the more complicated drug molecules.

A “biomimetic” lipid phase with a lipid composition that approximates that of monkey intestinal epithelial cells (15 mM $PI_{10}DPPS_{10}DPPC_{30}DPPE_{30}SPM_{20}$/9.75 mM cholesterol) was also studied using LSER models. Retention factors determined for 15 mM $PI_{10}DPPS_{10}DPPC_{30}DPPE_{30}SPM_{20}$/9.75 mM cholesterol were highly correlated (r^2=0.99) with retention factors determined using the simpler

lipid phase 15 mM $DPPG_{20}DPPC_{80}$/9.75 mM cholesterol. LSER models determined for both of these systems were also very similar. LSER models for these lipid phases were compared with an LSER model generated by Abraham, et al. for human intestinal absorption.[4] The LSER models for the biomimetic lipid phases were characterized by a large negative *b* term, a large positive *v* term, a small positive *e* term, and small negative *s* and *a* terms. The LSER model for human intestinal absorption was characterized by a large negative *b* and *a* terms, a large positive *v* term, a small positive *e* term, and a small positive *s* term.

Future LSER-based studies of liposome/water partitioning are nearly limitless. While the LSER models determined in these studies have been built using chromatography data, LSER models could be built using data determined for partitioning systems using a wide variety of methods including equilibrium dialysis[5], calorimetry[6,7], and spectrophotometry.[8] Another possible future direction might be the study of peptide interactions with lipid bilayers using LSER models. Liposome/water partitioning of peptides is a very important topic because of the implication of peptide-lipid interactions on the structure and function of various cell membranes.

Vesicles Formed Spontaneously by Short-Chain Lipids and Long-Chain Lipids

Another study presented in this dissertation focused on the characterization of novel pseudostationary phases formed by short-chain lipids (1,2-Dihexanoyl-*sn*-Glycero-3-Phosphocholine, DHPC, 6:0) and long-chain lipids (1,2-Dipalmitoyl-*sn*-Glycero-3-[Phospho-*rac*-(1-glycerol)] (Sodium Salt), DPPG, 16:0 and 1,2-Dipalmitoyl-*sn*-Glycero-3-Phosphocholine, DPPC, 16:0). When mixed in an aqueous medium in the proper amounts, short-chain lipids and long-chain lipids spontaneously form unilamellar vesicles.[9,10] These vesicles are ideal for EKC experiments because they are spontaneously formed and they are homogenously sized. The size of these vesicles as a function of DHPC content was determined by dynamic light scattering. As a general trend, the size of these aggregates decreased with the addition of more DHPC. Retention of neutral solutes in an EKC system using these vesicles as a pseudostationary phase was determined as a function of DHPC concentration. Retention factors for these solutes displayed a parabolic relationship with mole percent DHPC content. Using linear solvation energy relationships (LSER) models, this behavior is likely caused by changes in the lipid phase cohesiveness, hydrogen bond donor ability, and dipolarity that occur as a function of DHPC content. Finally, the retention behavior of all of the retention factors determined using DPPG/DHPC/DPPC vesicle phases exhibit high correlation with retention factors determined for 15 mM $DPPG_{20}DPPC_{80}$ liposomes prepared by extrusion.

The temperature dependence and thermodynamic parameters of vesicle/water partitioning for lipid phases comprised of spontaneous vesicles formed by short-chain and long-chain lipids was also

studied. EKC retention factors were determined for a set of 20 neutral aromatic solutes from 15 °C to 70 °C. Vesicle/water partition coefficients were determined from these retention factors and chromatographic phase ratios estimated for 15 mM $DPPG_{20}DHPC_{50}DPPC_{30}$ and 15 mM $DPPG_{20}DHPC_{70}DPPC_{10}$. Both of these lipid phases exhibited nonlinear third-order van't Hoff plots. This behavior is indicative of a heat capacity change (ΔC_p) associated with the transfer of the solute from the aqueous phase to the lipid phase that is linearly dependant on temperature. The thermodynamic parameters including the free energy change (ΔG), the enthalpy change (ΔH), the entropy change (ΔS), and the heat capacity change (ΔC_p) associated with vesicle/water partitioning were determined using the non-linear van't Hoff plots for 15 mM $DPPG_{20}DHPC_{50}DPPC_{30}$. The thermodynamic parameters determined for 15 mM $DPPG_{20}DHPC_{50}DPPC_{30}$ were not comparable to the behavior associated with the classical hydrophobic effect that is often associated with bulk organic solvent/water partitioning systems or the nonclassical hydrophobic effect that is often associated with biliayer membrane/water partitioning systems.

Vesicles formed from short-chain lipids and long-chain lipids are a very attractive lipid phase for chromatography experiments because they form spontaneously and do not require extrusion or sonication to obtain a homogenous size distribution. For these reasons, this system might be an ideal lipid medium for proteins and receptors for affinity capillary electrophoresis experiments. Affinity separations are based on the use of an immobilized protein or receptor to capture a specific molecule based on highly selective biospecific binding.[11] Although some affinity capillary electrophoresis methods use receptors or proteins in the free solution of the background buffer[12], some of these molecules lose their activity outside of a lipid matrix.[13] The P-glycoprotein (P-gp) does not retain its activity outside of the lipid matrix. P-gp is the main contributor to multidrug resistance (MDR) in humans. MDR describes the glycoprotein-mediated efflux of xenobiotics, waste products, and toxic agents from the interior of cell membranes. Unfortunately, the bioavailability of many important chemotherapy agents and anti-cancer drugs is inhibited by MDR.[12] The assessment of P-gp affinity has therefore become an important step in drug development. Wainer et al. have developed an immobilized P-gp-based liquid chromatography stationary phase that allows the determination of drug-P-gp binding.[15-24] A capillary electrophoresis version of this method would offer a free solution, rather than immobilized affinity phase for the separation. This advantage would decrease column preparation time significantly and remove the possibility that the immobilization procedure could alter the activity of the glycoprotein.

The thermodynamic study presented for 15 mM $DPPG_{20}DHPC_{50}DPPC_{30}$ and 15 mM $DPPG_{20}DHPC_{70}DPPC_{10}$ offered some interesting results. The partial specific molar volumes for both of these lipid phases could not be determined experimentally and therefore the chromatographic phase ratio was estimated rather than determined over the entire temperature range. This limitation

likely introduced errors to the thermodynamic parameters calculated for 15 mM $DPPG_{20}DHPC_{50}DPPC_{30}$. The fit of the partition coefficients determined for 15 mM $DPPG_{20}DHPC_{70}DPPC_{10}$ was not very good and therefore thermodynamic parameters could not be calculated for that lipid phase. It is possible that these two lipid phases are not good candidates for thermodynamic studies using chromatographic methods. Isothermal titration calorimetry (ITC) offers a direct method for determining thermodynamic parameters associated with partitioning systems rather than relying on the fit of partitioning data to third-order nonlinear van't Hoff relationships. Parallel ITC and hydrophobic interaction chromatography (HIC) studies have shown differences between thermodynamic parameters determined by calorimetry relative to van't Hoff relationships.[25]

Quantitative Structure-Activity Relationship for the Prediction of Skin Permeability Coefficients Using Liposome Electrokinetic Chromatography

Finally, a quantitative structure-activity relationship was developed to predict skin permeability coefficients from three solute descriptors: liposome electrokinetic chromatography (LEKC) retention factors, molecular weight, and a descriptor of hydrogen bonding determined using the solute structure. This model was generated using a set of 44 solutes including neutral aromatic solutes, ionizable aromatic solutes, and neutral aliphatic solutes. The model was validated using the same set of solutes by the leave-one-out approach and favorably compared with other models used for the prediction of skin permeability coefficients using similar descriptors.[26-29] Future studies should focus on adding more compounds to the training and validation sets in order to improve and fully test this model.

Works Cited

1. Saito, H.; Araiso, T.; Shirahama, H.; Koyama, T. Dynamics of the Bilayer/Water Interface of Phospholipid-Vesicles and the Effect of Cholesterol: A Picosecond Fluorescence Anisotropy Study. *J. Biochem.* **1991**, *109* (4), 559-565.
2. Bernik, D.L.; Negri, R.M. Local Polarity at the Polar Head Level of Lipid Vesicles Using Dansyl Fluorescent Probes. *J. Coll. Inter. Sci.* **1998**, *203*, 97-105.
3. Abraham, M.H.; Chadha, H.S.; Whiting,G.S.; Mitchell, R.C. Hydrogen Bonding.32. An analysis of water-octanol and water-alkane partitioning and the delta-log-P parameter of Seiler. *J. Pharm. Sci.* **1994**, *83* (8), 1085-1100.
4. Zhao, Y. H.; Le, J.; Abraham, M.H.; Hersey, A.; Eddershaw, P.J.; Luscombe, C.N.; Boutina, D.; Beck, G.; Sherborne, B.; Cooper, I.; Platts, J.A.; Evaluation of Human Intestinal Absorption Data and Subsequent Derivation of a Quantitative Structure-Activity Relationship (QSAR) with Abraham Descriptors. *J. Pharm. Sci.* **2001**, *90* (6), 749-784.
5. Pauletti, G.M.; Wunderli-Allenspach, H.; Partition coefficients in vitro: artificial membranes as a standardized distribution model. *Eur. J. Pharm. Sci.* **1994**, *1* (5), 273-282.
6. Zhang, F.; Rowe, E.S.; Titration Calorimetric and Differential Scanning Calorimetric Studies of the Interactions of n-Butanol with Several Phases of Dipalmitoylphosphatidylcholine. *Biochemistry*. **1992**, *31*, 2005-2011.
7. Rowe, E.S.; Zhang, F.; Leung, T.W.; Parr, J.S.; Guy, P.T.; Thermodynamics of Membrane Partitioning for a Series of n-Alcohols Determined by Titration Calorimetry: Role of Hydrophobic Effects. *Biochemistry*. **1998**, *37*, 2430-2440.
8. Pola, A.; Michalak, K.; Burliga, A.; Motohashi, N.; Kawase, M.; Determination of lipid bilayer/water partition coefficient of new phenothiazines using the second derivative of absorption spectra method. *Eur. J. Pharm. Sci.* **2004**, *21* (4), 421-427.
9. Gabriel, N.E.; Roberts, M.F. “Spontaneous Formation of Unilamellar Vesicles.” *Biochemistry.* **1984**, *23*, 4011-4015.
10. Gabriel, N.E.; Roberts, M.F. “Interaction of Short-Chain Lecithin with Long-Chain Phospholipids: Characterization of Vesicles That Form Spontaneously.” *Biochemistry.* **1986**, *25*, 2812-2821.
11. Cunico, R.L.; Gooding, K.M.; Wehr, T. Affinity Chromatography and Related Techniques. *Basic HPLC and CE of Biomolecules*, Bay Bioanalytical Laboratory: Richmond, CA, 1998; Chapter 10.
12. Gao, J.; Mrksich, M.; Mammen, M.; Whitesides, G.M. Affinity Capillary Electrophoresis: Using Capillary Electrophoresis to Study the Interactions of Proteins with Ligands. *In High*

Performance Capillary Electrophoresis: Theory, Techniques, and Applications; Khaledi, M.G., Ed.; John Wiley and Sons, Inc.: New York, 1998; 947-972.

13. Rigaud, J.L.; Pitard, B.; Levy, D. Reconstitution of membrane proteins into liposomes: application to energy-transducing membrane proteins. *Biochim. Biophys. Acta*. **1995**, *1231*, 223-246.
14. Wang, R.B.; Kuo, C.L.; Lien, L.L.; Lien, E.J. Structure-activity relationship: analyses of p-glycoprotein substrates and inhibitors. *J. Clin. Pharm. and Ther*. **2003**, *28*, 203-228.
15. Lu, L.; Leonessa, F.; Clarke, R.; Wainer, I.W. Frontal chromatographic analysis of drug interactions with immobilized P-glycoprotein. *Clin. Can. Res*. **1999**, *516*, 3833S.
16. Zhang, Y.X.; Leonessa, F.; Clarke, R.; Wainer, I.W. Development of an immobilized P-glycoprotein stationary phase for on-line liquid chromatographic determination of drug-binding affinities. *J. Chrom. B*. **2000**, *739* (1), 33-37.
17. Pham, Y.T.; Regina, A.; Farinotti, R.; Couraud, P.O.; Wainer, I.W.; Roux, F.; Gimenez, F. Interactions of racemic mefloquine and its enantiomers with P-glycoprotein in an immortalised rat brain capillary endothelial cell line, GPNT. *Biochim. Biophys. Acta*. **2000**, *1524* (2-3), 212-219.
18. Lu, L.L.; Leonessa, F.; Clarke, R.; Wainer, I.W. Competitive and allosteric interactions in ligand binding to P-glycoprotein as observed on an immobilized P-glycoprotein liquid chromatographic stationary phase. *Mol. Pharm.* **2001**, *59* (1), 62-68.
19. Lu, L.L.; Leonessa, F.; Baynham, M.T.; Clarke, R.; Gimenez, F.; Pham, Y.T.; Roux, F.; Wainer, I.W. The enantioselective binding of mefloquine enantiomers to P-glycoprotein determined using an immobilized P-glycoprotein liquid chromatographic stationary phase. *Pharm. Res.* **2001**, *18* (9), 1327-1330.
20. Moaddel, R.; Lu, L.L.; Baynham, M.; Wainer, I.W. Immobilized receptor- and transporter-based liquid chromatographic phases for on-line pharmacological and biochemical studies: a mini-review. *J. Chrom. B*. **2002**, *768* (1), 41-53.
21. Williams, M.L.; Wainer, I.W. Role of chiral chromatography in therapeutic drug monitoring and in clinical and forensic toxicology. *Ther. Drug. Monitor*. **2002**, *24* (2), 290-296.
22. Di Marco, M.P.; Edwards, D.J.; Wainer, I.W.; Ducharme, M.P. The effect of grapefruit juice and seville orange juice on the pharmacokinetics of dextromethorphan: The role of gut CYP3A and P-glycoprotein. *Life. Sci*. **2002**, *71* (10), 1149-1160.
23. Woodland, C.; Koren, G.; Wainer, I.W.**;** Batist, G.; Ito, S. Verapamil metabolites: potential P-glycoprotein-mediated multidrug resistance reversal agents. *Can. J. Phys. Pharm*. **2003**, *81* (8), 800-805.
24. Moaddel, R.; Bullock, P.L.; Wainer, I.W. Development and characterization of an open tubular column containing immobilized P-glycoprotein for rapid on-line screening for P-glycoprotein substrates. *J. Chrom. B.* **2004**, *799* (2), 255-263.

25. Chen, W.Y.; Huang, H.M.; Lin, C.C.; Lin, F.Y.; Chan, Y.C. Effect of Temperature on Hydrophobic Interaction between Proteins and Hydrophobic Adsorbents: Studies by Isothermal Titration Calorimetry and the van't Hoff Equation. *Langmuir*. **2003**, *19*, 9395-9403.
26. Flynn, GL Physicochemical determinants of skin absorption. In *Principles of Route-to-Route Extrapolation for Risk Assessment*; Edited by T.R. Garrity and C.J. Henry, Elsevier: New York. 1990; 93-127.
27. Potts, R.O.; Guy, R. Predicting Skin Permeability. *Pharm. Res.* **1992**, *9*, 663-669.
28. Ren, S.; Das, A.; Lien, E.J. QSAR Analysis of Membrane Permeability to Organic Compounds. *J. Drug. Target.* **1996**, *4* (1), 103-107.
29. Martinez-Pla, J.J.; Martin-Biosca, Y.; Sagrado, S.; Villaneuva-Camanas, R.W.; Medina-Hernandez, M.J. Biopartitioning micellar chromatography to predict skin permeability. *Biomed. Chrom.* **2003,** *17*, 530-537.
30. Bouwstra, J.A.; Gooris, G.S.; Dubbelaar, F.E.R.; Ponec, M. Cholesterol sulfate and calcium affect stratum corneum lipid organization over a wide temperature range. *J. Lip. Res.* **1999**, *40*, 2303-2312.

Appendix A-1

Lipid Structures

Lipid Name	Structure[1]	Molar Mass (g/mole)[1]	Partial Specific Volume (cm^3/g)[2]
1,2-Dipalmitoyl-*sn*-Glycero-3-[Phospho-*rac*-(1-glycerol)] (Sodium Salt) (DPPG, 16:0)	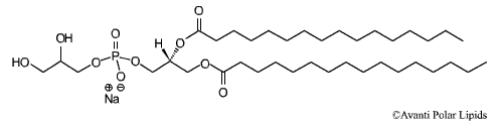	744.96	1.011[2]
1,2-Dipalmitoyl-*sn*-Glycero-3-Phosphocholine (DPPC, 16:0)	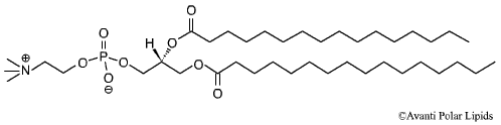	734.05	0.954[2]
1,2-Dihexanoyl-*sn*-Glycero-3-Phosphocholine (DHPC, 6:0)	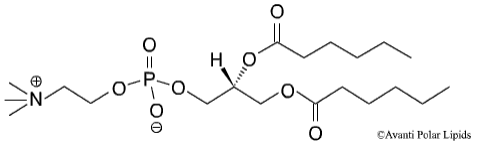	453.51	0.870[2]
Cholesterol	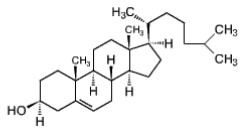	386.66	0.949[3]
(2S,3R,4E)-2-acylaminooctadec-4-ene-3-hydroxy-1-Phosphocholine	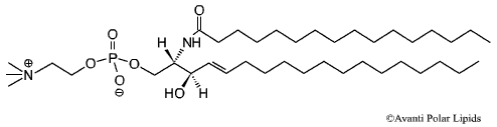	703.03	[redacted]

Lipid Name	Structure[1]	Molar Mass (g/mole)[1]	Partial Specific Volume (cm^3/g)[2]
(Chicken Egg Sphingomyelin)			[redacted]
1,2-Dipalmitoyl-*sn*-Glycero-3-Phosphoethanolamine (DPPE, 16:0)	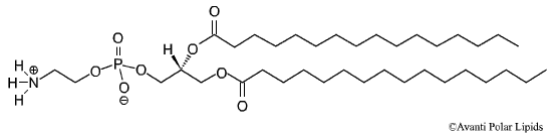	691.97	
1,2-Dipalmitoyl-*sn*-Glycero-3-[Phospho-L-Serine] (Sodium Salt) (DPPS, 16:0)	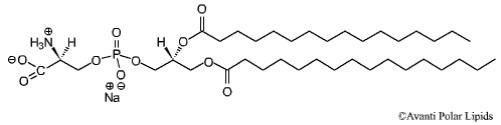	757.96	
L-a-Phosphatidylinositol (Soybean PI)	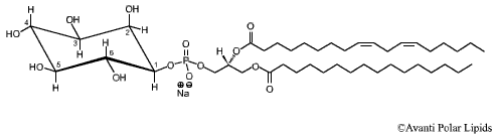	857.05	

1. Avanti Polar Lipids website, http://www.avantilipids.com, (accessed June 2004)
2. Marsh, D. CRC *Handbook of Lipid Bilayers*, CRC Press: Boca Raton, 1990; Section II.9.4.
3. Durchschlag, H. Specific Volumes of Biological Macromolecules and Some Other Molecules of Biological Interest. In *Thermodynamic Data for Biochemistry and Biotechnology*; Hinz, H.J., Ed.; Springer-Verlag: Berlin, **1986**.

Appendix A-2

Solute Structures, Molecular Weights, Octanol/Water Partition Coefficients, and Abraham Descriptors

Solute Name	Solute Structure[1]	Molecular Weight[1]	log $P_{o/w}$[2]	pK_a	E[3]	S[3]	A[3]	B[3]	V[3]
1,4-dioxane		88.11	-0.27		0.3290	0.7500	0.0000	0.6400	0.6810
1-methylnaphthalene	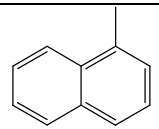	142.2	3.87		1.344	0.900	0.000	0.200	1.226
2,4,6-trichlorophenol	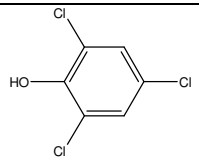	197.45	3.69	6.19[5]					
2,4-dichlorophenol	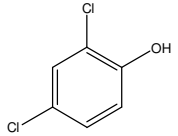	163.00	3.06	7.89[5]					
2,4-dimethylphenol	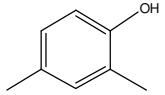	122.17	2.30	10.60[5]	0.8430	0.8000	0.5300	0.3900	1.0570
2-amino-4-nitrophenol	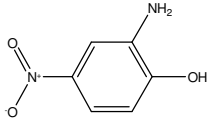	154.13	1.53	3.10[5]					

Solute Name	Solute Structure[1]	Molecular Weight[1]	log $P_{o/w}$[2]	pK_a	E^3	S^3	A^3	B^3	V^3
2-chlorophenol	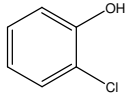	128.56	2.15	8.56[5]	0.8530	0.8800	0.3200	0.3100	0.8980
2-ethoxyethanol	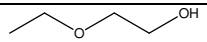	90.12	-0.32		0.2370	0.5000	0.3000	0.8300	0.7900
2-methoxypyridine	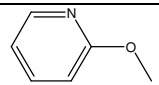	109.13	1.36		0.641	0.760	0.000	0.470	0.875
2-napthol	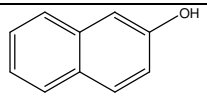	144.17	2.70	9.63[5]	1.5200	1.0800	0.6100	0.4000	1.1440
3,4-dimethylphenol	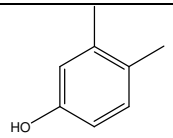	122.17	2.23	10.36[5]	0.8300	0.8600	0.5600	0.3900	1.0570
3,5-dimethylphenol	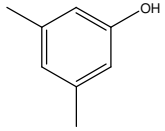	122.17	2.35		0.820	0.840	0.570	0.360	1.057
3-bromophenol	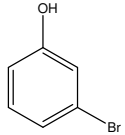	173.01	2.99		1.060	1.150	0.700	0.160	0.950
3-bromoquinoline	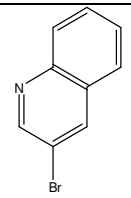	208.06	3.24	2.69[4]	1.6400	1.2300	0.0000	0.4200	1.2193

Solute Name	Solute Structure[1]	Molecular Weight[1]	log $P_{o/w}$[2]	pK_a	E^3	S^3	A^3	B^3	V^3
3-chlorophenol	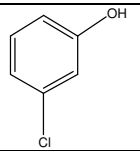	128.56	2.50		0.909	1.060	0.690	0.150	0.898
3-methyl benzyl alcohol	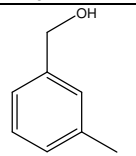	122.17	1.60		0.815	0.900	0.330	0.590	1.057
3-nitrophenol	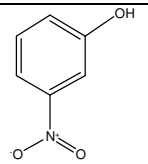	139.11	2.00	8.36[5]	1.0500	1.5700	0.7900	0.2300	0.9490
3-phenylpropanol	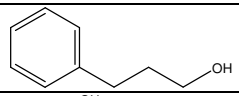	136.19	1.88		0.821	0.900	0.300	0.670	1.198
4-amino-2-nitrophenol	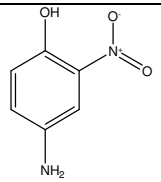	154.13	0.96	7.80[5]					
4-bromophenol	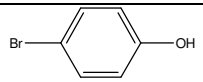	173.01	2.59	9.37[5]	1.080	1.170	0.670	0.200	0.950
4-chloro-3,5-dimethylphenol	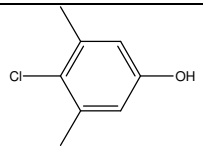	156.61	3.39	9.70[5]					

Solute Name	Solute Structure[1]	Molecular Weight[1]	log $P_{o/w}$[2]	pK_a	E^3	S^3	A^3	B^3	V^3
4-chloro-3-methylphenol	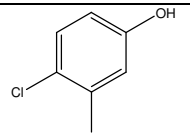	142.58	3.10		0.9200	1.0200	0.6500	0.2200	1.0380
4-chloroacetophenone	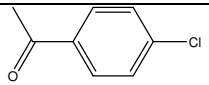	154.60	2.32		0.955	1.090	0.000	0.440	1.136
4-chloroanisole	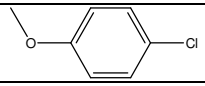	142.58	2.78		0.838	0.860	0.000	0.240	1.038
4-chlorophenol	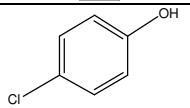	128.56	2.39	9.41[5]	0.915	1.080	0.670	0.200	0.898
4-chlorotoluene	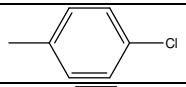	126.59	3.33		0.705	0.670	0.000	0.070	0.980
4-ethylphenol	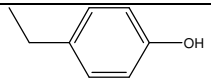	122.17	2.40	10.17[5]	0.8000	0.9000	0.5500	0.3600	1.0570
4-fluoroacetophenone	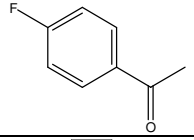	138.14	1.72		0.690	1.020	0.000	0.470	1.032
4-fluorophenol	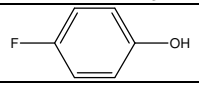	112.10	1.77		0.670	0.970	0.630	0.230	0.793
4-methyl benzyl alcohol	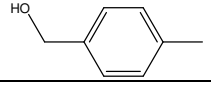	122.17	1.58		0.810	0.880	0.330	0.600	1.057
4-nitrophenol	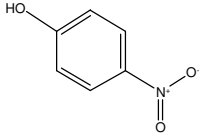	139.11	1.91	7.15[5]	1.0700	1.7200	0.8200	0.2600	0.9490

Solute Name	Solute Structure[1]	Molecular Weight[1]	log $P_{o/w}$[2]	pK_a	E^3	S^3	A^3	B^3	V^3
4-nitrotoluene	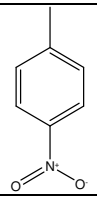	137.14	2.37		0.870	1.110	0.000	0.280	1.032
acetaminophen	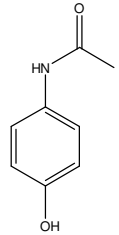	151.16	0.31	9.71[4]	1.0600	1.6300	1.0400	0.8600	1.1724
acetophenone	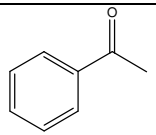	120.15	1.58		0.8180	1.0100	0.0000	0.4800	1.0140
aniline	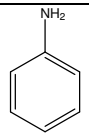	93.13	0.84	4.87[5]	0.955	0.960	0.260	0.410	0.816
antipyrine	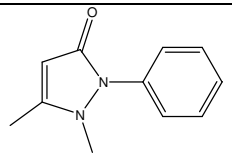	188.23	0.38	1.45[4]	1.3200	1.5000	0.0000	1.4800	1.5502
benzaldehyde	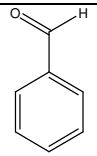	106.12	1.48		0.820	1.000	0.000	0.390	0.873

Solute Name	Solute Structure[1]	Molecular Weight[1]	log $P_{o/w}$[2]	pK_a	E[3]	S[3]	A[3]	B[3]	V[3]
benzene		78.11	2.13		0.6100	0.5200	0.0000	0.1400	0.7160
benzonitrile	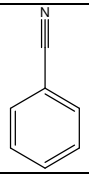	103.12	1.56		0.742	1.110	0.000	0.330	0.871
benzyl alcohol	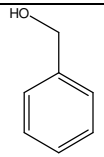	108.13	1.01		0.803	0.870	0.330	0.560	0.916
bifonazole	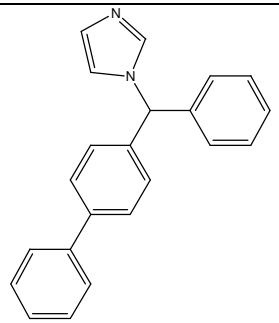	310.40	4.77		2.4100	2.2500	0.0000	1.1200	2.5006
bromobenzene	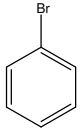	157.01	2.99		0.8820	0.7300	0.0000	0.0900	0.8910
butanol	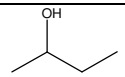	74.12	0.76		0.2200	0.4200	0.3700	0.4800	0.7310

Solute Name	Solute Structure[1]	Molecular Weight[1]	log $P_{o/w}$[2]	pK_a	E[3]	S[3]	A[3]	B[3]	V[3]
butyl benzoate	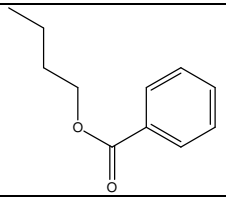	178.23	3.84		0.6680	0.8000	0.0000	0.4600	1.4950
butyrophenone	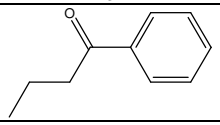	148.2042	2.77		0.7970	0.9500	0.0000	0.5100	1.2957
caffeine	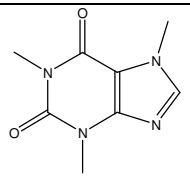	194.19	-0.16	0.60[4]	1.5000	1.6000	0.0000	1.3300	1.3632
carbamazepine	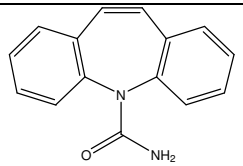	236.27	2.45		2.1500	2.0700	0.5200	1.1300	1.8106
carbon disulfide	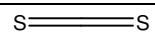	76.13	1.94		0.8770	0.2100	0.0000	0.0700	0.4910
chloramphenicol	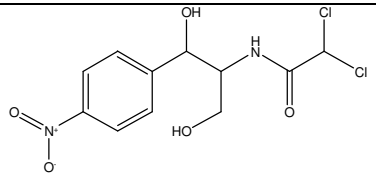	323.13	1.14	11.03[4]	1.8500	0.7200	0.3500	2.0900	2.0728
chlorobenzene	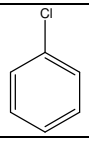	112.56	2.89		0.7180	0.6500	0.0000	0.0700	0.8390

Solute Name	Solute Structure[1]	Molecular Weight[1]	log $P_{o/w}$[2]	pK_a	E^3	S^3	A^3	B^3	V^3
chloroform	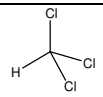	119.38	1.97		0.4250	0.4900	0.1500	0.0200	0.6170
clotrimazole	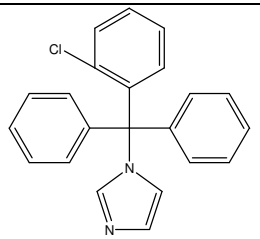	344.84			2.5500	2.6000	0.0000	1.0800	2.6230
decanol	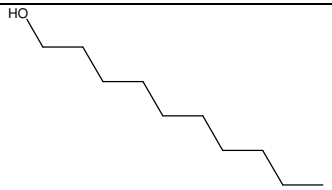	158.28	4.57		0.1910	0.4200	0.3700	0.4800	1.5760
dexamethasone	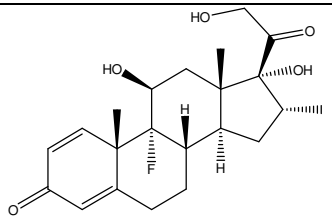	392.47	1.72		2.0400	3.5100	0.7100	1.9200	2.9132
diethylstilbestrol	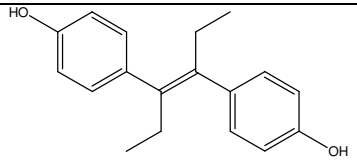	268.35	5.07		1.6000	1.7500	1.2600	0.7700	2.2440

Solute Name	Solute Structure[1]	Molecular Weight[1]	log $P_{o/w}$[2]	pK_a	E^3	S^3	A^3	B^3	V^3
estradiol	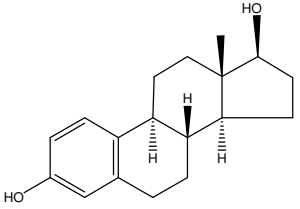	272.39	2.29		1.8000	1.7700	0.8600	1.1000	2.1988
ethanol		46.07	-0.37		0.2460	0.4200	0.3700	0.4800	0.4490
ethyl benzoate	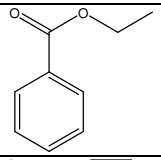	150.18	2.64		0.6890	0.8500	0.0000	0.4600	1.2140
ethylbenzene	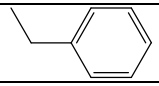	106.17	3.15		0.6130	0.5100	0.0000	0.1500	0.9982
heptanol	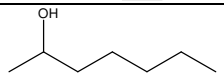	116.20	2.72		0.2110	0.4200	0.3700	0.4800	1.1540
hexanol	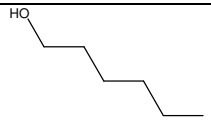	102.18	2.03		0.2100	0.4200	0.3700	0.4800	1.0130
hexanophenone	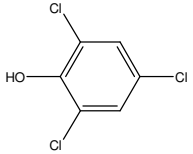	176.26							

Solute Name	Solute Structure[1]	Molecular Weight[1]	log $P_{o/w}$[2]	pK_a	E^3	S^3	A^3	B^3	V^3
hydrocortisone	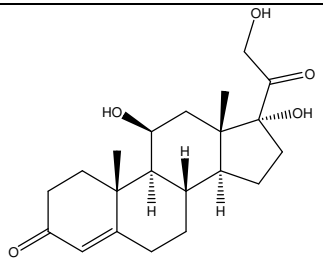	362.47	1.20		2.0300	3.4900	0.7100	1.9000	2.7976
iodobenzene	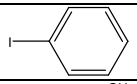	204.01	3.25		1.1880	0.8200	0.0000	0.1200	0.9750
m-cresol	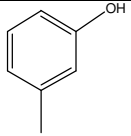	108.14	1.96	10.09[5]	0.822	0.880	0.570	0.340	0.916
m-dichlorobenzene	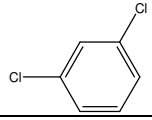	147.00	3.53		0.847	0.730	0.000	0.020	0.961
methanol		32.04	-0.50		0.2780	0.4400	0.4300	0.4700	0.3080
methyl benzoate	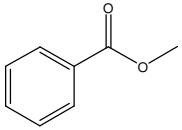	136.15			0.7330	0.8500	0.0000	0.4600	1.0730
methyl hydroxybenzoate	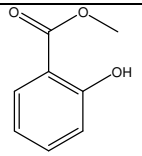	152.14	2.34	9.87[5]					

Solute Name	Solute Structure[1]	Molecular Weight[1]	log $P_{o/w}$[2]	pK_a	E^3	S^3	A^3	B^3	V^3
methyl-2-methyl benzoate	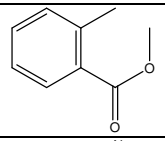	150.18	2.70		0.772	0.870	0.000	0.430	1.214
metronidazole	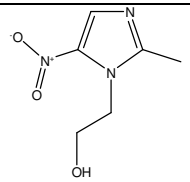	171.16	-0.16	2.50[4]	1.0500	1.6000	0.1800	1.0300	1.1919
naphthalene	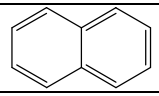	128.17	3.30		1.340	0.920	0.000	0.200	1.085
nifedipine	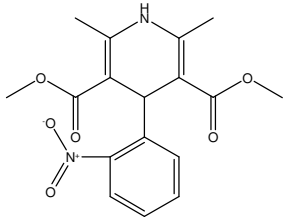	346.34	2.86		1.5000	2.4500	0.2300	1.4500	2.4945
nifuroxime	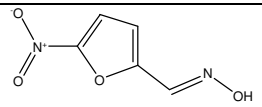	156.10	0.30		1.1300	0.9800	0.6900	0.6000	0.9669
nitrobenzene	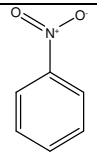	123.11	1.85		0.871	1.110	0.000	0.280	0.891
nonanol	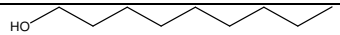	144.26	4.26		0.1930	0.4200	0.3700	0.4800	1.4350
o-cresol	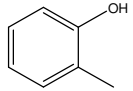	108.14	1.95	10.29[5]	0.8400	0.8600	0.5200	0.3000	0.9160

Solute Name	Solute Structure[1]	Molecular Weight[1]	log $P_{o/w}$[2]	pK_a	E^3	S^3	A^3	B^3	V^3
octanol	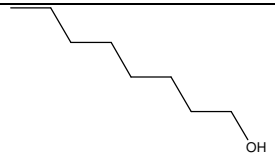	130.23	3.00		0.1990	0.4200	0.3700	0.4800	1.2950
o-dichlorobenzene	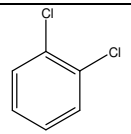	147.00	3.43		0.872	0.780	0.000	0.040	0.961
o-xylene	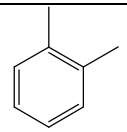	106.17	3.12		0.663	0.560	0.000	0.160	0.998
p-cresol	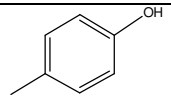	108.14	1.94	10.29[5]	0.8200	0.8700	0.5700	0.3100	0.9160
p-dichlorobenzene	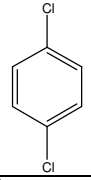	147.00	3.44		0.825	0.750	0.000	0.020	0.961
pentanol	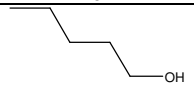	88.15	1.31		0.2190	0.4200	0.3700	0.4800	0.8720
pentoxifylline	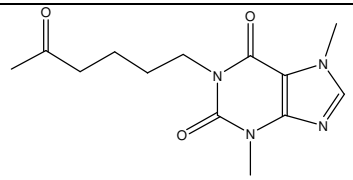	278.31	0.29	0.30[4]	1.6400	2.2800	0.0000	1.8400	2.0834

Solute Name	Solute Structure[1]	Molecular Weight[1]	log $P_{o/w}$[2]	pK_a	E^3	S^3	A^3	B^3	V^3
phenethyl alcohol	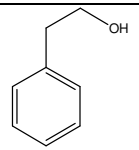	122.17	1.36		0.784	0.830	0.300	0.660	1.057
phenol	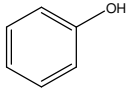	94.11	1.46	9.99[5]	0.8050	0.8900	0.6000	0.3000	0.7750
phenyl acetate	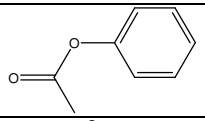	136.15	1.49		0.661	1.130	0.000	0.540	1.073
phenyl benzoate	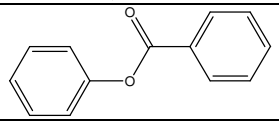	198.22	3.59		1.330	1.420	0.000	0.470	1.540
prednisolone	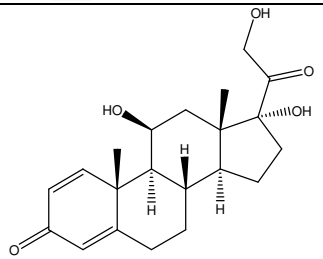	360.45	1.62		2.2100	3.1000	0.7100	1.9200	2.7546
prednisone	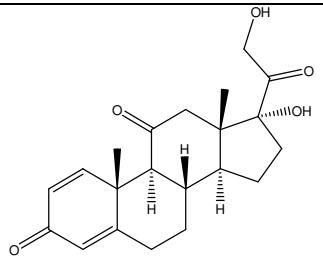	358.43	1.46		2.1400	3.5800	0.3600	1.8900	2.7116
propanol	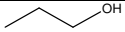	60.10	0.25		0.2360	0.4200	0.3700	0.4800	0.5900

Solute Name	Solute Structure[1]	Molecular Weight[1]	log $P_{o/w}$[2]	pK_a	E^3	S^3	A^3	B^3	V^3
propiophenone	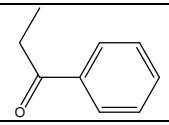	134.18	2.19		0.8040	0.9500	0.0000	0.5100	1.1548
propyl benzoate	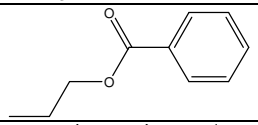	164.20	3.08		0.6750	0.8000	0.0000	0.4600	1.3540
propylbenzene	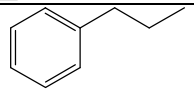	120.19	3.72		0.6040	0.5000	0.0000	0.1500	1.1390
p-xylene	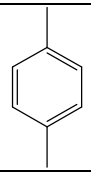	106.17	3.15		0.613	0.520	0.000	0.160	0.998
quinoline	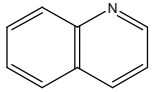	129.16	2.03	4.90[4]	1.2700	0.9700	0.0000	0.5400	1.0443
styrene	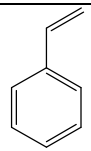	104.15	2.95		0.8490	0.6500	0.0000	0.1600	0.9550
tetrachloroethylene	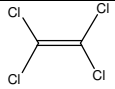	165.83	3.40		0.6390	0.4400	0.0000	0.0000	0.8370
thiamphenicol	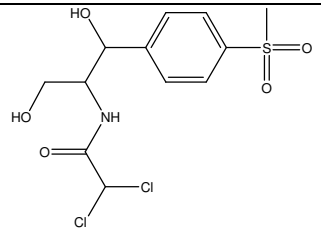	356.22			2.2600	3.3000	0.9000	2.0300	2.3204

Solute Name	Solute Structure[1]	Molecular Weight[1]	log $P_{o/w}$[2]	pK_a	E^3	S^3	A^3	B^3	V^3
thymol	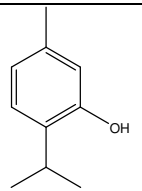	150.21	3.30	10.62[5]					
tolnaftate	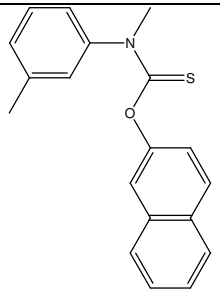	307.41			2.9700	2.2000	0.0000	0.9300	2.3949
toluene	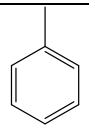	92.10	2.73		0.6010	0.5200	0.0000	0.1400	0.8570
trichloroethylene	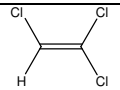	131.39	2.61		0.5240	0.3700	0.0800	0.0300	0.7150
valerophenone	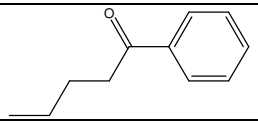	162.23			0.7950	0.9500	0.0000	0.5000	1.4366
water	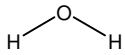	18.01	-1.15		0.0000	0.4500	0.8200	0.3500	0.1670

1. Solute structures and molecular weights taken from: Chemfinder website. http://www.chemfinder.com. (accessed May 2004). CambridgeSoft Corporation.

2. All log $P_{o/w}$ values taken from: Hansch, C.; Leo, A.; Hoekman, D.; *Exploring QSAR: Hydrophobic, Electronic, and Steric Constants*; American Chemical Society; Washington, DC, 1995.
3. Abraham solute descriptors taken from: Abraham, M.H.; Chadha, H.S.; Whiting,G.S.; Mitchell, R.C. Hydrogen Bonding.32. An analysis of water-octanol and water-alkane partitioning and the delta-log-P parameter of Seiler. *J. Pharm. Sci.* **1994**, *83* (8), 1085-1100.
4. pK_a values for neutral drugs taken from : Craig, P.N. Cumulative Subject Index and Drug Compendium. Vol. 6. In Hansch, C.; Sammes, P.G.; Taylor, J.B. (eds) Comprehensive Medicinal Chemistry, Pergamon Press, Oxford, 1990, p 237-965
5. pKa values for neutral aromatic solutes taken from: Lide, D.R.; *CRC Handbook of Chemistry and Physics* [Online Edition] **2003**.

Appendix A-3

Description of Abraham Solute Descriptors and System Coefficients

Abraham Solute Descriptors	System Coefficients
V, McGowan's characteristic volume	v, Cohesiveness/cavity formation
B, Hydrogen bond accepting ability	b, Hydrogen bond donating ability
A, Hydrogen bond donating ability	a, Hydrogen bond accepting ability
S, Dipolarity/polarizability	s, dipolarity/polarizability
E, Excess molar refraction	e, ability to interact with solute n- or π- electrons

Appendix A-4

Stepwise Regression for 15 mM $DPPG_{20}DPPC_{80}$, 15 mM cholesterol in 25 mM MES pH 6.0

All complete models were built in the format:

$$\log K_p = k_1 \log k + k_2 \frac{MW}{100} + k_3 H_b + k_4 \qquad \textbf{Equation A-4.1}$$

In order to verify the significance of each descriptor, incremental models were built by adding one descriptor at a time, ie.:

$$\log K_p = k_2 \frac{MW}{100} + k_4 \qquad \textbf{Model A-4.1}$$

$$\log K_p = k_3 H_b + k_4 \qquad \textbf{Model A-4.2}$$

$$\log K_p = k_1 \log k + k_4 \qquad \textbf{Model A-4.3}$$

$$\log K_p = k_2 \frac{MW}{100} + k_3 H_b + k_4 \qquad \textbf{Model A-4.4}$$

$$\log K_p = k_1 \log k + k_2 \frac{MW}{100} + k_4 \qquad \textbf{Model A-4.5}$$

$$\log K_p = k_1 \log k + k_3 H_b + k_4 \qquad \textbf{Model A-4.6}$$

$$\log K_p = k_1 \log k + k_2 \frac{MW}{100} + k_3 H_b + k_4 \qquad \textbf{Model A-4.7}$$

Stepwise regression was performed in three steps by calculating *F-to-enter* values for all descriptors not included in the model at each step and *F-to-remove* values for all descriptors already included in the model at each step. After each step, the descriptor with the largest significant *F-to-enter* value was added to the model and the descriptor with the smallest non-significant *F-to-remove* value was removed from the model.

Given two models, **Model A-4.3** and **Model A-4.5**, $SS_{reg}(3)$ is the regression sum of squares for **Model A-4.3** and $SS_{reg}(5)$ is the regression sum of squares for **Model A-4.5**. Therefore,

$$SS_{reg}\left(\log k, \frac{MW}{100}\right) = SS_{reg}(5) - SS_{reg}(3) \qquad \textbf{Equation A-4.2}$$

and $SS(\log k, MW/100)$ represents the sum of squares due to adding $MW/100$ to the model including only $\log k$ (**Model A-4.3**). The mean square due to adding $MW/100$ to **Model A-4.3** is calculated using:

$$MS_{reg}\left(\log k, \frac{MW}{100}\right) = \frac{SS_{reg}\left(\log k, \frac{MW}{100}\right)}{df} \qquad \textbf{Equation A-4.3}$$

where the degrees of freedom associated with $SS(\log k, MW/100)$, df, is calculated as the difference between the degrees of freedom in **Model A-4.6** ($df_{reg}(6)$) and the degrees of freedom in **Model A-4.1** ($df_{reg}(1)$):

$$df = df_{reg}(5) - df_{reg}(3) = 2 - 1 = 1 \qquad \textbf{Equation A-4.4}$$

Therefore,

$$MS_{reg}(\log k, \frac{MW}{100}) = SS_{reg}(\log k, \frac{MW}{100}) \qquad \textbf{Equation A-4.5}$$

The residual mean square for the more complicated model (**Model A-4.5** in this case) is calculated as:

$$MS_{res}(5) = \frac{SS_{res}(5)}{df_{res}(5)} \qquad \textbf{Equation A-4.6}$$

To calculate a partial F value to check the significance of the addition $MW/100$ to **Model A-4.3**, $MS(\log k, MW/100)$ is compared to $MS_{res}(6)$ for **Model A-4.5**:

$$F = \frac{MS_{reg}\left(\log k, \frac{MW}{100}\right)}{MS_{res}(5)} \qquad \textbf{Equation A-4.7}$$

A correlation matrix for the descriptors of this model is included in **Table A-4.1**. A summary of the regression sum of squares and residual sum of squares for this model is included in **Table A-4.2**.

Step 1

$\log k$ was added to the model because it has the best correlation with $\log K_p$ as per the correlation matrix included in **Table A-4.1**.

Next, *F-to-enter* was calculated for $MW/100$ and H_b:

$$F-to-enter\left(\frac{MW}{100}\right) = \frac{SS_{reg}(5) - SS_{reg}(3)}{MS_{res}(5)} = \frac{(28.77 - 22.31)}{\left(\frac{5.46}{41}\right)} = 48.51$$

$$F-to-enter(H_b)=\frac{SS_{reg}(6)-SS_{reg}(3)}{MS_{res}(6)}=\frac{(30.05-22.31)}{\left(\frac{4.18}{41}\right)}=75.92$$

The critical value for F at the 95% confidence interval with df=1 and 41 is 4.08.

The F-*to-enter* value for H_b was the largest significant F value and therefore H_b was added to the model.

Step 2

F-*to-remove* values were calculated for log k and H_b:

$$F-to-remove(\log k)=\frac{SS_{reg}(6)-SS_{reg}(2)}{MS_{res}(6)}=\frac{(30.05-15.05)}{\left(\frac{4.18}{41}\right)}=147.13$$

$$F-to-remove(H_b)=\frac{SS_{reg}(6)-SS_{reg}(3)}{MS_{res}(6)}=\frac{(30.05-22.31)}{\left(\frac{4.18}{41}\right)}=75.92$$

The critical value for F at the 95% confidence interval with df=1 and 41 is 4.08.

Therefore, both log k and H_b were deemed significant at the 95% confidence interval and neither were removed.

The F-*to-enter* value for MW/100 was calculated:

$$F-to-enter\left(\frac{MW}{100}\right)=\frac{SS_{reg}(7)-SS_{reg}(6)}{MS_{res}(7)}=\frac{(30.81-30.05)}{\left(\frac{3.42}{40}\right)}=8.89$$

The critical value for F at the 95% confidence interval with df=1 and 40 is 4.08.

Therefore, MW/100 is significant at the 95% confidence interval and was added to the model.

Step 3

F-*to-remove* values were calculated for log k, H_b, and MW/100:

$$F-to-remove(\log k)=\frac{SS_{reg}(7)-SS_{reg}(4)}{MS_{res}(7)}=\frac{(30.81-23.84)}{\left(\frac{3.42}{40}\right)}=81.52$$

$$F-to-remove(H_b)=\frac{SS_{reg}(7)-SS_{reg}(5)}{MS_{res}(7)}=\frac{(30.81-28.77)}{\left(\frac{3.42}{40}\right)}=23.86$$

$$F-to-remove\left(\frac{MW}{100}\right)=\frac{SS_{reg}(7)-SS_{reg}(6)}{MS_{res}(7)}=\frac{(30.81-30.05)}{\left(\frac{3.42}{40}\right)}=8.89$$

The critical value for F at the 95% confidence interval with df=1 and 40 is 4.08.

Therefore, log k, H_b, and MW/100 are significant at the 95% confidence interval and none are removed from the model.

Table A-4.1-Correlation matrix for 15 mM $DPPG_{20}DPPC_{80}$, 15 mM cholesterol in 25 mM MES pH 6.0.

	log K_p	**log k**	**MW/100**	**H_b**
log K_p	1.00			
log k	0.65	1.00		
MW/100	0.11	0.58	1.00	
H_b	0.44	0.06	0.06	1.00

Table A-4.2 - Regression sum of squares and residual sum of square for mM $DPPG_{20}DPPC_{80}$, 15 mM cholesterol in 25 mM MES pH 6.0.

Model #	Descriptors	Regression Sum of Squares	Regression Degrees of Freedom	Residual Sum of Squares	Residual Degrees of Freedom
1	MW/100	3.84	1	30.38	42
2	H_b	15.05	1	19.17	42
3	log k	22.31	1	11.92	42
4	MW/100, H_b	23.84	2	10.39	41
5	log k, MW/100	28.77	2	5.46	41
6	log k, H_b	30.05	2	4.18	41
7	log k, MW/100, H_b	30.81	3	3.42	40

Appendix A-5

Stepwise Regression for 15 mM $DPPG_{20}DPPC_{80}$, 15 mM cholesterol in 25 mM HEPES pH 7.5

Refer to **Appendix A-4** for a discussion of the stepwise regression procedure.

A correlation matrix for the descriptors of this model is included in **Table A-5.1**. A summary of the regression sum of squares and residual sum of squares for this model is included in **Table A-5.2**.

Step 1

log k was added to the model because it has the best correlation with log K_p as per the correlation matrix included in **Table A-5.1**.

Next, $F\text{-}to\text{-}enter$ was calculated for MW/100 and H_b:

$$F-to-enter\left(\frac{MW}{100}\right)=\frac{SS_{reg}(5)-SS_{reg}(3)}{MS_{res}(5)}=\frac{(27.82-24.12)}{\left(\frac{6.40}{41}\right)}=23.70$$

$$F-to-enter(H_b)=\frac{SS_{reg}(6)-SS_{reg}(3)}{MS_{res}(6)}=\frac{(29.87-24.12)}{\left(\frac{4.35}{41}\right)}=54.20$$

The critical value for F at the 95% confidence interval with df=1 and 41 is 4.08.

The $F\text{-}to\text{-}enter$ value for H_b was the largest significant F value and therefore H_b was added to the model.

Step 2

$F\text{-}to\text{-}remove$ values were calculated for log k and H_b:

$$F-to-remove(\log k)=\frac{SS_{reg}(6)-SS_{reg}(2)}{MS_{res}(6)}=\frac{(29.87-15.05)}{\left(\frac{4.35}{41}\right)}=139.68$$

$$F-to-remove(H_b)=\frac{SS_{reg}(6)-SS_{reg}(3)}{MS_{res}(6)}=\frac{(29.87-24.12)}{\left(\frac{4.35}{41}\right)}=54.20$$

The critical value for F at the 95% confidence interval with df=1 and 41 is 4.08.

Therefore, both log k and H_b were deemed significant at the 95% confidence interval and neither were removed.

The $F\text{-}to\text{-}enter$ value for MW/100 was calculated:

$$F-to-enter\left(\frac{MW}{100}\right)=\frac{SS_{reg}(7)-SS_{reg}(6)}{MS_{res}(7)}=\frac{(30.05-29.87)}{\left(\frac{4.17}{40}\right)}=1.73$$

The critical value for F at the 95% confidence interval with df=1 and 40 is 4.08.

Therefore, MW/100 is not significant at the 95% confidence interval and was not added to the model.

Table A-5.1-Correlation matrix for 15 mM $DPPG_{20}DPPC_{80}$, 15 mM cholesterol in 25 mM HEPES pH 7.5

	log K_p	**log k**	**MW/100**	**H_b**
log K_p	1.00			
log k	0.57	1.00		
MW/100	0.11	0.58	1.00	
H_b	0.44	0.07	0.06	1.00

Table A-5.2- Regression sum of squares and residual sum of square for mM $DPPG_{20}DPPC_{80}$, 15 mM cholesterol in 25 mM HEPES pH 7.5

Model #	Descriptors	Regression Sum of Squares	Regression Degrees of Freedom	Residual Sum of Squares	Residual Degrees of Freedom
1	MW/100	3.84	1	30.38	42
2	H_b	15.05	1	19.17	42
3	log k	24.12	1	10.11	42
4	MW/100, H_b	23.84	2	10.39	41
5	log k, MW/100	27.82	2	6.40	41
6	log k, H_b	29.87	2	4.35	41
7	log k, MW/100, H_b	30.05	3	4.17	40

Appendix A-6

Stepwise Regression for Octanol/Water

Refer to **Appendix A-4** for a discussion of the stepwise regression procedure.

A correlation matrix for the descriptors of this model is included in **Table A-6.1**. A summary of the regression sum of squares and residual sum of squares for this model is included in **Table A-6.2**.

Step 1

log $P_{o/w}$ was added to the model because it has the best correlation with log K_p as per the correlation matrix included in **Table A-6.1**.

Next, *F-to-enter* was calculated for *MW*/100 and H_b:

$$F-to-enter\left(\frac{MW}{100}\right)=\frac{SS_{reg}(5)-SS_{reg}(3)}{MS_{res}(5)}=\frac{(24.51-19.66)}{\left(\frac{9.72}{41}\right)}=20.46$$

$$F-to-enter(H_b)=\frac{SS_{reg}(6)-SS_{reg}(3)}{MS_{res}(6)}=\frac{(27.59-19.66)}{\left(\frac{6.63}{41}\right)}=49.04$$

The critical value for F at the 95% confidence interval with *df*=1 and 41 is 4.08.

The *F-to-enter* value for H_b was the largest significant F value and therefore H_b was added to the model.

Step 2

F-to-remove values were calculated for log k and H_b:

$$F-to-remove(\log k)=\frac{SS_{reg}(6)-SS_{reg}(2)}{MS_{res}(6)}=\frac{(27.59-15.05)}{\left(\frac{6.63}{41}\right)}=77.55$$

$$F-to-remove(H_b)=\frac{SS_{reg}(6)-SS_{reg}(3)}{MS_{res}(6)}=\frac{(27.59-19.66)}{\left(\frac{6.63}{41}\right)}=49.04$$

The critical value for F at the 95% confidence interval with df=1 and 41 is 4.08.

Therefore, both log k and H_b were deemed significant at the 95% confidence interval and neither were removed.

The $F\text{-}to\text{-}enter$ value for MW/100 was calculated:

$$F-to-enter\left(\frac{MW}{100}\right)=\frac{SS_{reg}(7)-SS_{reg}(6)}{MS_{res}(7)}=\frac{(27.70-27.59)}{\left(\frac{6.53}{40}\right)}=0.67$$

The critical value for F at the 95% confidence interval with df=1 and 40 is 4.08.

Therefore, MW/100 is not significant at the 95% confidence interval and was not added to the model.

Table A-6.1-Correlation matrix for octanol/water.

	log K_p	**log $P_{o/w}$**	***MW/100***	***H_b***
log K_p	1.00			
log $P_{o/w}$	0.57	1.00		
***MW*/100**	0.11	0.58	1.00	
H_b	0.44	0.07	0.06	1.00

Table A-6.2- Regression sum of squares and residual sum of square for octanol/water

Model #	Descriptors	Regression Sum of Squares	Regression Degrees of Freedom	Residual Sum of Squares	Residual Degrees of Freedom
1	MW/100	3.84	1	30.38	42
2	H_b	15.05	1	19.17	42
3	log $P_{o/w}$	19.66	1	14.57	42
4	MW/100, H_b	23.84	2	10.39	41
5	log $P_{o/w}$, MW/100	24.51	2	9.72	41
6	log $P_{o/w}$, H_b	27.59	2	6.63	41
7	log $P_{o/w}$, MW/100, H_b	27.70	3	6.53	40